

UNCLASSIFIED

AD 412012

DEFENSE DOCUMENTATION CENTER

FOR

SCIENTIFIC AND TECHNICAL INFORMATION

CAMERON STATION, ALEXANDRIA, VIRGINIA



UNCLASSIFIED

NOTICE: When government or other drawings, specifications or other data are used for any purpose other than in connection with a definitely related government procurement operation, the U. S. Government thereby incurs no responsibility, nor any obligation whatsoever; and the fact that the Government may have formulated, furnished, or in any way supplied the said drawings, specifications, or other data is not to be regarded by implication or otherwise as in any manner licensing the holder or any other person or corporation, or conveying any rights or permission to manufacture, use or sell any patented invention that may in any way be related thereto.

412012

AD No. 412012

DDC FILE COPY

JPRS: 19,701

17 June 1963

OTS: 63-~~2047~~³¹

7

TRANSLATIONS FROM INZHENERNO-FIZICHESKIY ZHURNAL

(Journal of Engineering Physics)

No 2, 1963

- USSR -

DDC
RECEIVED
AUG 12 1963
TISIA B

U. S. DEPARTMENT OF COMMERCE

OFFICE OF TECHNICAL SERVICES

JOINT PUBLICATIONS RESEARCH SERVICE

Building T-30

Ohio Drive and Independence Avenue, S.W.
Washington 25, D. C.

Price: \$4.00

FOREWORD

This publication was prepared under contract for the Joint Publications Research Service as a translation or foreign-language research service to the various federal government departments.

The contents of this material in no way represent the policies, views or attitudes of the U. S. Government or of the parties to any distribution arrangement.

PROCUREMENT OF JPRS REPORTS

All JPRS reports may be ordered from the Office of Technical Services. Reports published prior to 1 February 1963 can be provided, for the most part, only in photocopy (xerox). Those published after 1 February 1963 will be provided in printed form.

Details on special subscription arrangements for JPRS social science reports will be provided upon request.

No cumulative subject index or catalog of all JPRS reports has been compiled.

All JPRS reports are listed in the Monthly Catalog of U. S. Government Publications, available on subscription at \$4.50 per year (\$6.00 foreign), including an annual index, from the Superintendent of Documents, U. S. Government Printing Office, Washington 25, D. C.

All JPRS scientific and technical reports are cataloged and subject-indexed in Technical Translations, published semimonthly by the Office of Technical Services, and also available on subscription (\$12.00 per year domestic, \$16.00 foreign) from the Superintendent of Documents. Semiannual indexes to Technical Translations are available at additional cost.

TRANSLATIONS FROM INZHENERNO-FIZICHESKIY ZHURNAL
(Journal of Engineering Physics)

- USSR -

No. 2, 1963

Following is the translation of all articles except the last one in the Russian-language periodical Inzhenerno-fizicheskiy zhurnal (Journal of Engineering Physics), Vol. 6, No. 2, Publishing House of the Academy of Sciences, Belorussian SSR, Minsk, February 1963, pages 3-138. Authors' names accompany each article.

TABLE OF CONTENTS

	<u>Page</u>
Experimental Investigation of Heat Transfer and Critical Thermal Loads in Boiling Water Under Conditions of Free Movement.....	1
Consideration of Heat Exchange and the Relationship of Viscosity to Temperature in the Problem of the Flow of a Viscous Liquid Between Two Rotating Concentric Cylinders.	13
An Investigation of the Influence of the Diameter of a Pipe on the Size of the Critical Thermal Load for Boiling Water.....	27
Measurement of the Temperature of an Arc Jet.....	39
Fluctuations of Temperature and Thermal Stresses in a Turbine Blade During Periodic Changes of Gas Temperature...	50
The Study of the Mechanism of Moisture Transfer in the Drying of Colloidal Capillary-Porous Bodies.....	63
The Influence of the Mineralogical Composition of Argillaceous Soils on their Properties.....	82

	<u>Page</u>
The Breakdown of Heated Metals and Alloys in an Air Stream at Supersonic Velocities.....	94
The Effect of Transverse Mass Flow on the Resistance and Heat Exchange Associated With the Turbulent Flow of a Compress Gas.....	111
Performance of Porous Electrodes in a Diffusion Process of Reagent Supply.....	124
Electrical Analogue Solution, by Ohmic Resistance Circuits, of the System of Differential Equations for Heat and Mass Transfer.....	139
Transitional Heat Conductivity in Multi-layered Media. II. Double-Layered Systems and the Determination of Minimum Heating Time for a System of a Given Heat Capacity.....	148
On the Heat Conductivity of an Unlimited Flat Wall.....	160
Temperature Waves in Elastic Strains.....	168
The Anisothermal Flow of Real Gas in a Gas Pipeline.....	179
Concerning the Fields of a Turbulent Flow Velocity in a Cyclone Chamber.....	191
A Study of the Kinetics of Thermal Decomposition of Ethane by the Single-Pulse Shock-Tube Method.....	203
The Effect of an Electrical Field on a Continuous Liquid Jet..	212
Thermal Mass Exchange in Anisotropic Bodies.....	218
Similarity and Modeling Conditions of Arcless Electro-smelting Processes.....	223
Thermal Stresses and Heat Release in Rectangular Cross-Section Units.....	231
Concerning the Critical Diameter of Spherical Thermal Insulation.....	236
First International Congress of Chemical Engineering (CHISA) in BRNO.....	239

EXPERIMENTAL INVESTIGATION OF HEAT TRANSFER
AND CRITICAL THERMAL LOADS IN BOILING WATER
UNDER CONDITIONS OF FREE MOVEMENT

V.S. Golovin, B.A. Kol'chugin, and D.A.
Labuntsov, Power Institute imeni G.M.
Krzhizhanovskiy, Moscow

The results are given of an investigation of heat transfer and critical thermal loads in boiling water under conditions of free movement. Tests were conducted on horizontal silver pipes with an external diameter of 5 mm over a range of pressure changes of from 10 to 2000 $\text{n}\cdot\text{cm}^{-2}$.

Despite its urgency and practical significance, heat transfer in the boiling of water under conditions of free movement has been studied insufficiently, especially in the area of high pressures. Only a few experimental investigations are known which are devoted to this question [1,2]. There is also only a limited number of works devoted to critical thermal loads while boiling water in a large volume. There is only one investigation in the range of pressure changes of from 10 to 2000 $\text{n}\cdot\text{cm}^{-2}$ [3].

This work has the purpose of expanding and adding to the already available material; however, great attention has been devoted to the accuracy of measurements and to the cleanliness of the surface being investigated.

The experimental unit was made in the form of

a vertical cylindrical vessel in which the testing section was laid horizontally. An outlet condenser was welded to the upper surface of the bottom of the vessel. All elements of the test unit were made of stainless steel.

The testing section was a tube about 150 mm long and 5-4 mm in diameter. The tube was made of 99.99% silver.

A thermal load on the tube was created by a low voltage alternating current. The current in the circuit was measured by an astatic ammeter of the 0.5 class which was connected to a measuring transformer of a current of the same class. The voltage drop in the tube of the testing section was measured by a 0.5 class A.C. voltmeter

The temperature inside the tube was measured with a platinum resistance thermometer of special construction. The thermometer was connected into the measuring circuit with a low-resistance D.C. potentiometer. The graduation of the thermometer was accomplished by the All-Union Scientific Research Institute of the Committee of Standards, Measures, and Measuring Instruments. The error of the thermometer does not exceed 0.04 degrees K.

Before assembling the unit, the tube of the testing section was cleaned with fine-grained emery cloth and was polished with a paste from the State Optical Institute [4]. After assembly salt-free water was poured into the unit and its deaeration was accomplished by boiling at atmospheric pressure. In order to eliminate oxygen completely from the water,

hydrazine (N_2H_4) was added to it and the unit was sealed. The salt content of the water which was added did not exceed $0.7 \text{ g}\cdot\text{m}^{-3}$ of NaCl.

After the pressure in the unit reached the assigned value, the reading was set on the master manometer and for a specific thermal load $q = 0$ the temperature inside the tube was measured; under these conditions the temperature corresponded to the saturation temperature (T_s , °K). Then a certain thermal load was set on the test tube and measurements were made of the voltage drop in it, the current strength, and the temperature inside the tube. In doing this the pressure in the unit was kept constant; this was checked by the constancy of the readings of the manometer which performed the role of a sensitive indicator. It should be noted that the divergences in the values of the saturation temperature in one series of tests at the same manometer reading did not exceed the measurement error of the thermometer. Upon completion of a series of tests the pressure in the unit was lowered to atmospheric pressure. After this samples of water were selected for chemical analysis. Then the working section was removed from the unit for examination.

The coefficient of heat transfer was calculated according to the formula

$$\alpha = \frac{q}{T_i - \delta T_w - T_s}.$$

The employment of a platinum resistance thermometer and silver as the material of the test tube made it possible to obtain sufficiently high accuracy in measuring the coefficient of heat transfer. Thus the average quadratic error does not exceed 14% even under the most unfavorable conditions (pressure of $2000 \text{ n}\cdot\text{cm}^{-2}$, small thermal loads).

Numerous effective tests of heat transfer have shown that with no single material (copper, silver, nickel-plated copper) at a pressure over $98 \text{ n}\cdot\text{cm}^{-2}$ is it possible to obtain a clean tube surface if steps are not taken to remove completely the oxygen which is dissolved in the water. During the conduct of the test the surface is covered with a loose black-colored coating of the oxides of the metals with which the water comes in contact during the test.

The data on heat transfer which is obtained for such a surface is very unstable. With the same specific thermal loads the values of the heat transfer coefficients which are obtained when conducting the test in the direction of increasing the thermal load are lower than the values which are obtained when conducting the test in the opposite direction. For small specific thermal loads ($q = 1 \cdot 10^5 \text{ watts}\cdot\text{meters}^{-2}$) the divergences in the values of the heat transfer coefficients can reach 300%. If during operation on the upper branch of the curve $\alpha = f(q)$ the load is momentarily lowered to zero and then returned to the previous value, the value of the heat transfer coefficient will correspond to the level of the lower branch of the curve (Figure 1). As can be seen from the graph, such

data cannot be considered as being satisfactory. Figure 1 also contains test points from work [1]. A comparison of them makes it possible to presume that the upward swing of the points as indicated in work [2], especially when $q > 0.5 \cdot 10^6$ and for high pressures, apparently is explained by the considerable contamination of the surface of the tube.

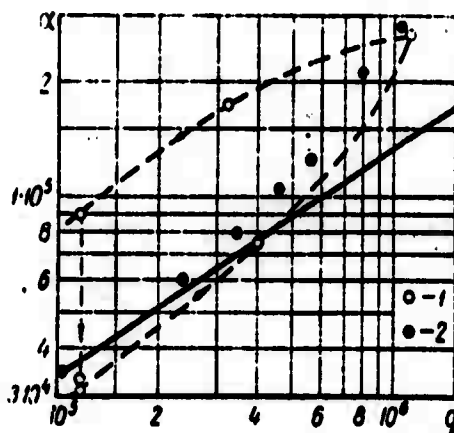


Figure 1. Test data on coefficients of heat transfer.

1 -- our data when $p = 725 \text{ n}\cdot\text{cm}^{-2}$; 2 -- data [2] when $p = 730 \text{ n}\cdot\text{cm}^{-2}$; the solid line corresponds to the data for a clean silver surface.

In order to prevent the accumulation of oxides and to obtain a practically clean surface, hydrazine was added to the water (5-7 g.m⁻³):



It is significant that only water and nitrogen result from the reaction. Therefore, the employment of small doses of hydrazine should not have significant influence on the data on heat transfer. As a check a series of tests was conducted in which the amount of hydrazine which was used was five times greater than normal; however, the data on heat transfer remained practically the same.

In conducting the tests while employing hydrazine the occurrence of pretreatment of the surface became noticeable. The tests showed that stable and reproducible data on heat transfer are obtained only after about one hour of operation of the heating surface under a high thermal load. Thus the employment of hydrazine and the pretreatment of the surface made it possible to obtain reliable, repetitive results on heat transfer for all ranges of change of thermal load and pressure.

The results of the tests are given in the table below; the remarks give a short description of the surfaces after the tests. The salt content of the water after the tests was in the range of 3.6-7.0 g.m⁻³ of NaCl.

Table

Results of tests on heat exchange

$q \cdot 10^{-6}$	ΔT	$q \cdot 10^{-6}$	ΔT	$q \cdot 10^{-6}$	ΔT	$q \cdot 10^{-6}$	ΔT
<i>Опыт № 43</i>		0,456	17,30	0,175	12,01	$T_s = 581,37^\circ \text{K}$	
$T_s = 5^\circ 2,21^\circ \text{K}$		0,244	13,90	0,29	14,72	1,14	5,99
2,23	9,16	0,123	10,00	$T_s = 372,98^\circ \text{K}$		0,266	3,17
1,18	7,11	0,356	16,13	1,01	24,79	<i>Опыт № 56</i>	
0,47	4,62	<i>Опыт № 44</i>		0,586	19,12	$T_s = 608,07^\circ \text{K}$	
0,247	3,42	$T_s = 582,29^\circ \text{K}$		0,386	16,42	1,79	5,11
0,595	4,63	2,17	8,85	0,212	13,40	0,182	2,03
0,596	4,65	0,261	3,75	0,109	10,56	$T_s = 623,44^\circ \text{K}$	
1,44	6,73	0,152	2,67	0,313	15,13	1,35	3,24
1,44	7,00	0,355	3,54	<i>Опыт № 55</i>		0,379	2,14
$T_s = 507,25^\circ \text{K}$		$T_s = 507,28^\circ \text{K}$		$T_s = 581,37^\circ \text{K}$		0,15	1,35
0,172	5,61	2,18	12,55	2,19	7,93	0,245	1,61
2,00	13,09	0,84	9,11	1,15	6,27	0,71	2,42
1,16	11,05	0,30	5,92	0,355	3,46	$T_s = 608,07^\circ \text{K}$	
0,60	8,59	0,123	4,06	0,149	2,51	0,690	2,42
0,198	5,26	0,46	6,68	$T_s = 607,76^\circ \text{K}$		<i>Опыт № 57</i>	
0,09	3,86	$T_s = 456,32^\circ \text{K}$		0,128	1,83	$T_s = 637,65^\circ \text{K}$	
0,383	6,72	1,59	17,52	0,374	2,69	0,575	1,20
$T_s = 456,27^\circ \text{K}$		0,85	14,69	0,705	3,36	0,341	1,06
1,63	18,27	0,493	12,28	1,16	4,00	0,196	0,85
1,21	16,99	0,116	6,54	1,77	4,79	0,114	0,65
0,641	14,23	0,281	9,87	1,77	5,13	0,254	0,89
0,353	11,54	$T_s = 435,60^\circ \text{K}$		1,75	5,14		
0,142	7,86	1,17	22,08	1,13	4,20		
0,250	10,04	0,605	18,35	0,40	2,67		
$T_s = 405,68^\circ \text{K}$							
1,17	22,50						
0,86	20,52						

Key:

1. Test

Note: Test No 44 was conducted in a completely

clean tube. The remaining tests were conducted in clean tubes with negligible deposits.

At pressures over $1000 \text{ n}\cdot\text{cm}^{-2}$ the heating surface usually grew somewhat "dull" after the conduct of the tests although it still retained a metallic luster. This is explained by the formation of an insignificant deposit which did not influence the level of heat transfer and which made it possible to describe such a boiling surface as being practically clean.

The data which was obtained (Figure 2) is well-described throughout the entire range of pressures and thermal loads which were investigated by the empirical formula

$$\alpha = 4 \left(q \frac{T_s}{T_{cr} - T_s} \right)^{2/3} .$$

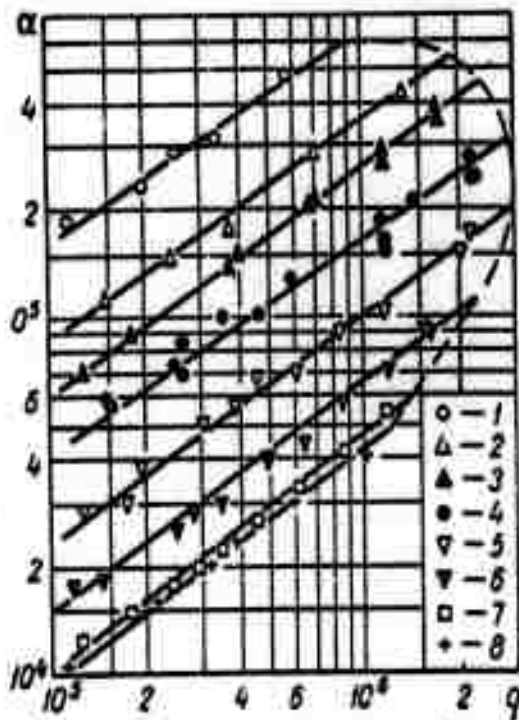


Figure 2. Test data on the coefficient of heat transfer α (watts·meters⁻²·degrees⁻¹) for various specific thermal loads q (watts·meters⁻²) and pressures p (n·cm⁻²).

1 -- 1970; 2 -- 1660; 3 -- 1365; 4 -- 974;
5 -- 302; 6 -- 108; 7 -- 29.4; 8 -- 9.8.

Deviations of test data from the data obtained by this formula do not exceed $\pm 25\%$. It should be noted that the relationship of the coefficients of heat transfer to the specific load and pressure generally were similar to the relationships given in work [2].

The method of preparing and conducting the tests for critical thermal loads was the same as in the tests on heat transfer. The critical thermal load was determined from the readings of a voltmeter and

ammeter at the moments of time preceding the burnout of the test tube.

A graph (Figure 3) of the relationship $q_{cr} = f(p)$ was constructed from the results of the tests. The nature of this relationship is basically similar to the data obtained in work [3]; however, the numerical values of q_{cr} in our tests are lower. It should be noted that in work [3] nichrome [nickel-chromium-iron alloy] plates set on edge were used as the heating surface, i.e., the conditions under which the tests in work [3] were conducted differed from ours.

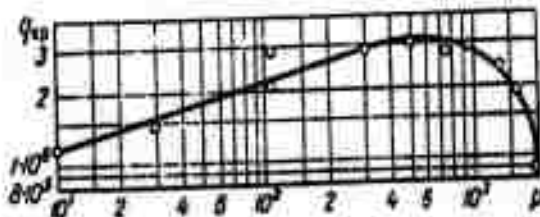


Figure 3. Relationship of the critical specific thermal load q_{cr} (watts·meters⁻²) to the pressure p (n·cm⁻²).

Symbols

α -- coefficient of heat transfer; q -- specific thermal load; q_{cr} -- critical specific thermal load; T_1 -- temperature inside the tube; T_s -- saturation temperature of the water; T_{cr} -- critical temperature of the water; T_w -- temperature drop in the wall of the experimental tube considering the heat release

in it.

Summary

Experimental data is obtained on boiling heat transfer to demineralized water from horizontal silver tubes having a 5 mm external diameter. The pressure and heat fluxes in the experiments varied over the range of 10-2000 ($\text{n}\cdot\text{cm}^{-2}$) and from $1\cdot 10^5$ ($\text{watts}\cdot\text{meters}^{-2}$) up to the critical fluxes respectively.

Stability and fair reproducibility of boiling heat transfer data were attained only with surfaces working not less than an hour at high thermal loads, provided the surface is kept sufficiently clean during the test.

At high pressures and considerable heat fluxes the boiling surface was found to be intensely covered with the oxide film. This fact can probably be explained by the presence of oxygen dissolved in the water. As a result the reproducibility of data is not achieved and heat transfer coefficients may differ rather significantly. The use of hydrazine ($5-7\text{g}\cdot\text{m}^{-3}$) made the boiling surface sufficiently clean over the entire pressure range, thus excluding the above-mentioned undesirable phenomena.

The critical heat fluxes from the horizontal silver tubes to the boiling water are evaluated over the pressure range of from 10-2000 ($\text{n}\cdot\text{cm}^{-2}$). The critical thermal load was determined by the burnout of the test tube.

BIBLIOGRAPHY

1. Cichelli, M., and Bonilla, C., Trans. ASME, 41, No 6, 1945.
2. Borishenskiy, V.M., Bobrovich, G.I., and Minchenko, F.P., Collection: Voprosy teploobmena i gidravliki dvukhfaznykh sred (Problems of Heat Transfer and Hydraulics in Two-phase Media), State Publishing House for Power Literature, 1961.
3. Kazakova, Ye.A., Collection: Voprosy teploobmena pri izmenenii agregatnogo sostoyaniya veshchestva (Problems of Heat Transfer during Change of the Aggregate State of a Substance), State Publishing House for Power Literature, 1953.
4. Vayner, Ya.V. et al., Spravochnik po zashchitno-dekorativnym pokrytiyam (Handbook on Protective-decorative Coverings), State Scientific Technical Publishing on Machine Building Literature, 1951.

CONSIDERATION OF HEAT EXCHANGE AND THE RELATIONSHIP
OF VISCOSITY TO TEMPERATURE IN THE PROBLEM OF THE
FLOW OF A VISCOUS LIQUID BETWEEN TWO ROTATING CON-
CENTRIC CYLINDERS

(on the theory of an unloaded bearing)

S.K. Aslanov
State University imeni
N.G. Chernyshevsky,
Saratov

A generalization of the problem of Professor N.P. Petrov on the movement of a lubricant in a symmetrical layer of an arbitrary thickness between rotating cylinders is examined for the case when heat exchange and the relationship of viscosity to temperature are considered.

Let us examine the established flow of a viscous liquid between two round coaxial cylinders of unlimited length of radii R_1 and R_2 ($R_2 > R_1$) which are rotating about a common axis with constant angular velocities ω_1 and ω_2 . In work [1] which laid a foundation for the hydrodynamic theory of lubrication, Professor N.P. Petrov gave a precise solution to this problem in his hypothesis on a constant coefficient of viscosity $\mu = \mu_0$, i.e., neglecting the influence of internal heat release on liquid friction. However, an experiment [2] indicates that the thermal effect in the layer is generally considerable and makes it necessary to take into account the relationship of viscosity to the temperature T . This investigation is based on the approximation of P.A. Filonov [3]

$$\mu = \mu_0 \exp[-\delta(T - T_0)] \quad \delta > 0, \quad (1)$$

the advantage of which will subsequently become clear. The remaining thermal physical characteristics of a liquid, in particular the coefficient of thermal conductivity λ , in view of their slight relationship to temperature, are assumed to be constant.

If we ignore the mass forces and take into account the unlimited length of the cylinders and the axial symmetry of the flow, then the equations of Navye-Stoks and of the influx of heat [4] in the case under consideration will give the following basic system of equations

$$\begin{aligned} \frac{\rho v^2}{r} &= \frac{dp}{dr}, \quad v_r = v_z = 0, \quad v_\varphi = v(r), \quad p = p(r), \\ \frac{d\tau}{dr} + \frac{2\tau}{r} &= 0, \quad \tau = \mu \left(\frac{dv}{dr} - \frac{v}{r} \right), \\ \frac{1}{r} \left(r\lambda \frac{dT}{dr} \right) + \frac{\tau^2}{l\mu} &= 0, \quad T = T(r) \end{aligned} \quad (2)$$

with the extreme conditions:

$$\begin{aligned} T &= T_0, \quad v = v_1 = \omega_1 R_1 \quad \text{when } r = R_1, \\ T &= T_1, \quad v = v_2 = \omega_2 R_2 \quad \text{when } r = R_2. \end{aligned} \quad (3)$$

From the second equation of (2) we immediately obtain

$$\tau = \mu \left(\frac{dv}{dr} - \frac{v}{r} \right) = \mu r \frac{d}{dr} \left(\frac{v}{r} \right) = \frac{C_0}{r^2}. \quad (4)$$

This means that for the displacement of a viscous layer an amount of work $Q = \tau V/l$ should be expended per unit of area; this work is given off in the flow in the form of heat and is lost through the walls of the cylinders under the established regime.

Thus from (1)-(4) a border problem occurs for temperature and speed fields in a dimensionless form:

$$\theta'' + \frac{1}{\xi} \theta' + \frac{a}{\xi^4} \exp \theta = 0; \quad (5)$$

$$\frac{d}{d\xi} \left(\frac{u}{\xi} \right) = \frac{b}{\xi^3} \exp \theta; \quad (6)$$

$$\theta = 0, \quad u = 1 \quad \text{when} \quad \xi = 1; \quad (7)$$

$$\theta = \theta_0, \quad u = u_0 \quad \text{when } \xi = \xi_0 > 1; \quad (8)$$

$$\theta = \delta(T - T_0), \quad \theta_0 = \delta(T_1 - T_0), \quad \xi = \frac{r}{R_1}, \quad \xi_0 = \frac{R_2}{R_1},$$

$$u = \frac{v}{v_1}, \quad u_0 = \frac{v_2}{v_1}, \quad a = \frac{C_0^2 \delta}{I \lambda \mu_0 R_1^2}, \quad b = \frac{C_0}{\mu_0 v_1 R_1}. \quad (9)$$

A nonlinear equation like (5) has already been used by us [5]. Introducing the new variables

$$\theta = y(x) - 2x, \quad x = \ln \frac{\sqrt{a}}{\xi},$$

we will have the equation

$$y'' + \exp y = 0$$

Integrating it, the general solution (5) can be presented in a final form as

$$\theta = \ln \frac{2C_1^{2/3}}{\text{ch}^2(C_2 + C_1 \sqrt{a} \ln \xi)}, \quad C_1 > 0. \quad (10)$$

From this the integration of (6) gives

$$u = AC_1 \xi \operatorname{th}(C_2 + C_1 \sqrt{a} \ln \xi) + C_3 \xi, \quad (11)$$

where

$$A = \frac{2b}{\sqrt{a}} = \pm \frac{2}{v_1} \sqrt{\frac{T\lambda}{\mu_0 \delta}} \quad (12)$$

(plus corresponds to $C_0 > 0$ and minus to $C_0 < 0$).

In order to find the arbitrary constants C_0 , C_1 , C_2 , and C_3 we have four limiting conditions of (7) and (8). In particular, in satisfying the border conditions for temperature Θ , we obtain

$$\begin{aligned} C_2 &= \operatorname{Arch}(C_1 \sqrt{2}), \quad \xi_1 = \xi_0 \exp\left(-\frac{\Theta_0}{2}\right), \\ C_3 + C_1 \sqrt{a} \ln \xi_0 &= \operatorname{Arch}(C_1 \xi_1 \sqrt{2}). \end{aligned} \quad (13)$$

In accordance with the existence of inverse hyperbolic functions, we have

$$C_1 \sqrt{2} > 1, \quad C_1 \xi_1 \sqrt{2} > 1. \quad (14)$$

As will be shown later, $\xi_1 > 1$ and the second inequality will become immaterial. Fulfilling the marginal conditions for speed u gives

$$C_2 = 1 - AC_1 \operatorname{th} C_2, \quad (15)$$

$$u_0 - \xi_0 = AC_1 \xi_0 [\operatorname{th}(C_2 + C_1 \sqrt{a} \ln \xi_0) - \operatorname{th} C_2],$$

which can be written in a more convenient form if we use (13) as:

$$C_2 = 1 \pm A \sqrt{C_1^2 - 1/2} \quad (16)$$

(plus corresponds to $C_2 < 0$, minus to $C_2 > 0$),

$$\operatorname{sh}(C_1 \sqrt{a} \ln \xi_0) = B, \quad B = \frac{2C_1 \xi_1 (u_0 - \xi_0)}{A \xi_0}. \quad (17)$$

The positive nature of the argument of the left part ($C_1 > 0$, $\xi_0 > 1$) results in $B \geq 0$, i.e.

$$A > 0 \text{ when } u_0 > \xi_0 \quad (\omega_2 > \omega_1),$$

$$A < 0 \text{ when } u_0 < \xi_0 \quad (\omega_2 < \omega_1). \quad (18)$$

Based on this, a sign is selected in (12) and consequently for the arbitrary constant C_0 . Its value is found from (17) and (9).

$$\sqrt{a} = \sqrt{\frac{\delta}{1 + \mu_0} \frac{|C_0|}{R_1}} = \frac{\operatorname{Arsh} B}{C_1 \ln \xi_0} = \frac{\ln(B + \sqrt{B^2 + 1})}{C_1 \ln \xi_0}. \quad (19)$$

As a result all the constants are expressed through C_1 . In order to determine C_1 in the second relationship of (15) we will exclude C_2 and \sqrt{a} with the help of (13) and obtain

$$\frac{u_0 - \xi_0}{A \xi_0 C_1} = \pm \sqrt{1 - \frac{1}{2C_1^2 \xi_1^2}} - \left(\pm \sqrt{1 - \frac{1}{2C_1^2}} \right). \quad (20)$$

The selection of a possible sign is limited by the conditions of (18). From this, according to (13), the plus sign occurs simultaneously only when

$$\xi_1 > 1, \quad C_1 > 0. \quad (21)$$

In the remaining two probable cases $C_2 < 0$. Solving equation (20), we then find the constant

$$C_1 = \frac{A \xi_0}{4(u_0 - \xi_0)} \left\{ \left[2 \left(\frac{u_0 - \xi_0}{A \xi_0} \right)^2 + \left(1 - \frac{1}{\xi_1} \right)^2 \right] \left[2 \left(\frac{u_0 - \xi_0}{A \xi_0} \right)^2 + \left(1 + \frac{1}{\xi_1} \right)^2 \right] \right\}^{1/2}. \quad (22)$$

The second solution $C_1 = \infty$ is not applicable since it results in infinite values of the temperature. It remains to select the sign for the constant C_2 . For this purpose we will require that the solution we have found provides a continuous limiting transition to a flow regime with a constant viscosity $\mu = \mu_0$, i.e., so that when $\mu \rightarrow \mu_0$ ($\delta \rightarrow 0$), it would turn into N.P. Petrov's solution [1, 4]. Because in the given case the value $A \rightarrow \infty$, (22) takes on the appearance

$$C_1 = \frac{A\xi_0}{4(u_0 - \xi_0)} \left| 1 - \frac{1}{\xi_1^2} \right|. \quad (23)$$

consequently values C_1 and C_2 also tend to proceed toward infinity. Applying (23) in (17) and (14) gives

$$B = \frac{1}{2} \left| \xi_1 - \frac{1}{\xi_1} \right|, \quad \sqrt{a} C_1 \ln \xi_0 = |\ln \xi_1|. \quad (24)$$

For the limit when $\delta = 0$, Θ , according to (9), turns to zero and (10) along with the first equation (13) results in the relationship

$$\frac{\text{ch}(C_2 + C_1 \sqrt{a} \ln \xi)}{\text{ch} C_2} = \xi. \quad (25)$$

From this with the help of (15) we visualize (11) as

$$u = \xi + \frac{A}{2C_1} \text{sh}(C_1 \sqrt{a} \ln \xi)$$

or considering (24)

$$u = \xi + \frac{A}{4C_1} \left(\xi^{|\ln \xi_1 / \ln \xi_0|} - \xi^{-|\ln \xi_1 / \ln \xi_0|} \right). \quad (26)$$

If we assume that $\xi_1 = \xi_0 > 1$, then using (23) it is possible to obtain

$$u = \frac{\xi^2 (u_0/\xi_0 - 1/\xi_0^2) - (u_0/\xi_0 - 1)}{(1 - 1/\xi_0^2) \xi}$$

or in the dimensional variables of (9)

$$v = \frac{r^2 (\omega_2 R_2^2 - \omega_1 R_1^2) - (\omega_2 - \omega_1) R_1^2 R_2^2}{(R_2^2 - R_1^2) r}, \quad (27)$$

which coincides precisely with N.P. Petrov's solution [1, 4]. Another possible assumption in (26) that $\xi_1 = 1/\xi_0$ gives as a result an expression which is different from (27). Thus in order to observe the limiting transition to the case of constant viscosity it is necessary that $\xi_1 > 1$ and consequently condition (21) determines the identical selection of the sign of C_2 . From this it is possible to draw the conclusion that $\xi_1 = 1$ is the upper limit of the existence of a stationary regime for the flow which we have examined, i.e., when $\xi_1 \leq 1$, the heat which is given off as a result of internal friction does not succeed in passing through the walls of the cylinders to the outside and creates the non-stationary condition of the flow. In dimensional terms, the limit of the established regime is expressed as follows:

$$T_1 - T_0 < \frac{2}{\delta} \ln \frac{R_2}{R_1}. \quad (28)$$

Thus (10)-(13), (16), (19), and (22) represent an exact solution of Professor P.N. Petrov's problem considering the influence of internal heat release on the process of liquid friction. As a result of this the liquid in the layer is heated and the temperature reaches a maximum:

$$\theta_{\max} = \ln \frac{2C_1 a \xi_2}{C_2 a - 1}, \quad \text{th}(C_2 + C_1 \sqrt{a} \ln \xi_2) = \frac{1}{C_1 \sqrt{a}}. \quad (29)$$

It can be shown that when $\xi_1 \geq \xi_0$ ($T_1 \leq T_0$), the latter always takes place.

A trivial case $\omega_1 = \omega$, ($u_0 = \xi_0$) is obtained similarly to the regime of constant viscosity, for formulas (23) and (24) retain their force. The unlimited nature of C_2 simplifies (11):

$$u = (AC_1 \text{th} C_2 + C_3) \xi = \xi \quad \text{или} \quad v = \omega_1 r,$$

i.e., the entire layer moves as a whole.

In order to portray the influence of the dissipative factor on the movement of a cylindrical layer of a viscous liquid we will calculate, on the

basis of (4), the value of the moment of the frictional forces on the internal cylinder

$$M = \int_0^{2\pi} |r| R_1 d\varphi = 2\pi |C_0|.$$

The case of a slide bearing which is most interesting from an engineering point of view is characterized by the parameters $\mu_0 = 0$ ($\omega_2 = 0$) and $\xi_0 \approx 1$ (smallness of clearance). Then (19) and (22) give:

$$m = \frac{M}{M_0} = \xi_1 \frac{\ln(B + \sqrt{B^2 + 1})}{B}, \quad \xi_1 = \exp \frac{\delta}{2} (T_0 - T_1),$$

$$B = \frac{\xi_1}{2} \left\{ \left[\frac{2}{A^2} + \left(1 - \frac{1}{\xi_1} \right)^2 \right] \left[\frac{2}{A^2} + \left(1 + \frac{1}{\xi_1} \right)^2 \right] \right\}^{1/2}. \quad (30)$$

The correction which is obtained for heat transfer can be expressed by known criteria of similarity if (12) is expressed as:

$$A = \pm \frac{1}{\text{Re}} \left[\frac{K \text{Ga}}{\text{Pr} \delta T_0} \right]^{1/2}, \quad \text{Re} = \frac{v_1 R_1}{\nu_0},$$

$$\text{Pr} = \frac{\mu_0 c_p g}{\lambda}, \quad \text{Ga} = \frac{8\pi g R_1^3}{\nu_0^2},$$

$$K = \frac{1 c_p T_0}{2\pi R_1}, \quad \nu_0 = \frac{\mu_0}{\rho}.$$

As an example of the practical employment of the above-developed theory numerical calculations were performed for a bearing with a rotor radius $R_1 = 0.025$ m and with cylinder oil having the following thermophysical characteristics [2]:

$$T_0 = 40^\circ\text{C}, \mu_0 = 0.675 \text{ n}\cdot\text{sec}\cdot\text{m}^{-2},$$

$$\lambda = 142.5 \cdot 10^{-3} \text{ watts}\cdot\text{meters}^{-1}\cdot\text{degrees}^{-1},$$

$$\rho = 9.64 \text{ n}\cdot\text{sec}^2\cdot\text{m}^{-4},$$

$\delta = 0.097 \text{ degrees}^{-1} \text{ C}$ (gives an average deviation from experimental values of μ of 3-4% in the temperature range from 15-65°C).

According to (29) and (30) we obtain the results:

1. $T_1 = T_0$ (same temperature conditions of the cylinder and bearing). When $\omega_1 = 1200$ rev/min, $m = 0.433$, i.e., the correction for heat transfer is equal to approximately 57%, $T_{\text{max}} = 52.5^\circ\text{C}$. Of course such an increase in the temperature in the lubricant layer cannot be neglected since it will lead to a greater than double decrease in the resistance moment. When $\omega_1 = 300$ rev/min $m = 0.913$ (correction 9%), $T_{\text{max}} = 41.5^\circ\text{C}$.

2. $T_1 = 20^\circ\text{C}$ (different temperature conditions of the cylinder and bearing). $\omega_1 = 1200$ rev/min, $m = 0.662$ (a correction of 34%), $T_{\text{max}} = 41.5^\circ\text{C}$. It is fully understandable that the influence of the thermal effect will decrease together with temperature T_1 .

It should be noted that in the framework of a hyperbolic approximation of the relationship $\mu(T)$,

basis of (4), the value of the moment of the frictional forces on the internal cylinder

$$M = \int_0^{2\pi} |r| R_1 d\varphi = 2\pi |C_0|.$$

The case of a slide bearing which is most interesting from an engineering point of view is characterized by the parameters $\mu_0 = 0$ ($\omega_2 = 0$) and $\xi_0 \approx 1$ (smallness of clearance). Then (19) and (22) give:

$$\begin{aligned} m = \frac{M}{M_0} &= \xi_1 \frac{\ln(B + \sqrt{B^2 + 1})}{B}, \quad \xi_1 = \exp \frac{\delta}{2} (T_0 - T_1), \\ B &= \frac{\xi_1}{2} \left\{ \left[\frac{2}{A^2} + \left(1 - \frac{1}{\xi_1}\right)^2 \right] \left[\frac{2}{A^2} + \left(1 + \frac{1}{\xi_1}\right)^2 \right] \right\}^{1/2}. \end{aligned} \quad (30)$$

The correction which is obtained for heat transfer can be expressed by known criteria of similarity if (12) is expressed as:

$$\begin{aligned} A &= \pm \frac{1}{\text{Re}} \left[\frac{K \text{Ga}}{\text{Pr} \delta T_0} \right]^{1/2}, \quad \text{Re} = \frac{v_1 R_1}{\nu_0}, \\ \text{Pr} &= \frac{\mu_0 c_p g}{\lambda}, \quad \text{Ga} = \frac{8\pi g R_1^3}{\nu_0^2}, \\ K &= \frac{1 c_p T_0}{2\pi R_1}, \quad \nu_0 = \frac{\mu_0}{\rho}. \end{aligned}$$

As an example of the practical employment of the above-developed theory numerical calculations were performed for a bearing with a rotor radius $R_1 = 0.025$ m and with cylinder oil having the following thermophysical characteristics [2]:

$$T_0 = 40^\circ\text{C}, \quad \mu_0 = 0.675 \text{ n}\cdot\text{sec}\cdot\text{m}^{-2},$$

$$\lambda = 142.5 \cdot 10^{-3} \text{ watts}\cdot\text{meters}^{-1}\cdot\text{degrees}^{-1},$$

$$\rho = 9.64 \text{ n}\cdot\text{sec}^2\cdot\text{m}^{-4},$$

$$\delta = 0.097 \text{ degrees}^{-1} \text{ C (gives an average deviation from experimental values of } \mu \text{ of 3-4\% in the temperature range from 15-65}^\circ\text{C)}.$$

According to (29) and (30) we obtain the results:

1. $T_1 = T_0$ (same temperature conditions of the cylinder and bearing). When $\omega_1 = 1200$ rev/min, $m = 0.433$, i.e., the correction for heat transfer is equal to approximately 57%, $T_{\max} = 52.5^\circ\text{C}$. Of course such an increase in the temperature in the lubricant layer cannot be neglected since it will lead to a greater than double decrease in the resistance moment. When $\omega_1 = 300$ rev/min $m = 0.913$ (correction 9%), $T_{\max} = 41.5^\circ\text{C}$.

2. $T_1 = 20^\circ\text{C}$ (different temperature conditions of the cylinder and bearing). $\omega_1 = 1200$ rev/min, $m = 0.662$ (a correction of 34%), $T_{\max} = 41.5^\circ\text{C}$. It is fully understandable that the influence of the thermal effect will decrease together with temperature T_1 .

It should be noted that in the framework of a hyperbolic approximation of the relationship $\mu(T)$,

the distribution of speeds and temperatures in a layer, as is not difficult to show, is expressed by Bessel's function with the argument $\text{const } |C_0|/\xi$. Therefore, the problem under consideration cannot be solved for the general case. It is only in the particular case of a small clearance between cylinders that one can finally find [4] all arbitrary constants from the four marginal conditions.

Symbols

r , φ , and z are the radial, angular and axial (directed along the common axis of the cylinders) cylindrical coordinates; V_r , V_φ , and V_z are the component speeds in the corresponding directions; ρ is the density; p is the pressure; I is the mechanical equivalent of heat; τ is the stress of the internal friction in the layer; M_0 is the resistance moment of the cylinder in the assumed case where $\mu = \mu_0 = \text{const}$; Ga is the Galileo number; K is the specific heat content per unit of length of the periphery of the cylinder; and c_p is the thermal capacity.

Summary

The stationary flow of a viscous liquid in an arbitrary space between rotating coaxial cylinders of infinite length is studied and the relationship between the temperature and friction heat and viscosity of the flow is taken into account. The law of this relationship is assumed to be exponential. Then the problem is reduced to the integration of a non-linear equation. This integration is performed rigorously

and all the boundary conditions are satisfied completely. As a result a closed rigorous solution is obtained for the case of constant temperatures of cylinders, and the limits of the given stationary flow conditions are shown. A comparison is made with the case of constant viscosity.

BIBLIOGRAPHY

1. Petrov, N.P., Inzhenernyy zhurnal (Engineering Journal), 1883.
2. Golubev, A.I., Collection: Treniye i iznos v mashinakh (Friction and Wear in Machines), Vol 12, Publishing House of the Academy of Sciences of the USSR, 1958.
3. Filonov, P.A., Dvizheniye nefti po trubam (The Movement of Oil through Pipes), State Publishing House for Petroleum Literature, 1930.
4. Targ, S.M., Osnovnyye zadachi teorii laminarnykh techeniy (The Main Problems of the Theory of Laminary Currents), GITTL, 1951.
5. Aslanov, S.K., Neft' i gaz (Petroleum and Gas), No 12, 1961.

AN INVESTIGATION OF THE INFLUENCE OF THE
DIAMETER OF A PIPE ON THE SIZE OF THE
CRITICAL THERMAL LOAD FOR BOILING WATER

R.A. Rybin
Central Boiler - Turbine
Institute imeni I.I.
Polzunov, Leningrad

Results are given of the experimental investigation of the influence of the diameter of a pipe on the size of the critical thermal load for gravimetric velocities of water of from 16,000 to 70,000 $\text{n}\cdot\text{m}^{-2}\cdot\text{sec}^{-1}$, steam content at the outlet from the pipe of up to 10% by weight, and a pressure of $101.3\cdot 10^5 \text{n}\cdot\text{m}^{-2}$.

There is a small number of published works in which a special study was made of the influence of the diameter of a channel on the size of the critical thermal load [3, 7, 9, 10]. In particular, the influence of diameter on the critical thermal flow q_{cr} when water is flowing in vertical pipes at a temperature below the saturation temperature and at a pressure of $25.4\cdot 10^5 \text{n}\cdot\text{m}^{-2}$ was investigated in work [7]. It was found that with a decrease of the diameter from 4 to 1 mm the critical thermal flows increase, but with a change in diameter from 4 to 6 mm they remain unchanged. In work [9] it was not noted that the diameter of the pipe influenced q_{cr} for changes of diameter from 4 to 12 mm and at pressures of $P = (101.3-202.6)\cdot 10^5 \text{n}\cdot\text{m}^{-2}$. As in work [7], the tests were conducted on water which was not heated to the saturation temper-

ature.

In investigating critical thermal flows in flat slotted channels [3] at a pressure of $143 \cdot 10^5 \text{ n} \cdot \text{m}^{-2}$, the authors came to the conclusion that a change in the width of a slot from 1.4 to 2.5 mm does not affect the size of the critical thermal load.

V.S. Chirkin and V.P. Yukin [10] conducted tests with ring apertures on water which was not heated to the saturation temperature and at a pressure close to atmospheric pressure. They established that a change in the width of the aperture space from 0.5 to 2.5 mm increases the critical thermal flow. Further increase in the width of the aperture up to 5 mm has no influence on q_{cr} .

From this short list of works it is apparent that the question of the influence of the diameter of a channel on the magnitude of the critical heat flow has been studied insufficiently and requires further investigation.

We conducted an investigation of the influence of the diameter of a pipe on the magnitude of the critical thermal load for the flow of a water-steam mixture with a gravimetric steam content at the exit of the channel of up to 10%, gravimetric flow speeds of $\gamma' \omega_0 = (1.6-7.0) 10^4 \text{ n} \cdot \text{m}^{-2} \text{ sec}^{-1}$, and pressure in the circuit of $101.3 \cdot 10^5 \text{ n} \cdot \text{m}^{-2}$. The tests were conducted in an experimental unit consisting of a closed circulating system with forced circulation (Figure 1).

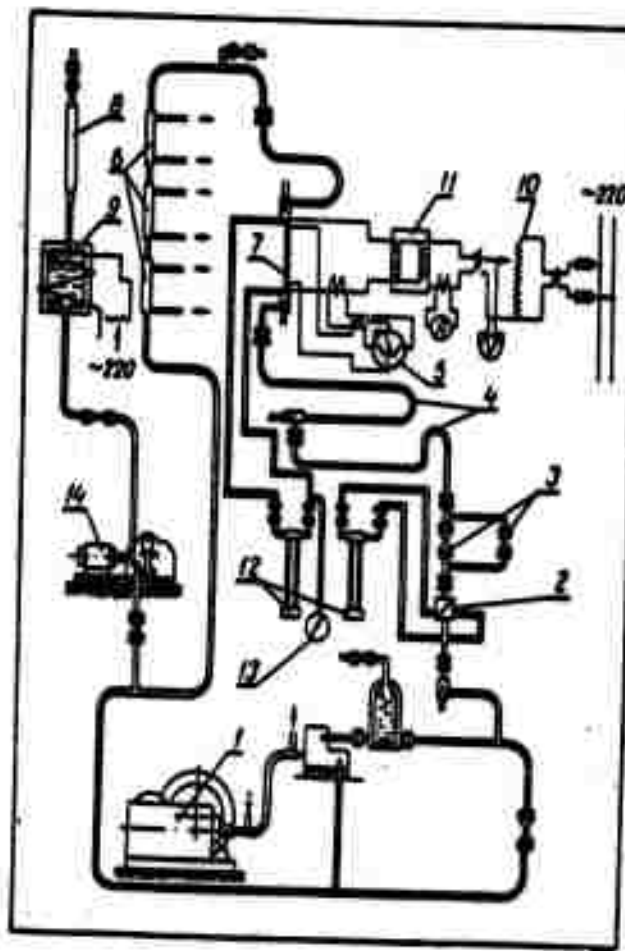


Figure 1. Diagram of the experimental unit.
 1 -- circulating pump; 2 -- measuring diaphragm;
 3 -- regulating valves; 4 -- heaters; 5 --
 wattmeter; 6 -- refrigerator condenser;

7 -- experimental section; 8 -- ion exchange filters; 9 -- deaerator; 10 -- autotransformer; 11 -- power transformer; 12 -- differential manometers; 13 -- master manometer; 14 -- feeder pump.

The experimental section and also the heater and vaporizer were heated with A.C. current. The heated part of each experimental section was preceded by an unheated hydrodynamic stabilization section 250 mm long. The tests were conducted in tubes with internal diameters of 2.05, 3.8, 5.3, 6.3, 7.6, and 10.2 mm. The relative length of all investigated pipes was equivalent to 40 diameters. This latter situation was caused, first of all, by the fact that according to the results of some experiments [4, 8] where $l/d = 15-20$, the relative length does not affect the size of the critical thermal load and, secondly, by the desire to have water at the intake into the experimental section which was not heated to the saturation temperature while the steam content at the outlet was 10%.

Method of measuring and of conducting the tests. In the course of conducting the tests the expenditure of water was measured through the use of a throttle piece; the temperature of the water at the input and of the steam-water mixture at the outlet from the experimental section were measured with chromel-aluminum thermocouples placed in mixing glasses; the pressure of the water before the test section was measured with a master manometer; and the electric

power supplied to the experimental tube was measured with a wattmeter. The onset of a crisis was gauged by the reddening of the tube. With this the load was thrown off from the tube. However, there were cases, mostly for small diameter tubes (5.3, 3.8, and 2.5 mm) when the load could not be thrown off and the pipe ruptured. The reddening always occurred in the upper part of the pipes.

Results of tests. In analyzing the test data the steam content at the outlet from the operating tube which was determined from the thermal balance equation was taken as the critical steam content x . The critical thermal flow was determined from the formula

$$q_{cr} = \frac{W_d}{\pi d l}$$

In connection with the fact that the transition from bubble boiling to pellicular boiling is a consequence of a profound hydrodynamic reconstruction of the flow [5, 6], it is preferable to relate the change in value of the critical thermal load not to the gravimetric steam content x but to the true volumetric steam content φ . Because the question of the determination of φ for a broad range of pressures, velocities, and steam contents is in the study stage, it is possible, based on works [1, 2], as a first approximation to use, rather than φ , the value of the volumetric expanded steam content β , inasmuch as in the area $\beta = 0-0.85$, the value φ is proportional to β , which is found from the formula

$$\beta = \left(1 + \frac{1-x}{x} \frac{\gamma''}{\gamma'} \right)^{-1}.$$

The tests showed that with a decrease in the diameter of the pipe in the range of changes of the parameters β and $\gamma' \omega_0$ under study, the critical thermal load increases.

The initial test data (such a treatment was used earlier by other authors) for $q_{cr} = f(\beta)$ for different values of $\gamma' \omega_0$ and d was treated as follows (Figure 2):

$$q_{cr} d^n = a + b\beta. \quad (1)$$

Coefficients a , b , and n depend on $\gamma' \omega_0$. The median line is drawn by the smallest squares method. A comparison of the values of $q_{cr} d^n = f(\beta)$ for different values of $\gamma' \omega_0$ in the range under consideration shows that in the given area of change of gravitational velocities and steam contents the influence of $\gamma' \omega_0$ on q_{cr} is negligible. This makes it possible to obtain the relationship

$$q_{cr} = f(\beta, d),$$

which generalizes the results of our tests with a spread of $\pm 20\%$ (Figure 3).

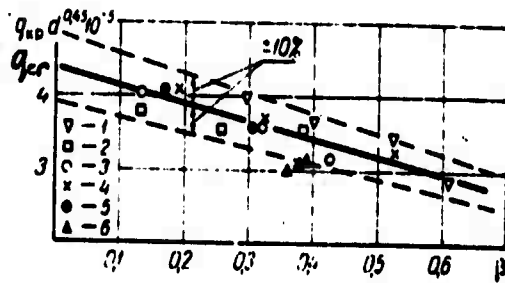


Figure 2. Relationship of the critical thermal load to the volumetric expended steam content for tubes of different diameters when $\gamma' \omega_0 = 45,000 \text{ n} \cdot \text{m}^{-2} \cdot \text{sec}^{-1}$.

1 -- $d = 2.05 \text{ mm}$; 2 -- 3.8 ; 3 -- 5.3 ;
 4 -- 6.3 ; 5 -- 7.7 ; 6 -- 10.2 .

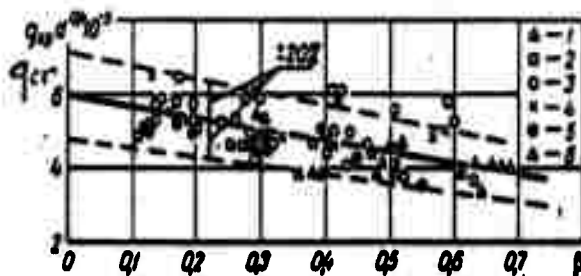


Figure 3. Relationship of the critical thermal load to the volumetric expended steam content when $\gamma' \omega_0 = (1.6-7.0)10^4 \text{ n} \cdot \text{m}^{-2} \cdot \text{sec}^{-1}$ and the tube diameters are as shown in Figure 2.

The empirical formula which describes the curve shown in Figure 3 is $q_{cr} = (6.0 - 3.05\beta)d^{0.4}10^5$.

The graph in Figure 4 is an attempt to generalize the data on the influence of the diameter of a channel on the value of the critical thermal load using the criteria of the system proposed by S.S. Kutateladze [6] [See Note]. The expended volumetric steam content β is taken as the parameter which determines the influence of steam content.

[Note]: The influence of the criterion $\frac{v}{g} \left(\frac{\gamma' - \gamma''}{\sigma} \right)^{3/2}$ in the case being considered (water at $P = (100-180)10^5 \text{ n}\cdot\text{m}^{-2}$), according to the data of V.M. Borishanskiy [11], can be neglected.

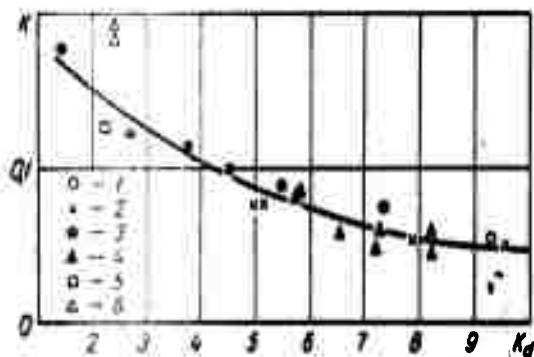


Figure 4. Relationship of criterion K to K_d when $K_w = 40$ and $\beta = 0.6$.
 1 -- $d = 13$ mm, $P = 101.3 \cdot 10^5 \text{ n}\cdot\text{m}^{-2}$;
 2 -- $d = 8.2, 9.9,$ and 5.3 mm, $P = 151.9 \cdot 10^5 \text{ n}\cdot\text{m}^{-2}$;
 3 -- $d = (2.05-10.2)$ mm, $P = 101.3 \cdot 10^5 \text{ n}\cdot\text{m}^{-2}$ (all Central Boiler-Turbine Institute);

4 -- d = 8.2 mm, P = (101.3, 143, 162.8, and 182.3) 10^5 n·m⁻² [10]; 5 -- aperture = 2.46 mm, P = 143·10⁵ n·m⁻² [3]; 6 -- d = 3 mm, P = 101.3·10⁵ n·m⁻² [4].

The graph in Figure 4 contains test data from a number of authors [3, 4, and 10] for one value of criterion $K_w = 40$ and $\beta = 0.6$. Criterion

$$K_w = \omega \cdot \sqrt[4]{\frac{\gamma' - \gamma''}{\sigma g^2}}.$$

The lack of a sufficient amount of test data for tubes of various diameters for different pressures, steam contents, and velocities made it impossible to construct similar curves for other values of the criterion K_w and the parameter β .

From the graph it is apparent that with a decrease of the criterion $K_d = d \left(\frac{\sigma}{\gamma' - \gamma''} \right)^{-1/2}$, the value of the criterion $K = q_{cr} (3600 r \sqrt{g r' \sqrt{\sigma (\gamma' - \gamma'')}})^{-1}$ increases. This under other equal conditions gives evidence of the increase of the critical thermal load with a decrease in the diameter of the channel. The path of the curve $K = f(K_d)$ provides a basis for assuming that for values of criterion K_d greater than 10, the latter will cease influencing K . This conclusion is supported qualitatively by works [8] and [11].

The nature of the influence of channel diameter on the value of the critical thermal load apparently can be explained by the fact that with a decrease in

the channel diameter the characteristic size of the freely-formed steam phase decreases due to the action of the hydraulic pressure of the flowing liquid. In this the portion of the heating surface which is in simultaneous contact with the steam decreases; this increases the stability of the two-phase surface layer [11]. In order under these conditions to break down the stability of the surface two-phase layer, it is necessary to increase the number of steam formation centers which are participating in the process. Under other equivalent conditions the latter is achieved by increasing the thermal load.

Symbols

l -- heated length of the operating pipe;
 d -- internal diameter of the operating pipe; q_{cr} -- critical thermal flow (load); w_0 -- speed of circulation (speed of the water at the saturation temperature); W_{el} -- electric power measured in the operating section.

Summary

The effect of the chamber diameter on the thermal load at the transition of bubble boiling to film boiling is examined. The experiments were carried out in a circuit with forced water circulation.

During the experiments the weight rate changed from 17,000 to 70,000 $n \cdot m^{-2} \cdot sec^{-1}$; vapor content variations at the outlet were up to 10%; the channel diameter was from 2 to 10 mm and the pressure was maintained at $101.3 \cdot 10^5 n \cdot m^{-2}$. The relative length of

the pipes was $l/d = 40$.

The channel diameter was found to have an important influence on the critical load.

An empirical formula was obtained which makes it possible to estimate the effect of the channel diameter on the critical thermal load over the range of parameter changes under study.

BIBLIOGRAPHY

1. Armand, A.A., Collection: Par vysokogo davleniya v energetike (High Pressure Steam in Power Engineering), State Publishing House on Power Literature, 1950.
2. Armand, A.A., and Nevstruyeva, Ye.I., Izv. Vsesoyuznogo teplotekhnicheskogo instituta imeni F.E. Dzerzhinskogo (News of the All-Union Thermal Engineering Institute imeni F.E. Dzerzhinskiy), No 2, 1950.
3. Dzheket, Rourti, Tserbi., Voprosy yadernoy energetiki (Problems of Nuclear Power Engineering), No 4, 1958.
4. Doroshchuk, V.Ye., and Frid, F.P., Teploenergetika (Thermal Power Engineering), No 9, 1959.
5. Kutateladze, S.S., Izv. AN SSSR OTN (News of the Academy of Sciences of the USSR: Department of Engineering Sciences), No 4, 1951.
6. Kutateladze, S.S., "Scientific Reports of the College," Energetika (Power Engineering), No 2, 1959.

7. Ornatskiy, T.P., Teploenergetika (Thermal Power Engineering), No 6, 1960.

8. Styrikovich, M.A., Miropol'skiy, Z.L., Shitsman, M.Ye., Mostinskiy, I.L., Stavrovskiy, A.A., and Faktorovich, L.Ye., Teploenergetika (Thermal Power Engineering), No 5. 1960.

9. Subbovin, V.I., Zenkevich, B.A., Sudnitsyn, S.A., Krotov, V.I., and Peskov, O.L., Collection: Issledovaniye teplootdachi k paru i vode, kipyashchey v trubakh pri vysokikh davleniyakh (Investigation of Heat Transfer to Steam and Water Boiling in Pipes at High Pressures), Atomic Literature Publishing House, 1958.

10. Chirkin, V.S., and Yukin, V.P., ZhTF, No 7, 1956.

11. Borishanskiy, V.M., ZhTF, No 2, 1956.

12. Subbotin, V.I., Zenkevich, B.A., Sudnitsyn, S.A., Ivashkevich, A.A., Sergeyev, N.D., and Peskov, O.L., Collection: Issledovaniye teplootdachi k paru i vode, kipyashchey v trubakh pri vysokikh davleniyakh (Investigation of Heat Transfer to Steam and Water Boiling in Pipes at High Pressures) (under the editorship of N.A. Dollezhal'), Atomic Literature Publishing House, 1958.

MEASUREMENT OF THE TEMPERATURE
OF AN ARC JET

Ye.V. Garkavyy

Results are given of the measurement of the temperature at the axis of an arc jet and of the temperature distribution along a radius as related to certain parameters of the discharge by means of a determination of the relative intensities of spectral lines and through an investigation of the hydrogen line contours of the Balmer $H\beta$ series.

Over the course of a number of years high temperature gas jets obtained through high current arc discharges have been a subject of very broad study. Recently they have also come under spectroscopic investigation. This has been based, first of all, on the fact that high temperature jets are of great interest in theoretical and applied spectroscopy. as a new source of light and, secondly, on the necessity of measuring one of the basic parameters which characterize arc jets -- temperature. Spectroscopic methods of measuring temperature make it possible to determine not only a local value of an indicated parameter at some point in the jet but also make it possible to find the temperature distribution for a cross section and along the length of the jet, which in a number of cases is a matter of considerable interest.

In this work the object of our research was a high temperature arc jet which was obtained with the help of a nitrogen-stabilized high-current D.C. arc discharge. Such units have already been described in publications [1, 2]. It is necessary to note only that a graphite cathode and a copper anode served as the electrodes. A cylindrical aperture in the anode served as an outlet for the jet into the atmosphere. The stabilizing gas was fed into the discharge chamber tangentially to the interior surface.

The spectra of the jet were recorded with the help of ISP-28 and ISP-51 spectrographs. The cross section of the jet was sharply directed at slits in the spectrographs at a distance of 2-3 mm from the outlet aperture. The focusing of the cross section of the jet at a slit of a spectrograph made it possible to find the temperature distribution along the radius of the jet according to the distribution of intensity across the spectrum. This was accomplished by recomputing the measured intensities of spectral lines taken for the lateral profile to find the radial distribution. The coefficients cited in work [3] were used for the recomputation.

The dispersion of the spectrographs in the area of line H_{β} amounted to 40 Å/mm for the ISP-51 and 65.5 Å/mm for the ISP-28, which made it possible to determine with sufficient accuracy the half-width of the line which had been changed in our tests in the range from 15 to 70 Å, depending on the temperature of the jet.

The method of measuring the temperature according

to the broadening of line $H\beta$ consisted of the following. Based on the experimentally measured half-width of line $(\Delta\lambda)_{1/2}$, a determination was made of the normal intensity of the field

$$F_0 = \frac{(\Delta\lambda)_{1/2}}{\alpha}.$$

The coefficient α was taken from the theoretical contour of line $H\beta$ as calculated by Griem, Kolb, and Shen [4]. Then according to the formula $F_0 = 2.61en^{2/3}$ the density of charged particles n was calculated where, in accordance with the theory of Griem, Kolb, and Shen, $n = n_e = n_i$. Having thus determined the electron density and keeping in mind the fact that the admixtures of graphite and copper in the jet do not exceed 2-3%, it is possible with a sufficient degree of accuracy to find the temperature, using the relationship of the electron density to the temperature for pure nitrogen [5]. Because the escape of the jet occurred into the atmosphere, for this purpose the relationship of n_e to T for a pressure of $9.8 \cdot 10^4 \text{ n}\cdot\text{m}^{-2}$ was used.

The values of the temperature which were calculated for the broadening of line $H\beta$ were compared with the results of measuring the temperature according to the relative intensities of the spectral lines. For measuring the temperature according to Ornshteyn's method, lines of one-time ionized carbon of 2509, 2512, and 2836-37 Å were used. The probabilities of transitions for these lines were taken from Maecker [6]. The formula for calculating the temper-

ature was

$$T = \frac{E_1 - E_2}{K} \left(\ln \frac{\lambda_2 A_1 g_1}{\lambda_1 A_2 g_2} \frac{I_2}{I_1} \right)^{-1}.$$

In determining the temperature according to the relative intensity of the spectral lines it was assumed that there was local thermodynamic equilibrium in the jet; this was checked by us and found to exist as applied to an arc jet [7].

The temperature values which were calculated from the same spectrum according to the CII lines and the half-width of line H_β correspond well with each other as can be seen from the table. The measurement of the temperature according to the broadening of line H_β in the presence of small admixtures obviously is more dependable than measuring according to the relative intensity of spectral lines. This is based on the fact that the probabilities of transitions for spectral lines are not known with sufficient accuracy. For lines CII which were used in this work the probabilities of transitions were determined with an error of 20-25%, which can cause an error in measuring the temperature of up to 35%. On the other hand, the half-width of line H_β can be determined with an error of a few percent which could cause an error in the temperature value on the order of 10%. Unfortunately the upper limit of the temperatures which can be measured in arc jets from the broadening of hydrogen lines is approximately 16,000-18,000°K; over this value the determination of the temperature becomes ambiguous in view of the decrease in electron

density which occurs with further increase in the temperature because of thermal expansion.

Table
Comparison of temperatures measured by
 $H\beta$ and by CII lines

Temperature at the axis of the jet, °K			
By $H\beta$	By CII		T_{av}
	$\frac{2509 \text{ \AA}}{2836}$ 37 \AA	$\frac{2512 \text{ \AA}}{2836}$ 37 \AA	
15450	16300	15550	15750
17000	17500	16850	17100
14300	14800	13950	14400
15800	17000	16250	16350
14400	14000	14800	14400

The value of the temperature at the axis of the jet and especially the nature of the temperature distribution along the radius of the jet depend essentially on the parameters of the discharge and the geometry of the discharge chamber. In experiments

on determining the relationship of the temperature on the axis of the jet to the power which is applied to the discharge (Figure 1), the length of the anode was constant and was equal to 50 mm and the diameter of the outlet aperture varied from 12 to 15 mm, which had no significant effect on the value of the axial temperature. The temperature distribution along the radius of the jet under these conditions was parabolic; as can be seen from Figure 2, the higher the temperature is at the axis of the jet, the steeper will be the parabola. If at a temperature of 14,000-15,000°K the temperature distribution curve corresponds to a parabola of the third degree, then for 18,000°K at the axis it is close to a quadratic parabola.

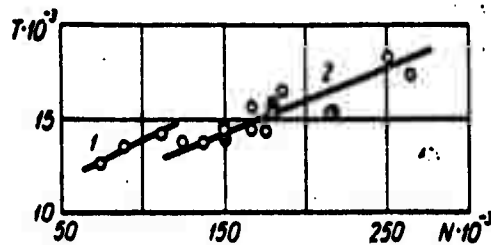


Figure 1. Relationship of the temperature $T(^{\circ}\text{K})$ at the axis of a jet to the power N (watts) which is applied to the discharge for two different expenditures of stabilizing gas.

1, 2 -- $G = 5.6; 6.5$ ($\text{g}\cdot\text{sec}^{-1}$)

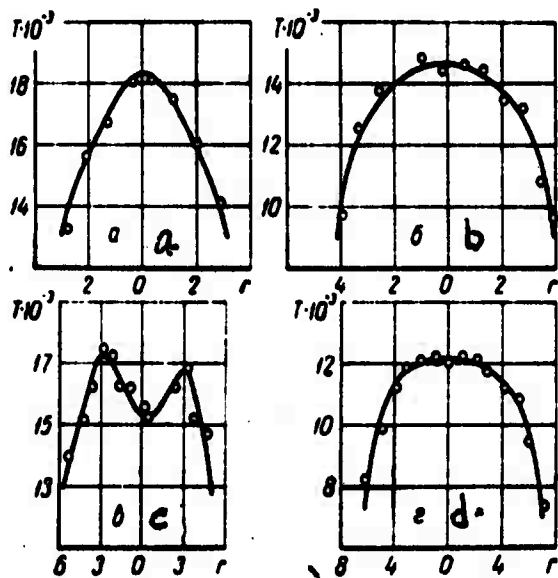


Figure 2. Distribution of temperature $T(^{\circ}\text{K})$ along the radius of a jet r (mm)
 a, b, c, d -- $N = 250; 160; 235; 269 \cdot 10^3$ (watts);
 $G = 6.55; 6.5; 10.75; 13.6$ ($\text{g} \cdot \text{sec}^{-1}$); $d = 12;$
 $12; 13.7; 15.5$ (mm) accordingly; $l = 50$ mm for
 a, b, and c and 100 mm for d.

The temperature distribution acquires a completely different character in the case of an increase in the expenditure of stabilizing gas to 11-14 g·sec⁻¹ when the geometry of the discharge chamber remains unchanged. In this case the maximum temperature is displaced approximately 3 mm from the center and a temperature dip appears at the jet axis which increases as the expenditure of stabilizing gas rises. The lowering of the temperature at the axis of the jet is rather considerable. For an expenditure of nitrogen of 14.5 g·sec⁻¹, for example, the depth of the dip, i.e., the difference between the maximum and axial temperatures, reaches 4,000-5,000°K.

Both the appearance of the dip and some asymmetry in the temperature distribution along the radius of the jet are based apparently on the intensification of the twisting of the jet during the increase in the expenditure of the stabilizing gas which is fed into the discharge chamber tangentially to the internal surface. The influence of the twisting depends significantly on the geometry of the discharge chamber and in particular on the length of the anode and the diameter of the outlet aperture (Figure 3). As is apparent from the graph, the temperature dip should lessen with an increase in the anode length and the diameter of the outlet aperture at the anode for an unchanging expenditure of the stabilizing gas and should disappear completely in the straight-line portion of the curve. And actually when the length of the anode is increased from 50 to 100 mm and the expenditure of gas remains unchanged, as does the

diameter of the outlet aperture, the temperature dip at the axis of the jet does disappear and the temperature distribution again assumes the shape of a parabola (Figure 2d). In this case the jet temperature is lowered somewhat and the temperature profile becomes fuller than in the case of a short anode. The temperature distribution curve which is given in Figure 2d corresponds approximately to a parabola of the fourth degree. This effect can apparently be explained by the fact that in a long anode there is better mixing of the cold and hot gas. In addition there is also the not completely excluded influence of the twisting. The flattening of the temperature profile for an increase in the length of the anode can also be explained in part by the change in the cooling conditions (increased removal of heat).

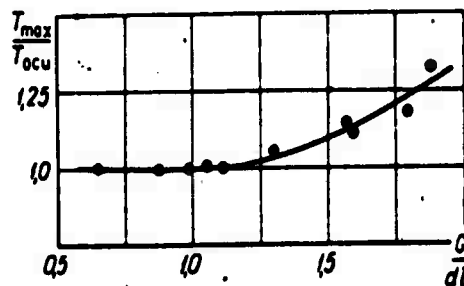


Figure 3. Relationship of the ratio of the maximum temperature T_{max} to the temperature at the axis of the jet T_{axis} with respect to the parameter G/dl ($g \cdot sec^{-1} \cdot cm^{-2}$).

All these phenomena of course require further investigation. However, it is now possible to conclude that by selecting certain discharge parameters and a certain geometry for the discharge chamber it is possible for some interval of temperatures to obtain a jet arc with a selected temperature distribution along the radius.

Symbols

T -- temperature of the jet; n_e -- electron density; n_i -- ion density; e -- electron charge; E -- excitation level energy; K -- Boltzman's constant; g -- statistical weight of the level; λ -- wave length; A -- probability of transition; I -- relative intensity of a spectral line; G -- expenditure of stabilizing gas (nitrogen); N -- discharge power; d -- diameter of the outlet aperture; l -- length of the anode.

Summary

The relationship of the temperature of the axis of an arc jet to the discharge power (Figure 1) is determined. Temperature distributions with respect to jet radius are plotted and discussed for various discharge parameters (Figure 2). The results of temperature measurements obtained by two different methods are compared.

BIBLIOGRAPHY

1. Shashkov, A.G., Yas'ko, O.I., Sergeev, V.L., and Yurevich, F.V., Inzhenerno-fizicheskiy zhurnal (Journal of Engineering Physics), No. 1, 1962.

2. Dzhon, Veyd, Shveyzer, Ios., Voprosy raketnoy tekhniki (Problems of Rocket Engineering), No 8, 1960.

3. Pearce, W.J., Conference on Extremely High Temperatures, Boston, Massachusetts, March 18-19, 1958.

4. Griem, H.R., Kolb, A.C., and Shen, K.J., Physics Rev., 116, page 4, 1959.

5. Martinek, F., Thermodynamic and Transport Properties of Gases, Liquids, and Solids, McGraw-Hill Book Company, New York-Toronto-London, page 130, 1959.

6. Maecker, H., Ztschr. Phys., 135, page 13, 1953.

7. Garkavyy, Ye.V., Inzhenerno-fizicheskiy zhurnal (Journal of Engineering Physics), No. 8, 1962.

FLUCTUATIONS OF TEMPERATURE AND THERMAL
STRESSES IN A TURBINE BLADE DURING PERIODIC
CHANGES OF GAS TEMPERATURE

Ye.P. Plotkin and Ye.I. Molchanov
All-Union Thermal Engineering Institute
imeni F.E. Dzerzhinskiy, Moscow

On the basis of the methods of approximate calculation simple relationships have been derived for evaluating temperature fluctuations of a blade and results are given of the calculation of thermal stresses which occur in blades during fluctuations of gas temperature.

In the process of operating gas turbine units one often encounters regimes where the rotor and stator blades are under conditions of periodically changing gas temperature. Considerable fluctuations in the gas temperature can occur because of the unstable operation of the combustion chamber or, during transitional stages, because of a change in the power of the gas turbine unit. In this the amplitude of the fluctuations can exceed by several times the difference of the gas temperatures of the initial and final heat regimes.

The gas temperature fluctuations cause corresponding fluctuations in the blade temperatures, especially of the thin edges which warm and cool considerably faster than the bulky center part of the blades. The resulting unevenness in the temperature throughout the cross section of a blade can be the reason for the appearance of thermal stresses. It is a matter of great practical interest to evaluate the change

in temperature and in thermal stresses in blades with the purpose of discovering the effect of gas temperature fluctuations on the strength of blades which are operating under conditions of high temperatures and stresses.

The difficulty of solving a non-stationary problem of thermal conductivity concerning the distribution of temperature in a blade means that one cannot obtain an analytical expression which is suitable for concrete analysis. However, it is possible to use the method of the approximate calculation of the blade temperature for a non-stationary regime [1] in order to discover, with a degree of accuracy which is sufficient for practical application, the effect of various factors such as the profile of the cross section of the blade, the conditions of heat transfer, the physical properties of the blade metal, the period and amplitude of the gas temperature fluctuations, etc.

At the basis of the method of approximate calculation is the assumption that in the heating of the blade the main flow of heat is normal to the surface and that the flow of heat along the skeletal line of the cross section is small and can be neglected. This makes it possible to consider each section of a blade cross section as a plate with a thickness of $\delta = 2h$.

A comparison of an approximate solution with an exact one [1] obtained on a hydraulic integrator shows that our assumption does not lead to a significant error for practically encountered conditions of

heat transfer and the physical properties of blade material.

For a plate which has heat transfer from two sides it is possible to establish the equation

$$\frac{dt}{d\tau} = k(t_g - t), \quad (1)$$

where $k = \frac{\alpha \psi}{c\gamma h}$.

The coefficient $\psi = \frac{t_g - t_s}{t_g - t}$ which is introduced into criterion k and which characterizes the inequality of distribution of the temperature throughout the plate, according to the theory of regular operation, is approximately equal to $\psi \approx (1 + Bi/3)^{-1}$.

Let us examine equation (1) for change in gas temperature according to the harmonic law

$$t_g = t_0 + \bar{t}_g \sin 2\pi \frac{\tau}{T}. \quad (2)$$

Introducing the dimensionless temperature of the plate $\theta = \frac{t - t_0}{t_g}$ we obtain the equation

$$\frac{d\theta}{d\tau} + k\theta = k \sin 2\pi \frac{\tau}{T}. \quad (3)$$

Let us accept $k = \text{const}$ in the solution, i.e., we will not consider the change of α , c , and γ with the change of temperature and time, and let us accept the value of ψ as being unchanged. The solution of

equation (3) takes on the form

$$\theta = \frac{\sin(2\pi\tau/T) - (2\pi/kT)\cos(2\pi\tau/T)}{1 + (2\pi/kT)^2} + A \exp(-k\tau), \quad (4)$$

where the constant A is easily determined from the initial condition. For large values of τ the second member of the solution approaches zero and

$$\theta = \left[1 + \left(\frac{2\pi}{kT} \right)^2 \right]^{-1/2} \sin \left(2\pi \frac{\tau}{T} - \varphi \right). \quad (5)$$

Thus from solution (5) it follows that the average temperature of the plate \bar{t} performs a simple harmonic fluctuation, the phase of which does not coincide with the phase of the fluctuation of the gas temperature

$$t = t_0 + \bar{t} \sin \left(2\pi \frac{\tau}{T} - \varphi \right), \quad (6)$$

where the amplitude of the fluctuations

$$\bar{t} = \bar{t}_g \left[1 + \left(\frac{2\pi}{kT} \right)^2 \right]^{-1/2}, \quad (7)$$

and the displacement of the phase of the fluctuations

$$\varphi = \text{arctg} \frac{2\pi}{kT}. \quad (8)$$

As is apparent from (7) and (8), the relative amplitude of the temperature fluctuations of a plate $\bar{\theta} = \bar{t}/\bar{t}_g$ and the angle of the displacement of the phase φ depend on the parameter

$$kT = \frac{\alpha \psi}{c\gamma h} T. \quad (9)$$

Based on relations (7) and (8) it is possible to calculate the temperature fluctuations of different parts of a blade, for example, the edges, considering them as plates with a corresponding thickness $\delta = 2h$.

The calculation of specific variants makes it possible to learn the effect of various factors. From an analysis of the curves (Figure 1) of the relationship $\bar{\theta} = \bar{t}/\bar{t}_g$ to the thickness δ and the fluctuation period T it is clearly apparent that even for relatively high values of the coefficient of heat transfer ($\alpha = 1163 \text{ watts}\cdot\text{meters}^{-2}\cdot\text{degrees}^{-1}$), fluctuations with a period of less than 0.5 sec will have little effect on the temperature of a blade. This means that pulsations of the gas temperature behind the combustion chamber of high and medium frequency (10 cycles or more) are of no danger with respect to the strength of the blades of a gas turbine. Low frequency fluctuations of t_g (1.5-3 cycles) behind the combustion chamber affect only the temperature of very thin edges (about 0.5 mm), and in this the amplitude of the temperature fluctuations of the edges can be 15% from the amplitude of the fluctuations of the gas temperature.

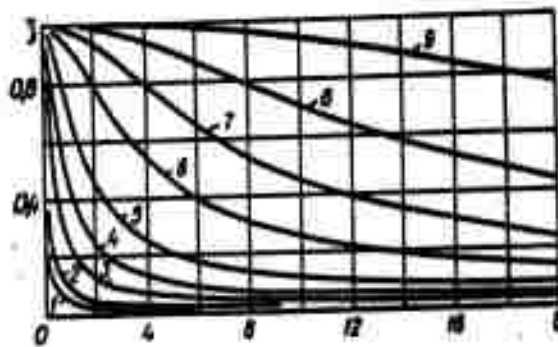


Figure 1. Relationship of the relative amplitude of the fluctuations of temperature $\bar{\theta}$ to the thickness δ (mm) for different values of T (sec).

1 -- 0.5; 2 -- 1; 3 -- 3; 4 -- 6; 5 -- 12;
6 -- 30; 7 -- 60; 8 -- 120; 9 -- 300.

A stronger effect on the temperature of the blade edges is caused by transitional processes which occur in regulating the power of the gas turbine unit and which occur with a period for the fluctuations of several seconds or more. In this the temperature field of the blade changes considerably and the temperature of the thin edges practically "follows" the temperature of the gas. A significant role in such regimes is played by the thickness of the edge; an increase in thickness considerably lowers the relative amplitude of the temperature fluctuations.

The average temperature of the thicker center

part of the cross section of a blade changes little with gas temperature fluctuations, at least for fluctuations, at least for fluctuation periods of up to 20 seconds. It should be noted that in evaluating the temperature of the center part of a cross section, the average temperature t of the equivalent plate still does not fully characterize the temperature field in this part of the cross section because the amplitude of the temperature fluctuations of the surface can be somewhat higher. In order to determine the temperature of the surface in the average part of the cross section it is possible to use the known solution [2] for the propagation of heat waves in a plate when the temperature of the environment performs harmonic fluctuations.

With the help of a hydraulic integrator an exact solution was obtained for a change of the temperature field of a rotor blade of a turbine during fluctuations of the gas temperature. The cross section of the blade was divided into 33 units; the thermo-physical properties c , γ , and λ of steel were accepted according to a temperature of 400°C ; the coefficient of heat transfer was accepted as a constant for the surface equal to $930 \text{ watts}\cdot\text{meters}^{-2}\cdot\text{degrees}^{-1}$.

Figure 2 shows graphs of temperature fluctuations of the exhaust edge and center of a blade. These graphs were constructed according to the results of the calculations.

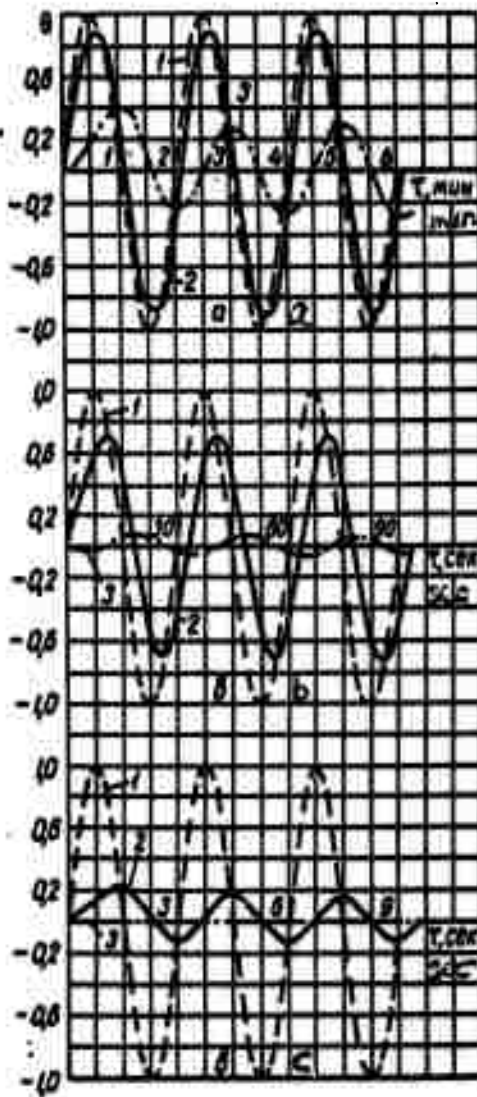


Figure 2. Temperature fluctuations of a turbine blade for gas temperature fluctuations (solution on a hydraulic integrator).

1 -- gas temperature; 2 -- temperature of the

exhaust edge; 3 -- temperature of the center of the blade; a, b, c -- T (sec) -- accordingly 120, 30, 3.

For small periods of fluctuations ($T = 3$ sec), the temperature of the center part of the blade does not change while at the same time the amplitude of the temperature fluctuations of the edge ($\delta = 1.6$ mm) comprises 12% of the amplitude of the fluctuations of \bar{t}_g . As the period of the fluctuations increases, the relative amplitude $\bar{\theta}$ of the fluctuations of the temperature of the edge grows, reaching in a period $T = 2$ minutes the value $\bar{\theta} = 0.90$. In this there is also an increase in the temperature fluctuations in the thicker center part of the cross section ($\bar{\theta} = 0.27$). It should be noted that the surface temperature in this part of the cross section fluctuates with an amplitude of $\bar{\theta} = 0.30$, slightly exceeding the amplitude of the temperature fluctuations of the center.

A comparison of the results of an accurate solution on a hydraulic integrator with the results of an evaluation of the temperature fluctuations of a blade according to the approximate method, as described above, show that approximate calculations performed without considering the longitudinal flow of heat along the blade section permit a sufficiently correct evaluation of the temperature fluctuations of a blade, although they do give somewhat inflated values for the temperature of the edge for gas temperature fluctuations.

The considerable unevenness of the temperature in

a cross section of a blade which occurs during gas temperature fluctuations causes thermal stresses in the blades. The evaluation of the size and nature of these stresses is a matter of interest. For this reason, using temperature fields obtained with the help of a hydraulic integrator, we calculated the thermal stresses in a rotor blade for gas temperature fluctuations of from 300 to 500°C with a period of $T = 2$ minutes. This case corresponds to actual fluctuations of t_g which occurred during idling of the turbine while adjusting its operation. The calculation of the temperature stresses was conducted according to the relationships for unevenly heated rods [3, 4]. The normal radial stresses σ_z in a cross section of an unevenly heated blade are equal to:

$$\sigma_z = E \left\{ \frac{\int_F E \beta t dF}{\int_F E dF} + y \frac{\int_F E \beta t y dF}{\int_F E y^2 dF} + x \frac{\int_F E \beta t x dF}{\int_F E x^2 dF} - \beta t \right\}.$$

The thermal stresses, as is apparent from the graph (Figure 3), change according to the harmonic law, periodically causing expansion or contraction. The maximum value of these stresses and the displacement of the phase are the same for different points of the cross section. The maximum stress occurs at the exhaust edge where it reaches a value of $\sigma_z = \pm 1140 \cdot 10^5$ $\text{n} \cdot \text{m}^{-2}$.

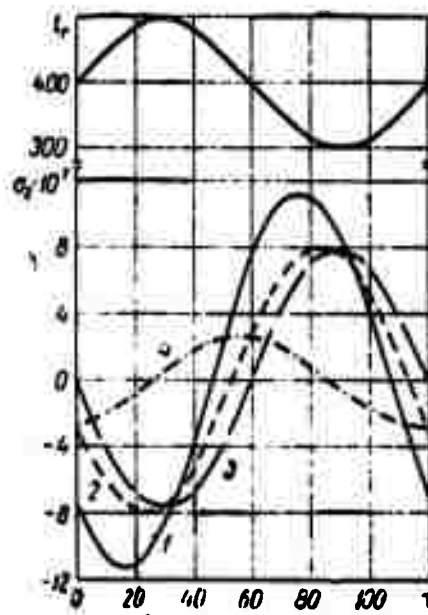


Figure 3. Temperature stresses σ_z ($\text{n}\cdot\text{m}^{-2}$) in a turbine blade ($T = 120$ sec).
 1, 2 -- at the exhaust and intake edges;
 3, 4 -- on the convex and concave surfaces.

The calculations which were made confirm the fact that because of gas temperature fluctuations in the process of operating a gas turbine unit it is possible to have considerable fluctuations in temperature and thermal stresses in the blades. These fluctuations of temperature and stresses can have a significant effect on the long-term strength of the blade material and can lead to early breakdown [5].

Symbols

t_g -- temperature of the surrounding gas; t -- average temperature of a plate; t_s -- surface temperature

of a plate; t_0 -- amplitude of the gas temperature fluctuations; τ -- time; T -- period of a gas temperature fluctuation; α -- coefficient of heat transfer; c -- thermal capacity of the blade material; λ -- coefficient of thermal conductivity; h -- half the thickness of a plate; E -- module of elasticity; β -- coefficient of linear expansion; x, y -- coordinates of points of a cross section relative to the main axes of the thermalelastic curvature of the blade; γ -- specific gravity of the blade material.

Summary

Approximate methods are presented for solving a temperature field of a turbine blade with gas temperature fluctuations. Simple relations for the temperature change of various parts of the blade are derived based on the fluctuation period, heat transfer conditions, physical properties of the metal, and blade shape.

Gas temperature fluctuations of high frequency are found to have actually no effect on the blade temperature field because of unstable operating conditions of the combustion chamber. Gas temperature fluctuations with transient operational processes of the turbine resulting from the action of the control system and characterized by lower frequency cause considerable temperature changes in the blade, especially of its thin edges. These changes may result in additional thermal stresses.

BIBLIOGRAPHY

1. Plotkin, Ye.P., and Molchanov, Ye.I.,
Collection: Povysheniye parametrov para i moshchnostey

agregatov v teploenergetike (Raising the Parameters of Steam and the Power of Units in Thermal Power Engineering) (under the editorship of A.S. Gorshkov, V.Ye. Doroshchuk, and N.V. Kuznetsov), State Publishing House for Power Engineering Literature, 1961.

2. Lykov, A.V., Teploprovodnost' nestatsionarnykh protsessov (Thermal Conductivity of Non-stationary Processes), State Publishing House for Power Engineering Literature, 1948.

3. Birger, I.A., Rukovodstvo dlya konstruktorov po raschety na prochnost' gazoturbinnnykh dvigateley (Handbook for Designers for Calculating the Strength of Gas Turbine Engines), No 2, State Publishing House of the Ministry of Defense, 1956.

4. Malinin, N.N., Izv. AN SSSR, OTN (News of the Academy of Sciences of the USSR, Department of Engineering Sciences), No 4, 1954.

5. Kostochkin, Yu.V., and Odina, I.A., Izv. AN SSSR OTN, Metallurgiya i toplivo (News of the Academy of Sciences of the USSR, Department of Engineering Sciences, Metallurgy and Fuel), No 1, 1960.

THE STUDY OF THE MECHANISM OF MOISTURE
TRANSFER IN THE DRYING OF COLLOIDAL
CAPILLARY-POROUS BODIES

N.V. Churayev
Kalininskiy Peat Institute,
Moscow

The results are described of experiments in the study of the mechanism of moisture transfer and of the processes of structure formation of colloidal capillary-porous bodies of various dispersities.

Methods which are based on the utilization of a radioactive indicator have been developed for the investigation of the hydrous properties and the moisture transfer mechanism in the drying of colloidal capillary-porous bodies [1-5]. With the help of these methods a study has been conducted of processes of the isothermal drying of samples of peat and clays (balls of a size of 7-10 mm). The tests were conducted in a drying unit [1] using two repetitions and passing air through the chamber at the rate of 1-3 liters/minute and while maintaining a temperature of 20-25°C. and a relative humidity of 10-30%.

Figure 1 shows the graphs which were obtained from a series of test samples and which reflect the relationship of the drying speed, sample volume, volumetric weight of the samples, coefficient β_0 , and the values of the integral criterion of phase transformation to the moisture content [1]. Based on these graphs the values $q_f = q_i$ have been calculated

which indicate the speed of removal of the moisture which is evaporated within the pores. The values of the difference $q - q_0 = q_1$ indicate the speed of drying which is based on the evaporation from the surface of the sample of water which reached there in the form of liquid.

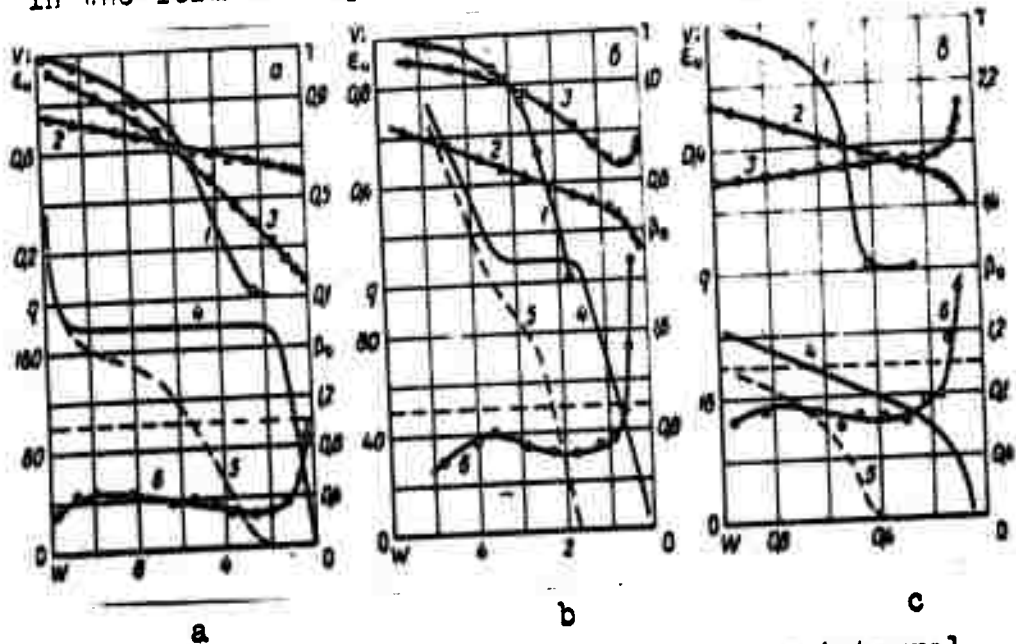


Figure 1. Change of values of the integral criterion of the phase transformation ξ_i (1), of the volume of the samples V (cm^3) (2) and their volumetric weight γ ($\text{g}\cdot\text{cm}^{-3}$) (3), of the speed of drying q ($\% \cdot \text{hour}^{-1}$) (4) and its component q_0 ($\% \cdot \text{hour}^{-1}$) (5), and also coefficient β_0 (6) in relation to the moisture content of samples W (g/g) which decreases during the course of the drying.

a -- peat moss, $R = 15\%$; b -- sedge peat, $R = 30\%$, dispersed; c -- humbrine.

The main results obtained from an analysis of the test data are shown in the following table.

Table
Results of the observation of the drying of samples of different soils

№ образца (1)	Характеристика образца (2)	P _c , мг (3)	Содержание частиц менее 1 мк. % (4)	Критические значения влажности, % (6)				Коэффициенты объемной усадки		Количество воды, перенесенной жидкостным механизмом, % (9)		
				W _{K1}	W _{K2}	W _{K3}	W _{N=100} = W _{Фк} (7)	β ₁	β ₂	M ₀	M	
												q ₀ , %/час (5)
1	Сфагновый переходный торф, R=15% (10)	60	5	176	180	—	30	30	0,047		35	44
2	Осоковый торф, R=30% (11)	115	12	82	190	—	75	70	0,130		31	37
3	Пушицево-сфагновый торф, R=40% (12)	125	20	65	170	45	35	30	0,183	1,17	29	45
4	Осоковый торф, R=30%, переработан 1 раз (13)	100	20	97	160	90	70	75	0,313	0,84	18	32
5	Медум-торф, R=25%, переработан 5 раз (14)	105	25	83	155	40	45	45	0,56	0,61	4	16
6	Медум-торф, R=25%, пептизирован NaOH (15)	95	40	85	130	50	45	50	1,22	1,40	H	H
7	Песок, 0,1—0,25 мм (16)	1100	0	6,8	4	—	0,6	0	0		100	100
8	Глуковецкий каолин (17)	630	H	18	22	—	5	2	0,59		14	52
9	Гумбрин (18)	430	H	20	35	10	13	14	1,78	2,2	38	56

Keys:

1. Sample number
2. Description of sample
3. Content of dry matter (in milligrams)
4. Content of particles smaller than 1 micron, %

5. Speed of drying, %/hour
6. Critical values of moisture content, %
7. $W_N = 100 - W_{\text{physico-chemical}}$
8. Coefficients of volumetric shrinkage
9. Quantity of water transferred by the liquid mechanism, %
10. Sphagnous transitional peat, R = 15%
11. Sedge peat, R = 30%
12. Eriophorous-sphagnous peat, R = 40%
13. Sedge peat, R = 30% processed once
14. Medium peat, R = 25%, processed five times
15. Medium peat, R = 25%, peptized with NaOH
16. Sand, 0.1-0.25 mm
17. Glukhovetskiy Kaolin
18. Humbrine

Note: H indicates the lack of experimental data.

The results of the tests make it possible to draw the following conclusions with respect to the mechanism of the processes which occur in drying test samples of colloidal capillary-porous bodies. In natural peat of low dispersity (No 1 and 2 in the

table), in connection with the high strength of the structural elements from large plant fibers, the shrinkage is not large ($\beta = 0.05-0.13$) and its rate in accordance with known theories [6], does not change throughout the entire course of the drying (Figure 1a). The low values of coefficient β_0 indicate an intensive entry of air into the samples which leads to a continuous decrease in their volumetric weight. The retreat of the evaporation front leads to a lowering of the values of ϵ ; from the very beginning of the drying. For this reason, as can be seen from the table, the role of the fluid mechanism for samples No 1 and 2 in a period with a constant drying speed is very important. Up to 30-35% of all the moisture is drawn to the surface of the sample in the form of liquid. This, in all probability, is facilitated by the plant residue which creates a capillary net which more or less drains the sample.

As the degree of dispersion of the peat increases as a result of its decomposition (sample No 3), mechanical processing (samples No 4 and 5), or spontaneous dispersion (sample No 6), there is a change in the mechanism of the processes of moisture transfer and structure formation during drying. The decrease in the size of the pores [7] leads to an increase in the strength of the capillary contraction [8] and the breakdown of the plant residue does not prevent further deformation of the samples. As a result of this the coefficients of volumetric shrinkage in highly dispersed peat increase to $\beta = 0.2-0.6$, as had been noted earlier by [9]. Similar relationships

occur also in mineral soils; as their degree of dispersion and hydrophilicity increase, the shrinkage processes develop ever more effectively, as is apparent from a comparison of the coefficients of β in the table. The transition to a liquid transfer mechanism occurs in highly dispersed samples of peat at low levels of moisture content. As can be seen from the table, the portion of the moisture which is transferred by the liquid mechanism becomes lower as the dispersion of the peat grows. Thus in the case of drying dispersed peat, the transfer of moisture in the form of vapor acquires basic importance.

An element which was common for all tested samples except sand was the gradual increase in the role of the liquid mechanism of transfer in the course of the drying, as is apparent from an analysis of the graphs of ξ ; and $\eta\xi$; . This may be connected with a decrease in the size of the air-conducting pores as a result of shrinkage and also with an increase in the moisture gradient in the sector between the retreating evaporation front and the surface of the sample. It should be noted that these conclusions do not coincide with the results obtained earlier in the study of thermal moisture conductivity [3, 10]. There, as is known, the role of moisture transfer in the form of vapor, on the contrary, increased as the moisture content of the peat decreased. These differences are connected, however, only with structural characteristics of the test samples and with the conditions under which the tests were conducted. The tests on thermal moisture conductivity were conducted with heat

and moisture insulated samples of pulverized peat of various moisture contents and, in these tests, the structure of the samples was formed spontaneously during the course of the drying. Therefore, if, for example, in the first case the dry peat was a large-pored powder, then in the drying tests the peat in the dried state would have a fine-pored "stone" structure. The change in the initial structure of the samples, which has a significant influence on the moisture transfer mechanism, can be used to control these processes.

As is apparent from the graphs in Figure 1b and c and from the table, the coefficient of volumetric shrinkage β does not remain constant in highly dispersed samples. For a moisture content W_p which is close to the content W_{pc} of physico-chemical bond water, the rate of shrinkage changes and the values of β increase to 0.6-2.2. The intensification of the shrinkage when $W < W_p$ is connected, in all probability, with the manifestation of the forces of molecular interaction which progress according to the measure of the amount of water removed and of the drawing together of the particles [11]. In this case there is a squeezing out of the air from the pores by the spontaneously deforming sample, which follows from an analysis of the values of coefficient β , which increase toward the end of the drying. This leads in turn to a noticeable increase in the values of the volumetric weight of the samples.

The interaction between the particles ends with the formation of strong condensation and

crystallization structures, after which the shrinkage of the material stops. In dispersed peat the end of the shrinkage was observed when $W = 15-25\%$ less than W_{pc} , which has also been confirmed by the results of other research [12, 13]. Let us note that the system of drying the samples has a vital effect on the course of the structure-forming processes. Thus, for example, in tests with clays (under conditions of $\beta_0 = 1$) the shrinkage ceased upon reaching a moisture content which corresponded to the maximum hygroscopicity [14, 15]. In our tests, when $\beta_0 < 1$ at the beginning of the drying (see Figure 1), the shrinkage of the samples of clays ended at lower values of moisture content. Similar conclusions also follow from works [16] and [17].

It is characteristic that in the case when the drawing together of particles by capillary forces which is required for a manifestation of the forces of molecular interaction is not achieved (as occurred, for example, in roughly dispersed sphagnum peat and kaolin), the breaking points on the shrinkage graphs will be lacking entirely. It should be noted that breaking points for W_β on the shrinkage graphs had not been detected previously. This is explained by the fact that the research was conducted, as a rule, on samples of considerable size. The formation of a crust on the surface of such samples limited the development of shrinkage, and a considerable difference between the moisture content of the surface and of the heart of the sample masked the influence of its hydrous properties and structure.

Let us now examine the sequence of the removal of various categories of moisture (in accordance with the classification of P.A. Rebinder [6, 18]) when drying samples. Figure 2 shows the results of determining the content of different categories of connected water in sedge peat of different moisture contents. The measurements were performed by the radioactive indicator method [2] for peat samples, the moisture content of which was changed by drying within the range of from 710 to 10%. On the graph the values of the moisture content of the peat at which the measurements of the total amount of solvent water in the peat $W_s = W_{\text{internal}} + W_{\text{immobilized}} + W_{\text{physico-chemical}}$ are placed along the horizontal axis.

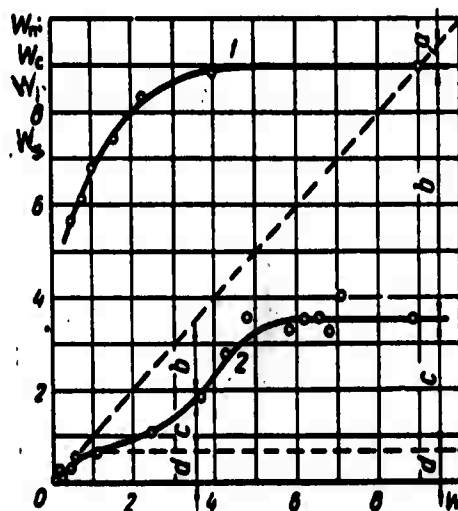


Figure 2. Content of free (a), capillary (b), immobilized plus intracellular (c), and physico-chemically connected (d) water in sedge peat ($R = 30\%$) for different moisture

contents W (g/g).

1 -- values of complete moisture capacity

W_c (%);

2 -- quantity of solvent water W_s (%).

The measured values of W_s and the values of the complete moisture capacity of this peat W_c as taken from works [19] are given along the vertical axis. The horizontal broken line indicates the content of physico-chemically connected water which is constantly in moist peat and which is 70% for the given sample. Using this graph it is possible to follow the change in content of various categories of water in the process of removing water from the peat.

For high moisture content of the peat which is greater than its full moisture capacity $W > W_c$, for example, when $W = 950\%$, the tested peat, as is apparent from the graph, contains free water $W_{free} = 50\%$, capillary water $W_{cap} = 550\%$ [See Note], intracellular and immobilized water $W_{com} = W_{intracell} + W_{immob} = 280\%$, and physico-chemically connected water $W_{pc} = 70\%$. The drying of peat leads at first to a loss of free water and then, when $W < W_c$, to the removal of the weakly connected water of the large pores. The role of the shrinkage of the material is still not noticeable at this stage of drying. The capillary forces are not sufficiently strong in order for the deformation of the framework of the material to occur. This is concirned in particular by works [8] and [16], where it was shown by direct measurements that the forces of capillary contraction and the

shrinkage of the sample do not occur in the initial stage of drying.

[Note]: As is known, the category of capillary water is not determined by the indicator method and therefore does not enter into the measured values of W_e .

In the case of further lowering of the moisture content, when the capillary pressure forces grow, it becomes possible to squeeze out the intracellular and immobilized water. This also is facilitated by the shift of the dispersion and ion equilibrium in the direction of the compact coagulation which occurs with a lowering of the moisture content of the system. In this case the intracellular and immobilized water become capillary water and are evaporated during the drying. The same water removal process as a result of a decrease in the combined water content for unchanged values of the capillary water content is observed during the mechanical pressing of water out of the peat [5, 7]. When the water content of sedge peat is lowered to approximately 400%, there is also a noticeable decrease in its absorptive ability [19] and complete moisture capacity (see Figure 2) which can be explained in part by the irreversible changes which occur during the dehydration of gels and plant residue.

Figure 3 shows the results of one of the tests of drying samples with the radioactive marking of only the intracellular water; these results confirm our position. A fraction of 0.25-1.0 mm of lowland sedge peat which had been washed on sieves and which

consisted of mainly plant residue was placed in a flask and covered with a concentrated solution of a radioactive indicator (Na_2SO_4 with S^{35}). After three days the batch was washed on a filter with a 4% solution of non-radioactive Na_2SO_4 until the indicator was completely gone from the free water. Little balls were formed from the sample which had thus been prepared and their drying was observed. As a result of such preparation the samples were marked with only intracellular water into which only a small quantity of radioactive marking was diffused during the three days. Because the capillary water of the peat contained the non-active salt in higher concentration, the reverse diffusion of the indicator from the intracellular water into the free water was artificially hampered. As can be seen from Figure 3, The radioactive marking appeared on the surface of the sample with a large delay, only after more than half of the water which had been contained in the peat was separated from it. Because this sample contained basically only capillary and intracellular water, the results of the test clearly indicate that at first pure water which filled the large capillary passages was removed and only later was the marked intracellular water removed.

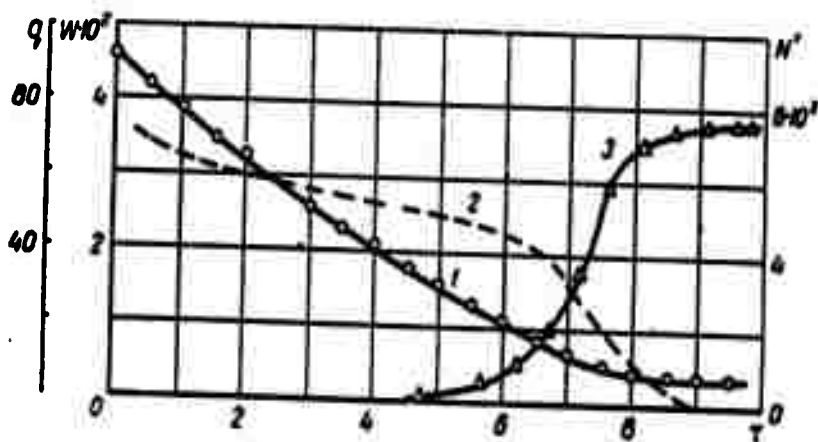


Figure 3. Results of observations of the drying of a roughly dispersed fraction of sedge peat with radioactive marking of the intracellular water.

- 1 -- moisture content of the sample W (g/g);
- 2 -- speed of drying q ; 3 -- specific activity of the surface of the sample N' (impulses/min⁻¹).

After the removal of the weakly connected intracellular and immobilized water, the dehydration of the microcapillaries begins. As can be seen from Figure 2, when the moisture content is close to 200-250%, practically no weakly connected water remains in the peat being tested. The beginning of the removal of water with higher connecting energy, which corresponds to the first critical moisture content, leads to a change in the drying speed. As can be

seen from Figure 1, for this moisture content there is also a change in the mechanism for transferring moisture; the transfer of moisture primarily in the form of vapor gives way to liquid transfer which occurs along a system of micropores. The β , coefficients in this increase, which is evidence that air is being squeezed out of the pores as a result of shrinkage and of the elimination of the internal evaporation front. The capillary contraction forces, as was shown in [8], reach a maximum value for W_{k1} .

The removal of microcapillary water ends when the moisture content of the peat is close to the content of W_{pc} . At this moisture content the drying mechanism again changes. The removal of the physico-chemically connected water begins, as evidenced by the fact that in all cases there was a coincidence of the second critical point on the drying curves, W_{k2} with $W_N = 100 = W_{pc}$ (see table). The removal of the most strongly connected water is accompanied by irreversible changes (hydrophobization) of the colloid fraction of peat [20]. The agreement of the second critical point with the W_{pc} content has been shown in a series of works for other dispersed materials [6, 21, 22].

The results of the research indicate that in accordance with the views of P.A. Rebinder [18] the removal of different categories of water during drying occurs in a strictly set sequence depending on the energy of its connection with the solid phase. The data which we have obtained confirms the results of the research of M.F. Kazanskiy [23] and L.A. Lepilkina and F.M. Polonskaya [24] which were obtained

by other methods of analysis. The specifics of the hydrous properties and structure of the samples of peat under study which contain intracellular and immobilized water leads, as was shown above, to some differences in the nature of the transfer of moisture and shrinkage which have been studied in the work.

It should be noted that the conclusions which we have made on the mechanism of moisture transfer apply only to the case of isothermal drying under the established conditions of the test regime. They cannot however be applied to other methods and systems of drying. However, such investigations can be conducted in each particular case with the help of methods of research which have been developed. The employment of these methods makes it possible to analyze phenomena which take place in the drying of materials which can be used in developing optimum systems for technological processes.

Symbols

q -- speed of drying; γ -- volumetric weight; β_0 -- coefficient; ϵ -- integral criterion of phase transformation; P_d -- content of dry matter in the test samples; q_0 -- speed of drying (in a period of constant speed); W_{k1} , W_{k2} -- moisture content corresponding to the first and second critical points on graphs of the speed of drying; W_β -- moisture content at which a change in the coefficient of volumetric shrinkage was observed; $W_{N=100}$ -- moisture content corresponding to the end of the removal of the radioactive indicator to the surface of the

sample; β_1, β_2 -- coefficients of volumetric shrinkage in the initial period and at the end of the drying; M_0, M -- quantity of moisture transferred to the surface of a sample by the liquid mechanism during a period of constant drying and during the entire period of drying, expressed as a percentage of the total quantity (solvent indicator) of water; $W_{\text{intracell}}$, W_{immob} -- accordingly, the content of intracellular and immobilized water.

Summary

The mechanism of moisture transfer and the process of structure formation in the drying of colloidal capillary-porous bodies of various dispersities (peat, clay) are studied using previously developed methods.

In the drying process the liquid mechanism becomes more important at the first critical point on the plot of the drying rate. The second critical point corresponds to the beginning of the removal of the physico-chemical bond water. A change in the shrinkage rate in highly dispersed samples is observed at low values of moisture content. This phenomenon results from the action of molecular forces. It is shown that the sequence of removal of various kinds of moisture from the material being dried depends on the bond energy of the solid phase.

BIBLIOGRAPHY

1. Churayev, N.V., Inzhenerno-fizicheskiy zhurnal (Engineering-Physics Journal), No 12, 1962.
2. Collection: Novyye fizicheskiye metody

Issledovaniya torfa (New Physical Methods of Investigating Peat), under the editorship of M.P. Volarovich and N.V. Churayev, State Publishing House for Power Literature, 1960.

3. Churayev, N.V., Kolloidnyy zhurnal (Colloid Journal), Vol 22, No 5, 1960.

4. Volarovich, M.P., and Churayev, N.V., Kolloidnyy zhurnal (Colloid Journal), Vol 21, No 2, 1959.

5. Volarovich, M.P., and Churayev, N.V., Issledovaniye torfa pri pomoshchi radioaktivnykh izotopov (Investigation of Peat with the Help of Radioactive Isotopes), Publishing House of the Academy of Sciences of the USSR, 1960.

6. Lykov, A.V., Teplo- i massoperenos v protsessakh sushki (Heat and Mass Transfer in Drying Processes), State Publishing House for Power Literature, 1956.

7. Volarovich, M.P., Gamayunov, N.I., Starikova, Z.A., and Churayev, N.V., Kolloidnyy zhurnal (Colloid Journal), Vol 21, No 3, 1959.

8. Ostrikov, M.S., et al., Kolloidnyy zhurnal (Colloid Journal), Vol 22, No 4, Vol 23, No 1, 1961.

9. Kurchunov, S.S., Torfyanaya promyshlennost' (The Peat Industry), No 8, 1946.

10. Volarovich, M.P., Gamayunov, N.I., and Churayev, N.V., Kolloidnyy zhurnal (Colloid Journal), Vol 22, No 5, 1960.

11. Nerpin, S.V., and Deryagin, B.V., Collection: Issledovaniya v oblasti poverkhnostnykh sil (Research in the Field of Surface Forces), Publishing House

of the Academy of Sciences of the USSR, 1961, page 156.

12. Kurdyumov, S.V., Trudy ukrainskogo instituta inzhenerov vodnogo khozyastva (Works of the Ukrainian Institute of Marine Engineers), Kiev, 1960, page 77.

13. Ivanov, Ye.Ya., Doctoral dissertation. Joint Council of the Department of Engineering Sciences of the Academy of Sciences of the Belorussian SSR, Minsk, 1961.

14. Myaglichenko, A.F., Inzhenerno-fizicheskiy zhurnal (Engineering-Physics Journal), No 2, 1960.

15. Kazanskiy, M.F., and Verezomskaya, A.L., IFZh (Engineering-Physics Journal), No 10, 1961.

16. Marachevskiy, I.I., et al., IFZh (Engineering-Physics Journal), No 8, 1960.

17. Kazanskiy, M.F., Kulandina, A.N., and Lutsik, P.P., IFZh (Engineering-Physics Journal), No 2, 1960.

18. Rebinder, P.A., Vsesoyuznoye nauchno-tekhnicheskoye soveshchaniye po intensivatsii protsessov i uluchsheniyu kachestva materialov pri sushke (All-Union Scientific Technical Conference on the Intensification of Processes and the Improvement of the Quality of Materials in Drying) (Plenary Session), Publishing House of Trade Unions, 1958.

19. Grebenshchikova, A.A., Pochvovedeniye (Soil Management), No 9, 1956, Torfyanaya promyshlennost' (Peat Industry), No 6, 1958.

20. Apushkin, K.K., Torfyanay promyshlennost' (Peat Industry), No 2, 1946.

21. Dushchenko, V.P., Pochvovedeniye
(Soil Management), No 5, 1958.

22. Kazanskiy, M.F., IFZh (Engineering-Physics
Journal), No 6, 1958.

23. Kazanskiy, M.F., Kolloidnyy zhurnal
(Colloid Journal), Vol 21, No 5, 1959; Doklady
Akademii nauk SSSR (Reports of the Academy of Sciences
of the USSR), Vol 130, No 5, 1960.

24. Lepilkina, L.A., and Polonskaya, F.M.,
IFZh (Journal of Engineering Physics), No. 10, 1958;
No 11, 1958.

**THE INFLUENCE OF THE MINERALOGICAL COMPOSITION OF
ARGILLACEOUS SOILS ON THEIR PROPERTIES**

**N.Ya. Kharkhuta and Yu.M. Vasil'yev
Branch of the All-Union Scientific Re-
search Institute for Roads and Highways,
Leningrad**

Experimental data is cited which indicates the influence of the mineralogical composition of argillaceous fractions of soils on their physico-mechanical properties and stability under the action of water and frost.

The influence of the mineralogical composition of argillaceous soils on their structural properties has been revealed through appropriate tests of soil mixtures which had been selected so as to have a predominance of minerals of different groups in their argillaceous fraction. Soil mixtures were prepared from pulverized soil, sand, and different clays. Concrete clay (ascanite from a deposit near Makharadze) served as a component for obtaining soil mixtures of which the argillaceous fraction consisted mainly of montmorillonite. Cambrian clay (Leningrad) was used to obtain soil mixtures in which minerals of the hydrated mica group predominated in the argillaceous fraction; kaolinite soil mixtures were prepared from clays of the Glukhovskoye and Latnenskoye deposits.

The components were selected in such a way so as to obtain soil mixtures which in one case would have the same granulometric composition of the mixtures and in the other case would have the same specific surface. In preparing mixtures of the same granulo-

metric composition, the argillaceous part was selected according to the total content of particles smaller than 0.002 mm.

If we consider that in the case of the predominance of minerals of the montmorillonite group the argillaceous fraction consists mainly of particles of considerably smaller sizes than in other soils, then the selected mixtures can only arbitrarily be indicated as having a certain granulometric composition. Nevertheless, in evaluating soils for engineering-construction purposes where there is also not a division of the argillaceous fraction, all these mixtures will be considered as being soils which have the same granulometric composition.

The specific surface was found by calculating the moisture equivalent for the flattening [raskatyvaniye] limit so that according to the measurements of Deryagin and Karasev [1], the thickness of the film of the bond water would be 0.15-0.20 microns. In this, according to Grim [2], the assumption was made that the thickness of the film of bond water was independent of the mineralogical composition of the soil. The determination of the specific surface was also performed using the measurements of Avgustinik and Dzhansis [3].

For each of the soils which were prepared in this way, the fluidity [tekuchest'] point, plasticity point, and ultimate strength were determined. An evaluation of the degree of compaction was performed based on the results of the "standard compacting" which has found wide employment in road, airfield, and

other types of construction. In this the optimum moisture content ω , and the maximum standard density δ_{\max} were determined. The soils were also tested for creep [polzuchest'], which made it possible to compare their degree of resistance to external loads and to learn the nature of the deformation change with respect to time. The tests for strength and creep were conducted during the deformation of soil by a round stamp. The form with the soil had a diameter of 100 mm and was 127 mm high; with a diameter for the stamp of 30 mm this minimized the effect of the bottom and sides of the form. Execution was accomplished with a lever press with a water load. In the test for creep the stamp was loaded through the lever press with an instantaneous unstressed load which was maintained over the course of 30 minutes. The size of the load was selected so that the stress on the surface of the soil would be one half the ultimate strength of the soil. By an ultimate strength σ_p we mean a stress on the surface at the point of contact of the stamp and the soil at which it begins to break down. The ultimate strengths are determined according to the curves of the relationship of reversible deformation to the stress for soils with optimum moisture content which are compacted to the maximum standard density [4]. The soils were also tested for creep under the same conditions.

A determination was also made of the effect of the mineralogical composition of the soils on the frequencies corresponding to their maximum tixotropic lowering of strength [this work was conducted with the

participation of V.M. Iyevlev, M.I. Kapustin, and Yu.N. Starodumov/. For this purpose an "Askaniya" vibration stand was used which made it possible to obtain different vibration regimes with frequencies of up to 600 cycles. Here the soils were placed in a cylindrical form which was 100 mm in diameter and 127 mm high and which was securely attached to the vibration table of the stand. From the surface the pressure was conducted through a stamp 98 mm in diameter by the pull of rubber lines so as to obtain a stress of $0.2 \cdot 10^5 \text{ n} \cdot \text{m}^{-2}$. The vibration regime was selected so that the acceleration which was developing during the oscillating movements was in all cases equal to 8 g. At the same time separate identical samples of soil were subjected to vibrations of various frequencies which made it possible to find such values for them which met the maximum tixotropic lowering of the strength of the soils. The latter were established from a volumetric weight of soil which was obtained in a set time and which at these frequencies reached a maximum value and also visually from the abundant formation of moisture and from the rapid and considerable deformation.

In order to obtain a more complete description of the effect of the mineralogical composition on the construction properties of soils it was necessary to compare their tendency toward swelling and frost heave. The soil samples were prepared in ring forms with an internal diameter of 102 mm and a height of 82 mm [5]. The sides of the forms consisted of separate rings which provided for free increase of the soil volume during

swelling and frost heave. The lower part of the forms consisted of a water chamber connected with pipes which provided for continuous feeding of water which could come either without pressure or with some small pressure which in these cases was taken as being equal to the height of the sample.

In testing for swelling, soils with a moisture content of $0.8 \omega_p$ (ω_p is the flattening limit) were formed to densities at which the volume of the pores containing air was 5% of the total volume of the samples. The water saturation was conducted under pressure. The freezing of the samples was conducted in a cooling chamber at a temperature of -5°C which was automatically maintained with an accuracy of $\pm 1^{\circ}$. The forms which were placed in the cooling chamber were insulated with slag cotton so as to provide for freezing the soil only from above. This freezing proceeded at a speed of 1.5-2 cm/day. Water was supplied to the lower parts of the samples without pressure.

All tests were repeated no less than five times. Departures from the average did not exceed 10-15%; therefore, the accuracy of the determinations can be considered as being satisfactory.

The results of the work are presented in the table below; the graph in Figure 1 gives the relationship of the flattening level to the content of argillaceous particles of different mineralogical composition in the soil mixtures. The creep curves are given in Figure 2. No noticeable effect of the mineralogical composition on the frequencies of maximum tixotropic lowering of strength was detected. Under these con-

ditions they were in the range from 150 to 200 cycles.

Table
Results of testing soil mixtures of different mineralogical composition

Грунты (1)	Содержание в % фракций различных размеров (мм) (2)						Предел текучести, % (4)			Число пластичности (6)	Результаты стандартного уплотнения (7)		Набухание, % (10)	Морозное пучение, % (11)	Предел прочности, 10 ⁻³ (к.м-г) (12)	
	0.5-0.25	0.25-0.10	0.10-0.05	0.05-0.01	0.01-0.002	менее 0.002 (3)	Граница раскатывания (5)	максимальная плотность, г/см ³ (8)	оптимальная влажность, % (9)		Морозное пучение, % (11)					
											27	17				10
I. Однородного гранулометрического состава (3)																
гидрослюдистый (4)	—	6	12	14	45	23	27	17	10	1,77	17,9	5,9	2,05-6			
монтмориллонитовый (5)	1	3	15	13	45	23	52	26	26	1,53	26,0	16,6	5,94-5			
каолинистый (на латненской глине) (6)	1	8	10	14	44	23	28	18	10	1,72	18,2	6,0	20,45-6			
каолинистый (на глуховской глине) (7)		4	14	11	48	23	27	17	10	1,71	18,4	5,7	19,85-6			
II. С одинаковой удельной поверхностью (8)																
гидрослюдистый (4)	—	1	13	14	49	23	28	18	10	1,77	17,2	6,4	1,95-6			
монтмориллонитовый (5)	1	2	17	14	52	14	42	22	20	1,55	26,0	12,9	5,44-5			
каолинистый (на латненской глине) (6)	1	2	12	14	49	22	30	18	12	1,70	18,3	6,4	15,05-6			
каолинистый (на глуховской глине) (7)	—	1	14	11	49	25	28	18	10	1,69	19,0	6,7	15,45-6			

Keys:

- | | |
|--|------------------------|
| 1. Soils | 4. Fluidity limit, % |
| 2. Content in % of fractions of different sizes (mm) | 5. Flattening limit, % |
| 3. Less than 0.002 | |

- | | |
|--|--|
| 6. Plasticity number | 7. Results of standard compaction |
| 8. Maximum density, grams/cm ³ | 9. Optimum moisture content, % |
| 10. Swelling | 11. Frost heave, % |
| 12. Ultimate strength, 10 ⁻⁵ (n·m ⁻²) | 13. The same granulometric composition |
| 14. Hydrated mica | 15. Montmorillonite |
| 16. Kaolinite (Latnenskaya clay) | 17. Kaolinite (Glukhovskaya clay) |
| 18. Same specific surface | |

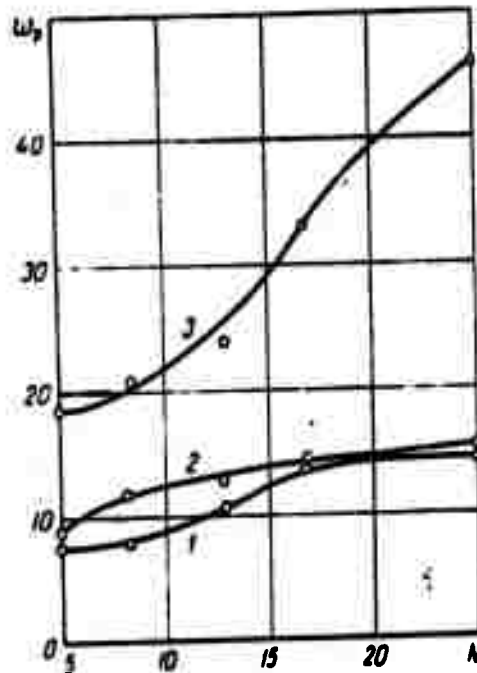


Figure 1. Relationship of the flattening limit ω_p (%) to the quantity of argillaceous particles N (%).

- 1 -- Kaolinite soils; 2 -- hydrated mica soils;
3 -- montmorillonite soils.

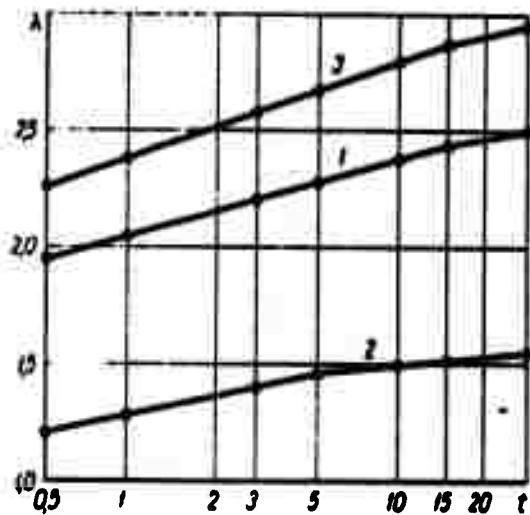


Figure 2. Relationship of the deformation in the process of creep λ (mm) to the time t (min).

1, 2, and 3 -- See Figure 1.

From the table it is apparent that the fluidity and flattening limits of hydrated mica and kaolinite soils are close to each other, but for montmorillonite soil they are considerably higher, especially when soils are compared which have the same granulometric composition but not the same specific surface. The somewhat specific position of the montmorillonite soil can be explained by the mobility of its crystalline latticework which leads to an increase in the specific

surface and consequently in the content of bond water. Therefore the maximum standard density of this soil was considerably lower and the optimum moisture content higher than in hydrated mica and kaolinite soils where these parameters were close to each other. A large amount of mechanical work was always expended in order to remove the water; therefore, in order to obtain the same density, montmorillonite soils require the expenditure of considerably more mechanical work than is the case with hydrated mica and kaolinite soils.

The ultimate strengths of the hydrated mica and kaolinite soils were the same but were 15-20% lower for the montmorillonite soils. This difference can be considered insignificant and can be ascribed to the lower absolute density of the montmorillonite soil.

From Figure 2 it is apparent that the development of deformation in the process of creep in all three soils is qualitatively the same; in semilogarithmic coordinates this process can be reflected by a straight line. At the same time it should be noted that for the same relative state of the soils and the same relative load the deformation of hydrated mica soils is considerably less. The montmorillonite soils were the most pliable with respect to an incident load. The kaolinite soils occupy an intermediate position; however, in their deformative properties they are closer to the montmorillonite soils than to the hydrated mica soils. The data which has been obtained makes it possible to conclude that the influence of the mineralogical composition of the argillaceous fraction of soils on the nature of deformation, its magnitude,

and also on the ultimate strength and compactness is limited to a change in the quantitative indices and therefore can always be taken into account through simple tests. Such tests include those for standard compaction and determination of the deformation module and ultimate strengths of soils.

It is apparent from the table that if the swelling of hydrated mica and kaolinite soils is practically the same, the swelling of montmorillonite soils is much higher; this can be ascribed completely to the properties of the mobile crystalline latticework of these minerals. Apparently the tests for swelling can serve as an indirect method of detecting minerals of the montmorillonite group in soils.

The mineralogical composition of the argillaceous fraction has a significant effect on the extent of frost heave, as has already been noted earlier [6, 7]. The kaolinite soils have low frost resistance. The frost heave of these soils was three times as great as for montmorillonite soils and 8-10 times as great as for hydrated mica soils. The hydrated mica soils have the greatest frost resistance; the montmorillonite soils occupy an intermediate position but are closer to the hydrated mica soils.

The great tendency of kaolinite soils toward frost heave in a number of cases makes them unacceptable for use in building foundations under such engineering installations as road and airfield surfaces, the upper portion of a railroad bed, etc. Even the presence of relatively small amounts of minerals of the kaolinite group in the argillaceous fraction of soils

can lower their resistance to frost actions, as is apparent from the test data shown in Figure 3 [4]. From the table and Figure 3, for example, it is apparent that if the argillaceous fraction of cohesive soil consists of 20-25% kaolinite, its frost heave will be 1½-2 times higher than when the soil fraction consists only of minerals of the hydrated mica group.

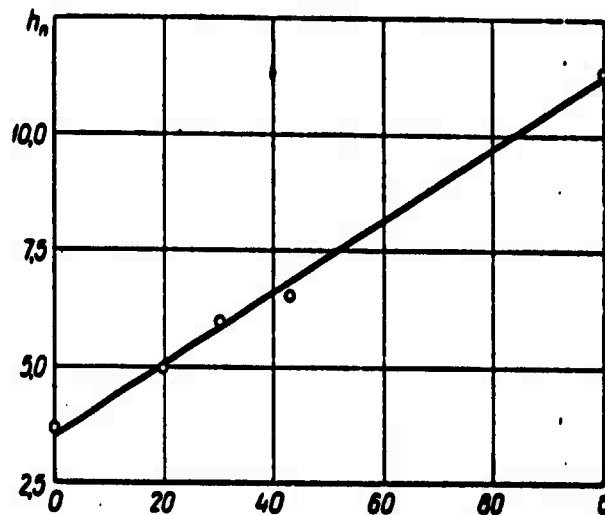


Figure 3. Relationship of frost heave h_n (%) of polymineral soil to the content of minerals of the kaolinite group in its argillaceous fraction c (%).

Thus the influence of the mineralogical content of soils on their water and frost resistance is very considerable and absolutely must be taken into account.

Summary

Experimental data is presented which shows the effect of the mineral composition of the argillaceous fraction of soils on their mechanical properties.

It is concluded that this effect on the ultimate strength of the soil, on its compositions, as well as on the change mechanism and on deformation may be found easily by simple tests. The effect of the mineral composition is considerable with respect to the action of water or frost. Montmorillonite soils show the maximum swelling while kaolinites display the maximum frost heave.

BIBLIOGRAPHY

1. Deryagin, B.V., and Karasev, V.V., Doklady Akademii nauk SSSR (Reports of the Academy of Sciences of the USSR), Vol 101, No 2, 1955.
2. Grim, R.Ye., Mineralogiya glin (Mineralogy of Clays), Institute of Linguistics, 1956.
3. Avgustinik, A.I., and Dzhansis, V.D., Zhurnal prikladnoy khimii (Journal of Applied Chemistry), Vol 24, No 4, 1951.
4. Kharkhuta, N.Ya., Vasil'yev, Yu.M., and Orkhimenko, R.K., Uplotneniye gruntov dorozhnykh nasypey (Compaction of the Soils of Road Fills), State Publishing House for Auto Transport Literature, 1958.
5. Kharkhuta, N.Ya., and Vasil'yev, Yu.M., Inzhenerno-fizicheskiy zhurnal (Journal of Engineering Physics), No 9, 1960.
6. Ducker, A., Strasse und Autobahn, No 3, 1956.
7. Kharkhuta, N.Ya., and Vasil'yev, Yu.M., Deformatsiya gruntov dorozhnykh nasypey (Deformation of the Soils of Road Fills), State Publishing House for Auto Transport Literature, 1957.

**THE BREAKDOWN OF HEATED METALS AND ALLOYS
IN AN AIR STREAM AT SUPERSONIC VELOCITIES**

L.Ya. Nesgovorov and V.I. Prosvirin,
Institute of Engineers of the Civil
Air Fleet USSR, Riga

The high temperature oxidation of metals and alloys in an air stream at high speeds which is accompanied by the corrosive-erosive breakdown and combustion of the material of a sample is investigated. The relationship of the average speed of the corrosive-erosive breakdown of metals and alloys to a series of active factors is established.

The high temperature oxidation of metals and alloys in a gaseous stream has been studied by a number of researchers [4-7] and has been conducted in heated furnaces through which various gas mixtures have been circulated at speeds not in excess of $10 \text{ m}\cdot\text{sec}^{-1}$.

In order to conduct such research in an air stream at high velocities a special unit was designed which consisted of a cylinder-type aerodynamic tube and a heating device (Figure 1). The methods for conducting the experiment were also worked out.

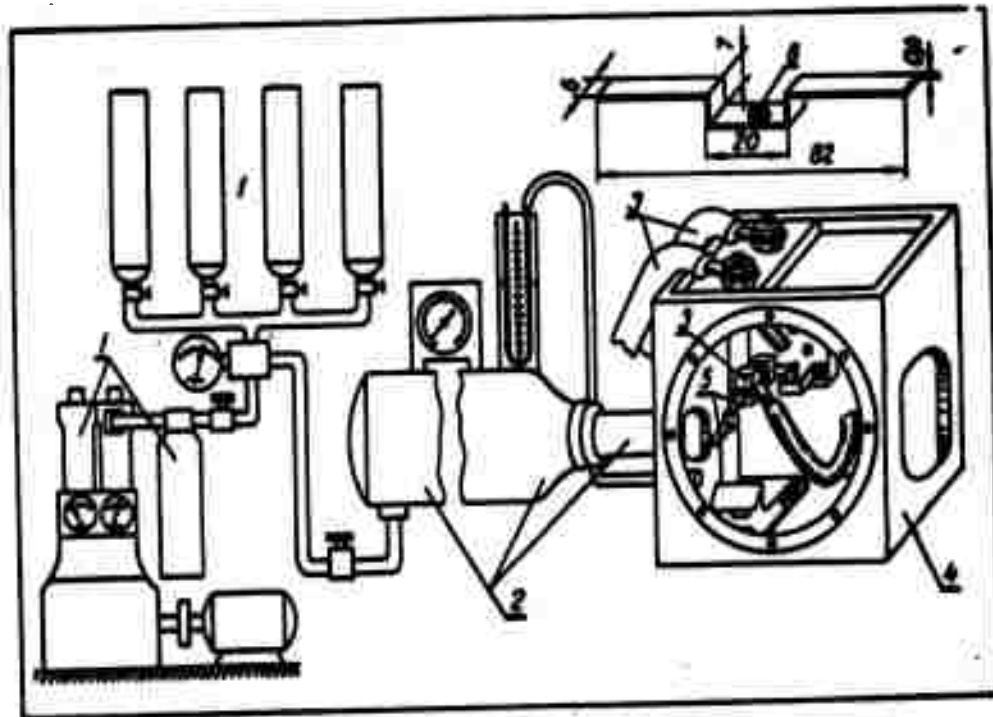


Figure 1. General diagram of the unit.

- 1 -- compressor part with operating cylinder;
 2 -- forechamber with operating nozzle; 3 --
 elements of the electroheating system; 4 -- oper-
 ating part of the aerodynamic tube; 5 -- sample;
 6 -- computer element.

Air was forced into the operating cylinders under a pressure of $5.9 \cdot 10^6 \text{ n} \cdot \text{m}^{-2}$ with the help of a four step compressor which had devices for cooling the air between the steps and at the exhaust. In the operating cylinders the compressed air was cooled to

the temperature of the surrounding atmosphere which was taken as 288°K . The condensed moisture was removed from the compressed air when it passed through the water-separating columns of the compressor and with the help of the drain taps of the operating cylinders. Thus the main mass of the moisture was removed from the air in the operating cylinders and on the way to them.

During the outflow of the compressed air from the cylinders into the forechamber its temperature is lowered, which causes a lowering of the deceleration temperature. Thus, for example, in the investigation when the flow speed changed from $M = 1.3$ to $M = 3.0$, the deceleration temperature was determined according to the temperature in the forechamber which was measured during the course of the experiment. Inasmuch as the departure of the deceleration temperature from the temperature of the surrounding atmosphere was insignificant and the moisture content from this was increased very little, the air in the pipe was sufficiently dry. The approximate value of the absolute moisture content was $9.81 \cdot 10^{-3} \text{ n} \cdot \text{m}^{-3}$.

The test sample which had a special form (Figure 1) was heated by the passage of an electric current. The measurement of the temperature of the sample was conducted by an optic method with an accuracy of $\pm 10^{\circ}$ in the range of temperatures under investigation ($1073\text{-}1273^{\circ}\text{K}$). The speed of the air movement was $0 \leq M \leq 3$. The time of action of the air flow was changed from 10 to 120 seconds. The angle of incline of the sample with respect to the direction of the wind

flow speed (angle of attack of the substance) was equal to $0 - \pi/3$ radians.

The order of conduct of the experiment was as follows. Before the start of the experiment the control-regulating apparatus was set in the position for the operating regime: $T = \text{const}$, $M = \text{const}$, $\tau = \text{const}$, $\alpha_{\text{at}} = \text{const}$.

An operating nozzle which was set for a certain M number was readied; the desired angle of attack of the sample was set. After setting the desired temperature in the optical pyrometer and the desired exposure on the time relay a signal was given at which there was a simultaneous change of the sample temperature and flow speed (M number) to the operating levels, which required 2 to 3 seconds. When the sample and pyrometer temperatures were equal, the "beginning of exposure" signal was given and the time relay was activated simultaneously. In the process of exposure special care was given to maintaining the constancy of the air flow speed and the sample temperature (fine regulation of the temperature was accomplished through the use of a ballast rheostat). Each new regime was operated with several control samples in order to establish an ampere-speed relationship (determination of the current strength required to maintain the equilibrium temperature of the sample for a certain air flow speed). This provided for rapid heating of the sample to the assigned temperature. The air flow speed was determined by measuring the difference between the full pressure in the forechamber and the static pressure in the operating cross section

(the cross section in which the sample was located). The test samples were prepared from calibrated sheet material. The test material was Armco iron and complex alloys with iron and nickel bases.

The determination of the total loss of weight of the sample was made by removing the scale which remained on it with a special reagent. The scale from the samples of Armco iron was removed with a reagent of the following composition: 10% H_2SO_4 + 1% formalin + H_2O ; treating time -- 2.5 minutes; reagent temperature -- 308 to 313°K. In order to determine the corrosive action of the reagent with respect to the pure metal (the determination of the protective action of the inhibitor -- formalin), 50 non-oxidized samples were treated in the given reagent for 15 minutes. The average loss of weight of the samples after treatment was $4.905 \cdot 10^{-6}$ g, i.e., within the limits of accuracy of analytical scales.

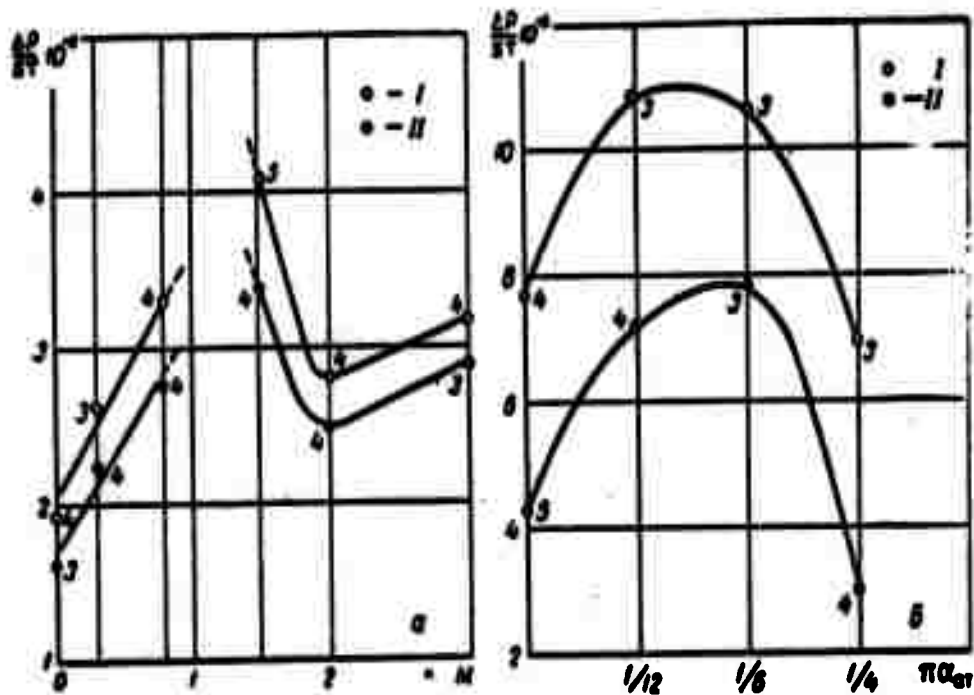
The removal of the oxide film from the sample alloys was performed with a reagent of the following composition: 20% HCl + 5% HNO_3 + 5% H_3PO_4 + H_2O . The temperature of the reagent for the iron alloy was 333°K; for the nickel alloys it was 353°K; the treatment time was 3 minutes. In order to determine the loss of weight of the non-oxidized sample due to the etching action of the reagent 50 samples of each alloy were treated at the indicated temperatures with a 15 minute exposure. The loss of weight was 1.5% for the first alloy and 2% for two other alloys. The calculation of the corrosive-erosive breakdown applied not to the whole sample but to an element of it con-

sisting of a disc 5 mm in diameter which had been cut with a calibrated punch from the center part of the sample after it had been subjected to a blowing action (Figure 1). The initial weight of such a disc (equal, for example, to $915 \cdot 10^{-6}$ n for the first alloy) was determined by a statistical method.

For this, 100 discs were cut from those places on a calibrated sheet which occupied a similar position to that of the cutting of discs following the blowing of the sample. Then the weight of the cut discs was measured and a frequency curve was constructed from data. In this it turned out that the weight of 90% of the discs from the first alloy was in the range from $910 \cdot 10^{-6}$ to $918 \cdot 10^{-6}$ n and only 10% had an average deviation of a magnitude of $\pm 8 \cdot 10^{-6}$ n from the average statistical weight. Thus the initial weight of a disc was taken as being the average number from 90 measurements of different discs.

A quantitative indicator of the breakdown process was the loss of weight (ΔP) which occurred in the formation of the scale. The total result of the decomposition of the sample during the operating regime was determined from the average value of 3 to 8 experimental points.

In studying the heat resistance of Armco iron in an air stream at high velocities the following factors were investigated: air stream speed, sample temperature, time of exposure, and angle of attack of the sample. The results of some basic tests are shown in Figure 2.



a

b

Figure 2. The corrosive-erosive breakdown of Armco iron in an air stream.

a -- relationship of the average speed of breakdown $\frac{\Delta P}{\sigma \tau}$ ($\text{n} \cdot \text{m}^{-2} \cdot \text{sec}^{-1}$) to the speed of the oncoming air stream (to the M number),

$T = 1073^\circ\text{K}$; $\alpha_{\text{at}} = 0$ radians; I, II -- $\tau = 10$;

30 sec; b -- relationship of the average speed

of breakdown $\frac{\Delta P}{\sigma \tau}$ ($\text{n} \cdot \text{m}^{-2} \cdot \text{sec}^{-1}$) to the angle of attack of the sample α_{at} (radians),

$M = 1.5$; $\tau = 10$ sec; I, II -- $T = 1173^\circ\text{K}$;

1073°K; 3, 4, 5 -- number of averaged experimental points.

In order to explain the influence of the air stream speed on the speed of breakdown of iron the following characteristics were taken: current density (or average gravimetric expenditure per unit of area of the pipe) and the average flow of kinetic energy per unit of area of the pipe; these were determined by the appropriate means [9].

The action of an air stream on heated metals and alloys is manifested in the corrosive-erosive breakdown of their surface layer. The extent of the corrosive (physico-chemical) action of a gas stream on a sample is characterized by the speed of scale formation which depends [10] on the speed of bringing atoms from the media which border on the scale (from the gas or metal) to the dividing surfaces between these media and the scale and on the speed of diffusion through the scale.

The speed of bringing oxygen atoms depends on the speed of movement of the gaseous medium (air) over the metal being oxidized. In an aerodynamic tube the parameter which describes the number of air particles (and consequently the number of atoms of oxygen) and their speed of movement is the gravimetric expenditure of air per unit of area of the cross section of the tube.

The erosive (mechanical) action of the air flow on the sample occurs under the action of the tangential stresses from the friction forces in the border layer, the action of which can be evaluated approximately from the change in kinetic energy of the air flow.

In a subsonic flow regime the influence of the air flow speed (M number) on the corrosive-erosive breakdown of Armco iron can be explained with the help of curves (Figure 3). From Figure 2a it is evident that in the interval from $M = 0$ to $M = 8$ the speed of the corrosive-erosive breakdown increases, which corresponds to the increase of I_w and E_{kin} in this interval

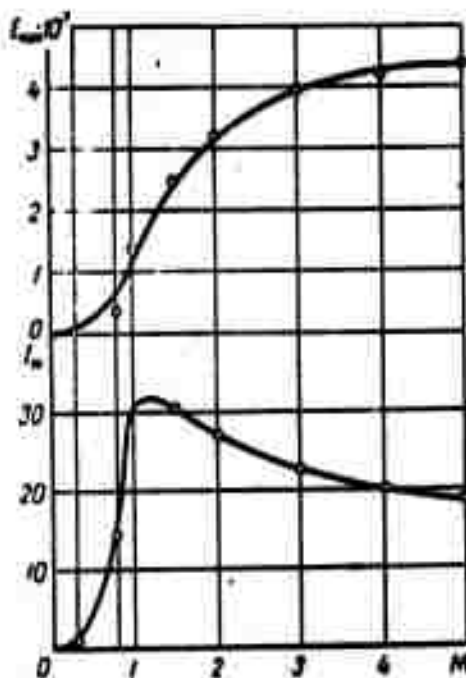


Figure 3. Relationship of the average flow of kinetic energy through a unit of area of a pipe E_{kin} (joules·sec⁻¹·m⁻²) and the average density of the current I_w (kg·sec⁻¹·m⁻²) to the speed of the air stream (M number).

The transition from subsonic to supersonic speeds has not been investigated due to the absence

of a stationary flow regime, the presence of a sharp increase in aerodynamic loads and vibrations which introduce distortions into the experiment, and the impossibility of exact measurement of the values of the parameters of the air flow.

At supersonic speeds ($M > 1$) the nature of the flow changes due to the appearance of a compression jump in front of the sample.

In order to explain the effect of the flow speed on the speed of corrosive-erosive breakdown it is necessary in this case to consider the change in the parameters of the air flow at the compression jump. In the supersonic regime of the flow up to the number $M \approx 1.8-2.0$ (Figure 2a) there is a lowering of the average speed of the corrosive-erosive breakdown which corresponds to the lowering of the gravimetric expenditure when $M > 1$ (Figure 3) and to the lowering of the kinetic energy behind the jump. Despite the increase in the total supply of kinetic energy in the range of M 's under study, the portion of kinetic energy acting on the sample decreases because part of the kinetic energy is lost in the compression jump. At a considerable increase in the speed of the flow ($M > 2$), the portion of kinetic energy acting on the sample will increase, which will cause a small increase in the speed of the corrosive-erosive breakdown of the Armco iron.

An increase in the exposure time from 10 to 30 seconds (Figure 2a) caused a lowering of the average speed of breakdown throughout the entire range of M numbers which were being investigated.

This indicates that the scale on the Armco iron under the conditions of the experiment possesses protective properties and that as a whole the process of the breakdown of the Armco iron at the selected temperatures has a corrosive character.

The results of the investigation of the influence of the angle of attack on the corrosive-erosive breakdown showed that the air stream has the maximum destructive action on a sample of Armco iron of an angle of attack of approximately $\pi/6$ radians both for subsonic (the experimental data is not given here) and supersonic velocities of the air stream (Figure 2b). Similar results were obtained in dusty gas streams [11, 12] at high subsonic speeds. Such investigations of an air stream are unknown. The maximum breakdown of the sample at an angle of attack of $\pi/6$ radians can be explained with the help of Newton's impact theory (considering the viscosity of the medium).

The maximum speed of the corrosive-erosive breakdown at an angle of attack of $\pi/6$ radians should be connected with the fuller utilization of the kinetic energy of the molecules of air upon impact with the surface of the sample. This condition is met for a certain ratio of normal and tangential components (with respect to the surface of the sample) of the quantity of movement of air molecules.

The initial investigation of the influence of temperature on the heat resistance of the first alloy was conducted in an immobile gas medium (Figure 4a).

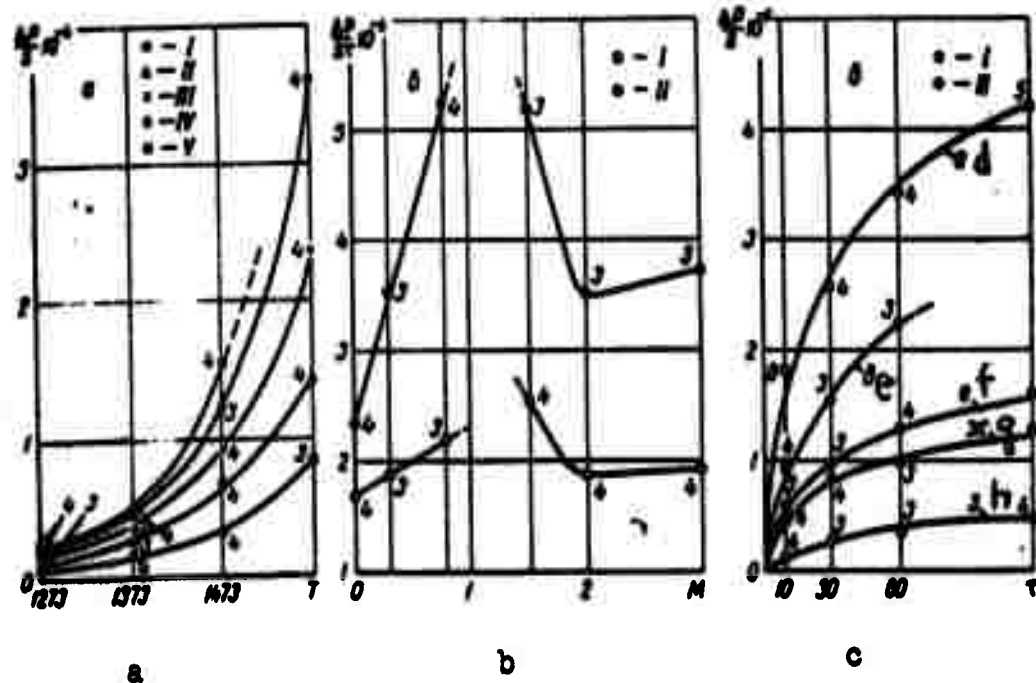


Figure 4. The kinetics of the corrosive-erosive breakdown of alloys with iron and nickel bases.

a -- relationship of the loss of weight of the samples of the first alloy $\frac{\Delta P}{\tau}$ (n/m^2) to the temperature of the sample T ($^{\circ}K$), $M = 0$;

$\alpha_{at} = 0$ radians; I to V -- $\tau = 10; 30; 60; 120; 36$ seconds;

b -- relationship of the average speed of the corrosive-erosive breakdown of an alloy $\frac{\Delta P}{\epsilon \tau}$ ($n \cdot m^{-2} \cdot sec^{-1}$) to the air stream speed (M number), $\tau = 10$ seconds;

$\alpha_{at} = 0$ radians; I and II -- $T = 1373; 1473^{\circ}K$;

c -- comparative evaluation of the heat resistance of alloys with an iron base, nickel bases, and

of Armco iron, $M = 0.8$; $\alpha_{at} = 0$ radians;
I and II -- $T = 1273; 1473^{\circ}\text{K}$; d -- Armco iron;
e, h -- alloys with an iron base; f, g -- alloys
with a nickel base; 3, 4, 5 -- number of
averaged experimental points.

For all tests of exposure the relationship of the loss of weight to the temperature had the same character. Up to a certain temperature area of $1373^{\circ}\text{K} \leq T \leq 1423^{\circ}\text{K}$ oxidation proceeds slowly; at temperatures above the indicated area the heat resistance decreases sharply and this is expressed in a sharp increase in the weight loss of the sample.

The sharp decrease in the heat resistance of an alloy having an iron base at $T \geq 1373^{\circ}\text{K}$ coincided with the appearance of an external, easily removable (upon cooling) layer of oxide on the surface of the sample. This oxide (on a cooled sample) had a dull gray cast and possessed magnetic properties.

The sharp drop in the heat resistance of the first alloy in the temperature range from 1373 - 1423°K for the case of double-layered scaling on the alloy can be connected with a phenomenon which has already been observed in a series of works [1] -- the vaporization of Cr_2O_3 at temperatures from 1373 - 1473° . If the oxide enters into the composition of a more complex oxide (for example, of the type of the spinels $\text{NiO}\cdot\text{Cr}_2\text{O}_3$, $\text{FeO}\cdot\text{Cr}_2\text{O}_3$, etc.), then there is a preliminary breakdown of this complex oxide.

From the outer layer of the scale of the alloy the oxide Cr_2O_3 vaporizes with the preliminary breakdown

of oxides of the type of the spinels $\text{FeO}\cdot\text{Cr}_2\text{O}_3$ and $\text{NiO}\cdot\text{Cr}_2\text{O}_3$.

The relationship of the speed of the corrosive-erosive breakdown of the first alloy to the air stream speed (Figure 4b) was investigated in the range of speeds $0 \leq M \leq 3$ at the temperatures of 1373°K and 1473°K . The exposure time was 10 seconds. An explanation of the course of the given of the given relationships at subsonic and supersonic speeds was accomplished with the help of averaged parameters of the air stream I_w and E_{kin} (Figure 3) similarly to the explanation for Armco iron. The higher speeds of the breakdown of an alloy at the temperature 1473°K in comparison with the temperature 1373°K were based on the more intensive course of the secondary reactions in the scaling of the alloy, which causes an intensification of the erosive breakdown of the scaling.

Heat resistance of the first alloy was compared with that of the second alloys and Armco iron at $M = 0.8$ and $T = 1473^\circ$ and 1273°K respectively (4c).

Figure 4c shows the time relationships of the loss of weight in corrosive-erosive breakdown. The fading nature of these curves points to the prevalence of the corrosive process in the total process of breakdown and to the protective properties of the scale of the test materials.

Iron at $T = 1273^\circ\text{K}$ and at a flow speed of $M = 0.8$ in a period of 120 seconds lost approximately 7.5 times more weight than the first alloy (curves d and e). At $T = 1473^\circ\text{K}$ in an immobile medium the

heat resistance of the first alloy differed little from the heat resistance of the second alloys; whereas in an air flow at $M = 0.8$ and at the same temperature the heat resistance of the first alloy was considerably lower than that of the nickel alloys (curves f, g, and e). In addition, the alloys with an iron base experienced combustion in high-velocity gas streams.

In our experiment, for example, burning of the first alloy was observed at $T \approx 1493^\circ\text{K}$ and an air stream speed of $M \geq 0.8$.

The possibility of the manifestation of such a process of burning is provided by the high iron content in the alloy. In an immobile gaseous medium a sample of the first alloy experienced complete breakdown as a result of melting at $T = 1643^\circ\text{K}$. We had found earlier that the burning of iron in an air stream occurred at $M \geq 0.8$ and $T \approx 1373^\circ$, which coincides with some calculations on the determination of the theoretical consumption of air (of the air stream speed) required in order to maintain a stable burning process.

Symbols

T -- sample temperature; M -- coefficient for the speed of the stream; τ -- exposure time; α_{at} -- angle of attack of the sample; $\Delta P/s$ -- relative loss of weight of the sample; $\Delta P/s\tau$ -- average speed of the breakdown of the sample material; I_w -- current density; E_{kin} -- average flow of kinetic energy through a unit of area of the pipe.

Summary

The results of a study of heat resistance of metals and alloys in an oxidizing medium at high velocity are presented. For the experiments a special unit was designed and appropriate methods were worked out. As a result of the investigation a relationship was established between the average velocity, the time of heating, the sample temperature, and the orientation of the sample to the air stream. Combustion of iron and iron-bearing alloys was also found in an air stream moving at a high velocity. The heat resistance of iron and of some heat resistant alloys in an air stream at a high velocity were compared.

BIBLIOGRAPHY

1. Ignatov, D.V., and Shangunova, P.D., O mekhanizme okisleniya splavov na osnove nikelya i khroma (The Mechanism of the Oxidation of Alloys of Nickel and Chromium), Publishing House of the Academy of Sciences of the USSR, 1960.
2. "The Speed of Scale Formation from Metals and Alloys," Uchenyye zapiski Leningradskogo universiteta imeni A.A. Zhdanova (Scientific Notes of the Leningrad University imeni A.A. Zhdanov), 1954.
3. Tomashev, N.D., Teoriya korrozii i zashchita metallov (The Theory of Corrosion and the Protection of Metals), Publishing House of the Academy of Sciences of the USSR, 1959.
4. Murphy, D., Wood, W., and Jominy, W., Trans. Am. Soc. Steel Treat., 19, 193, 1931.

5. Baukloh, W., and Reif, O., Metallwirtschaft, 14, 1055, 1935.

6. Bourgraff, R., Stahl und Eisen, 60, 1940.

7. Schroeder, W., Arch. Eisenhüttenw., 6, 47, 1932.

8. Vinarov, S.M., Aviatsionnoye metallovedeniye. (Aviation Metal Working), State Publishing House of the Ministry of Defense, 1962.

9. Penkherst, R., and Khodler, D., Tekhnika eksperimenta v aerodinamicheskikh trubakh. (Techniques of Experimentation in Aerodynamic Pipes), Institute of Linguistics, 1955.

10. Arkharov, V.I., Okisleniye metallov pri vysokikh temperaturakh (The Oxidation of Metals at High Temperatures), State Publishing House for Metallurgical Literature, 1945.

11. Olesevich, K.V., Iznos elementov gazovykh trub pri rabote na tverdom toplive (Wearing of Elements of Gas Pipes When Operating with Solid Fuel), State Scientific Technical Publishing House for Machine Building Literature, 1959.

12. Prosvirin, V.I., and Fedosov, A.I., Inzhenerno-fizicheskiy zhurnal (Journal of Engineering Physics), No. 1, 1959.

5570
CSO: 1880-D

- - -

THE EFFECT OF TRANSVERSE MASS FLOW ON THE
RESISTANCE AND HEAT EXCHANGE ASSOCIATED
WITH THE TURBULENT FLOW OF A COMPRESSED GAS

P. N. Romanenko
V. N. Kharchenko,
Forest Engineering Institute,
Moscow

The results of experimental investigations are reported on the effects on heat exchange and resistance of various gases to injection through a porous diaphragm into a turbulent boundary layer on a horizontal plane.

One of the effective methods of protecting streamline surfaces from the action of high temperatures or kinetic energies is the injection of liquid or gas coolants into the flow through a porous diaphragm. For this, in order to design a porous cooler, it is necessary to have reliable methods of determining thermal flow and frictional resistance on the streamline surfaces upon the admission of mass into the gaseous flow. The turbulent boundary layer offers the most practical interest since it prevails in devices for which porous cooling is necessary. However, even in those cases when no transverse mass flow exists, a laminar boundary layer is established and the injection of the coolant disrupts the stabilized flow and changes the laminar flow into a turbulent flow. Consequently, the problem of heat exchange and resistance between the substance and the gas, moving relative to each other, during porous cooling leads to the establishment of methods for determining the coefficients of heat exchange and resistance in the conditions of a turbulent boundary layer.

Various approximation methods of an analytical solution of the problem have been developed, based on diagrams of the actual flow conditions and the introduction of a large number of slightly valid assumptions, and also additional experimental data [1-5, 7, 14, 16]. The results of experimental works on the effect on heat exchange and resistance of the injection of air into a turbulent boundary layer on a horizontal plane have been published in a number of works [2, 6, 8-11]. They show that with increased consumption of injected air, the coefficients of heat exchange and resistance are diminished. However, the values of these coefficients, obtained by various authors, at identical conditions, differs considerably.

A short summary of the works on porous cooling is given in [17].

The results of investigations on frictional resistance and heat exchange upon injection of air, helium, carbon dioxide, and freon-12 into a turbulent boundary layer of heated air on a porous horizontal plate are presented in the present work. Experiments were conducted on an experimental section (Fig. 1), representing a rectangular thermally-insulated duct which has a porous copper plate with a 50% porosity in the bottom membrane measuring 300x60x8 mm ([Note]: The plate was made by the Chair of Physical Metallurgy, Gor'kovskiy Polytechnic Institute). Dimensions of the experimental section were 420x150x80 mm.

Injection of gases through the porous plate was accomplished by excess pressure produced in the tank under the plate. The injected air was supplied to the tank from the air compressor receiver and the other gases from a bottle through a pressure reduction valve. The static pressure drop on the plate was checked by a differential mercury manometer. The consumption of injected gas was determined according to a previously constructed calibrated graph at certain temperatures and pressure differentials of the plate. At the given conditions, the volumetric porosity was determined on a special weighing device according to the volume of displaced water from the measuring tank by the gas passing through the plate. Weighing of the porous plate was done before and after the experiment.

The experimental section was part of the device described in [21].

The following quantities were measured during the experiment: air pressure and temperature at the heater outlet (front of the jet); the dynamic pressure, and also

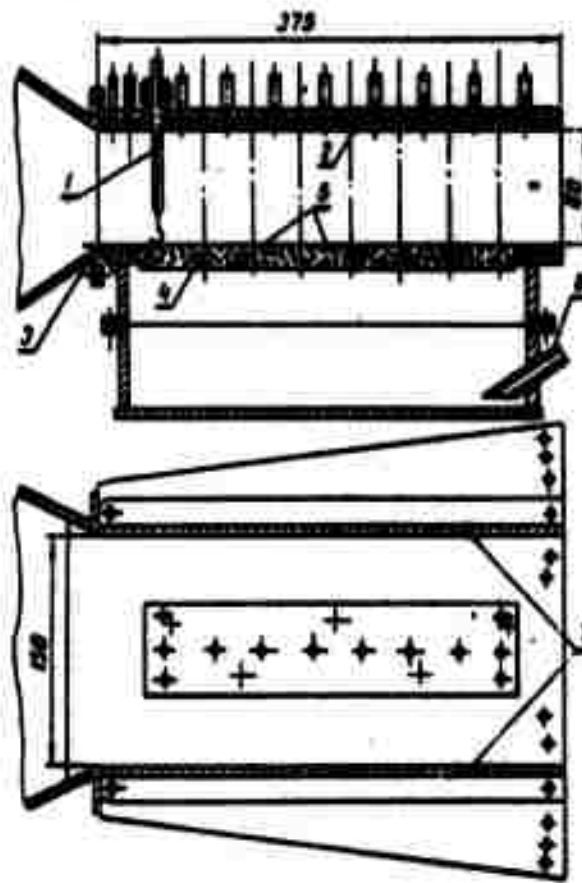


Fig. 1 Diagram of the Experimental Section

1. Pitot micro-tube
2. Static pressure check points
3. Boundary layer suction
4. Porous plate
5. Plate thermocouples
6. Injected-gas feed line
7. Side expandible membranes

the temperature of the air flow at 8 points along the length of the plate; the static pressure at 10 points; the temperature at five points on the inside surface and at five points on the outside surface of the plate; and the temperature of the injected gas in front of the plate.

The dynamic pressures in the boundary layer and in the streamline of the check points were measured with pitot micro-tubes connected to differential manometers filled with water or ethyl alcohol. Flow temperatures were measured with moveable chromel-alumel thermocouples at the same points as the dynamic pressures. A record of the air temperatures at all points was made on the tape of the electronic balancing potentiometer.

The pitot micro-tubes and micro-thermocouples were placed along the center of the plate by using a coordinate system which made it possible to measure the dynamic pressures and temperatures at check points 0.05 mm apart. Simultaneously, the fields of dynamic pressures and temperatures along the sides of the plate were measured at the first and last points. The measurements showed that the distribution of flow parameters along the width of the experimental section was uniform. Temperatures of the plate and also the injected gas were measured with chromel-alumel thermocouples and recorded with the aid of a PP-25 portable potentiometer.

For providing a build-up of the boundary layer at the front of the porous plate, suction of the boundary layer was carried out at a distance of 65 mm from flow intake onto the plate.

Prior to starting the experiment, the plate was heated to a prescribed temperature and held constant throughout the experiment. The required plate temperature for the given experiment was determined on the basis of previous works.

Reynolds number for the experiments ranged from 10^5 to 5×10^5 . The injection-rate ratio $\rho_w v_w / \rho_{1u_1}$ was measured from 1×10^{-4} to 7×10^{-3} , and the temperature of the air stream -- from 450° to 550°K . Temperature range of the plate was from 375° to 420°K and the flow velocity ranged from 25 to 75 meters/sec.

Graphs of the velocity distribution and temperatures for each cross section were plotted according to data from measurements of the dynamic and static pressures, flow temperatures at the check points of the boundary layer, and plate temperatures. The integral properties of the boundary layer; Θ , δ^* , and φ were determined

by these graphs. Graphs of the change of these properties along the length of the experimental section (along coordinate x) were then constructed. In addition, graphs of the change p , u_1 , T_1 , and ρ_1 along the length of the section were constructed. All these data were used to calculate the coefficient of frictional resistance c_f and heat flow q_w on the porous plate according to the integral impulse and energy relationships for the boundary layer.

For determining the flow rate in the boundary layer, the following initial equation was used:

$$u = \sqrt{2gh \frac{14}{\gamma}}. \quad (1)$$

The quantity γ , associated with the injection of air, was determined from the equation of state, $p = \gamma RT$, according to the measured pressure p in the cross section in question and according to temperature T at the given point of the boundary layer.

For determining the specific weight γ (or density ρ) of the mixture during injection of He, CO₂, and freon-12, the following ratios were used.

In [12] it was shown that in the case of turbulent flow around a horizontal porous surface one can use

$$\frac{\rho_w - \rho'}{\rho_w} \approx \frac{u}{u_1}. \quad (2)$$

The tangential force of friction on the membrane

$$\tau_w = \mu_w \left(\frac{du}{dy} \right)_w. \quad (3)$$

On the other hand,

$$\tau_w = \frac{c_f}{2} \rho_1 u_1^2. \quad (4)$$

The specific mass input of injected gas is expressed by the equation

$$j = \rho_w v_w - D_w \left(\frac{d\rho'}{dy} \right)_w. \quad (5)$$

or

$$j = \rho_w u_w \quad (6)$$

From equation (2) we have:

$$\left(\frac{du}{dy}\right)_w = -\left(\frac{d\rho'}{dy}\right)_w \frac{u_1}{\rho_w} \quad (7)$$

After substituting the expression for the velocity gradient on the membrane in equation (3), by means of equation (4) we will obtain

$$\left(\frac{d\rho'}{dy}\right)_w = -\frac{\rho_w c_f}{\mu_w} \frac{2}{\rho_1 u_1} \quad (8)$$

Then on the basis of equations (5) and (6) it is possible to write

$$\frac{\rho_w}{\rho_w} \left(1 + D_w \frac{\rho_w c_f}{\mu_w} \frac{\rho_1 u_1}{2 \rho_w u_w}\right) = 1, \quad (9)$$

from which

$$\rho_w' = \rho_w [1 + (Sc b_1)^{-1}]^{-1}, \quad (10)$$

where

$$Sc = \frac{\nu_w}{D_w}; \quad b_1 = \frac{\rho_w u_w}{\rho_1 u_1} \frac{2}{c_f}$$

The density of the two-component gas mixture in the boundary layer is

$$\rho = \frac{p}{gRT} \quad (11)$$

The gas constant of the mixture, R , is determined according to the formula

$$R = R_1 \left(1 - \frac{\rho'}{\rho}\right) + R' \left(\frac{\rho'}{\rho}\right) \quad (12)$$

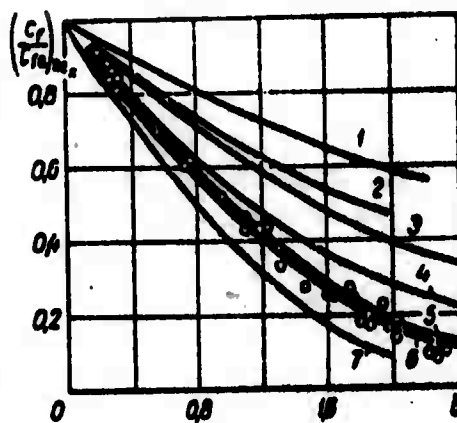


Fig. 2 Comparison of experimental data with results of various authors for the coefficient of resistance upon injection of air into a turbulent boundary layer on a horizontal plate: 1-[19]; 2-[10]; 3-[4]; 4-[3]; 5-[11]; 6-[16]; 7-[18]

From equations (11) and (12) we have:

$$\rho = \frac{p}{gR_1 T} + \rho' \left(1 - \frac{R'}{R_1}\right). \quad (13)$$

The partial density ρ' of the injected gas is expressed by equation (2)

$$\rho' = \rho_w \left(1 - \frac{u}{u_1}\right). \quad (14)$$

Taking into account equations (13), (14), and (10), we bring equation (1) to the following form:

$$u = \left\{ 2h \gamma_h \left[\frac{p}{gR_1 T} + \left(1 - \frac{R'}{R_1}\right) \frac{\rho_w}{1 + \frac{1}{Sc b_1}} \left(1 - \frac{u}{u_1}\right) \right]^{-1} \right\}^{1/2}. \quad (15)$$

Equation (15) represents a third degree equation with regard to the desired quantity u :

$$\frac{1}{u_1} \frac{\rho_w}{1 + \frac{1}{Sc b_1}} \left(1 - \frac{R'}{R_1}\right) u^3 - \left[\frac{p}{gR_1 T} + \left(1 - \frac{R'}{R_1}\right) \frac{\rho_w}{1 + \frac{1}{Sc b_1}} \right] \times \quad (16)$$

$$\times u^2 + 2h \gamma_h = 0.$$

The flow velocities in the boundary layer were determined according to equation (16). The membrane permeability parameter b_1 was calculated for the given specific flows of the injected gas $\rho_w u_w$ and the measured parameters of the streamline $\rho_1 u_1$ according to the formula

$$b_1 = \frac{\rho_w u_w}{\rho_1 u_1 St Pr^{1/2}}. \quad (17)$$

The Stanton number was determined from the heat balance equation

$$St = \frac{\rho_w u_w c_{pw} (T_w - T_s)}{\rho_1 u_1 c_{p1} (T_s - T_w)}. \quad (18)$$

For determining the inherent values of the resistance coefficient c_f along the length of the streamline surface, the integral relationship of impulses was used:

$$\frac{d\Theta}{dx} + \left(\frac{H+2}{u_1} \frac{du_1}{dx} + \frac{1}{\rho_1} \frac{d\rho_1}{dx} \right) \Theta - \frac{\rho_w u_w}{\rho_1 u_1} = \frac{c_f}{2}, \quad (19)$$

where

$$\Theta = \int_0^{\delta} \frac{\rho u}{\rho_1 u_1} \left(1 - \frac{u}{u_1} \right) dy; \quad H = \frac{\delta^*}{\Theta}; \quad \delta^* = \int_0^{\delta} \left(1 - \frac{\rho u}{\rho_1 u_1} \right) dy.$$

The values of the dimensionless coefficient of heat exchange, St , were determined by two independent methods: from the heat balance equation (18) and from the integral energy ratio

$$\frac{d\varphi}{dx} + \left[\frac{1}{u_1} \frac{du_1}{dx} + \frac{1}{T_c - T_w} \frac{d(T_c - T_w)}{dx} - \frac{1}{\rho_1} \frac{d\rho_1}{dx} \right] \varphi - \frac{(c_{p1} T_1 - c_{pw} T_w) \rho_w u_w}{c_p (T_c - T_w) \rho_1 u_1} = St, \quad (20)$$

where

$$\varphi = \int_0^{\delta} \frac{\rho u}{\rho_1 u_1} \left[\frac{T_1 - T_w}{T_c - T_w} \right] dy.$$

All the quantities encountered in equations (19) and (20), in addition to c_f and St , were determined from experimental data.

Experimental data for the effect of transverse flow of air, helium, carbone dioxide, and freon-12 on the resistance and heat exchange during non-gradient turbulent flow of air around a horizontal surface were correlated in the form of graphic relationships:

$$\left(\frac{c_f}{c_{f0}} \right)_{Re_x} = f(b) \quad \text{и} \quad \left(\frac{St}{St_0} \right)_{Re_x} = f(b_T),$$

where

$$b = \frac{\rho_w u_w}{\rho_1 u_1} \frac{2}{c_{f0}}; \quad b_T = \frac{c_{pw} \rho_w u_w}{c_{p1} \rho_1 u_1} \frac{1}{St_0}.$$

For determining c_{f0} , special experiments were

conducted. A horizontal impermeable membrane was blasted with air at the temperature of the membrane and at values of $Re_x = u_1 x / \nu_1$, which occurred in the tests with a transverse injected gas. The coefficient of resistance c_{f_0} was determined from the experimental data from the integral impulse relationship

$$\frac{c_{f_0}}{2} = \frac{d\theta_0}{dx} \quad (21)$$

The depth of impulse loss θ_0 during isothermal streamline with air flow of an impermeable horizontal membrane was calculated according to the formula

$$\theta_0 = \int_0^{\delta} \frac{u}{u_1} \left(1 - \frac{u}{u_1} \right) dy.$$

In addition, values of c_{f_0} were calculated by the method of F. Clauser [14] and Bräzius' formula

$$\frac{c_{f_0}}{2} = 0,0296 \left(\frac{u_1 x}{\nu_1} \right)^{-0,2} \quad (22)$$

Test data for c_{f_0} , obtained from equation (21) and Clauser's method satisfactorily agree with data of formula (22).

The Stanton number, St_0 , was determined by the following formula [15]:

$$St_0 = \frac{0,0296 Re_x^{-0,2}}{1 + 0,874 Re_x^{-0,1} (Pr - 1)} \quad (23)$$

where $A=1.5 Pr^{-0.67}$

It is evident from Fig. 2 that an increase in the permeability parameter is accompanied by a drop in magnitude of the resistance coefficient and for $b \approx 2$ is almost 20% of c_{f_0} .

Preventing the general tendency of c_f/c_{f_0} to decrease with an increase in b for the data of the various works is essentially different. Our data was similar to

to the theoretical data of [3], based on Prandtl's hypothesis on the means of mixing; [16], based on the boundary zones of resistance; and the experimental work of [11], obtained in conditions which more closely approximated the conditions of our experiments. Works [4], [10], and [9] give too large, and work [18], too small an effect of the injection on the coefficient of resistance.

When injecting gases of different molecular weight, the most decrease of resistance results with the injection of gases with a low molecular weight (Fig. 3). Freon-12 reduces resistance considerably less than air and particularly helium, however, at identical inputs of injected gas, the effectiveness of helium is considerably greater in comparison with air than air in comparison with freon-12. Carbon dioxide takes an intermediate position between air and freon-12.

The effect of injecting gases of different molecular weight on the heat exchange is shown in Fig. 4. Data of this graph shows that injection of gases essentially reduces heat flow on the membrane. It is significant to note that injected gases of different molecular weight effect heat exchange in approximately the same way as they effect resistance. Helium, having a very large heat capacity, is a very effective coolant, whereas freon-12, with a heat capacity one-eighth the magnitude of helium (in the investigated conditions), only slight-

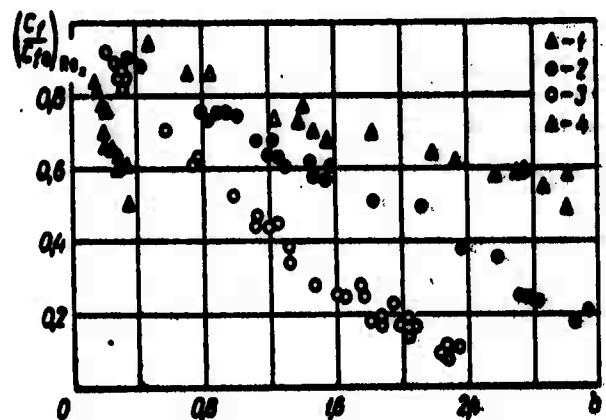


Fig. 3 Effect of the injection of various gases on the resistance coefficient: 1-freon-12; 2-CO₂; 3-air; 4-helium

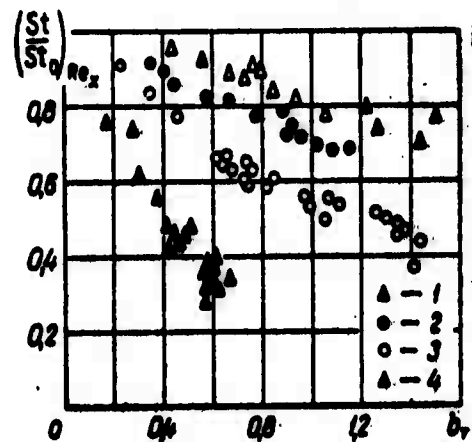


Fig. 4 Effect of the injection of various gases on the coefficient of heat exchange; 1-4; see Fig. 3

reduces heat exchange. The experimental points on the graphs for carbon dioxide and air with intermediate values of heat capacity fall between the points for freon-12 and helium.

SYMBOLS

D_w -- coefficient of diffusion
 h -- difference in manometer liquid levels
 γ_h -- specific gravity of liquid in manometer
 j -- specific mass input of injected gas
 R, R_1, R' -- respectively the gas constants for the mixture of air and injected gas, undisturbed flow, and the injected gas
 Re_x, Re_0 -- Reynolds' numbers of the undisturbed flow composed of x and Θ
 $T, T_1, T_2, T_w, T^*, T_1^*, T_e$ -- respectively, the temperatures of the boundary layer, undisturbed flow, injected gas in front of the plate, the plates, adiabatic drag of the boundary layer, adiabatic drag of the undisturbed flow, and the equilibrium temperature of the membranes
 ρ', ρ_w' -- partial density of the injected gas in the boundary layer and near the membrane
 Sc -- Schmidt number
 b_1 -- permeability parameter characterizing the effect substance transmission over the surface of a streamline body

Indices -- 1, parameters of the undisturbed flow; 0, parameters for a plane impermeable plate in isothermal flow; w , membrane parameters

SUMMARY

Gas injection into an air turbulent boundary layer decreases skin friction and heat transfer with small consumption of injected gas.

In the experiments, air, helium, carbon dioxide, and freon-12 were injected through a porous wall.

It is shown that with increase in the molecular weight of the injected gases, their effect on skin friction and heat transfer decreases.

ditions of reagent supply. The solution is obtained in a closed form and accounts for electrochemical electrode polarization and ohmic losses. Distribution of polarization and the process intensity are described by expressions (31) and (32) respectively.

BIBLIOGRAPHY

1. Rannie, W. E., Jet Prop. Lab. CIT, XI, 1947
2. Mickley, H. S., MIT, Cambridge, Mass., IX, 1952
3. Dorrance, W. H., and Dore, F. J., JAS, 21, No 6, 1954
4. Rubesin, M. W., NACA, TN 3341, 1954
5. Van Driest, E. R., Symposium on Mass Transfer Cooling for Hypersonic Flight, RAND, 1957
6. Leadon, B. M., and Scott, C. I., Rosemont Aero. Lab. Univ. Minn. Tech. Rept., No 126, II, 1956
7. Kalikhman, L. Ye., Zhurnal Tekhnicheskoy Fiziki (Journal of Technical Physics), 25, No 11, 1955
8. Rubesin, M. W., NACA, RM A 55, L13, 1955
9. Rubesin, M. W., Pappas, C. C., and Okuno, A. F., NACA, RM A 55119, XII, 1955
10. Tenderland, T., and Okuno, A. F., NACA, RM A 56, D 05, VI, 1956
11. Mickley, H. S., and Davis, R. S., NACA, TN 4017, XI, 1957
12. Mugalev, V. P., Trudy Moskovskogo Fiziko-Tekhnicheskogo Instituta (Works of the Moscow Physico-Technical Institute), No 4, Oborongiz, 1959
13. Mugalev, V. P., Ibid., No 5, 1959
14. Clauser, F. H., JAS, 21, No 2, 1954
15. Eckert, E. R., and Drake, R. M., Teoriya teplo - i massobmena (Theory of Heat and Mass Exchange) Gosenergoizdat, 1961
16. Kutateladze, S. S., and Leont'yev, A. I., PMTF, No 1, 1962
17. Hartnett, I. P., Masson, D. I., Gross, I. F., and Gasley, C. I., JAS, 27, No 8, 1960
18. Hacker, D. S., Jet Propulsion, 26, No 9, 1956
19. Pappas, C. C., and Okuno, A. F., JAS, 27, No 5, 1960
20. Clarke, I. H., Menkes, H. R., and Libby, P. A., JAS, 22, No 4, 1955
21. Romanenko, P. N., and Leont'yev, A. I., Trudy MIIT (Works of the Moscow Institute of Railway Transportation Engineers), No 139, Transzheldorizdat, Moscow, 1961

6368
CSO: 1880-D

PERFORMANCE OF POROUS ELECTRODES IN A
DIFFUSION PROCESS OF REAGENT SUPPLY

V.S. Bogotskiy and I.G. Gurevich,
Powers Engineering Institute,
Academy of Sciences Belorussian SSR,
Minsk

The problem concerning the distribution of the electrochemical process by means of electrochemical polarization and ohmic loss through a porous electrode of finite thickness, operating in a diffusion system, is investigated. A general solution in the closed form is given.

In applied electrochemistry, the use of porous electrodes, having a developed external surface, is associated with desire to intensify electrode processes to the maximum and at the same time to obtain noted specific properties.

In connection with this there is much significance in question about the effective use of such electrodes, explained by the macro-kinetic nature of the electrode process, leading to a non-uniform distribution of its intensity in the volume of the electrode.

In most of the published works [1-16], directly or indirectly related to the present question, the problem concerning the intensity of the electrode process in the volume of the electrode is solved (by one approach or another) analytically, issuing from the general theory of the field distribution in the electrolytic cell (Poisson's equation is used) by means of mass-transfer processes [13-15] or without such transfer [4-10]. In works [11, 12] the electrode is investigated as being

equipotential, but the distribution of intensity for the electrochemical process in the electrode is associated only with the process of mass transfer. In certain works [1-3, 16], distribution of process intensity in the electrode is studied with the use of an equivalent electrical circuit in place of an electrode reducing the problem to localization of currents in the elements of this circuit. The shortcomings of such a method include the difficulty of simulating the transport processes which, in the conditions of the investigated problem, are described (as given below) by non-linear equations [3].

In the present article, in contrast to the works of O. S. Ksenzhek [10, 12] and L. G. Ostin [11], the problem concerning the operation of a porous electrode in a diffusion system is investigated in a more general formulation and takes into account all forms of loss (both polarization and ohmic) for an electrode of finite thickness.

We will study study the following system (Fig. 1).

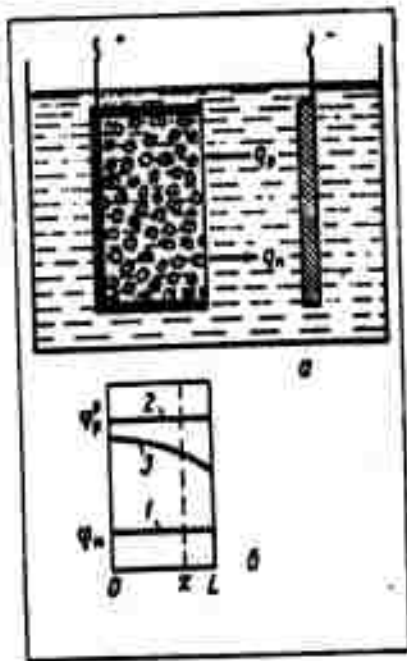


Fig. 1

a--electrical cell diagram; b--distribution of potential through the depth of the porous electrode: metallic skeleton of the electrode (1), electrolytic solution without current (2) and with a current (3)

A porous electrode of thickness L was submerged in an electrolytic chamber. In the present work, the case is investigated where the reagents are either electroneutral molecules or the corresponding ions of the electrolyte. It is suggested that transfer of electroneutral molecules of the reagent and product in the investigated system to the electrode--electrolytic chamber is accomplished only by means of molecular diffusion, and the transfer of ions of the electrolyte--by means of diffusion and migration in the electric field of the electrode.

It is further suggested that the ionic concentrations, comprising the working mixture and filling the electrode, considerably exceed the concentrations of the electroneutral molecules of the reagent and product. This condition makes it possible to study the conductivity of the mixture and, in addition, to disregard the diffusion potential formed due to non-uniform distribution of the ionic concentrations.

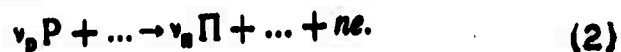
Conditions are provided for maintaining constant volume (in the electrolytic chamber at a certain distance from the electrode) concentrations of reagent c_r and product c_p or by means of chamber dimensions, or by means of a continuous supply of reagent and removal of the product formed.

In the steady state an amount of products equivalent to the magnitude of the current I flows to the electrode and an equal amount of products, formed in the course of the reactions, is removed from the electrode.

In the present work, during the study of the transport stages of the electrode process, the flow of electroneutral substances (reagent or product) are taken into account.

$$\bar{q}_i = -D_i \text{grad} c_i. \quad (1)$$

Suppose that in the electrode a reaction of the form below takes place



Assuming the visible surface of the electrode is sufficiently large in order to neglect edge effects, and the structure is very finely porous in order to have the possibility to be diverted from a concrete structure and to study the electrochemical reaction

occurring in the entire volume of the electrode (as first done by Ya. B. Zel'dovich [17]), and to possibly change to the study of a unidimensional problem.

Since the distribution of the intensity of the electrode process (true current density i) through the depth of the porous electrode is associated with both the distribution of reagent and product concentrations and the distribution of potential, then we will come to a system of two equations describing the function of the electrode. One of these is Fick's equation

$$c_p = -\frac{v_p s}{nFD_p} i, \quad (3)$$

and the other--Poisson's equation

$$\eta = sR_s i. \quad (4)$$

Prior to analysis of the system of equations (3) and (4), it is necessary to decide on the suitability of use of Poisson's equation in (4) because, generally speaking, it describes the distribution of the solution potential.

Neglecting the resistance of the metallic skeleton in comparison with the effective resistance of the mixture in the pores of the electrode $R_p = \text{constant}$, we obtain, independent of coordinate x , the dependence of the metal potential φ_M (line 1, Fig. 1, b) and, if there is no current, the potential of the solution (equilibrium) φ_p^p , also independent of x (line 2), then under load $\varphi_p = f(x)$ (curve 3).

The potential drop on the electrode surface in the absence of current is

$$\Delta\varphi^p = \varphi_M - \varphi_p^p, \quad (5)$$

and the potential drop for the electrode under load is

$$\Delta\varphi = \varphi_M - \varphi_p. \quad (6)$$

Then polarization of the electrode is

$$\eta = \Delta\varphi^p - \Delta\varphi = \varphi_p - \varphi_p^p. \quad (7)$$

Differentiating (7), we obtain

$$\frac{\partial \eta}{\partial x} = \frac{\partial \varphi_p}{\partial x}. \quad (8)$$

From the relationship (8), the suitability of using Poisson's equation in the form (4) is evident, whereas the condition of usage is included in order that the conductivity of the metallic skeleton of the electrode considerably exceeded the conductivity of the working mixture.

For the kinetic nature of the process (1) we take the expression from the theory of delayed discharge

$$i = j_0 \left\{ \frac{c_p^x}{c_p^0} \exp \left[\frac{aF}{RT} \eta \right] - \frac{c_n^x}{c_n^0} \exp \left[- \frac{(n-a)F}{RT} \eta \right] \right\}. \quad (9)$$

In order that the system of equations (3) and (4) proved to be complete, we find the relation between the localized values of concentrations of product and reagent which should make it possible to eliminate the concentration of the product from equation (9).

Writing Fick's equation (1) twice, once for the reagent and once for the product, and expressing the flow of the substance from the electrical magnitudes and coefficients of the reactions (2), we obtain respectively:

$$\frac{dc_p}{dx} = \frac{v_p}{nFD_p} I_x, \quad (10)$$

$$\frac{dc_n}{dx} = - \frac{v_n}{nFD_n} I_x. \quad (11)$$

Eliminating I_x from (10) and (11), we obtain, after differentiation, the interesting relation

$$c_n^x = c_n^L + \frac{v_n}{v_p} \frac{D_p}{D_n} (c_p^L - c_p^0). \quad (12)$$

For this, in order to change equation (12) from unknown values of concentrations on the frontal (with respect to the opposite electrode, i. e., for $x=L$) surface of the electrode c_p^L and c_n^L to given volume concentrations c_p^0 and c_n^0 , we will study the conditions of reagent diffusion from the electrolytic chamber to the

electrode. Assuming the distribution of concentrations of reagent and product in the diffusion layer near the frontal surface of the electrode as linear, we obtain the following expression for current per unit visible surface of the electrode:

$$I = \frac{nFD_p}{v_p} \frac{(c_p^v - c_p^l)}{\delta} \quad (13)$$

Then, using the expression for limiting current

$$I_{\text{npex}} = \frac{nFD_p}{v_p \delta} c_p^v \quad (14)$$

we obtain $c_p^l = \frac{v_p \delta}{nFD_p} I_{\text{npex}} (1 - \theta)$, where $\theta = \frac{I}{I_{\text{npex}}}$ - the coefficient of "charging" the electrode ($0 \leq \theta \leq 1$). Finally,

$$c_p^l = c_p^v (1 - \theta) \quad (15)$$

Similarly we obtain

$$c_n^l = c_n^v + \frac{v_n}{v_p} \frac{D_p}{D_n} c_p^v \theta \quad (16)$$

Taking into account equations (12), (15) and (16), equation (9) can be rewritten in the following form:

$$i = j_0 \left\{ \frac{c_p}{c_p^v} \exp \left[\frac{\alpha F}{RT} \eta \right] - \left[1 + \frac{c_p^v}{c_n^v} \frac{v_n}{v_p} \frac{D_p'}{D_n'} + \frac{c_p^v}{c_n^v} \left(\frac{D_p}{D_n} - \frac{D_p'}{D_n'} \right) \frac{v_n}{v_p} \theta - \frac{c_p^v}{c_n^v} \frac{v_n}{v_p} \frac{D_p'}{D_n'} \right] \exp \left[- \frac{(n - \alpha) F}{RT} \eta \right] \right\} \quad (9')$$

We introduce the following symbols:

$$v = \frac{v_n}{v_p}; \quad \xi = \frac{c_n^v}{c_p^v}; \quad d_{p,n} = \frac{D_p}{D_n}; \quad d_{p,n}' = \frac{D_p'}{D_n'}; \quad d_l = \frac{D_l}{D_l}$$

(for most porous electrodes $d=10^{-1}$ or 10^{-2} 12). If

the electrode decreases diffusion only by its structure without regard for the properties of the diffusing substance, then it is evident that $d_p = d_n$, i. e. $D_p/D_p = D_n/D_n$. Then the expression for i is simplified:

$$i = j_0 \left\{ \frac{c_p}{c_p^0} \exp \left[\frac{\alpha F}{RT} \eta \right] - \left(1 + \frac{\nu d'_{p,n}}{\xi} - \frac{\nu d'_{p,n}}{\xi} \frac{c_p}{c_p^0} \right) \times \right. \\ \left. \times \exp \left[- \frac{(n-\alpha) F}{RT} \eta \right] \right\} \quad (17)$$

and the system of equations (3) and (4) is rewritten:

$$c_p^0 = \frac{\nu_p j_0}{n F D_p} \left\{ \frac{c_p}{c_p^0} \exp \left[\frac{\alpha F}{RT} \eta \right] - \right. \\ \left. - \left(1 + \frac{\nu d'_{p,n}}{\xi} - \frac{\nu d'_{p,n}}{\xi} \frac{c_p}{c_p^0} \right) \exp \left[- \frac{(n-\alpha) F}{RT} \eta \right] \right\}. \quad (18)$$

$$\eta' = s R_s j_0 \left\{ \frac{c_p}{c_p^0} \exp \left[\frac{\alpha F}{RT} \eta \right] - \right. \\ \left. - \left(1 + \frac{\nu d'_{p,n}}{\xi} - \frac{\nu d'_{p,n}}{\xi} \frac{c_p}{c_p^0} \right) \exp \left[- \frac{(n-\alpha) F}{RT} \eta \right] \right\}.$$

Taking into account that for the conditions of the investigated problem (Fig. 1, a), the flow of the substance and current across the back surface of the electrode is zero and across the frontal surface is respectively equal to ν_p/nFI and I , we obtain the boundary conditions of the following form:

$$\eta' |_{x=0} = 0, \quad \eta' |_{x=L} = R_s I; \quad (19)$$

$$c_p |_{x=0} = 0, \quad c_p |_{x=L} = \frac{\nu_p}{n F D_p} I.$$

System (18) is a system of two non-linear differential equations of the second order.

We will rewrite the system of equations (18) and

boundary conditions (19) after previously being changed to a dimensionless coordinate from the condition $\zeta = x/L$ ($0 \leq \zeta \leq 1$), to dimensionless concentrations from the condition $c = c_p/c_p^0$ ($0 \leq c \leq 1$) and to dimensionless polarizations from the condition $u = \eta/R_p L$.

Then

$$c'' = A\psi \left\{ c \exp \left[\frac{\theta}{\Omega_{\text{пер}}} u \right] - (E - Mc) \exp \left[-\frac{(n-a)\theta}{\alpha \Omega_{\text{пер}}} u \right] \right\}, \quad (18')$$

$$u'' = \frac{A}{\theta} \left\{ c \exp \left[\frac{\theta}{\Omega_{\text{пер}}} u \right] - (E - Mc) \exp \left[-\frac{(n-a)\theta}{\alpha \Omega_{\text{пер}}} u \right] \right\}$$

and boundary conditions

$$u'|_{\zeta=0} = 0, \quad u'|_{\zeta=1} = 1;$$

$$c'|_{\zeta=0} = 0, \quad c'|_{\zeta=1} = \psi\theta, \quad (19')$$

where

$$A = \frac{I_0}{I_{\text{пер}}}; \quad I_0 = sLj_0; \quad \psi = \frac{D_p \beta}{D_p/L};$$

$$\Omega_{\text{пер}} = \frac{1}{R_p L} \frac{RT/\alpha F}{I_{\text{пер}}}; \quad E = 1 + \frac{v d_{p,n}}{\xi}; \quad M = \frac{v d_{p,n}}{\xi}.$$

Equating the first equation of the system (18) to the second we obtain

$$\frac{c''}{u''} = \psi\theta. \quad (20)$$

After a double integration of (20) taking into account the boundary conditions for $\zeta=1$ we have:

$$u = \frac{c}{K} + C_2, \quad (21)$$

where $K = \psi\theta$, and C_2 -- the second integration constant.

Substituting (21) into the first equation of system (18') we obtain

$$c'' = A\psi \left\{ K_1 c \exp(K_2 c) - (E - Mc) K_1^{\frac{\alpha-n}{\alpha}} \exp \left[\frac{\alpha-n}{\alpha} K_2 c \right] \right\}; \quad (22)$$

where $K_1 = \exp(\theta_2 \theta / \Omega \lim)$; $K_2 = 1/\Omega \lim \psi$.

We substitute the variable quantities according to

$$c = \ln z. \quad (23)$$

Then equation (22) can be rewritten

$$z' - f_1(z) z' + f_2(z) = 0 \quad (24)$$

with boundary conditions $z'|_{z=0} = 0$; $z'|_{z=1} = Kz_1$ ($z_1 = z|_{z=1}$).

Here

$$f_1(z) = \frac{1}{z};$$

$$f_2(z) = A\psi \left\{ -K_1 \ln z z^{K_1+1} + (E - M \ln z) K_1^{\frac{a-n}{a}} z^{\frac{a-n}{a} K_1+1} \right\}.$$

Substitution of $p(z) = z'(\zeta)$ makes it possible to reduce the order of equation (24) and bring it to the form of a Bernoulli equation

$$p' - f_1(z)p + f_2(z)p^{-1} = 0. \quad (24')$$

The boundary conditions are written respectively:

$$p(z)|_{z=z_1} = 0; p(z)|_{z=z_1} = Kz_1.$$

A subsequent substitution $q(z) = p^2(z)$ makes it possible to reduce equation (24') to a linear equation with variable coefficients

$$q' - 2f_1(z)q + 2f_2(z) = 0. \quad (24'')$$

Integrating (24'') by known methods and determining the integration constant from the boundary condition for $\zeta=1$:

$$q|_{z=z_1} = p^2|_{z=z_1} = K^2 z_1^2.$$

we obtain a solution in the following form:

$$q = z^2 \left\{ 2A\psi \left[K_1 z^{K_1} \left[\frac{\ln z}{K_1} - \frac{1}{K_1^2} \right] - EK_1^{\frac{a-n}{a}} \frac{z^{\frac{a-n}{a} K_1}}{\frac{a-n}{a} K_1} + \right. \right. \\ \left. \left. + MK_1^{\frac{a-n}{a}} z^{\frac{a-n}{a} K_1} \left[\frac{\ln z}{\frac{a-n}{a} K_1} - \frac{1}{\left(\frac{a-n}{a} K_1 \right)^2} \right] \right] \right\} +$$

$$\begin{aligned}
& + K^2 - 2A\psi \left\{ K_1 z_1^{K_1} \left[\frac{\ln z_1}{K_2} - \frac{1}{K_2^2} \right] - EK_1 \frac{z_1^{\frac{\alpha-n}{a} K_2}}{\frac{\alpha-n}{a} K_2} + \right. \\
& \left. + MK_1 \frac{z_1^{\frac{\alpha-n}{a} K_2}}{z_1^{\frac{\alpha-n}{a} K_2}} K_2 \left[\frac{\ln z_1}{\frac{\alpha-n}{a} K_2} - \frac{1}{\left(\frac{\alpha-n}{a} K_2 \right)^2} \right] \right\}.
\end{aligned}$$

In order to determine K_1 (explicitly and entering the constant of integration C_2 of equation (20) in it) we use the boundary condition for $S=0$: $q|_{z_0} = 0$.

A solution in the general form of the derived equation, with regard to K_1 , is difficult. For values of α and n , satisfying the relationship $\alpha - n/\alpha = -1$, the equation becomes quadratic and the following expression is derived for K_1 :

$$K_1 = Q + \sqrt{Q^2 - B} \quad (25)$$

where

$$\begin{aligned}
Q &= \frac{K^2 K_2^2}{4A\psi} (z_1^{K_2} [K_2 \ln z_1 - 1] - z_0^{K_2} [K_2 \ln z_0 - 1])^{-1}; \\
B &= \frac{EK_2 \left(\frac{1}{z_1^{K_2}} - \frac{1}{z_0^{K_2}} \right) - M \left(\frac{1}{z_1^{K_2}} [K_2 \ln z_1 + 1] - \frac{1}{z_0^{K_2}} [K_2 \ln z_0 + 1] \right)}{z_1^{K_2} [K_2 \ln z_1 - 1] - z_0^{K_2} [K_2 \ln z_0 - 1]}
\end{aligned}$$

and from which

$$C_2 = \frac{\Omega_{\text{пред}}}{\Theta} \ln(Q + \sqrt{Q^2 - B}). \quad (26)$$

Performing the reverse transformation from the change of z to the change of c , we obtain

$$c = \int_{c_0}^c \left\{ K^2 + 2A\psi \left[\frac{K_1}{K_2^2} (\exp[K_2 c] [K_2 c - 1] - \exp[K_2 c_1] [K_2 c_1 - 1]) + \right. \right.$$

$$\begin{aligned}
& + \frac{1}{K_1} \left(\frac{E}{K_2} (\exp[-K_2 c] - \exp[-K_2 c_1]) - \frac{M}{K_2} (\exp[-K_2 c] \times \right. \\
& \left. \times [K_2 c + 1] - \exp[-K_2 c_1] [K_2 c_1 + 1]) \right) \Bigg\}^{-1/2} dc. \quad (27)
\end{aligned}$$

The relationship between c and ζ (27) by a known approximation can be simplified. Considering that for the majority of ideal systems the quantity

$$K_2 c_1 = (1 - \theta) \frac{1}{\Omega_{\text{нрел}} \psi} \ll 1 \quad (K_2 c \ll K_2 c_1),$$

and replacing first two members of the expansion with $\exp(K_2 c)$ we derive the following expression instead of (27)

$$\begin{aligned}
\zeta \approx \int_{c_1}^c \left\{ 2A\psi \left(\frac{M}{K_1} + K_1 \right) c^2 - 2A\psi \frac{E}{K_1} c + K^2 - \right. \\
\left. - 2A\psi \left(\frac{M}{K_1} + K_1 \right) c_1^2 + 2A\psi \frac{E}{K_1} c_1 \right\}^{-1/2} dc. \quad (27')
\end{aligned}$$

Integrating (27') in the given limits we obtain

$$\zeta \approx \frac{1}{\sqrt{a}} \left[\text{Arch} \frac{2ac + b}{\sqrt{-\Delta}} - \text{Arch} \frac{2ac_1 + b}{\sqrt{-\Delta}} \right]. \quad (28)$$

where

$$\begin{aligned}
a &= 2A\psi \left(\frac{M}{K_1} + K_1 \right); \quad b = -2A\psi \frac{E}{K_1}; \\
\Delta &= 8A\psi \left(\frac{M}{K_1} + K_1 \right) \left\{ K^2 - 2A\psi \left(\frac{M}{K_1} + K_1 \right) c_1^2 + 2A\psi \frac{E}{K_1} c_1 \right\} - \\
&\quad - 4(A\psi)^2 \frac{E^2}{K_1^2}.
\end{aligned}$$

Then for the dimensionless concentration, the following expression can be written:

$$c \approx \frac{\sqrt{-\Delta} \operatorname{ch} \left[\zeta \sqrt{a} + \operatorname{Arch} \frac{2ac_0 + b}{\sqrt{-\Delta}} \right] - b}{2a} \quad (29)$$

Entering the concentration at the back surface of the electrode in (29), c_0 can be determined by means of solving the transcendental equation (29) with the boundary condition for $\zeta=1$:

$$c_1 = 1 - \Theta$$

The expression for the dimensionless polarization (21) can then be written in the following form:

$$u \approx \frac{\sqrt{-\Delta} \operatorname{ch} \left[\zeta \sqrt{a} + \operatorname{Arch} \frac{2ac_0 + b}{\sqrt{-\Delta}} \right] - b}{2aK} + \frac{\Omega_{\text{npex}}}{\Theta} \ln(Q' + \sqrt{Q'^2 - B'}) \quad (30)$$

where Q' and B' -- the values of Q and B taking into account the above assumptions.

The distribution of polarization and current through the porous electrode are described by the following expressions:

$$\eta \equiv \frac{RT}{aF} \frac{\Theta}{\Omega_{\text{npex}}} u \approx \frac{RT}{aF} \frac{\Theta}{\Omega_{\text{npex}}} \Theta \times \left\{ \frac{\sqrt{-\Delta} \operatorname{ch} \left[\zeta \sqrt{a} + \operatorname{Arch} \frac{2ac_0 + b}{\sqrt{-\Delta}} \right] - b}{2aK} + \frac{\Omega_{\text{npex}}}{\Theta} \ln(Q' + \sqrt{Q'^2 - B'}) \right\} \quad (31)$$

$$i \equiv \frac{j_0}{A\psi} c \approx \frac{1}{2} \frac{j_0 \sqrt{-\Delta}}{A\psi} \operatorname{ch} \left[\zeta \sqrt{a} + \operatorname{Arch} \frac{2ac_0 + b}{\sqrt{-\Delta}} \right] \quad (32)$$

The obtained solution of the problem, in the closed form, concerning the distribution of intensity of an electrochemical process through a porous electrode

(27) in a diffusion system and the expressions resulting from it (with the given assumptions) for polarization (31) and current (32) present the most difficulty for analysis. Overcoming this difficulty will be studied in subsequent reports.

SYMBOLS

- D_j -- diffusion coefficient of the j -component in the electrolyte
 D_j^e -- effective diffusion coefficient of the j -component in the porous electrode
 d -- coefficient of diffusion dilution at the electrode in comparison with diffusion in the free electrolyte
 ν_j -- stoichiometric coefficient in the j -component of the reaction
 s -- specific surface of the porous electrode
 R_p -- effective resistance of the operating mixture in the pores of the electrode
 n -- number of electrons participating in the reaction
 F -- Faraday's number
 α -- kinetic coefficient of the electrode reaction
 δ -- thickness of the diffusion layer at the frontal surface of the electrode
 Θ -- "charging" coefficient of the electrode
 ξ -- "contamination" coefficient of the reagent with the product of oxidation (reduction)
 $j_0 = j_0^i (c_n^v)^{\alpha/n} (c_p^v)^{1-\alpha/n}$ -- current exchange
 I_0 -- effective value of the current exchange on the porous electrode
 ψ -- variable (first introduced in 11) characterizing the relationship between the transport dilutions in the diffusion layer adjacent to the frontal surface of the electrode and inside the electrode
 Ω_{lim} -- the dissipation capability factor characterizing the relationship between electrode polarizability with a limiting current and the ohmic resistance filling its operating mixture

SUMMARY

The problem is solved on the distribution of the electrochemical process through the depth of a porous electrode of finite thickness under the diffusion con-

[Translator's note: In the preceding translation several Russian letters were used as subscripts and superscripts. Following is a list of those letters and their meanings as used in the text: P--(sub.) solution; P--(super.) equilibrium; (the remaining are subscripts), П--product; M--metal, Э--electrode; лрел--limiting]

BIBLIOGRAPHY

1. Coleman, J. J., Trans. Electrochem. Soc., 90, 545, 1946
2. Coleman, J. J., Journ. Electrochem. Soc., 98, 26, 1951
3. Euler, J. U., and Nonnenmacher, W., Electrochim. Acta, 2, 280, 1960
4. Daniel'-Bek, V. S., Zhurnal Fizicheskoy Khimii (Journal of Physical Chemistry), 22, No 6, 1948
5. Frumkin, A. N., Ibid., No 12, 1949
6. Ksenzhek, O. S., and Stender, V. V., Doklady Akademii Nauk SSSR (Reports of the Academy of Sciences USSR), 106, No 3, 1956
7. Ksenzhek, O. S., and Stender, V. V., Ibid., 107, No 2, 1956
8. Ksenzhek, O. S., and Stender, V. V., Zhurnal Fizicheskoy Khimii (Journal of Physical Chemistry), 31, No 1, 1957
9. Buvet, R., Guillou, M., and Warszawski, B., Electrochim. Acta, 6, 113, 1962
10. Ksenzhek, O. S., Zhurnal Fizicheskoy Khimii (Journal of Physical Chemistry), 36, No 3, 1962
11. Austin, L. G., Symposium on Fuel Cells, Chicago Meeting, Division of Petroleum Chemistry, Am. Chem. Soc., Sep 3-8, 1961
12. Ksenzhek, O. S., Zhurnal Fizicheskoy Khimii (Journal of Physical Chemistry), 36, No 2, 1962
13. Perskaya, R. M., and Zaydenman, I. A., Doklady Akademii Nauk SSSR (Reports of the Academy of Sciences USSR), 115, No 3, 1957
14. Zaydenman, I. A., and Perskaya, R. M., Zhurnal Fizicheskoy Khimii (Journal of Physical Chemistry), 33, No 1, 1959
15. Yusti, E., Pil'kun, M., Shaybe, V., and Vinzel', A., Vysokoaktivnyy vodorodnyy diffuzionnyy elektrod (The Highly Active Hydrogen Diffusion Electrode), Inostrannaya Literatura (Foreign Literature), 1962

16. Urbach, H. B., Symposium on Fuel Cells, Chicago Meeting, Division of Petroleum Chemistry, Am. Chem. Soc., Sep 8-13, 1961
17. Zel'dovich, Ya. B., Zhurnal Fizicheskoy Khimii (Journal of Physical Chemistry), 13, No 2, 1939

6368
GSO: 1880-D

ELECTRICAL ANALOGUE SOLUTION, BY OHMIC RESISTANCE
CIRCUITS, OF THE SYSTEM OF DIFFERENTIAL
EQUATIONS FOR HEAT AND MASS TRANSFER

L. A. Kozdoba

Institute of Naval Engineers, Odessa

A method for the electrical analogue solution, by ohmic resistance circuits, of the system of differential equations for heat and mass transfer is given [1, 2]. The results are compared with the numerical solution of [3].

The system of differential equations of heat and mass transfer in the unidimensional case with transfer coefficients, which depend on temperature t and moisture content u , $\lambda = \lambda(t, u)$ and $a' = a'(t, u)$, has the form [1, 2]:

$$\begin{aligned} \frac{\partial t}{\partial \tau} &= \frac{1}{c \gamma_0} \frac{\partial}{\partial x} \left(\lambda \frac{\partial t}{\partial x} \right) + \frac{e p}{c} \frac{\partial u}{\partial \tau} \\ \frac{\partial u}{\partial \tau} &= \frac{\partial}{\partial x} \left(a' \frac{\partial u}{\partial x} \right) + a' \delta \frac{\partial t}{\partial x} \end{aligned} \quad (1)$$

$0 < x < L.$

In 1, 2, boundary conditions for system (1) were introduced. The boundary conditions for the surface of $x=R$ of the plate (width and length are considerably larger than the thickness $2R$) (Fig. 1, a) with a symmetrical

distribution of temperature and moisture content, relative to the center plane ($x=0$), have the form:

$$-\lambda \left(\frac{\partial t}{\partial x} \right)_{x=R} + a [t_c - t(R, \tau)] + \rho (1-s) q'(\tau) = 0. \quad (2)$$

$$a' \gamma_0 \left(\frac{\partial u}{\partial x} \right)_{x=R} + a' \gamma_0 \delta \left(\frac{\partial t}{\partial x} \right)_{x=R} + q'(\tau) = 0. \quad (3)$$

Similar conditions can be written for the boundary $x=-R$. We shall assume, as in [3], that $a'\delta=0$, and simplify system (1). Then, if to write (1)-(3) in the finite implicit form, it is possible to introduce the expression for the parameters of the ohmic resistance circuits which a solution for temperatures (R^t -circuit) and moisture contents (R^u -circuit). Derivation of the expressions for the parameters of the R^t - and R^u -circuits is similar to the derivation in [4, 5]. For similarity with Kirchhoff's law for circuit junctions, it was necessary to determine the parameters of the R^t -circuit (Fig. 1, b) by the expressions:

$$R_i^t = R_N^t / \lambda_i; \quad (4)$$

$$R_{i,i}^t = \frac{\Delta \tau}{(c \gamma_0)_i h_i^2} R_N^t. \quad (5)$$

$$R_{i,ni}^t = \frac{\Delta V_{ni}^t k' \Delta \tau R_N^t}{(c \gamma_0)_i b_i h_i^2 (u_{i,k-1} - u_{i,n})}. \quad (6)$$

$$R_{a,i}^t = \frac{\lambda_i R_i^t}{a_i h_i}. \quad (7)$$

$$R_p^t = \frac{\Delta V_{ni}^t k' \lambda_i R_i^t}{\rho h_i (1-s) q'}. \quad (8)$$

and the parameters of the R^u -circuit (Fig. 1, c) -- by expressions

$$R_i^u = R_N^u / a_i. \quad (9)$$

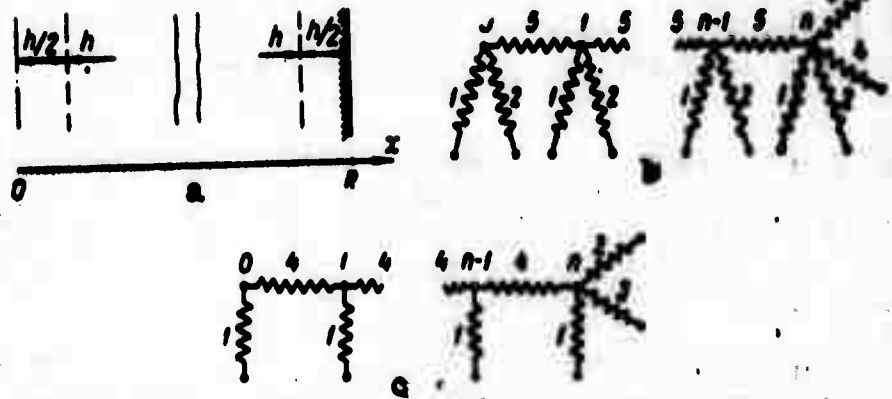


Fig. 1: a--division of the plate into elementary sections for solving the unidimensional symmetrical problem; b-- R^t -circuit: 1--resistors $R_{n,1}^t$, 2--resistors $R_{n,2}^t$, 3-- $R_{n,3}^t$, 4-- $R_{n,4}^t$, 5-- $R_{n,5}^t$. Voltage V_{\min}^t is supplied across the ends of resistors 1; voltage $V_{n,k}^t$ is removed at junctions 0 and n ; and voltages V_0^t and V_{\min}^t are supplied across resistors 3 and 4 respectively; c-- R^u -circuit: 1--resistor $R_{n,1}^u$, 2-- $R_{n,2}^u$, 3-- $R_{n,3}^u$, 4-- $R_{n,4}^u$. Voltages $V_{n,k-1}^u$ are supplied across the ends of resistors 1, $V_{n,k}^u$ is removed at junctions 0 and n ; and V_{\min}^u is removed at 2 and 3. V_0 --voltage simulating t_0 .

$$R_{i,1}^t = \frac{\Delta t}{h^2} R_{N,i}^t \quad (10)$$

$$R_{i,2}^t = \frac{\Delta V_{n,k}^t a_i \gamma_0 R_i^t}{q h_i} \quad (11)$$

$$R_i^u = \frac{\Delta V_{n,k}^u R_i^u}{\delta (t_0 - t_n)_{n-1}} \quad (12)$$

The R^t - and R^u -circuits for solving the unidimensional symmetrical problem are shown in Fig. 1. The space interval in regions $x=0$ and $x=R$ is taken as $h/2$,

the junctions $1, \dots, i$ are located at distances $x=ih$ from the middle ($i=0, 1, \dots, n$).

When the transfer coefficients are taken as constant, expressions (4)-(12) have the form:

$$R^i = R_N^i \quad (4')$$

$$R_c^i = \frac{a \Delta \tau}{h_i^2} R_N^i \quad (5')$$

$$R_{c,n}^i = \frac{a \Delta V_n^i k^i \Delta \tau R_N^i}{(u_{i,k-1} - u_{i,k}) b h_i^2} \quad (6')$$

$$R_a^i = \frac{\lambda R_N^i}{a h_i} \quad (7')$$

$$R_p^i = \frac{\Delta V_n^i k^i \lambda R_N^i}{\rho h_i (1-s) q} \quad (8')$$

$$R^u = R_N^u \quad (9')$$

$$R_c^u = \frac{a' \delta t}{h_i^2} R_N^u \quad (10')$$

$$R_q^u = \frac{\Delta V_n^u k^u a' \tau_0 R_N^u}{q' h_i} \quad (11')$$

$$R_c^u = \frac{\Delta V_n^u k^u}{\delta (t_c - t_n)_{k-1}} R_N^u \quad (12')$$

In the general case, unequal space and time intervals were chosen. Only the accuracy of solution depends on the magnitudes of h and Δt , while convergence and stability are independent of h and Δt , since the solution of finite divergent equations for R-circuits leads to an implicit system [6].

In the same way as in [4, 5], expressions were introduced for calculating the parameters of the R^v - and R^u -circuits for solving the system of equations of heat and mass transfer written in rectangular coordinates (two and three dimensional problems), for the system of equations written in cylindrical or polar coordinates, and for dimensionless equations in any coordinate system.

The method of solving problems of heat and mass transfer by electrical analogues is identical to the method for solving unsteady heat flow problems [4, 5], but the solution is parallel to R^v - and R^u -circuits (Fig. 1).

We shall determine the distribution of u in the m time interval according to the known distribution of u at the $(m-1)$ time interval and by the known boundary conditions at time m . The parameter of the R^u -circuit also depends on $(t_c - t_n)$ at the $(m-1)$ time interval.

After having obtained $(u_{1,k-1} - u_{1,k})$, we determine R_u^v and, according to the known distribution of temperatures and boundary conditions at $(m-1)$, we determine the distribution of temperatures in the m time interval.

It is possible to determine u by the known difference $(t_c - t_n)$ for interval m in the second approximation, however, experiments showed that it is restricted by one approximation.

Since the solution is discreet in space and time, then at each step it is possible to change the parameters of the R^v - and R^u -circuits with space and time in order to calculate the variability of the physical properties of the materials, boundary conditions, etc.

In tables 1 and 2 are presented the results of solving the system of differential equations of heat and mass transfer by electrical analogue for R^v - and R^u -circuits and the results of [3], derived by a numerical method.

The conditions and numerical solution were taken according to [3]. The relative error is

$$\Delta' = \frac{t_{2m} - t_n}{t_c} 100\%; \Delta'' = \frac{u_{2m} - u_n}{u_n} 100\%.$$

Problem: A wall, $2R=0.09$ meters, having an initial temperature $t_n=10^\circ\text{C}$ and an initial moisture content of $u_n=0.27$, was placed in an environment at $t_c=90^\circ\text{C}$.

Table 1. Distribution Temperature in the Wall

Time, hours	Distance from wall center										
	0.0	0.01125			0.0225	0.03375			0.045		
	Elec. anal-ogue	Elec. anal-ogue	Accor-ding to $\sqrt{3}$	Δ' , %	Elec. anal-ogue	Elec. anal-ogue	Accor-ding to $\sqrt{3}$	Δ' , %	Elec. anal-ogue	Accor-ding to $\sqrt{3}$	Δ' , %
0.0	11.0	11.0	10.00	1.11	12.0	14.5	10.00	5.000	17.0	17.345	-0.383
0.2	11.5	12.0	10.00	2.22	13.5	17.5	16.63	0.970	21.0	23.330	-2.590
0.4	14.0	14.5	13.10	1.55	16.5	19.5	19.45	0.055	23.0	25.735	-3.040
0.6	17.4	18.0	16.07	2.14	20.0	22.3	22.11	0.210	26.0	28.095	-2.330
0.8	20.0	20.8	18.90	2.11	22.5	25.0	24.63	0.410	28.0	30.335	-2.590
1.0	23.0	23.7	21.58	2.35	25.0	27.8	27.04	0.840	30.5	32.470	-2.190
1.2	24.9	25.5	24.14	1.51	26.5	29.3	29.32	-0.022	32.3	34.495	-2.440
1.4	27.2	27.8	26.56	1.38	29.0	31.5	31.49	0.011	36.2	36.420	-0.240
1.6	29.4	30.0	28.74	1.40	31.2	34.7	33.67	1.140	34.5	38.355	-4.280
1.8	31.7	32.3	30.92	1.53	33.5	35.8	35.62	0.200	36.2	40.090	-4.320
2.0	33.8	34.5	32.99	3.21	35.5	37.5	37.47	0.033	40.0	41.730	-1.930
2.2	36.0	36.6	34.96	1.82	37.6	39.8	39.23	0.630	42.0	43.295	-1.440
2.4	38.0	38.4	36.83	1.74	39.7	41.2	40.91	0.320	43.5	44.785	-1.430

Table 2. Distribution of Moisture Content in Wall

Time, hours	Distance from wall center										
	0.0	0.01125			0.0225	0.03375			0.045		
	Elec. anal-ogue	Elec. anal-ogue	Accor-ding to $\sqrt{3}$	Δ'' , %	Elec. anal-ogue	Elec. anal-ogue	Accor-ding to $\sqrt{3}$	Δ'' , %	Elec. anal-ogue	Accor-ding to $\sqrt{3}$	Δ'' , %
0.0	0.2700	0.2700	0.270	0	0.263	0.2460	0.270	-8.89	0.1610	0.2425	-30.18
0.2	0.2700	0.2700	0.270	0	0.266	0.2390	0.268	-10.74	0.1790	0.2410	-22.96
0.4	0.2700	0.2700	0.270	0	0.265	0.2410	0.266	-9.26	0.1930	0.2395	-20.93
0.6	0.2700	0.2700	0.270	0	0.261	0.2410	0.264	-8.52	0.2044	0.2375	-12.26
0.8	0.2700	0.2690	0.270	-0.37	0.261	0.2420	0.262	-7.40	0.2140	0.2360	-8.15
1.0	0.2700	0.2680	0.270	-0.74	0.260	0.2440	0.260	-5.92	0.2220	0.2340	-4.44
1.2	0.2690	0.2680	0.270	-0.74	0.259	0.2460	0.258	-4.44	0.2276	0.2325	-1.81
1.4	0.2686	0.2664	0.270	-1.33	0.258	0.2480	0.256	-2.96	0.2326	0.2305	0.78
1.6	0.2680	0.2656	0.269	-1.26	0.258	0.2490	0.255	-2.22	0.2360	0.2300	2.22
1.8	0.2670	0.2646	0.268	-1.26	0.258	0.2494	0.254	-1.70	0.2390	0.2290	3.70
2.0	0.2664	0.2638	0.267	-1.18	0.258	0.2520	0.253	-0.37	0.2400	0.2280	4.44
2.2	0.2656	0.2630	0.266	-1.11	0.257	0.2520	0.252	0	0.2360	0.2275	3.15
2.4	0.2640	0.2625	0.265	-0.92	0.256	0.2500	0.251	-0.37	0.2350	0.2285	3.15

$$\alpha = 10,44 \text{ см} \cdot \text{м}^{-2} \cdot \text{град}^{-1} \text{С}; \lambda = 0,93 \text{ см} \cdot \text{м}^{-1} \cdot \text{град}^{-1} \text{С};$$

$$c = 1,885 \text{ кдж} \cdot \text{кг}^{-1} \cdot \text{град}^{-1} \text{С}; \gamma_0 = 14715 \text{ н} \cdot \text{м}^{-2};$$

$$\rho = 2388,3 \text{ кдж} \cdot \text{кг}^{-1}; \delta = 10^{-3} \text{ н} \cdot \text{м}^{-1} \cdot \text{град}^{-1} \text{С};$$

$$\varepsilon = 0,1; K_i = 0,3; L_u = 0,08;$$

$$a = \lambda/c\gamma = 32,91 \cdot 10^{-6} \text{ м}^2 \cdot \text{сек}^{-1};$$

$$a' = aL_u = 2,63 \cdot 10^{-6} \text{ м}^2 \cdot \text{сек}^{-1};$$

$$q'(\tau) = \frac{a' \gamma_0 \mu_n K_i'}{R} = 6976 \cdot 10^{-4} \text{ н} \cdot \text{м}^{-2} \cdot \text{сек}^{-1};$$

$$b = \frac{q_0}{c} = 126,667^\circ \text{С}.$$

We take $h=0.01125$ meters. Dividing the plate into elementary sections was done according to the diagram in Fig. 1, a. Since the problem is symmetrical, the solution was carried out on half R^t - and R^u -circuits, and u and t were determined at the junctions where $x=0$ (center of plate), 0.01125 , 0.0225 , 0.03375 , and 0.045 meters (surface).

The resistance circuits consisted of class 0.2 variable resistance boxes with integrator charts used as the measuring diagram [7].

The temperature and moisture content of the wall surface ($x=0.045$ meters) were determined according to [3] as the half-sum between values t and u at a given time interval at point $x=0.03375$ meters and at imaginary point $x=0.05625$ meters.

Error in the solution due to $a\delta'=0$ was evaluated in [3].

Results are given in the tables for $\Delta\tau_{\text{exp}}=0.2$ hours. As the initial distribution in the experiment, the distribution of t and u , obtained for the time interval 0.2 hours, was taken which was also the initial distribution used in [3].

Selection of the initial distribution influences magnitudes of error Δ . The initial distribution according to tables 1 and 2 lead to a decrease of in the first steps of the solution in comparison with the initial distribution of [3].

In Fig. 2, the errors Δ^t and Δ^u are given for experiments at $\Delta\tau_{\text{exp}}=0.6$ hours. Increasing the first

step from 0.2 to 0.6 hours leads to an increase of error (compare tables 1 and 2 and Fig. 2).

The initial distribution of t and u in the experiment, the errors are given in Fig. 2, are the same in tables 1 and 2.

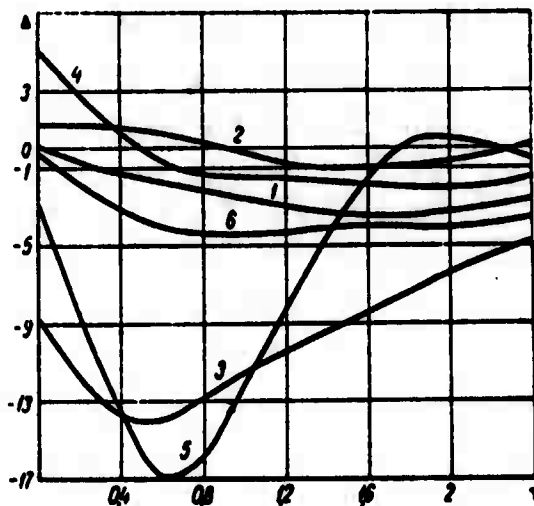


Fig. 2 Change of Δ^u (1, 3, and 5) Δ^t (2, 4, and 6)(%) with time at points at distances from the middle of the plate(meters):
1, 2--0.01125; 3, 4--0.03375;
5, 6--0.045

Relative errors were determined initially from the numerical solution [3] with the step $\Delta\tau=0.2$ hours (tables 1 and 2) with a correction in the first step.

From the tables and Fig. 2 it is evident that the error drops with increasing number of steps in time and after 5-6 steps is comparatively small.

By the corresponding selection of the initial distribution (similar correction introduced in the first steps of the numerical solution [8]), by the decrease of the time intervals in the first steps of the solution, and by the decrease of space intervals in the zones of sudden drop of t and u can reduce maximum errors and obtain time-interval errors not exceeding 2-3%.

In such a manner, electrical analogues of ohmic resistance circuits can successfully be used to solve the system of differential equations of heat and mass

transfer. The error, in comparison with the numerical solution after 5-6 steps in time, is small and sufficiently accurate for engineering practice.

SYMBOLS

- R^u -- electrical resistance of the circuit for determining moisture content (R^u -circuit)
 R^t -- electrical resistance of the circuit for determining temperature (R^t -circuit)
 R_N -- standard R-circuit resistor
-- interval of time $\tau = (\tau = 0, 1, 2, \dots)$
 ΔV_M -- greatest voltage drop (when determining u and t in a drying process, V_M is the minimum voltage)
 k -- factor for transposing from analogue parameters to voltages
 \mathcal{M} -- electrical analogue
 \mathcal{N} -- numerical
 C -- environment
 H -- initial

SUMMARY

The paper presents expression for calculation of parameters of ohmic resistance circuits in the system of differential equations of heat and mass transfer at variable physical parameters (1, 2).

The results of solving the test problem (3) (tables 1, 2 and Fig. 2) show that this method is sufficiently accurate for engineering practice.

BIBLIOGRAPHY

1. Lykov, A. V., Yavleniya perenosa v kapillyarno-poristykh telakh (The Phenomena of Transfer in Capillary-Porous Bodies), GITIL, 1954
2. Lykov, A. V., Teplo- i massobmen v protsessakh sushki (Heat and Mass Transfer in Drying Processes), Gosenergoizdat, 1956.
3. Yushkov, P. P., Works of the Institute of Power Engineering, Academy of Sciences, Belorussian SSR, No 10, published by the Academy of Sciences, Belorussian SSR, Minsk, 1959
4. Kozdoba, L. A., Inshenerno-fizicheskiy Zhurnal (Journal of Engineering Physics)
5. Kozdoba, L. A., "Reports of the Schools of Higher Learning," Energetika (Power Engineering), No 2, 1960
6. Beresin, I. S., and Zhidkov, N. P., Metody Vychisleniy (Calculation Methods), Vol II, Fizmatgiz, 1960
7. Fil'chakov, P. F., and Panchishin, V. I., Integratory (Integrators), EGDA, published by the Academy of Sciences, Ukrainian SSR, Kiev, 1961
8. Yushkov, P. P., Ibid. 3, No VI, published by the Academy of Sciences, Belorussian SSR, Minsk, 1958

6368

CSO: 1880-D

**TRANSITIONAL HEAT CONDUCTIVITY IN MULTI-LAYERED MEDIA. II.
DOUBLE-LAYERED SYSTEMS AND THE DETERMINATION OF
MINIMUM HEATING TIME FOR A SYSTEM OF A GIVEN
HEAT CAPACITY**

I. S. Zaydenman and G. F. Muchnik

The method is examined for the solution of contact problems with the breaking coefficient (Part I) is use for the solution of the "internal problems" for double-layered flat systems.

The differential equation for heat conductivity for the first and second layers is:

$$\frac{\partial t_1}{\partial \tau} = a_1 \frac{\partial^2 t_1}{\partial x^2}, \quad \frac{\partial t_2}{\partial \tau} = a_2 \frac{\partial^2 t_2}{\partial x^2}. \quad (1)$$

Limiting conditions (the problem is solved for the case of adiabatic partitions) are:

$$\lambda_1 \frac{\partial t_1}{\partial x} \Big|_{x=0} = 0; \quad (2)$$

$$t_1|_{x=x_1} = t_2|_{x=x_1}; \quad \frac{\partial t_1}{\partial x} \Big|_{x=x_1} =$$

$$= -\frac{\lambda_2}{\lambda_1} \frac{\partial t_2}{\partial x} \Big|_{x=x_1}; \quad (3)$$

$$\lambda_2 \frac{\partial t_2}{\partial x} \Big|_{x=x_2} = 0. \quad (4)$$

Initial conditions (fig. 1):

$$t_1(0, x) = t_0; \quad t_2(0, x) = 0. \quad (5)$$

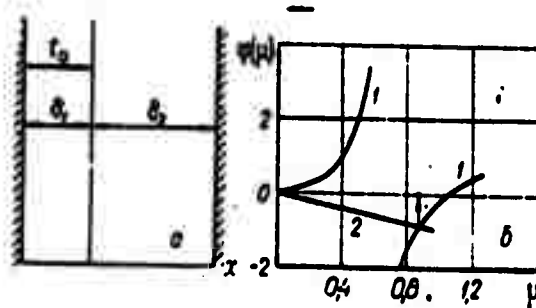


Fig. 1. Double-layered system: a- statement of the problem; b- determination of the first root of the characteristic equation:

$$1 - \text{tg} \mu_2 K_2'; 2 - \text{tg} \mu_1$$

Solution for separate layers:

$$t_1 = t_{\text{TERM}} + t_0 \sum_{i=1}^{\infty} \frac{2K_2 \sin \mu_{2i} \cos \mu_{1i} x \exp(-\mu_{2i}^2 \tau)}{\mu_{1i} (l \sin \mu_{1i} \sin \mu_{2i} - n \cos \mu_{1i} \cos \mu_{2i})}, \quad (6)$$

$$t_2 = t_{\text{TERM}} - t_0 \sum_{i=1}^{\infty} \frac{2 \sin \mu_{1i} \cos \mu_{2i} (x_2 - x) \exp(-\mu_{1i}^2 \tau)}{\mu_{1i} (l \sin \mu_{1i} \sin \mu_{2i} - n \cos \mu_{1i} \cos \mu_{2i})}, \quad (6a)$$

where

$$\mu_{1i} = \mu_{1i} \frac{\delta_1}{\sqrt{a_1}}; \quad \mu_{2i} = \mu_{1i} \frac{\delta_2}{\sqrt{a_2}};$$

$$l = \frac{\delta_1}{\sqrt{a_1}} K_2 + \frac{\delta_2}{\sqrt{a_2}}; \quad n = \frac{\delta_2}{\sqrt{a_2}} K_2 + \frac{\delta_1}{\sqrt{a_1}}; \quad K_2 = \frac{\sqrt{\lambda_2 c_2}}{\sqrt{\lambda_1 c_1}}.$$

Characteristic equation

$$K_2 \text{tg} \mu_2 = -\text{tg} \mu_1. \quad (6.b)$$

Terminal temperature of the system can be determined from the thermal balance

$$t_0 c_1 \delta_1 = t_{\text{TERM}} (c_1 \delta_1 + c_2 \delta_2), \quad t_{\text{TERM}} = t_0 \frac{c_1 \delta_1}{c_1 \delta_1 + c_2 \delta_2}, \quad (7)$$

because in the common form

$$t_{\text{TERM}} = t_0 \frac{c_1 \delta_1}{\sum_{i=1}^n c_i \delta_i}. \quad (7a)$$

Thermophysical properties of sheets are:

$$c_1 = 1.848 \cdot 10^6 \text{ J} \cdot \text{m}^{-3} \cdot \text{deg}^{-1}, \quad c_2 = 1.512 \cdot 10^6 \text{ J} \cdot \text{m}^{-3} \cdot \text{deg}^{-1},$$

$$a_1 = 1.36 \cdot 10^{-3} \text{ cm}^2 \cdot \text{sec}^{-1}, \quad a_2 = 0.97 \cdot 10^{-3} \text{ cm}^2 \cdot \text{sec}^{-1},$$

$$\lambda_1 = 0.252 \text{ w} \cdot \text{m}^{-1} \cdot \text{deg}^{-1}, \quad \lambda_2 = 0.147 \text{ w} \cdot \text{m}^{-1} \cdot \text{deg}^{-1},$$

$$\rho_1 = 0.03 \text{ cm}, \quad \rho_2 = 0.083 \text{ cm}.$$

From which

$$K_2 = 0.59, \quad \mu_2 = 2.66 \mu_1, \quad \mu_4 = 0.81 \mu_1.$$

Finally

$$l = \frac{0.03}{0.037} 0.59 + \frac{0.0835}{0.0312} = 3.136,$$

$$n = \frac{0.0835}{0.0312} 0.59 + \frac{0.03}{0.037} = 2.39.$$

Characteristic equation

$$0.59 \operatorname{tg}(2.66 \mu) = - \operatorname{tg}(0.81 \mu).$$

First root (fig. 1)

$$\mu_1 = 0.83,$$

$$\frac{l}{T \sqrt{a_1}} = 480^\circ \text{C}, \quad t_0 = 1700^\circ \text{C},$$

$$t_2 = 480 - 1700 \sum_{i=1}^{\infty} \varphi(\mu_i) \cos \mu_{2i}(x_2 - x) \exp(-\mu_i^2 \tau).$$

With a sufficiently large time period T , all terms of the series except the first can be ignored inasmuch as the row is rapidly fading.

Then $\varphi(\mu_1) = 0.555$,

$$t_2 = 480 - 1700 \cdot 0.555 \cdot \cos \mu_{21}(x_2 - x) \exp(-0.83^2 \tau).$$

With

$$x = x_2, \quad t_2 = 480 - 945 \exp(-0.69 \tau).$$

It often is required to determine the time necessary for warming up the extreme right layer to the temperature \bar{t} . This time can be

obtained from (6.a):

$$\tau(\bar{t}) = - \frac{2,303 \lg [\Theta/\varphi(\mu_1)]}{\mu_1} \quad (8)$$

Let us examine a double-layered system surrounded by adiabatic partitions, the retention capability of which is constant. This means that $c_1 \delta_1 + c_2 \delta_2 = \text{const}$. With $\mu = \text{const}$ and $\bar{t} = \text{const}$,

this leads to

$$c_1 \delta_1 = \text{const}, \quad c_2 \delta_2 = \text{const} \quad (9)$$

For such a system, time $\tau(\bar{t})$ possesses the following properties:

1. τ increases k times if: a) λ_1 and λ_2 are reduced k times; b) δ_1 and δ_2 are increased k times; c) the proportion δ_1/λ_1 is increased k times. In particular, τ becomes zero if δ_1/λ_1 and δ_2/λ_2 become zero.

2. τ does not depend on δ_1 if the corresponding $\lambda_1 \rightarrow \infty$ and, conversely on λ_1 if the corresponding $\delta_1 \rightarrow 0$.

On the basis of properties 1 and 2, it can be concluded that $\tau(\bar{t})$ is a homogeneous function of the first degree with respect to δ_1/λ_1 i.e.,

$$\tau(\bar{t}) = b_1 \frac{\delta_1}{\lambda_1} + b_2 \frac{\delta_2}{\lambda_2}, \quad (9.a)$$

where b_1 and b_2 are constant with respect to δ_1 and λ_1 .

We stress again that formula (9.a) holds true only when observing conditions (9). Actually, in the general case the warmingup process (cooling process) is determined by the Fourier criterium

$Fo = a\tau/\delta_2$, which can be easily shown if equation (1) is written

in dimensionless form

$$\frac{d\bar{\theta}}{dFo} = \frac{d^2\bar{\theta}}{dX^2}; \quad \bar{\theta} = f(Fo, X); \quad X = \frac{x}{\delta}.$$

For multilayered systems, as will be shown below in the example of the four-layered system, the conditions of similarity also hold true in observing the constancy of the criterion Fo , i.e., the reduction of all a_i by n times leads to an increase (τ) by n times, and a reduction of \int_1 (of all layers simultaneously) --- to the reduction τ ($\bar{\tau}$) by n^2 times.

However, with $c_1 \int_1 = \text{const}$ and $c_2 \int_2 = \text{const}$

$$Fo_1 = \frac{\lambda_1}{(c_1 \delta_1) \delta_1} \tau = A_1 \frac{\lambda_1}{\delta_1} \tau, \quad Fo_2 = \frac{\lambda_2}{(c_2 \delta_2) \delta_2} \tau = A_2 \frac{\lambda_2}{\delta_2} \tau,$$

i.e., hold true (9.a).

The solution of the problem for a two-layered system can be used for the solution of its own type of limiting problem -- determination of the minimum time necessary for the "extraction" from the first sheet of a certain amount of heat by means of contacting this sheet with a body "equivalent" to the remaining layers, which possesses the total terminal heat capacity $c_2 \int_2$ and the infinite heat con-

ductivity (the case of the infinite heat capacity of a body leads to the known problem of the first series with a zero limiting temperature). The thermal contact at the edge of the sheet is considered ideal. This problem, of course, can also be solved independently if we place as the second limiting condition

$$-\lambda_1 \frac{d\theta_1}{dx} \Big|_{x=\delta_1} = \bar{c}_2 \frac{d\theta_2}{d\tau}$$

or take a thermal balance equivalent to it

$$t_2(\bar{c}_2 \delta_2) = t_0 c_1 \delta_1 - c_1 \int_0^{\delta_1} t_1(x, \tau) dx.$$

However, we will immediately obtain the solution of this limiting problem as a separate case in the solution of the two-layered system.

As a matter of fact, from (9.a) with $\lambda_2 \rightarrow \infty$ we find

$$\tau(\bar{l}) = b_1 \frac{\delta_1}{\lambda_1} = \tau_{\min}. \quad (9.b)$$

This also is the sought minimum time necessary for the extraction of a specified amount of heat from the first sheet. For any system, consisting of N sheets, τ_{\min} will also determine the limiting

boundary, in which case we should take for the heat capacity of the second layer ($c_2 \delta_2$) in this case some equivalent heat capacity of the system

$$\left(\bar{c}_2 \delta_2 = \sum_{i=2}^N c_i \delta_i \right).$$

The overall solution of the limiting problem has the following form

$$t = t_{\text{TRM}} - t_0 \sum_{n=1}^{\infty} \frac{2 \cos \left(\mu_n \frac{x}{\delta_1} \right) \exp \left(-\mu_n^2 \frac{a_1 \tau}{\delta_1^2} \right)}{-\mu_n \sin \mu_n + [c_1 \delta_1 / c_2 \delta_2 + 1] \cos \mu_n}. \quad (9.c)$$

The characteristic equation

$$\operatorname{tg} \mu_n = -\mu_n \frac{c_2 \delta_2}{c_1 \delta_1}. \quad (9.d)$$

The series (9.c) quickly converges and, beginning with a specified $Fo = (Fo)_{\text{limiting}}$, all its terms become small in comparison to the

first.

Then

$$t = t_{\text{TRM}} - t_0 \frac{2 \cos \left(\mu_1 \frac{x}{\delta_1} \right) \exp \left(-\mu_1^2 \frac{a_1 \tau}{\delta_1^2} \right)}{-\mu_1 \sin \mu_1 + [c_1 \delta_1 / c_2 \delta_2 + 1] \cos \mu_1}. \quad (9.e)$$

For small values of Fo , the representation with $x = \delta_1$ can be written

$$T = \frac{t_0}{s} - \frac{t_0}{s[1 + b/\sqrt{s}]},$$

the original of which is

$$t(\delta_1, \tau) = t_0 - t_0 \exp(b^2 \tau) \operatorname{erfc}(b\sqrt{\tau}). \quad (9.f)$$

where $b = \sqrt{a_1 c_1 / c_2} \int_2$; $\operatorname{erfc} = 1 - \operatorname{erf}$; erf is a function of errors

For the comparison and evaluation of the formulas obtained above, the limiting problem was solved by the numerical method of terminal differences.

The basic equation and extreme conditions in the terminal differences can be presented in the form:

$$t_{m+1,n} = \frac{1}{\rho} t_{m,n-1} + \frac{\rho-2}{\rho} t_{m,n} + \frac{1}{\rho} t_{m,n+1}, \quad (10)$$

where $\frac{1}{\rho} = \frac{a_1 \Delta \tau}{(\Delta x)^2}$;

$$t_{0,0} = t_{0,1} = \dots = t_{0,N} = t_0; \quad (10.a)$$

$$t_{0,11} = t_{0,cr} = 0; \quad (10.b)$$

$$t_{m,0} = t_{m,1}; \quad (10.c)$$

$$t_{m+1,11} - t_{m,11} = k(t_{m,N} - t_{m,N+1}); \quad k = \frac{\lambda_1 \Delta \tau}{c_2 \delta_2 \Delta x}. \quad (10.d)$$

As can be seen from equations (10.c) and (10.d), for calculating temperature, two "zero" layers are introduced -- one, located to the left of the first layer (with index $n = 0$), and the other to the right of the last layer (with index $n = N+1$) at a distance of $\Delta x/2$ from the partition. These layers permit satisfying the limiting conditions of the mission.

The temperature of the partitions (i.e., points $x = \int_1$) is:

$$t_{m,cr} = \frac{t_{m,N+1} + t_{m,N}}{2} = t_{m,11}.$$

From which

$$t_{m,N+1} = 2t_{m,11} - t_{m,N}. \quad (11)$$

With the help of the relationship (11), the temperature of the layer ($N+1$) is determined. The temperature of the left zero layer is determined from the relationship (10.c). Substituting (11) in (10.d) we find

$$t_{m+1,11} = (1 - 2k)t_{m,11} + 2kt_{m,1}. \quad (11.a)$$

The solution has a physical significance (it does not violate the second law of thermodynamics) with $1-2k > 0$, i.e., $k < \frac{1}{2}$.

For the modulus p in equation (10), a value greater than 2 or equal to 2 should be taken. However, in the latter case, the points obtained from the solution will fluctuate about the true values, which is why it is recommended that $p=3$ be taken.

The calculation is made with the use of subsequent operations:

a) The temperature of the layer (N+1) is determined

$$t_{0, N+1} = 2t_{0, II} - t_{0, N}.$$

With

$$t_{0, II} = 0 \quad t_{0, N+1} = -t_{0, N};$$

b) The temperature of the inner sheet is determined, including the Nth layer by the formula

$$t_{1, n} = \frac{1}{3} (t_{0, n-1} + t_{0, n} + t_{0, n+1})$$

etc.

c) From the found values $t_{m, I}$ and $t_{m, II}$, $t_{m+1, II}$ is determined.

In this, $t_{m, II}$ is found from (11).

If $t_{0, II} = 0$, $t_{1, II} = 2kt_{0, I}$. The interval $\Delta \tau$ with $p = 3$

$$\Delta \tau = \frac{(\Delta x)^2}{3a}. \quad (11b)$$

Solution (11.a) can be broken into two components:

$$t_{m+1, II} = \Theta_1 + \Theta_2.$$

As the calculations show, the value Θ_2 assumes a stable value quite rapidly.

The temperature of the limit $t_{m+1, II}$ in this case can be found from the formula for the sum of the series (geometric progression) with the initial term Θ_2 and the denominator $(1-2k)$:

$$t_{m+1, II} = (1-2k)^m t_{0, II} + \Theta_2 \frac{1 - (1-2k)^m}{2k}. \quad (11.c)$$

It is recommended to take as t_0 the temperature of the boundary at some time interval m_0 after the start of the process (for example, $m_0 = 10$), and for θ_2 -- the average value between θ_2, m_0 and θ_2, term , where $\theta_2, \text{term} = 2 kt_{\text{term}}$.

Thus, with $m_0 = 10$, $t_{0, \text{II}} = 208.4^\circ\text{C}$, $\theta_2 = 19.7^\circ\text{C}$ from the accurate calculation $t_{41, \text{II}} = 376.5^\circ$, and from the formula (11.c) $t_{41, \text{II}} = 382.0^\circ\text{C}$. The error is 1.5%.

Figure 2 presents a comparison of the data for computation of the temperature of the partition of the second sheet obtained with the use of the operation and numerical methods of calculation, the convergence is sufficiently satisfactory.

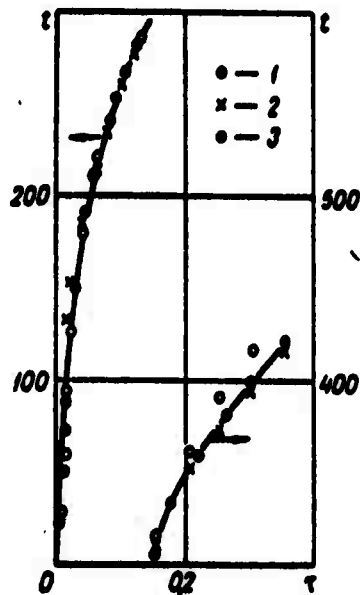


Figure 2. Comparison of calculation methods. 1- function of erf; 2- solution with the first term of the series; 3- numerical method.

From the drawing, it can be seen that with 0.05 seconds, formula (9.e)

should not be used, and with 0.15 seconds, formula (9.f) provides an error.

From (9.e) it can be determined

$$\tau_{\min} = \frac{2,303 \lg [\theta/\varphi(\mu_1)]}{\mu_1^2 a_1} z_1^2 \quad (12)$$

where

$$\varphi(\mu_1) = \frac{2 \cos \mu_1}{-\mu_1 \sin \mu_1 + \cos \mu_1 \cdot (1 + c_1 b/c_2 z_1)}$$

The values μ_1 and $\varphi(\mu_1)$ are presented in the table. With

$$c_1 \delta_1 = \text{const}$$

$$\tau_{\min} = - \frac{2,303 \lg |\Theta/\tau(\mu_1)|}{\mu_1^2} \frac{(c_1 \delta_1)^2}{\lambda_1} = b \frac{\delta_1}{\lambda_1},$$

which was noted above.

TABLE

Roots of the Characteristic Equation $\mu = -\mu c_2 \delta_2 / c_1 \lambda_1$ and functions $\varphi(\mu_1)$

$c_2 \delta_2 / c_1 \lambda_1$	μ_1	μ_2	μ_3	μ_4	$\varphi(\mu_1)$
20,00	1,60	4,720	7,860	11,00	0,036
15,00	1,61	4,725	7,865	11,00	0,047
10,00	1,63	4,730	7,870	11,00	0,070
7,50	1,65	4,740	7,875	11,00	0,091
5,00	1,69	4,750	7,880	11,01	0,131
3,75	1,72	4,765	7,890	11,02	0,158
2,50	1,79	4,790	7,900	11,03	0,213
1,50	1,90	4,850	7,930	11,05	0,277
1,25	1,96	4,870	7,950	11,07	0,304
0,75	2,11	4,970	9,010	11,10	0,342
0,50	2,29	5,080	8,095	11,17	0,357

Figure 3 shows data from the calculation with various terminal temperatures of the system, $\delta_1 = 0.03$ cm, $c_1 = 1.848 \cdot 10^6 \text{ J} \cdot \text{m}^{-3} \cdot \text{deg}^{-1}$,

$c_2 \delta_2 = 0.0125 \cdot 10^5 \text{ J} \cdot \text{m}^{-2} \cdot \text{deg}^{-1}$. (next page)

The curves obtained are the limiting curves for the multi-layered system with those c_1 and δ_1 and possessing the same retention capability c_2 and $\delta_2 = 0.033 \text{ cal} (\text{cm}^2 \cdot ^\circ\text{C})^{-1}$.

The results of the calculation $\tau(\bar{t})$ according to formula (9.a) are presented in figure 4. (next page)

As can be seen from the figure, all calculating points are well-plotted on straight lines, in which respect in all cases $b_2 = \text{const}$.

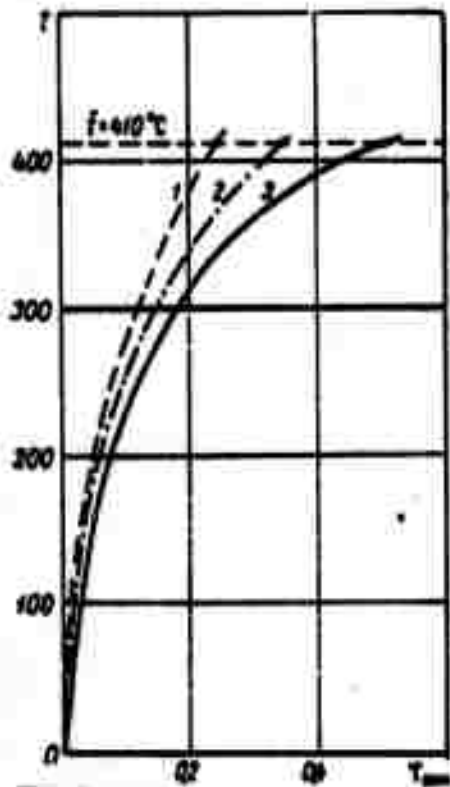


Fig. 3. Minimum time of heating the system:
 1- $t_{\text{term}}=530^{\circ}$, $t_0=1850^{\circ}\text{C}$; 2- $t_{\text{term}}=480^{\circ}\text{C}$, $t_0=1700^{\circ}\text{C}$; 3- $t_{\text{term}}=430^{\circ}\text{C}$, $t_0=1500^{\circ}\text{C}$

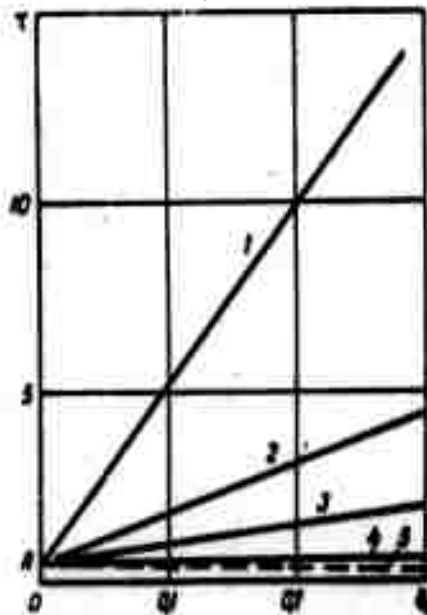


Fig. 4. Dependence of warming-up time τ (sec) of the system on the thickness of partition of the second sheet f_2 (cm) and coefficient of heat conductivity; 1-4 - λ_2 respectively equal to 0.126; 0.42; 0.84; 8.4 ($\text{W}\cdot\text{m}^{-1}\cdot\text{deg}^{-1}$); 5- for $\lambda_2 = \infty$

Symbols

t_{term} -- terminal temperature of the system; μ_1 -- root of the characteristic equation; δ_1, δ_2 -- thicknesses of layers; $\lambda_1, \lambda_2, c_1, c_2$ -- coefficients of heat conductivity and heat capacity of the layers; $\theta = t_{\text{term}} - \bar{t}$ -- dimensionless temperature; $\Delta \tau, \Delta x$ -- pulsating interval in time and space; m -- time index; n -- space; t_{II} -- temperature of a body with infinite heat conductivity.

Summary

By means of a general method, presented in Part I for some multilayer systems, the unsteady temperature field of each component of a two-layer adiabatic system with internal heat sources in one of the layers is found and analyzed. A minimum time required for heating such a system to the prescribed temperature is estimated both by the analytical and numerical methods. The exact solutions are given in the final form.

6367

CSO: 1880-D

ON THE HEAT CONDUCTIVITY OF AN UNLIMITED FLAT WALL

A. F. Khrustalev
Sevastopol Branch, Odessa Polytechnic Institute,
Sevastopol

A method is recommended for the three-dimensional stationary temperature field of an unlimited flat wall, half immersed in a heat-giving medium, while its other half gives off heat in a heat-sensitive medium.

We are designating the relative coefficient of heat exchange between the heat giving medium, the temperature of which changes only in the direction of the x-axis according to the law $T_1 = f(x)$, and the wall through h_0 , and the relative coefficient of

heat exchange between the wall and the heat-sensitive medium through h . We take the temperature of the heat-sensitive layer as equal to zero.

In such a formulation, the solution consists of the determination of the function $T(x, y, z)$ satisfying the Laplace equation

$$\frac{d^2 T}{dx^2} + \frac{d^2 T}{dy^2} + \frac{d^2 T}{dz^2} = 0 \quad (1)$$

and the limiting conditions

$$\pm \frac{dT}{dy} + hT = 0 \quad \text{where } y = \pm b, |x| < \infty, 0 < z < +\infty; \quad (2)$$

$$\pm \frac{dT}{dy} + h_0 T = h_0 f(x) \quad \text{where } y = \pm b, |x| < \infty, -\infty < z < 0. \quad (3)$$

With respect to the function $f(x)$, we assume that it can be represented in the interval $(-\infty, +\infty)$ by the cone-integral of Fourier, i.e.,

$$f(x) = \int_{-\infty}^{+\infty} A(\beta) \cos \beta x d\beta, \quad A(\beta) = \frac{1}{\pi} \int_{-\infty}^{+\infty} f(v) \cos \beta v dv. \quad (4)$$

We note that the case of a two-dimensional stationary temperature field of a flat wall which corresponds to $f(x) = \text{const}$ is examined in [3].

It is not difficult to verify that the function

$$T = \frac{1}{b} \int_{-\infty}^{+\infty} \cos \beta x d\beta \int_{-\infty}^{0-i\infty} B(u, \beta) \cos(\sqrt{u^2 - \beta^2 b^2} \rho) \exp(uv) du, \quad (5)$$

in which $y = \rho b$, $z = vb$, $B(u, \beta)$ is the arbitrary function of the effective parameter β and the complex parameter u , and the contour

of integration represents the entire simulated axis with the diversion of the origin of the coordinates in accordance with the hour hand and satisfies equation (1). It remains to satisfy conditions (2) and (3) which, on the basis of (5) with $\rho = 1$ respectively take the form:

$$\int_{-\infty}^{+\infty} \cos \beta x d\beta \int_{-\infty}^{0-i\infty} K(u, \beta) \exp(uv) du = 0 \quad \text{for } v > 0; \quad (6)$$

$$\int_{-\infty}^{+\infty} \cos \beta x d\beta \int_{-\infty}^{0-i\infty} \psi(u, \beta) \exp(uv) du = h_0 f(x) \quad \text{for } v < 0. \quad (7)$$

Here

$$K(u, \beta) = \frac{B(u, \beta)}{b^2} (hb \cos \sqrt{u^2 - \beta^2 b^2} - \sqrt{u^2 - \beta^2 b^2} \sin \sqrt{u^2 - \beta^2 b^2});$$

$$\psi(u, \beta) = K(u, \beta) \frac{h_0 b \cos \sqrt{u^2 - \beta^2 b^2} - \sqrt{u^2 - \beta^2 b^2} \sin \sqrt{u^2 - \beta^2 b^2}}{hb \cos \sqrt{u^2 - \beta^2 b^2} - \sqrt{u^2 - \beta^2 b^2} \sin \sqrt{u^2 - \beta^2 b^2}}.$$

Conditions (6) and (7) will be satisfied if

$$\int_{-i\infty}^{0-i+\infty} K(u, \beta) \exp(u, v) du = 0, v > 0; \quad (8)$$

$$\int_{-i\infty}^{0-i+\infty} \psi(u, \beta) \exp(uv) du = h_0 A(\beta), v < 0, \quad (9)$$

because having multiplied both parts of the equality (8) and (9) by $\cos \beta x$ and integrating by β from $-\infty$ to $+\infty$ with consideration of (4) we come respectively to equalities (6) and (7)

The paired integral equations (8) and (9) will be satisfied if $K(u, \beta)$ is regular in the range $\text{Re}(u) \leq 0, u \neq 0$, and

$\psi(u, \beta)$ is regular in the range $\text{Re}(u) > 0, u \neq 0$, and if these functions satisfy the requirements of the Jordan lemma in the corresponding ranges.

At the origin of coordinates $\psi(u, \beta)$, there should be a simple pole with the residue

$$\text{res } \psi(u, \beta) |_{u=0} = -\frac{h_0 A(\beta)}{2\pi i}$$

therefore

$$\text{res } K(u, \beta) |_{u=0} = -\frac{h_0 a(\beta) A(\beta)}{2\pi i}$$

$$a(\beta) = \frac{hb \text{ch } \beta b + \beta b \text{sh } \beta b}{h_0 b \text{ch } \beta b + \beta b \text{sh } \beta b}$$

For the construction $K(u, \beta)$, following [1 - 4], we form the infinitive product

$$\Pi(u, \beta) = \prod_{k=1}^{\infty} \frac{1 - u/a_k}{1 - u/b_k} \quad (10)$$

where a_k is the positive root of the equation

$$hb \cos \sqrt{u^2 - \beta^2 b^2} - \sqrt{u^2 - \beta^2 b^2} \sin \sqrt{u^2 - \beta^2 b^2} = 0, \quad (11)$$

and b_k is the positive root of the equation

$$h_0 b \cos \sqrt{u^2 - \beta^2 b^2} - \sqrt{u^2 - \beta^2 b^2} \sin \sqrt{u^2 - \beta^2 b^2} = 0, \quad (12)$$

in which $\Pi(u, \beta) = \frac{1}{\sqrt{a(\beta)}}$ for sufficiently large $|u|$ in the range

$$0 < \delta < \arg u < 2\pi - \delta.$$

Now, it is clear that

$$K(u, \beta) = -\frac{h_0 A(\beta)}{2\pi i} a(\beta) \frac{\Pi(u, \beta)}{u}, \quad (13)$$

and the functions

$$\begin{aligned} T &= -\frac{bh_0}{2\pi i} \int_{-\infty}^{+\infty} a(\beta) A(\beta) \cos \beta x d\beta \times \\ &\times \int_{-i\infty}^{0-i} \frac{\Pi(u, \beta) \cos(\sqrt{u^2 - \beta^2 b^2}) \rho \exp(iu) du}{u (hb \cos \sqrt{u^2 - \beta^2 b^2} - \sqrt{u^2 - \beta^2 b^2} \sin \sqrt{u^2 - \beta^2 b^2})} \\ &= -\frac{bh_0}{\pi} \int_{-\infty}^{+\infty} a(\beta) A(\beta) \cos \beta x d\beta \times \\ &\times \int_0^{\infty} \frac{\text{Im}[\Pi(in, \beta) \exp(iun)] \text{ch}(\sqrt{n^2 + \beta^2 b^2}) dn}{n (hb \text{ch} \sqrt{n^2 + \beta^2 b^2} + \sqrt{n^2 + \beta^2 b^2} \sin \sqrt{n^2 + \beta^2 b^2})} + \\ &+ \frac{bh_0}{2} \int_{-\infty}^{+\infty} \frac{A(\beta) \text{ch} \beta b \rho \text{ch} \beta x d\beta}{h_0 b \text{ch} \beta b + \beta b \text{sh} \beta b} \end{aligned} \quad (14)$$

satisfies equation (1) and the limiting conditions (2) and (3).

By the method presented in [1] → [3], we find the limiting value T and $\frac{dT}{dy}$ with $y \rightarrow \pm 0$, $\rho = 1$, and we also determine

the response T with $\rightarrow \pm \infty$:

$$\lim_{v \rightarrow \pm 0, \rho = \pm 1} T = \frac{h_0}{h - h_0} \int_{-\infty}^{+\infty} A(\beta) (\sqrt{a(\beta)} - 1) \cos \beta x d\beta.$$

$$\lim_{v \rightarrow \pm 0, \rho = \pm 1} \left[\pm \frac{dT}{dy} \right] = \frac{h_0}{h - h_0} \int_{-\infty}^{+\infty} A(\beta) (h - h_0 \sqrt{a(\beta)}) \cos \beta x d\beta.$$

$$\lim_{v \rightarrow \pm 0, \rho = \pm 1} \left[\pm \frac{dT}{dy} \right] = \frac{hh_0}{h - h_0} \int_{-\infty}^{+\infty} A(\beta) (1 - \sqrt{a(\beta)}) \cos \beta x d\beta.$$

$$\lim_{v \rightarrow +\infty} T = 0, \quad \lim_{v \rightarrow -\infty} T = bh_0 \int_{-\infty}^{+\infty} \frac{A(\beta) \operatorname{ch} \beta b \rho \cos \beta x d\beta}{h_0 b \operatorname{ch} \beta b + \beta b \operatorname{sh} \beta b}.$$

Let us examine another three-dimensional stationary temperature field of an unlimited flat wall with mixed limiting conditions:

$$\alpha T - \lambda \frac{dT}{dz} = 0 \quad \text{where } y = 0, \quad |x| < \infty, \quad |z| < \infty; \quad (15)$$

$$\frac{dT}{dy} + hT = 0 \quad \text{where } y = b, \quad |x| < \infty, \quad 0 < z < +\infty; \quad (16)$$

$$\frac{dT}{dy} + h_0 T = h_0 f(x) \quad \text{where } y = b, \quad |x| < \infty, \quad -\infty < z < 0. \quad (17)$$

With respect to the function $f(x)$ it is assumed that the expansion (4) is applicable.

The solution consists of determining the function $T(x, y, z)$ which satisfies equation (1) and the limiting conditions (15) - (17).

It is easy to be convinced that the function

$$T = \frac{1}{b} \int_{-\infty}^{+\infty} \cos \beta x d\beta \int_{-\infty}^{+\infty} B_1(u, \beta) \left[\cos \sqrt{u^2 - \beta^2} z \rho + \right.$$

$$\left. + \frac{ab \sin \sqrt{u^2 - \beta^2 b^2} \rho}{\lambda \sqrt{u^2 - \beta^2 b^2}} \right] \exp(uv) du \quad (18)$$

satisfies equation (1) and condition (15). It remains to satisfy conditions (16) and (17) which, on the basis of (18) assume the form:

$$\int_{-\infty}^{+\infty} \cos \beta x d\beta \int_{-i\infty}^{0-i\infty} K_1(u, \beta) \exp(uv) du = 0 \text{ where } \rho = 1, v > 0; \quad (19)$$

$$\int_{-\infty}^{+\infty} \cos \beta x d\beta \int_{-i\infty}^{0-i\infty} \phi_1(u, \beta) \exp(uv) du = h_0 f(x) \text{ where } \rho = 1, v < 0. \quad (20)$$

Here

$$K_1(u, \beta) = \frac{B_1(u, \beta) \varphi_1(u, \beta)}{\lambda b^2 \sqrt{u^2 - \beta^2 b^2}}$$

$$\begin{aligned} \varphi_1(u, \beta) = & hb^2 a \sin \sqrt{u^2 - \beta^2 b^2} + \lambda bh \sqrt{u^2 - \beta^2 b^2} \cos \sqrt{u^2 - \beta^2 b^2} + \\ & + ab \sqrt{u^2 - \beta^2 b^2} \cos \sqrt{u^2 - \beta^2 b^2} - \lambda (u^2 - \beta^2 b^2) \sin \sqrt{u^2 - \beta^2 b^2}; \end{aligned}$$

$$\phi_1(u, \beta) = \frac{\varphi_2(u, \beta)}{\varphi_1(u, \beta)} K_1(u, \beta);$$

$$\begin{aligned} \varphi_2(u, \beta) = & h_0 b^2 a \sin \sqrt{u^2 - \beta^2 b^2} + \lambda bh_0 \sqrt{u^2 - \beta^2 b^2} \cos \sqrt{u^2 - \beta^2 b^2} + \\ & + ab \sqrt{u^2 - \beta^2 b^2} \cos \sqrt{u^2 - \beta^2 b^2} - \lambda (u^2 - \beta^2 b^2) \sin \sqrt{u^2 - \beta^2 b^2}. \end{aligned}$$

As before, we find that

$$K_1(u, \beta) = - \frac{h_0 A(\beta) \varphi_1(0, \beta) \Pi_1(u, \beta)}{2\pi i \varphi_2(0, \beta) u}$$

where

$$\frac{\varphi_1(0, \beta)}{\varphi_2(0, \beta)} = \frac{ah \operatorname{sh} \beta b + \lambda h \beta \operatorname{ch} \beta b + ab \operatorname{ch} \beta b + \lambda \beta^2 \operatorname{sh} \beta b}{ah_0 \operatorname{sh} \beta b + \lambda h_0 \beta \operatorname{ch} \beta b + ab \operatorname{ch} \beta b + \lambda \beta^2 \operatorname{sh} \beta b};$$

$$\Pi_1(u, \beta) = \prod_{k=1}^{\infty} \frac{1 - u/a_k}{1 - u/b_k};$$

a_k and b_k are positive roots of the equation $\varphi(u, \beta) = 0$ and $\varphi_2(u, \beta) = 0$,
 in which $\Pi_1(u, \beta) = \sqrt{\frac{\varphi_1(0, \beta)}{\varphi_2(0, \beta)}}$ for sufficiently large u in the
 range $0 < \delta < \arg u < 2\pi - \delta$.

Now it is not difficult to establish that the function

$$\begin{aligned}
 T = & -\frac{bh_0}{2\pi i} \int_{-\infty}^{+\infty} \frac{\varphi_1(0, \beta)}{\varphi_2(0, \beta)} A(\beta) \cos \beta x d\beta \times \\
 & \times \int_{-\infty}^{+\infty} [\Pi_1(u, \beta) (\lambda \sqrt{u^2 - \beta^2 b^2} \cos \sqrt{u^2 - \beta^2 b^2} \rho + a b \sin \sqrt{u^2 - \beta^2 b^2} \rho) \times \\
 & \times \exp(uw) du |u \varphi_1(u, \beta)|^{-1} = \frac{h_0 b}{\pi} \int_{-\infty}^{+\infty} \frac{\varphi_1(0, \beta)}{\varphi_2(0, \beta)} A(\beta) \cos \beta x d\beta \times \\
 & \times \int_{-\infty}^{+\infty} \{ \operatorname{Im} [\Pi_1(in, \beta) \exp(inw)] (\lambda \sqrt{n^2 + \beta^2 b^2} \operatorname{ch} \sqrt{n^2 + \beta^2 b^2} \rho + \\
 & + a b \operatorname{sh} \sqrt{n^2 + \beta^2 b^2} \rho) dn | \ln \varphi_1(in, \beta) |^{-1} + \\
 & + \frac{h_0 b^2}{\pi} \int_{-\infty}^{+\infty} \frac{(\lambda b \operatorname{ch} \beta b \rho + a \operatorname{sh} \beta b \rho)}{\varphi_2(0, \beta)} A(\beta) \cos \beta x d\beta. \quad (21)
 \end{aligned}$$

The limiting values T and $\frac{dT}{dy}$ where $v \rightarrow \pm 0$, $\rho = 1$, and also
 the response T where $v \rightarrow +\infty$ has the form:

$$\begin{aligned}
 \lim_{v \rightarrow \pm 0, \rho=1} T &= \frac{h_0}{h-h_0} \int_{-\infty}^{+\infty} A(\beta) \left[\sqrt{\frac{\varphi_1(0, \beta)}{\varphi_2(0, \beta)}} - 1 \right] \cos \beta x d\beta, \\
 \lim_{v \rightarrow \pm 0, \rho=1} \frac{dT}{dy} &= \frac{h_0}{h-h_0} \int_{-\infty}^{+\infty} A(\beta) \left[h - h_0 \sqrt{\frac{\varphi_1(0, \beta)}{\varphi_2(0, \beta)}} \right] \cos \beta x d\beta;
 \end{aligned}$$

(cont. on next page) ↓

$$\lim_{\substack{y \rightarrow 0, \\ \rho = 1}} \frac{\partial T}{\partial y} = \frac{hh_0}{h-h_0} \int_{-\infty}^{+\infty} A(\beta) \left[1 - \sqrt{\frac{\varphi_1(0, \beta)}{\varphi_2(0, \beta)}} \right] \cos \beta x d\beta.$$

$$\lim_{\sigma \rightarrow +\infty} T = 0; \quad \lim_{\sigma \rightarrow -\infty} T = h_0 b^2 \int_{-\infty}^{+\infty} A(\beta) \frac{(\lambda \beta \operatorname{ch} \beta b \rho + a \operatorname{sh} \beta b \rho)}{\varphi_2(0, \beta)} \cos \beta x d\beta.$$

In conclusion, we note that if the function $f(x)$ is resolved in the Fourier sine integral, the problem is solved in an analogous manner; therefore, the assigned problem can be solved in the proposition that the function $f(x)$ can be represented by the Fourier integral in its general form.

Summary

A method is discussed in the paper for determination of a three-dimensional temperature field of an infinite flat wall under mixed boundary conditions (2), (3), and (15), (16), and (17).

An exact solution is obtained in the form of equations (14) and (21).

BIBLIOGRAPHY

1. A. M. Danilevskiy, Zapadny Naukovo-doslid institutu matem ta mekh, KhDU, 13, series 4, 1st edition, 1936
2. A. F. Khrustalev and B. I. Kogan, Izvestiya vysshikh uchebnykh zavedeniy Matematika (Bulletin of Higher Educational Institutions, Mathematics), No. 6, 1960
3. A. F. Khrustalev, Inzhenerno-fizicheskii zhurnal (Journal of Engineering Physics) No. 11, 1961
4. A. F. Khrustalev, Inzhenerno-fizicheskii zhurnal (Journal of Engineering Physics), No. 12, 1961.

6367

CSO: 1880-D

TEMPERATURE WAVES IN ELASTIC STRAINS

V. S. Khomenko
Hydrometeorological Institute, Odessa

On the basis of the thermodynamics of the reversible processes, the plane problem concerning periodic pressure of a rigid die on an elastic semiplane is examined.

Statement and Solution of the problem

With speeds of strain a little less than the speed of propagation of elastic waves, it is possible to proceed from the equation of the statistical theory of elasticity [1]. The latter in tensor symbols have the form [2, 3]:

$$\frac{d\sigma_{ij}}{dx_i} = 0, \quad \sigma_{ij} = (\lambda e - \gamma T) \delta_{ij} + 2\mu \varepsilon_{ij}, \quad (1)$$
$$e = \varepsilon_{ii}, \quad \gamma = \alpha(3\lambda + 2\mu).$$

In addition, the strains ε_{ij} are connected with displacements u_i by the relationships

$$\varepsilon_{ij} = \frac{1}{2} \left(\frac{\partial u_i}{\partial x_j} + \frac{\partial u_j}{\partial x_i} \right). \quad (2)$$

Subsequently, we will examine the plane stress condition, i.e., we will assume that $\sigma_{33} = 0$.

We set the axis $x_1 = x$ along the border of semiplane conditions, and the axis $x_2 = y$ vertically down. The displacements u_1 and u_2 can be expressed by the harmonic function φ and the function ψ in the

following manner [1, 2, 47]:

$$u_1 = -\frac{\lambda + 2\mu}{3\lambda + 2\mu} \int \frac{d\varphi}{dx} dy - y \frac{d\varphi}{dx} + \frac{d\Phi}{dx},$$

$$u_2 = \frac{4(\lambda + \mu)}{3\lambda + 2\mu} \varphi - y \frac{d\varphi}{dy} + \frac{d\Phi}{dy}, \quad \Delta\varphi = 0, \quad \Delta\Phi = \frac{\gamma}{2(\lambda + \mu)} T, \quad (3)$$

we place in force the absolute rigidity of a die under the letter

$$\frac{4(\lambda + \mu)}{3\lambda + 2\mu} \frac{d\varphi}{dx} + \frac{d^2\Phi}{dx dy} = 0 \quad \text{where} \quad |x| < a, \quad y = 0. \quad (4)$$

With the use of equality (3), it is possible to represent stresses σ_{12} and σ_{22} in the form:

$$\sigma_{12} = 2\mu y \frac{d^2\varphi}{dx dy} + 2\mu \frac{d^2\Phi}{dx dy},$$

$$\sigma_{22} = 2\mu \frac{d\varphi}{dy} - \frac{\mu\gamma}{\lambda + \mu} T - 2\mu y \frac{d^2\varphi}{dy^2} + 2\mu \frac{d^2\Phi}{dy^2}.$$

At the border of the semiplane with $y=0$, the tangential stress is absent

$$\frac{d\Phi}{dy} = 0, \quad (5)$$

with $|x| < a$ applied pressure

$$\sigma_{22} = 2\mu \frac{d\varphi}{dy} - \frac{\mu\gamma}{\lambda + \mu} T(x) + 2\mu \frac{d^2\Phi}{dy^2} = \quad (6)$$

and with $|x| > a = P_0(x) + P_1(x) \exp(j\omega t), \quad j = \sqrt{-1},$

$$\sigma_{22} = 0. \quad (7)$$

Subsequently, in complex values, only the effective part is assumed.

The functions P and P_1 are subject to determination from condition (4) and the given total force.

$$Q_0 + Q_1 \exp(j\omega t) = \int_{-a}^a P_0(x) dx + \exp(j\omega t) \int_{-a}^a P_1(x) dx. \quad (8)$$

From the equalities (6) and (7), we have the following limiting conditions for the function φ with $y=0$.

$$\frac{\partial \varphi}{\partial y} = \begin{cases} \frac{\gamma}{2(\lambda + \mu)} T(x) - \frac{\partial^2 \varphi}{\partial y^2} + \frac{1}{2\mu} [P_0 + P_1 \exp(j\omega t)], & |x| < a, \\ \frac{\gamma}{2(\lambda + \mu)} T(x) - \frac{\partial^2 \varphi}{\partial y^2}, & |x| > a. \end{cases} \quad (9)$$

For the determination of the temperature T , we use the equation for heat conductivity

$$\rho c \frac{\partial T}{\partial t} = k \Delta T + q. \quad (10)$$

As shown in the work 57, for the reversible processes the value q can be determined from the relationship

$$q = -\gamma T_0 \frac{de}{dt} = -\frac{4\mu\gamma T_0}{3\lambda + 2\mu} \frac{\partial^2 \varphi}{\partial y \partial t} - \frac{\gamma^2 T_0}{\lambda + \mu} \frac{dT}{dt}. \quad (11)$$

(From the results of the investigations of N. S. Fastov 67 it follows that the thermodynamic process can be considered as reverse with small frequencies of stress.) On the basis of equality (11) the equation of heat conductivity can be written in the following form

$$\left(\rho c + \frac{\gamma^2 T_0}{\lambda + \mu} \right) \frac{dT}{dt} = k \Delta T - \frac{4\mu\gamma T_0}{3\lambda + 2\mu} \frac{\partial^2 \varphi}{\partial y \partial t}. \quad (12)$$

If a heat exchange takes place on the boundary of the semiplane, the condition should be satisfied

$$\frac{dT}{dy} + \beta T = 0 \text{ where } y = 0. \quad (13)$$

On the strength of the equality (6) the function φ can be represented by the expression

$$\varphi(xyt) = \varphi_0(xy) + \varphi_1(xy) \exp(j\omega t), \quad \Delta \varphi_{0,1} = 0, \quad (14)$$

where φ_0 is the value of the function φ which corresponds to the constant component of pressure, and φ_1 is the complex amplitude of the variable component φ . It is not difficult to see that the temperature effects in the semiplane are caused by the exceptionally variable component of the pressure force. Therefore

$$T(xyt) = T_1(xy) \exp(j\omega t), \quad \Phi(xyt) = \Phi_1(xy) \exp(j\omega t). \quad (15)$$

For determining the values φ_1 , T_1 , and Φ_1 in accordance with the qualities (3), (5), (9), and (12)-(15), we have the following differential system:

$$\Delta \Psi_1 = 0, \quad \Delta T_1 = \frac{j\omega}{k} \left(\rho c + \frac{\gamma^2 T_0}{\lambda + \mu} \right) T_1 + \frac{4j\omega \mu \gamma T_0}{k(3\lambda + 2\mu)} \Psi_1, \quad (16)$$

$$\Delta \Phi_1 = \frac{\gamma}{2(\lambda + \mu)} T_1, \quad \Psi_1 = \frac{d\Phi_1}{dy}.$$

With $y=0$

$$\Psi_1 = \begin{cases} \frac{\gamma}{2(\lambda + \mu)} T_1(x) - \frac{d^2 \Phi_1}{dy^2} + \frac{1}{2\mu} P_1(x), & |x| < a, \\ \frac{\gamma}{2(\lambda + \mu)} T_1(x) - \frac{d^2 \Phi_1}{dy^2}, & |x| > a, \end{cases} \quad (17)$$

$$\frac{d\Phi_1}{dy} = 0, \quad \frac{dT_1}{dy} + \beta T_1 = 0.$$

Besides the conditions (17), it is necessary to require that the sought functions decrease towards infinity, and on the border of the semiplane with $|x| < a$, $y=0$ satisfied equality (4)

$$\frac{4(\lambda + \mu)}{3\lambda + 2\mu} \int_0^{\infty} \frac{d\bar{\Psi}_1}{dx} dy + \frac{d^2\bar{\Phi}}{dx^2} = 0. \quad (18)$$

For solution of the assigned mission, we use the Fourier transformation

$$\bar{f}(\xi y) = \int_{-\infty}^{\infty} f(xy) \exp(i\xi x) dx, \quad (19)$$

$$f(xy) = \frac{1}{2\pi} \int_{-\infty}^{\infty} \bar{f}(\xi y) \exp(-i\xi x) d\xi,$$

in which the simulated unit i does not interact with the temporary simulated unit j .

With the use of the transformations (19), the system of equations (16), (17) is written in the form

$$\begin{aligned} \frac{d^2 \bar{\Psi}_1}{dy^2} - \xi^2 \bar{\Psi}_1 &= 0, & \frac{d^2 \bar{T}_1}{dy^2} - (\xi^2 + jr) \bar{T}_1 &= js \bar{\Psi}_1, \\ \frac{d^2 \bar{\Phi}_1}{dy^2} - \xi^2 \bar{\Phi}_1 &= n \bar{T}_1, \end{aligned} \quad (20)$$

where

$$r = \frac{\omega}{k} \left(\rho c + \frac{\gamma^2 T_0}{\lambda + \mu} \right); \quad s = \frac{4\omega\mu\gamma T_0}{k(3\lambda + 2\mu)}; \quad n = \frac{\gamma}{2(\lambda + \mu)}.$$

With $y=0$

$$\begin{aligned} \bar{\Psi}_1 &= n \bar{T}_1(\xi) - \frac{d^2 \bar{\Phi}_1}{dy^2} + \frac{1}{2\mu} \bar{P}_1(\xi), \\ \frac{d \bar{\Phi}_1}{dy} &= 0, & \frac{d \bar{T}_1}{dy} + \beta \bar{T}_1 &= 0. \end{aligned} \quad (21)$$

Apart from the conditions (21), a limitation (18) is placed on the functions being sought which is connected with the absolute rigidity of the die. From this condition, with the use of the Fourier integral and the second equality (21) we obtain the integral equation

$$\int_{-\infty}^{\infty} \xi \exp(-i\xi x) d\xi \int_0^a \bar{\Psi}_1 dy = 0, \quad |x| < a. \quad (22)$$

Equation (22), on the strength of the parity of the function $\bar{\Psi}_1(\xi y)$ with respect to ξ (parity of the function $\Psi_1(xy)$ with respect

to ξ follow directly from the relationship (3) and the conditions of symmetry of vertical displacements) has the following solution satisfying the first equality (20) [7]:

$$\bar{\Psi}_1 = A j_0(a\xi) \exp(-|\xi|y), \quad (23)$$

where A is the constant subject to determination.

It is easy to prove that the solution of the equations (20) under conditions (21) and (23) are determined by the expressions:

$$\bar{T}_1 = \frac{sA}{r} \left[\frac{|\xi| - \beta}{V\xi^2 + jr - \beta} \exp(-yV\xi^2 + jr) - \exp(-y|\xi|) \right] j_0(a\xi), \quad (24)$$

$$\frac{1}{2\mu} \bar{P}_1(\xi) = -A \left[\frac{j|\xi| ns (|\xi| - \beta) (|\xi| - V\xi^2 + jr)}{r^2 (V\xi^2 + jr - \beta)} - 1 - \frac{ns}{2r} \right] j_0(a\xi). \quad (25)$$

The constant A, which is part of the relationship (23)-(25) is found from the normalization conditions (8)

$$Q_1 = \int_{-\infty}^{\infty} P_1(x) dx.$$

Determining from representation (25) the original and last used expression, we obtain

$$A = -\frac{\pi Q_1}{2\mu} \left[\int_0^{\infty} F(\xi) j_0(a\xi) \frac{\sin a\xi}{\xi} d\xi \right]^{-1},$$

where

$$F(\xi) = \frac{jns\xi(\xi - \beta)(\xi - \sqrt{\xi^2 + jr})}{r^2(\sqrt{\xi^2 + jr} - \beta)} - 1 = \frac{ns}{2r}$$

Transferring in equations (23) and (24) to the originals, we finally find

$$\Psi_1 = \frac{A}{2\pi} \int_{-\infty}^{\infty} j_0(a\xi) \exp(-|\xi|y - i\xi x) d\xi, \quad (26)$$

$$T_1 = \frac{sA}{\pi r} \int_0^{\infty} j_0(a\xi) \left[\frac{\xi - \beta}{\sqrt{\xi^2 + jr} - \beta} \exp(-y\sqrt{\xi^2 + jr}) - \exp(-y\xi) \right] \times \cos \xi x d\xi, \quad (27)$$

from which, in particular, we obtain the temperature limit

$$T_1(x) = \frac{sA}{\pi r} \int_0^{\infty} j_0(a\xi) \left(\frac{\xi - \beta}{\sqrt{\xi^2 + jr} - \beta} - 1 \right) \cos \xi x d\xi. \quad (28)$$

Peculiarities of Temperature Diffusion at the Limit

In many practical important cases, for example, with a free heat exchange with a surface, the coefficient of heat exchange β is a very small value which can be ignored (for example, for steel $\beta = 3.6 \cdot 10^{-6} \text{ cm}^{-1}$ [8] 7). In this simplest case, the diffusion of temperature at the limit of the semiplane has the form

$$T_1(x) = \frac{sA}{\pi r} \left[\int_0^{\infty} j_0(a\xi) \frac{\xi \cos \xi x}{\sqrt{\xi^2 + jr}} d\xi - \frac{E(a^2 - x^2)}{\sqrt{a^2 - x^2}} \right], \quad (29)$$

where $E(x)$ is a unitary function: $E=1$ with $x \geq 0$ and $E=0$ with $x < 0$.

We will show that the temperature of the limit of the semiplane is a limiting function. For this, with the use of the transformation of the package we write the integral (29) in the form
(next page)

$$I = \int_0^{\infty} j_0(a\xi) \frac{\xi \cos \xi x}{\sqrt{\xi^2 + jr}} d\xi = \frac{1}{\pi} \frac{d}{dx} \int_1^{\infty} \frac{K_0[\sqrt{j}r(x-a\tau)]}{\sqrt{\tau^2-1}} d\tau +$$

$$+ \frac{1}{\pi} \frac{d}{dx} \int_1^{\infty} \frac{K_0[\sqrt{j}r(x+a\tau)]}{\sqrt{\tau^2-1}} d\tau. \quad (30)$$

Here, $K_0(\tau)$ is a modification of the Bessel function of the second type of the zero order, and the value x , as a result of the symmetry of the problem, can be considered positive.

It is not difficult to see that only the first term in equality (30) can have singularity in the point $x=a$. For the isolation of this singularity, we note that the function $K_0(\tau)$ in point $\tau=0$ has an order of $\ln \tau$. On the basis of

this, in the vicinity of the point $x=a+0$, the integral (3) can be presented in the form

$$I = -\frac{1}{\pi\sqrt{2}} \frac{d}{dx} \int_1^{1+\delta} \frac{\ln \left| \frac{x}{a} - \tau \right|}{\sqrt{\tau^2-1}} d\tau + R(x), \quad (31)$$

where δ is a small positive value satisfying the inequality $\delta > 0$ with $x < a$, $\delta > \frac{x-1}{a}$ with $x > a$, and $R(x)$ is the function

which is regular with $x=a$.

Computing the integral (31), we find

$$I = \begin{cases} [2a(a-x)]^{-1/2} + R_1(x), & x = a-0; \\ R_2(x), & x = a+0. \end{cases}$$

These equalities, together with formula (28) indicate the limitation of the function T_1 in points $|x|=a$, inasmuch as $T_1(x) \rightarrow 0$ with $x \rightarrow \infty$, on the entire axis $y=0$.

From the relationship (29) with integration by parts, it is easy to obtain the asymptotic behavior of the function $T_1(x)$ 9;

(next page)

$$T_1(x) = -\frac{sA(jr)^{-\mu}}{\pi r x^2} \left[1 - \frac{3(2 + a^2 \sqrt{jr})}{2x^2 \sqrt{jr}} \right] + O(x^{-4}). \quad (32)$$

As can be seen from formula (32), the complex amplitude of the temperature gradation rapidly falls off with distance from the die.

Diffusion of Heat Sources

The complex amplitude q_1 of the density of heat sources, in accordance with equalities (11), (14), and (26) can be presented in the form

$$q_1 = -\frac{j\omega\gamma T_0}{\pi} \left[\frac{4\mu A}{3\lambda + 2\mu} \int_0^\infty j_0(a\xi) \exp(-\xi y) \cos \xi x d\xi + \frac{\pi\gamma}{\lambda + \mu} T_1(x, y) \right]. \quad (33)$$

From expression (33) it follows that the elastic strain of the semi-plane leads to the formation of volumetric sources of heat, the intensity of which drops off with distance from the die. In particular, near the edges of the die, from their internal side, there takes place a concentration of heat sources. Actually, with $y=0$

$$q_1 = -\frac{j\omega\gamma T_0}{\pi} \left[\frac{4\mu AE(a^2 - x^2)}{(3\lambda + 2\mu)\sqrt{a^2 - x^2}} + \frac{\pi\gamma}{\lambda + \mu} T_1(x) \right],$$

where, as shown above, $T_1(x)$ is a limited function.

With sufficiently small frequencies of strain, the second term in equality (33) can be ignored. In this case

$$q_1 = -\frac{4\sqrt{2}j\omega\gamma T_0 \mu A}{\pi(3\lambda + 2\mu)} \times \left[\frac{\sqrt{(y^2 - x^2 + a^2)^2 + 4x^2 y^2} + y^2 - x^2 + a^2}{(y^2 - x^2 + a^2)^2 + 4x^2 y^2} \right]^{1/4}. \quad (34)$$

At great distances from the start of the coordinates, we have

$$q_1 = \frac{My}{2\pi(x^2 + y^2)}, \quad M = -\frac{16j\omega\gamma T_0\mu A}{3\lambda + 2\mu}$$

Consequently, with a distance from the die, the amount q_1 acts as a heat dipole oriented along the y -axis and the moment which is equal to M .

We note in conclusion that the amount of heat which arises as a result of the elastic strain is proportional to the frequency of vibration.

Symbols

λ, μ -- Lamé's coefficient; σ_{ij} -- tensor of stress; ϵ_{ij} -- tensor of strain; δ_{ij} -- unitary tensor; T_0 -- absolute temperature of the medium; k -- coefficient of heat conductivity; α -- coefficient of linear expansion; β -- coefficient of heat exchange; c -- specific heat capacity; ρ -- density; q -- volumetric density of heat sources which arise as a result of the strain; $T(x)$ -- the desired function of propagation of temperature on the border of the semiplane; $P_0(x)$ -- the constant pressure component; $P_1(x)$ -- the complex amplitude of the periodic force of the frequency ω ; $j_0(x)$ -- the Bessel function of the zero order.

Summary

The two-dimensional contact plane problem on periodical pressure of rigid die on an elastic semiplane is solved through a single harmonic entering in the heat conduction equation as well. The system of equations obtained is solved using the Fourier transformation along with the coordinate. Then the problem is reduced to a solvable integral equation with respect to the amplitude of the periodical portion of the pressure applied to the die.

BIBLIOGRAPHY

1. L. A. Galin, Kontaknyye zadachi teorii uprugosti (Contact Problems of the Theory of Elasticity, GITIL, 1953).
2. E. Malan and G. Parkus, Termouprugi e napryasheniya, vyzvayemye statsionarnymi temperaturnymi pol'yami (Thermal Elastic Stresses Caused by Stationary Temperature Fields), State Physical-Mathematical Publishing House, 1959.
3. I. N. Sneddon and D. S. Berry, Klassicheskaya teoriya uprugosti (Classical Theory of Elasticity), State Physical-Mathematical Publishing House, 1961.
4. P. F. Pankovich, Teoriya uprugosti (Theory of Elasticity). United Scientific-Technical Publishers, 1939.
5. M. A. Biot, Journal of Applied Physics, 27, No.3, 1956.
6. N. S. Fastov, Fizika metallov i metallovedeniye (Physics of Metals and Metallurgy, 12, 3d issue, Academy of Sciences USSR Publishing House, 1961.
7. I. M. Ryzhik and I. S. Gradshteyn, Tablitsy integralov, summ, ryadov, i proizvedeniy (Tables of integrals, sums, series, and products) GITIL, 1951.
8. V. S. Shchedrov, Treniye i iznos v mashinakh (Friction and Wear in Machines), 10, Academy of Sciences USSR Publishing House, 1955.
9. A. Erdelyi. Asimptoticheskiye raslozheniya (Asymptotic Expansion), State Physical-Mathematical Publishing House, 1962 / 2. VII. 1962/

6367
CSO: 1880-D

THE ANISOTHERMAL FLOW OF REAL GAS IN A GAS PIPELINE

by B. V. Shalinov
Scientific-Research Institute of
Natural Gas, Moscow

Under investigation is a steady-state flow of thermodynamically imperfect gas in a gas pipeline, and the heat exchange with the surrounding medium is taken into account. A solution suitable for practical calculations was obtained by the use of the small parameter method.

In engineering practice, the distribution of the gas temperature over the length of the gas line is calculated by the well known V. G. Shukhov formula applying to thermodynamically ideal gas flowing at a low speed (1). There are cases when the gas temperature at the end of the pipeline is lower than the temperature of the surrounding ground (2). This does not agree with the V. G. Shukhov formula and shows that it is inaccurate with reference to the flow of gas. It is assumed that the temperature drop is caused by the fact that the gas is thermodynamically nonideal which has to be taken into account in case of considerable pressure changes (2). At any rate, no satisfactory quantitative estimate is available. I. A. Charnyy's monograph (1) cites a system of gas dynamic equations for real gas and examines in detail a case of adiabatic flow (the Joule-Thomson effect).

Below is the effect of nonideal gas on the temperature of a gas line where account is taken of the heat exchange with the surrounding medium on the basis of general equations of gas dynamic.

I. The initial equations are those of the law of mass preservation and the quantity of motion and balance of energy which, disregarding the uneven distribution over the gas line cross-section, looks like the following: $\gamma w f = G = \text{const.}$

$$d\left(\frac{w^2}{2g}\right) + \frac{dp}{\gamma} + dz + \frac{dx}{d} \lambda \frac{w^2}{2g} = 0, \quad (1)$$

$$d\left(\frac{w^2}{2g} + z + \frac{i}{A}\right) = \frac{K \Pi d}{GA} (T_0 - T) dx$$

and the equation of the state of real gas, for which the Bertlow equation (3) was used, is

$$\frac{pv}{RT} = 1 + \frac{9}{128} \frac{p}{p_c} \frac{T_c}{T} \left(1 - 6 \frac{T_c^2}{T^2}\right) = Z(p, T). \quad (2)$$

Deducting the second equation (1) from the third, we get the

heat inflow equation

$$di - A \frac{dp}{\gamma} = \frac{K \Pi d}{G} (T_0 - T) dx + \frac{dx}{d} A \lambda \frac{w^2}{2g}. \quad (3)$$

It is known (1) that in the case of gas flowing in a major gas line at a slow speed, the equation of the quantity of motion may disregard the changes in the speed-produced pressure and geometric height as compared to the changing piezometric pressure, and take

$$\frac{dp}{\gamma} = - \frac{dx}{d} \lambda \frac{w^2}{2g}. \quad (4)$$

Then the equation of the heat inflow can be represented with the same degree of accuracy as

$$di = \frac{K \Pi d}{G} (T_0 - T) dx \quad (5)$$

or, using the well known thermodynamic relation for an enthalpy (1),

as

$$c_p dT + A \left[v - T \left(\frac{\partial v}{\partial T} \right)_p \right] dp = \frac{K \Pi d}{G} (T_0 - T) dx. \quad (6)$$

The designations used here are well known and coincide with those taken in (1); the exceptions are T_0 — the temperature of the surrounding medium and K — the full coefficient of the heat transfer from the gas to the surrounding medium.

The problem is thus reduced to the integration of two nonlinear equations

$$-\frac{dp}{dx} = \frac{\lambda}{2gd} \left[\frac{G}{f} \right]^3 \frac{ZRT}{p},$$

$$\frac{dT}{dx} + \frac{9}{128} \frac{AR}{c_p} \frac{T_c}{p_c} \left[1 - 18 \frac{T_c^2}{T^2} \right] \frac{dp}{dx} = \frac{4K}{c_p d} \frac{f}{G} (T_0 - T) \quad (7)$$

with the initial conditions $p = p_1$, $T = T_1$ and $x = 0$.

To simplify the problem, we shall take λ , K , and c_p as constants of the gas-line length, and average Z_0 value as the coefficient of compressibility within the temperature and pressure range under consideration.

We shall introduce the dimensionless variables

$$x = \frac{x}{l}, \quad \pi = \frac{p}{p_c}, \quad \tau = \frac{T}{T_c}, \quad \tau_0 = \frac{T_0}{T_c}$$

and assuming that

$$s = \frac{9}{128} \frac{AR}{c_p} \frac{a}{b}, \quad a = \frac{l}{d} \frac{4K}{c_p} \frac{f}{G},$$

$$b = \frac{p_c^2}{Z_0 R l c_p} \frac{8g}{\lambda} \left[\frac{f}{G} \right]^3 K,$$

we shall change the equation system (7) to the following:

$$\frac{d\tau}{dx} = s \left[1 - \frac{18}{\tau^2} \right] \frac{\tau}{\pi} + a(\tau_0 - \tau),$$

(8)

$$\frac{d\pi}{dx} = -\frac{a}{b} \frac{\tau}{\pi}, \quad \pi = \pi_1, \quad \tau = \tau_1 \quad \text{при } x = 0.$$

II. In the case of an anadiabatic gas flow ($K \neq 0$), the solution of the equation system (8) can be obtained by the small parameter method (4).

In the majority of the actually important cases the parameter ϵ is very small. With $\epsilon = 0$ (ideal gas), the system (8) will look like the following:

$$\frac{d\varphi}{dx} = a(\tau_0 - \varphi), \quad \frac{d\psi}{dx} = -\frac{a}{b} \frac{\varphi}{\psi}. \quad (9)$$

Its solution, in keeping with the conditions $\varphi = \tau_1, \psi = \pi$, and $x = 0$, will be:

$$\begin{aligned} \varphi(x) &= \tau_0 + (\tau_1 - \tau_0) \exp(-ax), \\ \psi(x) &= \left[\pi_1^2 - \frac{2a\tau_0}{b}x - 2\frac{\tau_1 - \varphi(x)}{b} \right]^{1/2}. \end{aligned} \quad (10)$$

We shall further assume that

$$\tau = \varphi + \bar{\tau}, \quad \pi = \psi + \bar{\pi}. \quad (11)$$

From (8) and (9) we find: $\frac{d\bar{\pi}}{dx} = \frac{a}{b} \left[\frac{\varphi}{\psi} - \frac{\varphi + \bar{\tau}}{\psi + \bar{\pi}} \right]$,

$$\frac{d\bar{\tau}}{dx} = \frac{\epsilon}{\psi + \bar{\pi}} \left[\varphi + \bar{\tau} - \frac{18}{\varphi + \bar{\tau}} \right] - a\bar{\tau}. \quad (12)$$

$$\bar{\pi} = 0, \quad \bar{\tau} = 0 \quad \text{при} \quad x = 0.$$

We shall look for a solution of the latter system in the form of small parameter ϵ series. Bearing in mind that with $\epsilon = 0$.

$\bar{\pi}(x) \approx 0, \quad \bar{\tau}(x) \approx 0$, we get:

$$\begin{aligned} \bar{\pi}(x) &= \epsilon \bar{\pi}_1(x) + \dots, \\ \bar{\tau}(x) &= \epsilon \bar{\tau}_1(x) + \dots. \end{aligned} \quad (13)$$

The convergence of the series is insured by the Poincare theorem (4).

In the future we shall confine ourselves to the first terms of

expansion (13) in view of the low $\bar{\epsilon}$ value. Substituting (13) in (12)

and dividing the power series ($\varphi \neq 0, \Psi \neq 0$), we will find:

$$\begin{aligned} \frac{d\bar{\pi}_1}{dx} &= \frac{a}{b} \frac{1}{\psi} \left[\bar{\pi}_1 \frac{\varphi}{\psi} - \bar{\tau}_1 \right], \\ \frac{d\bar{\tau}_1}{dx} &= \frac{\varphi}{\psi} \left[1 - \frac{18}{\varphi^2} \right] - a\bar{\tau}_1, \end{aligned} \quad (14)$$

$$\bar{\tau}_1 = 0, \quad \bar{\pi}_1 = 0 \quad \text{при } x = 0.$$

The solution of the linear equations (14) is obtained in quadratures: $\bar{\tau}_1 = \frac{b}{a} (\varphi - \tau_0) \int_{\bar{\pi}_1}^{\psi} \left[\frac{18}{\varphi^2} - 1 \right] \frac{d\psi}{\varphi - \tau_0}$,

$$\bar{\pi}_1 = -\frac{a}{b\psi} \int_0^{\bar{\tau}_1} \bar{\tau}_1(x) dx, \quad (15)$$

and the relation $\varphi = \varphi(\Psi)$ is provided by the equations (10).

These integrals can be computed to a desired accuracy by approximate methods.

1. Let us examine in detail a case in which $\tau_1 = \tau_0$. The relations (10) and (15) are simplified:

$$\varphi(x) = \tau_0, \quad \psi(x) = \left[\bar{\pi}_1^2 - \frac{2a\tau_0}{b} x \right]^{1/2}, \quad (16)$$

$$\bar{\tau}_1 = \frac{b}{a} \left[\frac{18}{\tau_0^2} - 1 \right] \exp(-ax) \int_{\bar{\pi}_1}^{\psi} \exp(ax) d\psi.$$

We shall express the latter integral by the Gauss function

$$\operatorname{erf} \xi = \frac{2}{\sqrt{\pi}} \int_0^{\xi} \exp(-t^2) dt,$$

whose values are tabulated (5):

$$\bar{\tau}_1 = -\frac{\sqrt{\pi}}{2} \frac{b}{a\sqrt{c}} \left[\frac{18}{\tau_0^2} - 1 \right] \exp(c\psi^2) [\operatorname{erf}(\bar{\pi}_1 \sqrt{c}) - \operatorname{erf}(\psi \sqrt{c})]. \quad (17)$$

Disregarding the correction for pressure in the case of non-ideal gas which is very low, that is taking $\pi \approx \Psi$, we will present the solution as follows:

$$\pi = \left[\pi_1^2 - \frac{a}{c} x \right]^{1/2}, \quad \tau = \tau_0 - \tau^*,$$

$$\tau^* = \frac{\sqrt{\Pi}}{2} \cdot \frac{I_0}{\sqrt{c}} \exp(c \pi^2) [\operatorname{erf}(\pi_1 \sqrt{c}) - \operatorname{erf}(\pi \sqrt{c})], \quad (18)$$

$$I_0 = \frac{9}{128} \frac{AR}{c_p} \left[\frac{18}{\tau_0^2} - 1 \right], \quad c = \frac{b}{2\tau_0}.$$

It follows from (18) that τ will diminish or increase with the drop in initial pressure depending on whether τ_0 is less or more than the inversion temperature by $\tau_{inv.} = \sqrt{18}$.

It can be shown that function (18) is monotonic, and for this reason the maximum change in the gas temperature due to its nonideal characteristic, as compared with the initial temperature, occurs when

$$\pi = 0: \quad \tau_{max}^* = \frac{\sqrt{\Pi}}{2} \frac{I_0}{\sqrt{c}} \operatorname{erf}(\pi_1 \sqrt{c}). \quad (19)$$

2. Still more interesting from the point of view of applications is the case when $\tau_1 \neq \tau_0$. The following conditions are usually fulfilled

$$|\delta| = |\tau_1 - \tau_0| \ll 1, \quad b \gg 1, \quad \tau_0 \gg 1. \quad (20)$$

The function $F(\delta) = \frac{18}{\varphi^2} - 1$, where $\varphi(\delta) = \tau_0 + \delta \exp(-ax)$, we shall expand into the Maclaurin series with each fixed value x , disregarding the terms of the second order of the infinitesimal in

$$\text{relation to } \delta: \quad F(\delta) = \left(\frac{18}{\tau_0^2} - 1 \right) - \frac{36}{\tau_0^3} \delta \exp(-ax).$$

$$\text{Then } \tau_1 = \frac{b}{a} (\varphi - \tau_0) \left[\left(\frac{18}{\tau_0^2} - 1 \right) \int_{\tau_1}^{\varphi} \frac{d\psi}{\varphi - \tau_0} + \frac{36}{\tau_0^3} (\pi_1 - \psi) \right]. \quad (21)$$

To calculate the integral in (21), bearing in mind inequality (20), we shall replace (without much loss of accuracy) function $\psi(x)$ by a simpler one

$$\bar{\psi}(x) = \left[\pi_1^2 - \frac{2a\tau_0}{b} x \right]^{1/2},$$

whereupon the mentioned integral will be expressed by a Gauss function analogically to (16).

Taking $\pi \approx \psi \approx \bar{\psi}$, we shall express the final solution in the following form

$$\pi = \left\{ \pi_1^2 - \frac{a}{c} x - \frac{2}{b} (\tau_1 - \tau_0) [1 - \exp(-ax)] \right\}^{1/2},$$

$$\tau = \tau_0 + (\tau_1 - \tau_0) \exp(-ax) - \tau^*,$$

$$\tau^* = \frac{\sqrt{\pi}}{2} \frac{l_0}{\sqrt{c}} \exp(c\pi^*) [\operatorname{erf}(\pi_1\sqrt{c}) - \operatorname{erf}(\pi\sqrt{c})] - \quad (22)$$

$$- \frac{81}{32} \frac{AR}{c_p} \frac{\tau_1 - \tau_0}{\tau_0^3} (\pi_1 - \pi) \exp[-c(\pi_1^2 - \pi^2)],$$

$$l_0 = \frac{9}{128} \frac{AR}{c_p} \left[\frac{18}{\tau_0^2} - 1 \right], \quad c = \frac{b}{2\tau_0}.$$

Taking inequality (20) into account, it is quite possible to use formulas (18) instead of (22) for calculating π^* and τ^* .

3. In the case of a fully heat-insulated gasline ($K = 0$), an approximate solution can be obtained from (18) by a maximum change with $K \rightarrow 0$: $\tau = \tau_1 - \tau^*$, $\tau^* = l/(\pi_1 - \pi)$,

$$\pi = \left[\pi_1^2 - \frac{2a\tau_1}{b} x \right]^{1/2}, \quad l = \frac{9}{128} \frac{AR}{c_p} \left[\frac{18}{\tau_1^2} - 1 \right]. \quad (23)$$

It is similar to the linearized solution for Vander Waals' gas found in (1).

III. In addition to the other well defined parameters from a physical point of view, the distribution of the gas temperature over the length of the gas line depends on the full coefficient of heat transfer K characterizing the heat exchange with the surrounding medium. The methods of calculating it in concrete cases are found in (6) as well as in reference manuals on heat transfer.

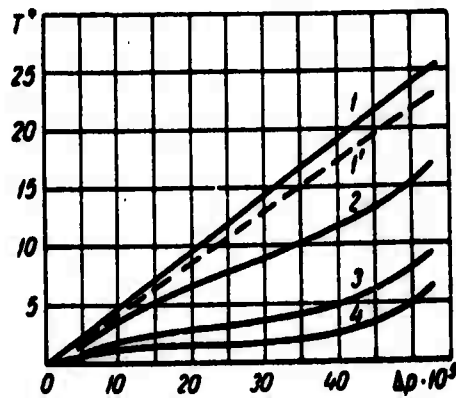


Fig. 1. Relationship between $T^*(^{\circ}\text{C})$ and

1 - $K=0$; 1' - $K=0(1)$; 2 - $K=1.16$; $G=1362.5$;
3 - $K=4.65$; $G=1362.5$; 4 - $K=1.16$; $G=681.25$.

Under turbulent conditions of gas flow in a gas line the coefficient K depends on hydraulic factors, but the range of its dependence on the Reynolds parameter is very narrow. In the case of high Re numbers, the coefficient K is actually determined by the heat-conducting properties of the surrounding medium and can be calculated by the Forheimer, Arons-Kutateladze formulas, etc. In practice, a certain average value of coefficient K is frequently used. According to the

Investigations by Pistol'kors, K may be taken (in terms of $\text{wt}/\text{m}^2 \times$ degree) as 1.16 for dry sand, 1.45 for damp clay and 3.49 for water-saturated sand. The latter value is recommended also by Shukhov and Leybenzon (6). In a turbulent gas flow K is larger than in a laminar flow; a fully heat-insulated gas pipeline reduces K to zero.

To estimate the effect of the thermodynamic non-ideal characteristic of gas on the temperature conditions of a gas line, calculations were made under the following conditions: $l = 120 \text{ km}$; $d = 0.8$; $\lambda = 0.0135$; methane gas; $T_0 = 190.5^\circ\text{K}$; $R = 53 \text{ m/deg.}$; $c_p = 2.219 \text{ kJ/kg} \times \text{deg.}$; $p_0 = 44.9 \times 10^5 \text{ n} \times \text{m}^{-2}$; $Z_0 = 0.93$.

Formulas (18) and (23) were used to calculate the drop in the gas temperature T^* produced by the changing pressure $\Delta p = p_1 - p$ with $p_1 = 53.9 \times 10^5 \text{ n/m}^2$, $T_1 = T_0 = 15^\circ\text{C}$ and various weight loss values G (in n/sec) and coefficient K (solid lines in fig. 1). The theoretical distribution of the gas temperature over the length of the gas line was calculated by formula (22) for real gas, and for a comparison with V. G. Shukov's formula (10) for ideal gas (Fig. 2).

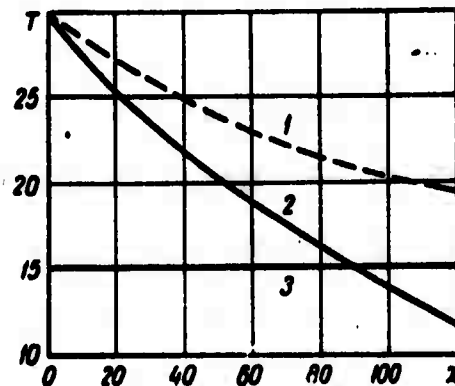


Fig. 2. Theoretical dependence of $T(^{\circ}\text{C})$ on x (km) with $p_1 = 53.9 \cdot 10^5 \text{ h.m}^{-2}$; $G = 1362.5 \text{ n.sec}^{-1}$; $K = 1.17 \text{ wt.m}^{-2} \cdot \text{deg}^{-1}$.

1 - through (10); 2 - through (22);
3 - ground temperature.

The calculation shows that:

1) the temperature curve corresponding to real gas runs considerably lower than the curve corresponding to V. G. Shukov's formula (10) under identical conditions (Fig. 2);

2) the drop in gas temperature caused by its non-ideal characteristic depends largely on the rate of flow of G and coefficient K : all other conditions being equal, it drops with a decreasing G , and increases with a decreasing K to a value corresponding to the Joule-Thomson effect with $K = 0$ (Fig. 1);

3) the non-ideal characteristics of the gas may cause its temperature to drop below that of the surrounding ground, which agrees with the natural observations (2).

The selection of a particular equation of state is not a matter of principle importance. The Bertlow equation, as is known (3), produces good results under moderate pressures, as in the case of methane in the field of pressure (0 - 100) 10^5 h x m⁻². In the particular case of K = 0, a comparison was made of the calculations based on formulas (23) and the similar I. A. Charnyy formulas for vander Waals' gases (Fig. 1) which are found to be practically the same within the temperature and pressure range under consideration.

Thus the V. G. Shukhov formula applicable to the flow of gas in a gas line under changing pressure shows over-estimated gas temperature values as it does not take into account the non-ideal characteristic of the gas. This should be borne in mind whenever it is important to know the gas temperature in a gas pipeline (the depth of the pipeline, the condensation of hydrocarbons and water, etc.).

A generalization of the outlined method of solution does not involve any serious difficulties in the case of the variable-length gas line K and T₀.

Bibliography

1. Charnyy, I. A., Osnovy Gazovoy Dinamiki (The Basis of Gas Dynamics), Gostoptekhzdat (State Publishing House of the Petroleum and Fuel Industry), Moscow, 1961.
2. Schorre, Charles E., Oil and Gas J., 53, No.21, 1954.
3. Karapet'yants, M. Kh., Khimicheskaya Termodinamika (Chemical Thermodynamics), Goskhimizdat (State Publishing House for Chemical Literature), Moscow, 1953.

4. Berezin, I. S., Zhidkov, N. P. Metody Vychisleniy (Calculation Methods), 1, 2, Fizmatgiz, Moscow, 1959.

5. Segal, B. I., Semendyayev, K. A. Pyatiznachnyye matematicheskiye tablitsy Five-Cipher Mathematical Tables. Publ. by the USSR Academy of Sciences, 1950.

6. Leybenzon, L. S. Sobraniye Trudov (Collected Works), 3, Publ. by the USSR Academy of Sciences, 1955.

5132
CSO: 1880-D

CONCERNING THE FIELDS OF A TURBULENT FLOW VELOCITY IN A CYCLONE CHAMBER

by V. A. Schwab,
Branch of the Omsk Institute of Railroad Engineers, Tomsk

The subject under consideration is the velocity field of a turbulent isothermal flow in a cylindrical chamber with a tangential supply of a medium, as a result of the generalization of the viscous movement with an average value of the "turbulent agitation" coefficient.

The characteristic features of the twisted turbulent flow produced in special cyclone or vortex chambers with a tangential supply of a medium are incorporated in the production of high pressure heating devices, in the designs of a number of separators, various types of pressure and feeder installations. From this point of view it would be interesting to generalize the experimental investigations of the velocity fields in such cyclone chambers on the basis of theoretical principles. In this sense there are some possibilities, if the turbulent movement in a cyclone chamber is to be considered as a result of the generalization of the viscous movement problem by using the average value of the "turbulent agitation" coefficient. In this case, as will be shown later, it would be possible to establish the velocity field in the peripheral region of the cyclone according to the input of the medium through the cyclone, the coefficient of the flow turbulence and the basic dimensions of the cyclone, and generalize the experimental investigations of the velocity fields.

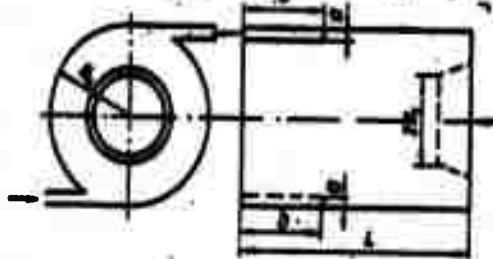


Fig. 1. Diagram of cyclone chamber

For this purpose we shall examine the movement of a medium in a cyclone chamber with a radius R_0 and L long (with an arbitrary value of the L/R_0 ratio) and its tangential supply through nozzles whose cross-section outlet area is determined by the product of dimensions

$\sum_{\sim} a_i b_i$ (Fig. 1). The exit of the medium from the cyclone is through an opening in radius R_1 and the R_1/R_0 ratio may have various values.

In the peripheral region of a cyclone ($r > R_1$) characterized by a tangential supply of a medium along the entire cyclone generator, there is practically no agitation in the direction z , which is normal in relation to the rotation plane; in that case, the movement in this region can be considered as a plane movement depending only on r and φ with the use of a cylindrical system of coordinates. The effect of the axial speed component u_z becomes substantial and a central part of the cyclone at $r < R_1$ where the cylindrical surface of radius R_1 is, as in the first approximation, the surface of the division of two different regions of medium movement, peripheral and central, which can simultaneously be considered as the surface corresponding to the "merger" of

the medium under the effect of centrifugal forces through the outlet opening of radius R_1 . In this connection, the division surface of radius R_1 is the boundary in the changing nature of the distribution of the transverse (rotating) speed component u_φ . As is known, the experimental data revealed that in the peripheral region ($r > R_1$) u_φ increases with the decreasing radius in accordance with the exponential relationship, and in the central part u_φ is approximately proportional to the radius, which practically corresponds to the quasi solid rotation of the medium.

In the case of the peripheral region of the cyclone (at $r > R_1$), assuming that the movement does not depend on coordinate s , and noting that the terms containing the derivatives $\frac{\partial}{\partial \varphi}$ are excluded in view of the flow symmetry, we will get a differential equation for a turbulent movement in the following form:

$$\begin{aligned} \bar{u}_r \frac{\partial \bar{u}_r}{\partial r} - \frac{\bar{u}_\varphi^2}{r} = -\frac{1}{\rho} \frac{\partial \bar{p}}{\partial r} + \\ + \nu \left(\frac{\partial^2 \bar{u}_r}{\partial r^2} + \frac{1}{r} \frac{\partial \bar{u}_r}{\partial r} - \frac{\bar{u}_r}{r^2} \right) - \frac{\bar{u}_r^3}{r} - \frac{\bar{u}_\varphi^3}{r}, \end{aligned} \quad (1)$$

$$\begin{aligned} \bar{u}_r \frac{\partial \bar{u}_\varphi}{\partial r} + \frac{\bar{u}_r \bar{u}_\varphi}{r} = \\ = \nu \left(\frac{\partial^2 \bar{u}_\varphi}{\partial r^2} + \frac{1}{r} \frac{\partial \bar{u}_\varphi}{\partial r} - \frac{\bar{u}_\varphi}{r^2} \right) - \frac{\partial}{\partial r} \overline{u_\varphi u_r} - 2 \frac{\bar{u}_\varphi \bar{u}_r}{r} \end{aligned} \quad (2)$$

and the continuous movement equation

$$\frac{\partial \bar{u}_r}{\partial r} + \frac{\bar{u}_r}{r} = 0, \quad (3)$$

where the solid line indicates the time - averaging operation, and the

dot the corresponding values of the pulsing speed components. In later presentations, all the transformations will refer only to time averages, and the averaging sign will therefore be omitted. As a result of the separation of variables and integration in (3), we get

$$ru_r = \text{const} = -\frac{q}{2\pi L}, \quad (4)$$

where q is the volumetric consumption of the medium through the nozzles. A negative sign indicates that the direction of the speed component u_r is toward the cyclone axis. By substituting the values u_r in (4), we find from equation (1)

$$\frac{1}{r} \left[u_r^2 + u_\varphi^2 + \overline{u_r^2} + \overline{u_\varphi^2} \right] = \frac{1}{\rho} \frac{dp}{dr}. \quad (5)$$

Bearing in mind that the viscous tangential tension in the case of movement under consideration is

$$\tau_{\varphi r} = \mu \left(\frac{\partial u_\varphi}{\partial r} - \frac{u_\varphi}{r} \right) = \mu r \frac{\partial}{\partial r} \left(\frac{u_\varphi}{r} \right),$$

and introducing the designation of the turbulent tension component

$$\overline{\tau}_{\varphi r} = -\overline{\rho u_\varphi' u_r'},$$

equation (2) can be expressed by tension

$$\rho \left(u_r \frac{\partial u_\varphi}{\partial r} + \frac{u_\varphi u_r}{r} \right) = \frac{\partial}{\partial r} (\tau_{\varphi r} + \overline{\tau}_{\varphi r}) + \frac{2}{r} (\tau_{\varphi r} + \overline{\tau}_{\varphi r}). \quad (6)$$

On the basis of the general principles of the semiempirical theory of turbulence, we will assume that

$$\overline{\tau}_{\varphi r} = Ar \frac{d}{dr} \left(\frac{u_\varphi}{r} \right), \quad (7)$$

and that the kinematic coefficient of the "turbulent viscosity" is

$$\varepsilon = \frac{A}{\rho} = \beta r \left| \frac{d}{dr} \left(\frac{u_\varphi}{r} \right) \right|. \quad (8)$$

If some average value of the coefficient $\epsilon = \epsilon_0$ can be taken in the region of flow, at $r > R_1$, equation (6) will amount to the following after the substitutions of the $\tau_{\varphi r}$ and $\tau_{\varphi r}$ values

$$u_{\varphi} \frac{\partial u_{\varphi}}{\partial r} + \frac{u_{\varphi} u_r}{r} = (\nu + \epsilon_0) \left(\frac{\partial^2 u_{\varphi}}{\partial r^2} + \frac{1}{r} \frac{\partial u_{\varphi}}{\partial r} - \frac{u_{\varphi}}{r^2} \right). \quad (9)$$

As $u_{\varphi} = u_{\varphi}(r)$, equation (9) can be presented as follows:

$$\frac{d^2 u_{\varphi}}{dr^2} + \frac{1+m}{r} \frac{du_{\varphi}}{dr} - \frac{1-m}{r^2} u_{\varphi} = 0, \quad (10)$$

where

$$m = q [2\pi L (\nu + \epsilon_0)]^{-1}. \quad (11)$$

equation (10) is a Euler type equation, and its two particular solutions should look like

$$u_{\varphi} = r^k.$$

The substitution of value u_{φ} in (10) produces

$$k^2 + mk - (1-m) = 0,$$

hence we have:

$$k_1 = -(m-1); \quad k_2 = -1.$$

The general solution of equation (10) is

$$u_{\varphi} = Ar^{-(m-1)} + Br^{-1}. \quad (12)$$

The arbitrary constants can be defined from the following considerations. A certain speed $u_{\varphi 0}$ is established near the cylindrical wall of the cyclone but not on the wall itself, so that

$$u_{\varphi} = u_{\varphi 0} \text{ при } r = R_0. \quad (13)$$

Besides, when $q = 0$, that is when the medium is not shifted in a radial direction but the established speed value $u_{\varphi 0}$ at $r = R_0$ continues, the speed component u_{φ} should be redistributed in accordance with the

rotation of liquid as a solid body. This movement can be produced by removing the entire medium flowing in through the nozzles to the cylindrical wall of the cyclone through specially made openings in that wall, as was experimentally proved in work (1). Obviously, an analogical case would be the rotation of a solid cylindrical wall when the circular movement of the medium on the external boundary is caused by viscous tensions on its surface, and in this case the medium inside the cycle chamber will rotate as a solid body.

Thus when $q = 0$, it is necessary to have $u_\varphi = Ar$ which is possible with $B = 0$. Using the boundary condition (13), we get the following final result for u_φ with $r > R_1$:

$$u_\varphi = u_{\varphi 0} (R/r)^n, \quad (14)$$

Where

$$n = m - 1 = q [2\pi L(\nu + \varepsilon_0)]^{-1}.$$

Thus the relationship characterizing the field of the rotational speed in the peripheral region of the cyclone with $r > R_1$ has been established. Relation (14) makes it possible to establish the effect on the velocity field of medium q , the length and radius of the cyclone, and coefficients ε_0 and ν . Here the value ε_0 is considerably greater than ν , which in most cases makes it possible to disregard the value of the latter. A quasi-solid rotation of the medium is initiated when $\varepsilon_0 + \nu \rightarrow \infty$, just as in $q = 0$. When the viscosity of the medium disappears, that is when $\varepsilon_0 + \nu \rightarrow 0$, it follows from (12) that

$$u_\varphi = B/r = u_{\varphi 0} R/r. \quad (15)$$

Comparing it with (14), we find the following condition:

$$m = q [2\pi L(\nu + \varepsilon_0)]^{-1} < 2. \quad (16)$$

Thus the meaning of relation (14), with low $\varepsilon_0 + \nu$ values, is limited by (16); consequently, with certain $\varepsilon_0 + \nu$ values it is possible to produce a movement in the cyclone only when the q values satisfy (16).

The value ε , defined by (8), we shall compute as the average magnitude within the peripheral portion of the cyclone at $r > R_1$. We shall assume that the "swirling method" l is proportional to radius $l = \alpha r$, where α is the constant subject to definition by experimental methods. From (8) and the additional use of (14) we will get the following for ε :

$$\varepsilon = \alpha^2 \frac{u_{\varphi 0} q R_0}{2\pi L \varepsilon_0} \left(\frac{R_0}{r}\right)^{n-1}.$$

Attributing the average value ε_0 to the average value of the radius in the zone under consideration $r_{cp} = \sqrt{R_0 R_1}$, we find

$$\varepsilon_0 = \alpha R_0 \sqrt{u_{\varphi 0} |u_{r0}|} \left(R_1/R_0\right)^{\frac{n-1}{4}}, \quad (17)$$

where

$$\frac{|u_{r0}|}{\frac{1-n}{4}} = q (2\pi L R_0)^{-1}. \quad (18)$$

The effect of multiplier R_1/R_0 may not be taken into account, as the index value of the experimental data on the used values $R_1/R_0 = 0.15-1$, does not exceed the range $\frac{1-n}{4} \approx 0.1-0.15$. The following assumption in this case would be fairly accurate

$$\varepsilon_0 = \alpha R_0 \sqrt{u_{\varphi 0} |u_{r0}|}. \quad (19)$$

The value of constant α is defined on the basis of the experimental

investigations of the velocity fields in cyclones. Since according to (14) and (18)

$$n = |u_{r0}| R_0 \varepsilon_0^{-1} - 1,$$

we will get the following, bearing in mind (19):

$$\alpha = \frac{1}{n+1} \sqrt{\frac{|u_{r0}|}{u_{\varphi 0}}}. \quad (20)$$

The values α , calculated by the experimental data (1, 2) in accordance with (20), are plotted on a graph (Fig. 2) in relation to $M = \sqrt{\frac{u_{r0}}{u_{\varphi 0}}}$, bearing in mind that the volumetric flow through the feed nozzle

$$q = u_{ax} \sum_n a_i b_i,$$

where u_{ax} is the speed of the incoming medium, we get for M , taking (18) into account,

$$M = \left(\frac{u_{ax}}{u_{\varphi 0}} \frac{\sum_n a_i b_i}{2\pi L R_0} \right)^{1/2}. \quad (21)$$

It follows from the graph (Fig. 2) that the value α is subordinated with precision to the linear relation

$$\alpha = 0,01 + 0,56 M. \quad (22)$$

The order of magnitude α agrees with the values obtained by L. A. Vulis and V. P. Ustimenko who considered the turbulent movement in a cyclone from the viewpoint of its qualitative conformity with a rotating tubular jet. Relation (22) was constructed by the use of the experimental data obtained by measuring the velocity fields in cyclones with a tangential supply of a medium only (1, 2). It should be emphasized that the result obtained in accordance with the formulation

of the problem characterizes the velocity field in a cylindrical cyclone where the medium is supplied tangentially. A partial supply of the medium through an axial nozzle in the central part of the cyclone accelerates the growing speed in the peripheral part of the cyclone (the n degree index is higher). This phenomenon can be explained by the support produced by the air mass introduced in the central part of the cyclone; it is confirmed by the tests made by D. N. Lyakhovskiy (2) in which the volume of air introduced through the axial nozzles amounted to one-third of that introduced by the tangential nozzles.

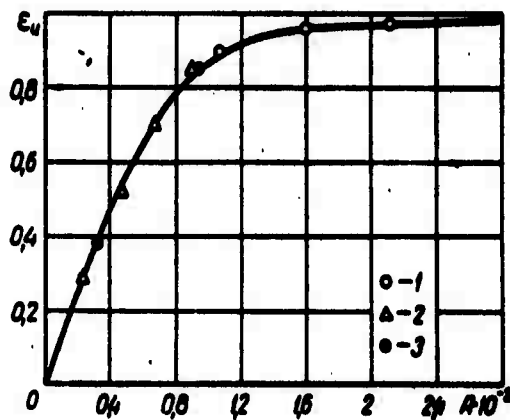


Fig. 2. Relationship between coefficient ϵ and dimensionless parameter M , according to experimental data.

1-Ivanov, Katanel'son, Pavlov; 2-Vulis, Ustimenko; 3-Schwab, Kapustin, Shabanov.

Thus the field of the velocity component u_p in the peripheral region of the cyclone ($r > R_1$) is defined by the exponential relation (14) in which the index of power n , taking (20) and (22) into account,

will be

$$n = M(0.01 \ 0.56M)^{-1} - 1. (23)$$

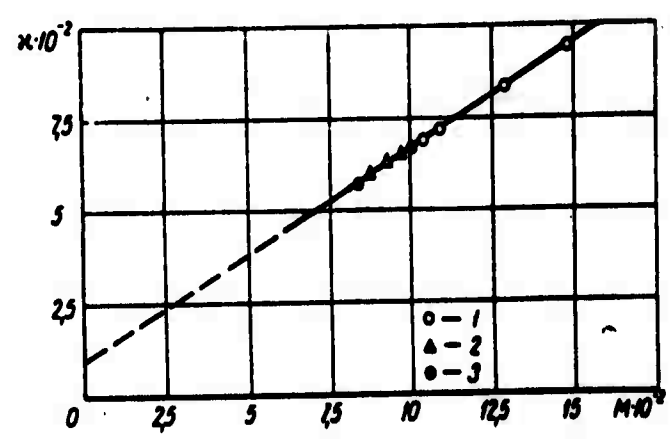


Fig. 3. Relationship between velocity drop $\epsilon_u = u_0/u_{px}$ of isothermal flow and dimensionless parameter

$$A = \frac{\sum a_i b_i}{2\pi R_0 L} \quad 1-3 \text{ --see Fig. 2.}$$

The relation $u_{\varphi 0} / u_{sx} = \epsilon_u$ included in (21) represents the coefficient of the decreasing speed which is defined by the preset speed near the cylindrical wall of the cyclone and the speed of the incoming medium. A reduction in the incoming speed u_{sx} to $u_{\varphi 0}$ near the wall of the cyclone is the result of the energy loss in the cyclone through friction tension on the cyclone walls, the outlet loss of speed and the loss involved in the central part of the cyclone in the activation of the air mass through the outlet opening, and other similar losses. The experimental data (1, 2) can be used to express the coefficient of the velocity loss by the following dimensionless relation

$$\varepsilon_u = f \left(\frac{\sum a_i b_i}{2\pi L R_0} \right),$$

as presented in the graph (Fig. 3). The use of the experimental coefficient value ε_u obviates the necessity of prescribing the velocity value $u_{\varphi 0}$ according to the experimental data in each concrete case in order to define the velocity field. It is a very important and test-proven fact that the field of rotational speed in the peripheral part of the cyclone, in accordance with the above conclusion, depends on the cross section area of the inlet nozzles but does not depend on the method of their distribution on the cyclone generator (assuming the same energy loss value at the end). This conclusion naturally does not affect the changes arising in the distribution of velocity components u_z .

In the central part of the cyclone, with $r < R_1$ and fairly low values R_1/R_0 (within the range of 0.15 - 0.4), the velocity field u_{φ} , as in the case of a solid body rotation, is described by a linear relation

$$u_{\varphi} = u_{\varphi R_1} \frac{r}{R_1},$$

where $u_{\varphi R_1}$ is determined by (14) with $r = R_1$. A smoothing-out process occurs at the joint of the speed velocity profiles u_{φ} , so that $\frac{du_{\varphi}}{dr} = 0$ with $r = R_1$.

Bibliography

1. Schwab, V. A., Kapustin, A. M., Shabanov, P. A. Sboruik nauchnykh trudov TEMIITA (Collected publications of the Moscow Engineering Institute), 34, 1961.

2. Ivanov, Yu. V., Katsnel'son, B. D., Pavlov, V. A., Bulis, L. A., Ustimenko, B. P., Lyakhovskiy, D. N. Voprosy Aerodinamiki i Teploperedachi (Aerodynamics and Heat Transfer in Boiler-Heating Processes) (edited by G. F. Knorre), Gosenergoizdat, 1958.

5132

CSO: 1880-D

A STUDY OF THE KINETICS OF THERMAL DECOMPOSITION OF ETHANE BY THE SINGLE-PULSE SHOCK-TUBE METHOD

by V. G. Knorre
G. I. Koslov

Power Institute im. G. M. Krzhishanovskiy, Moscow

The process of thermal decomposition of ethane has been studied before by various methods in the field of relatively low temperatures (3, 4, 5). But the data available on the total kinetics of high temperature ethane decomposition are still insignificant. We therefore initiated a study of this process by the method of a single-pulse shock tube described in work (1).

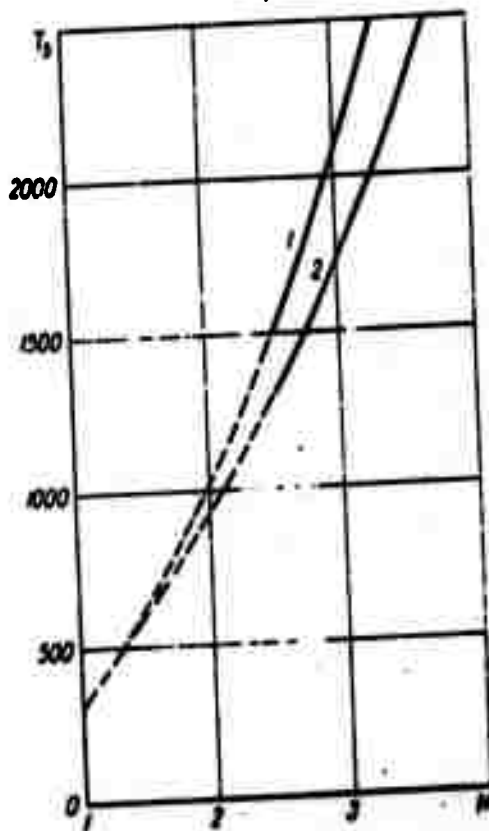


Fig. 1. The relationship between the temperature behind the reflected wave shock and the Mach number of the incident shock wave
1-for pure Ar; 2-5% mixture of $C_2H_6+95\% Ar$

An analysis of the reaction products was made on C_2H_6 , C_2H_4 , C_2H_2 , H_2 and in a number of tests on CH_4 . The pressure of the reacting gas in the high temperature "plug" during the tests amounted to about $405 \times 10^3 \text{ n x m}^{-2}$, and the reaction time between the tests fluctuated from 0.7×10^{-3} to 1.1×10^{-3} sec. The calculation of the gas temperature behind the reflected shock wave T_5 took into account the relationship between the ethane thermal capacity and the temperature on the assumption that the oscillation relaxation had been completed and there was no chemical reaction. The dependence of the theoretical temperature on the Mach number of the incident shock wave for a 5% mixture of $C_2H_6 + 95\%$ Ar is shown in Fig. 1. The mixtures containing ethane of the order of 1% temperature T_5 was calculated on the basis of calculation curves obtained for cases of pure argon and a 5% mixture of $C_2H_6 + 95\%$ Ar. The T_5 value was used as a temperature reaction T_p , with a correction for the reaction heat. The latter, in turn, was determined by an analysis of the reaction products that took into account the dependence of the thermal effects of the decomposition reaction of ethane, ethylene and acetylene on the temperature.

The tests were made in the interval of the Mach number values of an incident shockwave which extended the range of ethane transformation from about 2 to 90%. This made it possible to cover a reaction temperature range from 1,160 to 1,580° K in these relatively short reaction periods. It will apparently be quite difficult to rise to the region of still higher temperatures even by these methods.

Table

Speed-temperature dependence of ethane pyrolysis

Test No.	$P_1, \text{H} \cdot \text{m}^{-2}$	M	$P_2, \text{H} \cdot \text{m}^{-2}$	$T_2, ^\circ\text{K}$	Reaction time, sec. $\times 10^{-3}$	Initial ethane concentration in mixture $(\text{C}_2\text{H}_6)_0, \%$	Composition of the reaction products, %					K_2, sec^{-1}	$\log K_2$	$T_p, ^\circ\text{K}$	$10^4/T_p, \text{deg}^{-1}\text{K}$
							C_2H_6	CH_4	C_2H_4	C_2H_2	H_2				
139	15970	2.34	415000	1170	0.76	5.3	5.1	0	0	0	0.1	52	1.72	1170	8.53
146	9720	2.41	277000	1220	0.78	5.4	5.1	0	0	0	0.1	74	1.87	1210	8.25
140	14250	2.46	408000	1260	0.96	5.3	4.4	0.05	0.6	0	0.6	194	2.29	1230	8.12
145	19450	2.54	641000	1320	0.87	5.3	3.6	0.1	1.2	0	1.4	442	2.64	1270	7.87
138	12900	2.55	433000	1330	0.77	5.3	4.2	0.2	1.1	0	1.25	305	2.48	1290	7.75
144	6530	2.56	218000	1340	1.03	5.4	4.1	—	1.05	0	1.15	267	2.43	1290	7.75
136	11700	2.65	440000	1420	0.82	5.3	3.6	0.25	1.55	0	1.8	470	2.67	1370	7.30
134	10500	2.66	394000	1430	0.83	4.45	2.2	—	2.15	0	2.5	843	2.93	1400	7.15
137	10500	2.72	421000	1480	0.70	5.3	2.7	0.35	2.25	0.05	2.7	962	2.98	1400	7.15
132	10500	2.72	421000	1480	0.81	4.4	1.4	—	2.5	0.15	3.2	1420	3.15	1430	7.00
131	10500	2.76	442000	1520	0.76	4.4	1.4	—	2.5	0.2	3.2	1503	3.18	1470	6.80
142	9590	2.82	429000	1570	0.74	5.3	1.65	0.50	2.7	0.1	3.75	1580	3.20	1470	6.80
135	9590	2.84	436000	1590	0.84	4.45	0.95	0.55	2.55	0.55	3.85	1840	3.26	1510	6.62
141	8790	2.89	422000	1630	0.74	5.3	1.05	0.6	2.9	0.25	4.3	2180	3.34	1510	6.62
143	8050	2.99	424000	1730	0.98	5.4	0.65	0.9	3.0	0.5	4.8	2200	3.34	1580	6.33
151	15000	2.48	428000	1440	1.14	1.15	0.3	0.1	0.6	0.1	0.85	1180	3.07	1480	7.05
149	12900	2.62	424000	1570	0.89	1.15	0.1	0.25	0.55	0.3	1.2	2740	3.44	1530	6.53

To determine the order of the ethane reaction, tests were made with a 5% mixture of $\text{C}_2\text{H}_6 + 95\% \text{Ar}$ with the same M number but different pressures in the reacting gas. The figures on these tests are shown in the table under numbers 145; 138 and 144. A comparison of the reaction speed values in these tests reveals that the thermal decomposition of ethane does not depend a great deal on the pressure

changes within the approximate range of 202×10^3 to $607 \times 10^3 \text{ h} \times \text{m}^{-2}$, which indicates the first order of the reaction. The tests were made primarily with a 5% ethane - Ar mixture. Several tests were made with 1% ethane concentration in the mixture.

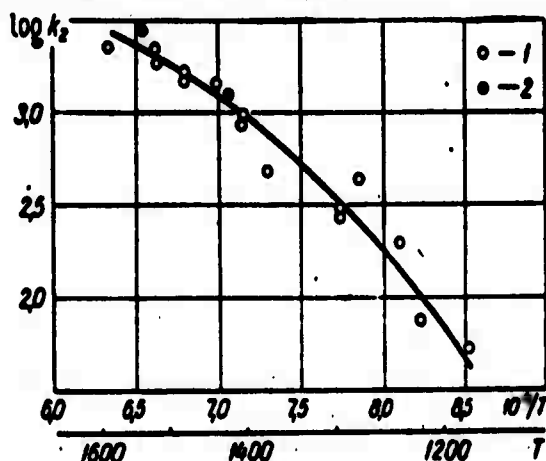


Fig. 2. Temperature dependence of the speed constant of the ethane pyrolysis process:

1-5% C₂H₆; 2-1% C₂H₆.

The test results were processed in accordance with the reaction of the first order. The primary experimental material and the calculation results of the reaction speed constant of the first order in the thermal decomposition of ethane k_2 are shown in the table. The temperature dependence k_2 is represented in Fig. 2. This chart shows that the activation energy of the thermal decomposition of ethane decreases with increasing reaction temperature. But as the latter increases, according to the table, the degree of ethane decomposition increases. Thus the seeming activation energy of this process decreases with the increasing decomposition of ethane. This result agrees with the

conclusion reached by Skinner and Ball (2). Figure 3 shows a comparison of our data with those of other authors obtained from a relatively low degree of ethane transformation. Thus in the tests carried out by Skinner and Ball the degree of transformation did not exceed 20%, and that is why their data are found within such a narrow temperature interval of 1,060-1,220° K. This graph shows that, given a temperature corresponding to a low degree of ethane decomposition (not more than 20%), the results of our tests well agree with the general tendency of the temperature dependence of the reaction speed constant k_2 . But at higher temperatures and degrees of decomposition the speed constants obtained in our tests will amount to only several percent of the values obtainable by extrapolating the data on corresponding low degree transformation k_{20} . This experimental result indicates that ethane pyrolysis occurs in a chain mechanism with the participation of free radicals. It is interesting to point out that k_2 does not depend on the ethane concentration in the initial mixture as implied in our work (2) and by our data. The k_2 dependence on the degree of transformation is apparently due to the inhibiting action of one of its decomposition products.

The graph represented in Fig. 3 can be used to determine k_{20} . The angle of incline of Arrhenius straight line drawn through the experimental data with a low degree of ethane transformation corresponds to the activation energy of 1,140 Joule $\times h^{-1}$. On the other hand, Skinner's and Ball's data indicate an activation energy equal to

870 Joule $\times h^{-1}$. Other researchers cite their own values.

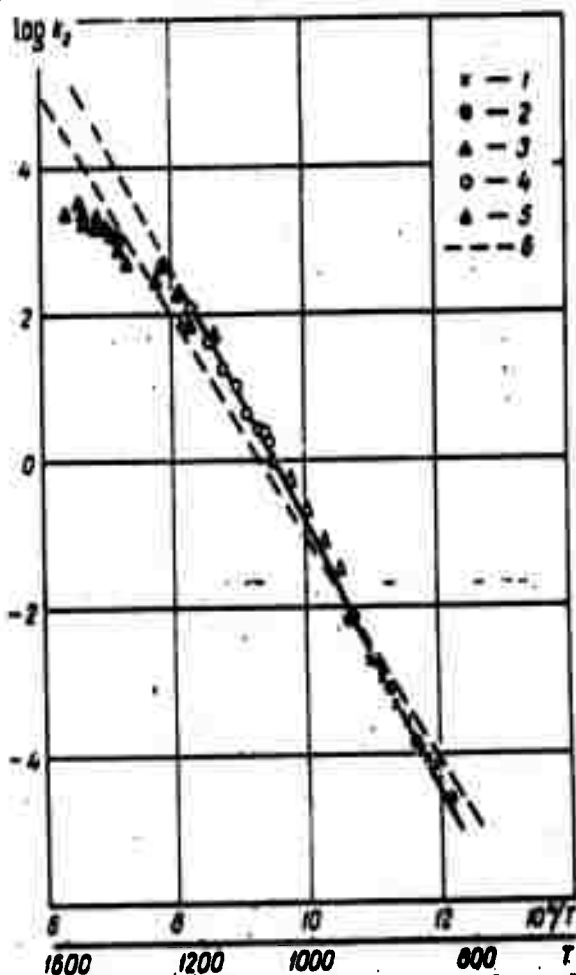


Fig. 3. Comparing the data on the temperature dependence of the speed constant of ethane pyrolysis:

- 1 - (4); 2 - (5); 3 - (3); 4 - (2); 5 - ours;
6 - a case of a calculation pre-exponent

It seems to us that the following method of determining the activation energy of ethane pyrolysis is more correct. The free atoms and radicals determining the speed of ethane pyrolysis can be produced by a break in either the C-H or the C-C bond in the ethane molecule. If the process is a monomolecular one, then, according to the theory, the pre-exponential factor should be of the order of the frequency

oscillations of the valent bonds in the molecule. In the case of an ethane molecule this frequency amounts to approximately $3,000 \text{ cm}^{-1}$. That means that the pre-exponential factor of the speed constant k_2 is equal to $9 \times 10^{13} \text{ sec}^{-1}$. An Arrhenius straight (dotted) line corresponding to this value of the pre-exponential factor is drawn across the experimental data (Fig. 3). The activation energy value calculated from the incline of the given straight line was found to be equal to $980 \pm 28 \text{ joule} \times \text{h}^{-1}$. We thus get the following expression for the ultimate speed constant of ethane pyrolysis:

$$k_{20} = 9 \cdot 10^{13} \exp \left(-\frac{69000}{RT} \right). \quad (1)$$

It would be interesting to compare the activation energy, thus defined, with the C-H and C-C bond-breaking energy in the ethane molecule. There are different values of these bond-breaking energies mentioned in literature and recommended by various authors. For example, the C-H bond-breaking energy values cited by various authors are found within the interval of $1,210 - 1,420 \text{ joule} \times \text{h}^{-1}$, and for the C-C bond in the interval of $840 - 1,200 \text{ joule} \times \text{h}^{-1}$. Thus the free radicals are probably originated by the following reaction



This is confirmed also by the appearance of methane in ethane pyrolysis products, especially at a high degree of transformation, whereas it is not found in ethylene and acetylene decomposition products. The inhibition of the ethane pyrolysis process with the

increasing degree of its transformation may be due to the elimination of radical CH_3 or atom H from the system (which invariably forms there) by one of the intermediate ethane decomposition products, such as H_2 , C_2H_4 , CH_4 or C_2H_2 . As shown in the table, the concentration of these substances in the reacting system reaches considerable proportions. In this case the primary products of ethane pyrolysis are ethylene and hydrogen. A little later the reaction products are found to contain methane whose concentration gradually increases in the course of ethane decomposition. Acetylene apparently forms from ethylene at higher temperatures and degrees of ethane pyrolysis. The question which of these components inhibits the ethane pyrolysis process can be decided by studying the effect of the addition of these gases to the initial ethane-argon mixture. This was done in work (2) where it was shown that the addition of hydrogen accelerates the ethane pyrolysis whereas the addition of methane and ethylene slows it down. Thus either one or both of these substances can inhibit the ethane decomposition process.

This problem, of course, requires further investigation. We will merely point out that any micromechanism pretending to describe the ethane pyrolysis process should explain that experimental fact. From this point of view it would be interesting to check the Rice-Hertzfeld mechanism which was further developed and modified in works (2, 4).

SUMMARY

The kinetics of ethane pyrolysis was studied in a single-pulse shock tube over the temperature range 1160 - 1580°K, the reaction time being about 1 msec. Total first order equation (1) describing the initial stage of ethane pyrolysis is given. The apparent activation energy falls with ethane decomposition.

Starting from the requirements and using the data obtained in the present work and reported, the conclusion is made on radical mechanism of the initial stage of the ethane pyrolysis described by equation (2).

BIBLIOGRAPHY

1. Kozlov, G. I., Knorre, V. G., IFZh Journal of Engineering Physics, No. 7, 1961.
2. Skinner, G. B., Ball, W. E., Journal of Phys. Chem., 64, 1025, 1960.
3. Davis, H. G., Williamson, K. D., Fifth World Petroleum Congress, Sec., LV, p. 4, 1959.
4. Steacie, E. W. R., Shane, G., Can. J. Res., 18, 203, 1940.
5. Kutchler, L. Theile, H., Z. physik. chem., 42, 359, 1939.

5132
CSO: 1880-D

THE EFFECT OF AN ELECTRICAL FIELD ON A CONTINUOUS LIQUID JET

by A. A. Semerchan
N. N. Kuzin
V. K. Isaykov

Institute of High-Pressure Physics, Moscow

Continuous liquid jets are now finding increasing application in the national economy, and the tendency is to increase their outflow speed. Under development is a hydraulic excavator designed to destroy rock at the speed of the water outflow which is faster than the speed of sound in the air. It is known (1) that a high-speed jet grows increasingly wider further away from the nozzle, assuming the shape of a cone consisting of a mixture of water and air, and its destructive capacity is thereby sharply reduced (2). The fight against the atomization of the jet is therefore assuming decisive importance in connection with hydraulic excavators which are used for destroying rocks located at considerable distances from the nozzle. It is believed possible to compress the jet with the use of an external electrical field if it can be electrified. The Institute of high-pressure physics of the USSR Academy of Sciences has therefore made a study of the effect of an electrical field on a continuous liquid jet. The nozzles used in the tests had a diameter of 0.5 to 2 mm. The speed of the jet was about 2.5 meters/sec. A high voltage rectifier capable of developing up to 20 kilovolts was used to create an electrical field. Up to 7 kilovolts the voltage was determined by a kilovolt meter, and above that by the spark gap in the discharger

installed at the rectifier outlet. The table on which the tests were made was covered with an insulating rubber mat so that all the items on the table were insulated from the ground. The observations were made visually and photographed with an exposure of $1/1250$ sec. The photographs were taken at a 40° angle to the jet trajectory plane, the lens being held at a level of the nozzle tip. It was first determined whether the jet coming out of the nozzle was electrified. As the jet went through a ring under a +6 kilovolt potential, individual drops of water were seen to detach themselves, swirl around the rim of the ring and adhere to it. In another test the water jet was aimed straight down between the plates of an air condenser which had +6 kilovolts in one armature and 0 in the other. The jet was first attracted to the +6 kilovolt plate, and, acquiring a positive charge upon contact, was repelled from that plate and attracted to the 0 plate. After that the phenomenon was repeated from the very beginning. The oscillation frequency of the jet depends on the distance between the plates, the potential of the positively charged plates, the nozzle diameter and the speed of the water outflow, etc. In our case the oscillation frequency per second equalled 2. The water jet coming out of the nozzle into the air was thus found to be charged. This is probably due to electrokinetic phenomena, but it is difficult to establish whether this electrization occurs in the nozzle or in the air.

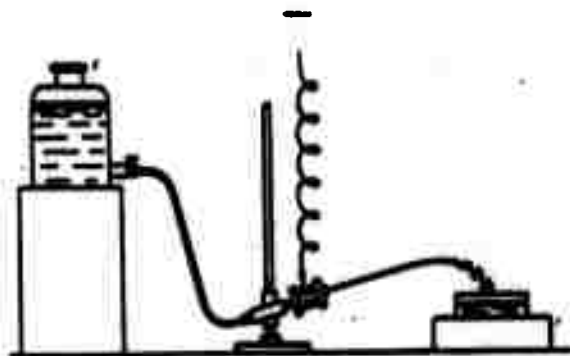


Fig. 1. Artificial electrization of water jet.

The authors assumed that one of the reasons for the atomization of the jet as it travels away from the nozzle was electrization. Actually, if the water drops receive a similar charge they repel each other thereby widening the jet spread. Experiments in the artificial electrization of the jet were therefore made for that purpose. When a high tension wire was connected directly to the metallic nozzle tip (Fig. 1), the jet took on the same charge as the tip. A metal level attached to an ebonite handle and connected to the nozzle tip with a high tension wire was then placed in contact with the jet. The level was repelled from such a test rod. The similarity of the jet charge signs was also confirmed by the determination of the drop charges. Two identical electroscopes were used. One of them was charged with the use of a metal ball on an ebonite handle near the nozzle by the repeated transfer of the same amount of charges. The second electroscope was charged by the water drops coming out of the nozzle and hitting the electroscope ball. Charged to the same potential by different methods, the two balls were connected; the electroscope needles remained in place which confirms the similarity of their charges.

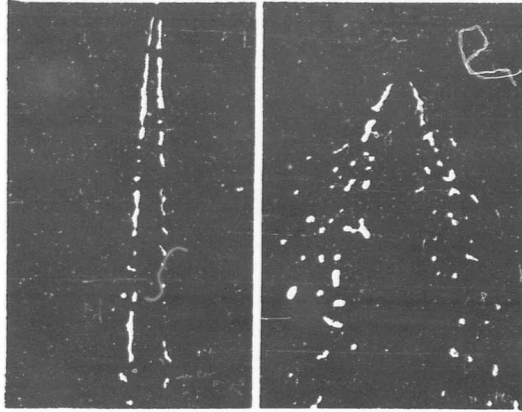


Fig. 2. a- Jet flowing out of two-opening nozzle; b- same jet with nozzle under high pressure.

A nozzle was built with two parallel openings with 0.8 mm diameters, spaced at 2 mm from each other. When a high voltage was passed to the nozzle, these jets repelled each other (Fig. 2). It is also obvious that the atomization of an artificially charged jet into drops is more intensive than that of an uncharged jet. Special tests showed (Fig. 3) that the atomization of a jet increases with the increasing application of a charge. At a distance of 350-400 mm from the nozzle the jet begins to atomize, and hits the target in the form of separate large drops. The dispersal of the drops is proportional to the applied charge. At a distance of 170-200 mm from the nozzle, small jets consisting of tiny water drops begin to branch off the main jet. The dispersion angle of the small jets widens with the increasing charge, reaching a maximum value up to 60° .

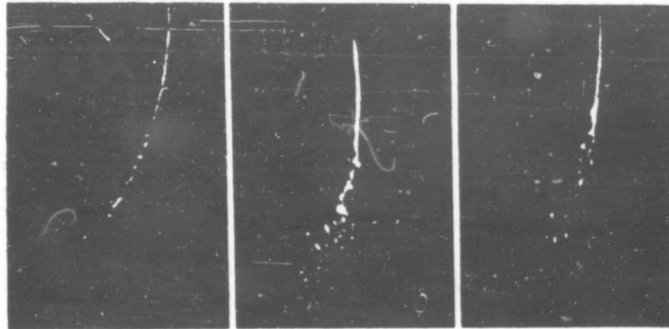


Fig. 3. Increasing jet atomization with increasing pressure

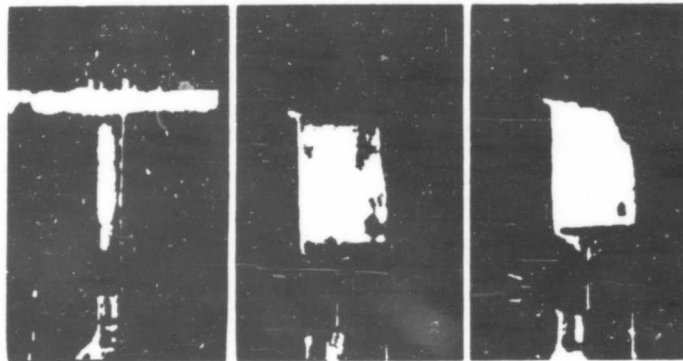


Fig. 4. a-a vertical upward jet;
 b-compression of jet with an analogously charged cylinder;
 c-jet cannot "break through" charged cylinder.

The electrified jet was contracted and passed through a reticular metal cylinder (for the convenience of observation) which was connected to the nozzle by a high voltage wire (Fig. 4, a, b). At some critical point the kinetic energy of the charged jet is not high enough to overcome the electrical field of the cylinder (Fig. 4, c). All the

above listed tests were made with ordinary tap water. Attempts to electrify kerosene and spindle oil jets (good dielectrics) did not produce any positive results: the potential did not produce any effect on the shape of the jet.

It was thus established that an electrified water jet breaks up in proportion to the jet potential. This break-up can to a large extent be controlled and reduced to a minimum with the use of charged focusing cylinders. At any rate, it may be stated that if the electrization of a jet is one of the reasons for its break-up, this factor can be reduced to a minimum by passing the jet through similarly charged cylinders, rings or bellows.

The above tests justify the hope that an increase in the compactness of the hydraulic excavator jets with the use of an electrical field may be quite effective.

Bibliography

1. Semerchan, A. A., Vereshchagin, L. F., Filler, F. M., Kuzin, N. N., Zhurnal Tekhnicheskoy Fiziki (Journal of Technical Physics), 28, No. 9, 1958.
2. Semerchan, A. A., Vereshchagin, L. F., Filler, F. M., Kuzin, N. N., IFZh (Journal of Engineering Physics), No. 3, 1960.

5132
CSO: 1880-D

THERMAL MASS EXCHANGE IN ANISOTROPIC

by N. I. Gamayunov
Kalinin Peat Institute, Moscow

Following (1, 2), the thermal mass exchange in anisotropic capillary-porous colloid bodies can be described by a system of equations.

$$\frac{\partial t}{\partial \tau} = \sum_{i=1}^3 C_i \frac{\partial^2 t}{\partial x_i^2} + \sum_{i=1}^3 D_i \frac{\partial^2 \theta}{\partial x_i^2}, \quad (1)$$

$$\frac{\partial \theta}{\partial \tau} = \sum_{i=1}^3 C_i' \frac{\partial^2 t}{\partial x_i^2} + \sum_{i=1}^3 D_i' \frac{\partial^2 \theta}{\partial x_i^2}, \quad (2)$$

where x_i represents the Cartesian coordinates ($i = 1, 2, 3$); t, θ are, respectively, the temperature and potential of the mass exchange;

$$C_i = a_i + \frac{\rho \delta_i a_{mi}}{c}; \quad D_i = \frac{\rho a_{mi} c_m}{c}; \quad C_i' = \frac{\delta_i a_{mi}}{c_m}; \quad D_i' = a_{mi}.$$

It is assumed here that the coefficients of heat and temperature conduction, moisture and potential conduction and the thermo-gradient coefficients δ_i differ in the direction of the coordinate axes. The other coefficients do not depend on the coordinates as they are the mass (volumetric) characteristic of the body.

We will find a solution of system (1), (2) for an anisotropic body representing a parallelepiped with the following dimensions $2l_1 \times 2l_2 \times 2l_3$ under boundary conditions:

$$t(x_1, x_2, x_3, 0) = f_1(x_1, x_2, x_3), \quad \theta(x_1, x_2, x_3, 0) = f_2(x_1, x_2, x_3), \quad (3)$$

$$t(l_i, \tau) = \varphi_i(\tau), \quad \theta(l_i, \tau) = \psi_i(\tau) \quad (4)$$

and symmetry conditions (it is assumed here that the coordinates

originate in the center of the paralleliped, and the solution takes into account only 1/8 of its volume)

$$\frac{\partial t(0, \tau)}{\partial x_i} = 0, \quad \frac{\partial \theta(0, \tau)}{\partial x_i} = 0. \quad (5)$$

After the successive application to equations (1), (2) and conditions (3)-(5) of the Laplace integral transformation by time and the Laplace finite transformation (3) or the Fourier cosine-transformation (4) by three coordinates and their combined solution, we get:

$$\bar{T} = (M_1 \gamma_1 - N_1 \gamma_2)/H; \quad \bar{\Theta} = (N_2 \gamma_2 - M_2 \gamma_1)/H, \quad (6)$$

where

$$\gamma_s = F_s + \Phi_s + \Psi_s, \quad s = 1, 2; \quad H = M_1 N_2 - M_2 N_1;$$

$$M_1 = D_1 p_1^2 + D_2 p_2^2 + D_3 p_3^2 + q; \quad N_1 = B_1 p_1^2 + B_2 p_2^2 + B_3 p_3^2;$$

$$M_2 = C_1 p_1^2 + C_2 p_2^2 + C_3 p_3^2; \quad N_2 = A_1 p_1^2 + A_2 p_2^2 + A_3 p_3^2 + q.$$

$$T(x_1, x_2, x_3, q) = \int_0^{\infty} \exp(-q\tau) t(x_1, x_2, x_3, \tau) d\tau;$$

$$\Theta(x_1, x_2, x_3, q) = \int_0^{\infty} \exp(-q\tau) \theta(x_1, x_2, x_3, \tau) d\tau;$$

$$\bar{T}(p_1, p_2, p_3, q) = \int_0^{l_1} \int_0^{l_2} \int_0^{l_3} T(x_1, x_2, x_3, q) \cos p_1 x \cos p_2 x \cos p_3 x dx_1 dx_2 dx_3;$$

$\bar{\Theta}, F_1, F_2$ are also transforms by three coordinates of functions θ, f_1, f_2 .

$$\Phi_1 + \Psi_1 = \frac{\sin \rho_1 l_1 \sin \rho_2 l_2 \sin \rho_3 l_3}{\rho_1 \rho_2 \rho_3} \sum_{i=1}^3 \rho_i^2 (A_i \bar{\varphi}_i + B_i \bar{\psi}_i);$$

$$\Phi_2 + \Psi_2 = \frac{\sin \rho_1 l_1 \sin \rho_2 l_2 \sin \rho_3 l_3}{\rho_1 \rho_2 \rho_3} \sum_{i=1}^3 \rho_i^2 (C_i \bar{\varphi}_i + D_i \bar{\psi}_i);$$

$$\bar{\varphi}_i(\rho) = \int_0^l \exp(-q\tau) \varphi_i(\tau) d\tau; \quad \bar{\psi}_i(\rho) = \int_0^l \exp(-q\tau) \psi_i(\tau) d\tau.$$

According to conditions (4), (5), the characteristic equations are recorded as follows:

$$\cos(\rho_1 l_1) = \cos \mu_k = 0, \quad \mu_k = (2k-1)\pi/2 \quad (k=1, 2, 3, \dots);$$

$$\cos(\rho_2 l_2) = \cos \mu_m = 0, \quad \mu_m = (2m-1)\pi/2 \quad (m=1, 2, 3, \dots);$$

$$\cos(\rho_3 l_3) = \cos \mu_n = 0, \quad \mu_n = (2n-1)\pi/2 \quad (n=1, 2, 3, \dots).$$

We shall use the inversion formula to change to the originals by the coordinates, equate the denominator of equations (6) with zero, find the roots q_j and, using the expansion theorem, we will get the final expression: (c) $t(x_1, x_2, x_3, \tau) =$

$$= \frac{1}{v_1 - v_2} \sum_{k=1}^{\infty} \sum_{m=1}^{\infty} \sum_{n=1}^{\infty} \sum_{j=1}^2 (-1)^{j+1} [M_{1j}^*(u_{1j} + v_{1j}) - N_{1j}^*(u_{2j} + v_{2j})], \quad (7)$$

$$= \frac{1}{v_1 - v_2} \sum_{k=1}^{\infty} \sum_{m=1}^{\infty} \sum_{n=1}^{\infty} \sum_{j=1}^2 (-1)^{j+1} [N_{2j}^*(u_{2j} + v_{2j}) - M_{2j}^*(u_{1j} + v_{1j})], \quad (8)$$

where

$$M_{1j}^* = \frac{A_1}{L_1^2} \mu_k^2 + \frac{A_2}{L_2^2} \mu_m^2 + \frac{A_3}{L_3^2} \mu_n^2 - v_j, \quad j=1, 2;$$

$$M_{2j}^* = \left(Fe_1 + \frac{1}{Lu_1} \right) \frac{A_1}{L_1^2} \mu_k^2 + \left(Fe_2 + \frac{1}{Lu_2} \right) \frac{A_2}{L_2^2} \mu_m^2 +$$

$$+ \left(Fe_3 + \frac{1}{Lu_3} \right) \frac{A_3}{L_3^2} \mu_n^2 - \nu_j;$$

$$N_{1j}^* = \frac{1}{\delta} \left(\frac{Fe_1 A_1}{\Delta_1 L_1^2} \mu_k^2 + \frac{Fe_2 A_2}{\Delta_2 L_2^2} \mu_m^2 + \frac{Fe_3 A_3}{\Delta_3 L_3^2} \mu_n^2 \right);$$

$$N_{2j}^* = \frac{1}{\delta} \left(\frac{A_1}{\Delta_1 L_1^2} \mu_k^2 + \frac{A_2}{\Delta_2 L_2^2} \mu_m^2 + \frac{A_3}{\Delta_3 L_3^2} \mu_n^2 \right);$$

$$A_i = \frac{a_{mi}}{a_m}; \quad L_i = \frac{l_i}{l}; \quad \Delta = \frac{\delta_i}{\delta};$$

$$a_m = \sqrt{a_{m1}^2 + a_{m2}^2 + a_{m3}^2}; \quad l = \sqrt{l_1^2 + l_2^2 + l_3^2}; \quad \delta = \sqrt{\delta_1^2 + \delta_2^2 + \delta_3^2};$$

$$\begin{aligned} \nu_j = \frac{1}{2} & \left\{ \frac{A_1 K_1}{L_1^2} \mu_k^2 + \frac{A_2 K_2}{L_2^2} \mu_m^2 + \frac{A_3 K_3}{L_3^2} \mu_n^2 + (-1)^{j+1} \left[\left(\frac{A_1 K_1}{L_1^2} \mu_k^2 + \right. \right. \right. \\ & \left. \left. \left. + \frac{A_2 K_2}{L_2^2} \mu_m^2 + \frac{A_3 K_3}{L_3^2} \mu_n^2 \right)^2 - 4 \left[\frac{A_1^2 \mu_k^2}{L_1^4 Lu_1} + \frac{A_2^2 \mu_m^2}{L_2^4 Lu_2} + \frac{A_3^2 \mu_n^2}{L_3^4 Lu_3} + \right. \right. \right. \\ & \left. \left. \left. + \frac{A_1 A_2 \mu_k \mu_m}{L_1^2 L_2^2} \left(\frac{1}{Lu_1} + \frac{1}{Lu_2} \right) + \frac{A_1 A_3 \mu_k \mu_n}{L_1^2 L_3^2} \left(\frac{1}{Lu_1} + \frac{1}{Lu_3} \right) + \right. \right. \right. \\ & \left. \left. \left. + \frac{A_2 A_3 \mu_m \mu_n}{L_2^2 L_3^2} \left(\frac{1}{Lu_2} + \frac{1}{Lu_3} \right) \right] \right]^{1/2} \right\}; \end{aligned}$$

$$K_i = 1 + Fe_i + 1/Lu_i, \quad i = 1, 2, 3; \quad Fe_i = \frac{\rho \delta_i}{c}; \quad Lu_i = \frac{a_{mi}}{a_i};$$

$$u_{j0} = 8 \int_0^1 \int_0^1 \int_0^1 f_s(x_1, x_2, x_3) \cos \mu_k \frac{x_1}{l_1} \cos \mu_m \frac{x_2}{l_2} \cos \mu_n \frac{x_3}{l_3} \times$$

$$\times d \frac{x_1}{l_1} d \frac{x_2}{l_2} d \frac{x_3}{l_3} \cdot \cos \mu_k \frac{x_1}{l_1} \cos \mu_m \frac{x_2}{l_2} \cos \mu_n \frac{x_3}{l_3} \exp(-\nu_j F_0 m);$$

$$v_{j0} = \frac{(-1)^{k+m+n+1} 8}{\mu_k \mu_m \mu_n} \int_0^{F_0 m} \left\{ \frac{A_1 \mu_k^2}{L_1^2} \left[\left(\frac{1}{Lu_1} + Fe_1 \right) \varphi_1(\theta) + \frac{Fe_1}{\delta_1} \psi_1(\theta) \right] + \right.$$

$$\begin{aligned}
& + \frac{A_2 \mu_m^2}{L_3^2} \left[\left(\frac{1}{Lu_2} + Fe_2 \right) \varphi_2(\theta) + \frac{Fe_2}{\delta_2} \psi_2(\theta) \right] + \frac{A_3 \mu_m^2}{L_3^2} \left[\left(\frac{1}{Lu_3} + Fe_3 \right) \varphi_3(\theta) + \right. \\
& \left. + \frac{Fe_3}{\delta_3} \psi_3(\theta) \right] \Bigg\} \exp \left\{ -\nu_l [Fo_m(\tau) - Fo_m(\theta)] \right\} dFo_m(\theta) \times \\
& \times \cos \mu_k \frac{x_1}{l_1} \cos \mu_m \frac{x_2}{l_2} \cos \mu_n \frac{x_3}{l_3} ; \\
& Fo_m(\tau) = \frac{a_m \tau}{l^2} ; Fo_m(\theta) = \frac{a_m \theta}{l^2} .
\end{aligned}$$

It is not difficult to extend the method of solution cited in the article to bodies of various configuration by using the Laplace, Fourier or Henkel finite transformations.

SUMMARY

A heat and mass transfer equation of an anisotropic capillary-porous colloidal body is solved in the paper. The body is a parallelepipedon $2l_1 \times 2l_2 \times 2l_3$ in size under boundary conditions (3) and (4) and symmetry conditions (5).

BIBLIOGRAPHY

1. Lykov, A. V., Teplo- i Massoobmen v Protsessakh Sushki (Thermal and Mass Exchange in Drying Processes). Gosenergoizdat, 1956.
2. Lykov, A. V., Mikhailov, Yu. A., Teoriya Perenosa Energii i Veshchestv (The Theory of Energy and Matter Transfer). Publ. by the Belorussian Academy of Sciences, 1959.
3. Collection of articles on Teplo- i massoobmen v protsessakh ispareniya (Thermal and Mass Exchange in Evaporation Processes), edited by A. V. Lykov. Publ. by the Academy of Sciences of the USSR, 1958.
4. Sneddon, A. I., Preobrazovaniya Fur'ye (The Fourier Transformation), Foreign Literature Publishing House, 1955.

5132
CSO: 1880-D

SIMILARITY AND MODELING CONDITIONS OF ARCLESS ELECTROSMELTING PROCESSES

by G. S. Nus

State Scientific Research Institute of Nonferrous Metals, Moscow

Under general stationary conditions dealt with in the formulas (8)-(29)* we shall assume that $\epsilon \gg 1$, as in the case of low values ϵ the effects produced by the polarization of a dielectric may be ignored. In this connection, we shall consider $\epsilon - 1 \approx \epsilon$. Otherwise a similarity analysis will lead to an additional equation condition in the sample and model of dielectric penetrability which, as will be seen later, does not have to be fulfilled in the case of high values ϵ .

An equation of motion is valid for any moment of time, and that means also for $\tau = 0, \frac{2\pi}{\omega}, \frac{4\pi}{\omega}, \dots$. Then it will be possible to include in it $\exp(j\omega\tau) = 1$ for a similarity analysis.

Replacing the dimensional magnitudes a, \dot{a}, a, \dot{a} in the equations by the dimensionless $A = \frac{a}{a_0}, \dot{A} = \frac{\dot{a}}{\dot{a}_0}, A = \frac{a}{a_0}, \dot{A} = \frac{\dot{a}}{\dot{a}_0}$ (where a_0 is the magnitude scale) and, excluding the scales, we will get dimensionless equations and the following binding equations between the scales:

- 1) from the equations of the electromagnetic field (8)

$$\frac{c_{co} \epsilon_0}{\omega_0 l_0^2} = \frac{u_0 \epsilon_0^2}{l_0 c_{co}} = \frac{c_{co} \epsilon_0}{c_{co}} = \frac{c_{co} u_0 \epsilon_0}{\omega_0 l_0 c_{co}};$$

- 2) from the equations of motion (9)

$$\frac{\rho_0 u_0}{\tau_0} = \frac{\rho_0 u_0^2}{l_0} = \frac{\rho_0}{l_0} = \rho_0 g_0 = \frac{\rho_0 u_0}{l_0^2} = \frac{c_{co} \epsilon_0^2}{\omega_0 l_0};$$

- 3) from the equations of heat transfer in the smelting (11)

$$\frac{l_0 l_0}{l_0^2} = k_0 c_{co} \epsilon_0^2 = \frac{c_{co}^2 \rho_0 g_0}{\tau_0};$$

- 4) from the equations of heat conduction (13)

$$k_0 c_{co} \epsilon_0^2 = q_{pe};$$

* The numeration of the formulas in this article is in accordance with (1) of which this work is a continuation.

5) from the boundary conditions (21), (23)

$$\frac{k_0 t_0}{l_0} = r_0 \rho_0 g_0 u_0 = a_0 t_0.$$

The others do not produce any binding equations*. We have 13 equation binding 19 unknown scales. Selecting the following 6 scales as independents $\rho_0 = \rho_*$; $\sigma_0 = \sigma_*$; $t_0 = t_*$; $c_{20} = c_{2*}$; $k_0 = k$; $g_0 = g$, and determining all the others from the binding equations by dividing the physical magnitudes into the scales, we will obtain the values of the dimensionless magnitudes.

If the unknown quantities are dimensionless characteristic equations, the solution of the entire system of dimensionless equations may be recorded in general terms as follows:

$$K^{IV} = K^{IV}(\Pi) = K^{IV}(X, Y, Z, L_I, L_{II}, \dots, L_I, Fo, Re_{Tps}, \dot{E}_{Tps},$$

$$Bi', Bi'', \theta_r, \theta_n, \dot{E}_n, V_n, Ko_*, Q_{ps}, Gr', \Sigma_1, K'_*, K'_{*1},$$

$$K'_{*2}, K'_{*3}, K''_*, K''_{*1}, K''_{*2}, R_{*1}, R_{*2}, R_{*3}, Pr_*, \Lambda_{*1}, \Lambda_{*2},$$

$$\Lambda_{*3}, C_*, C_{*1}, C_{*2}, C_{*3});$$

$$K^V = K^V(\Pi); K^V_{1,2,3} = K^V_{1,2,3}(\Pi); Po_1 = Po_1(\Pi),$$

$$\theta_{2,3} = \theta_{2,3}(\Pi); K''' = K'''(\Pi); Eu = Eu(\Pi). \quad (42)$$

where the function $f(\Pi)$ is introduced to simplify the recording. It can be understood as a function of a point in some region of multi-dimensional space Π ; the number of space dimensions is equal to the number of dimensionless magnitudes included in the sign of the function, and the region is determined by the possible values of these magnitudes.

The monodromic criteria here are:

*It is assumed that all the equations expressing boundary conditions are invariant in relation to scale transformations.

$$X = \frac{xg^{1/2} \sigma^{1/2}}{c^{1/2}}; \quad Y = \frac{yg^{1/2} \sigma^{1/2}}{c^{1/2}}; \quad Z = \frac{zg^{1/2} \sigma^{1/2}}{c^{1/2}};$$

$$L_{i, II, \dots, i} = \frac{l_{i, II, \dots, i} g^{1/2} \sigma^{1/2}}{c^{1/2}}; \quad \dot{E}_{r, p, n} = \frac{\dot{e}_{r, p, n}}{\rho_0^{1/2} c^{1/2}} \left(\frac{\sigma_0}{g}\right)^{1/2};$$

$$\Theta_{s, s, r, n} = \frac{t_{s, s, r, n}}{t_0}; \quad V_n = \frac{v_n}{c^{1/2}} \left(\frac{\sigma_0}{g}\right)^{1/2}; \quad \Sigma_s = \frac{\sigma_s}{\sigma_0};$$

$$Q_{p_0} = \frac{q_{p_0} \sigma^{1/2}}{k \rho_0 g^{1/2} c^{1/2}}; \quad R_{\sigma_1, \sigma_2, \sigma_3} = \frac{\rho_{\sigma_1, \sigma_2, \sigma_3}}{\rho_0};$$

$$\lambda_{\sigma_1, \sigma_2, \sigma_3} = \frac{\lambda_{\sigma_1, \sigma_2, \sigma_3} t_0 \sigma^{1/2}}{k \rho_0 g^{1/2} c^{1/2}};$$

$$C_{\sigma_1, \sigma_2, \sigma_3} = \frac{c_{\sigma_1, \sigma_2, \sigma_3} g^{1/2} t_0 \sigma^{1/2}}{k c^{1/2}}.$$

The polydromic criteria:

$$Fo = \frac{\lambda_0}{\rho_0 g c_0 l_i^2}; \quad Re_{r, p_0} = \frac{v_2 \rho_0 l_i}{\mu_0}; \quad Bi' = \frac{\alpha' l}{\lambda_0};$$

$$Bi'' = \frac{\alpha'' l}{\lambda_{\sigma_3}}; \quad Ko_{\sigma_1} = \frac{r}{c_{\sigma_1} t_0}; \quad Gr'_{\sigma_1} = \frac{\rho_{\sigma_1}^2 g l_i^3}{\mu_{\sigma_1}^2};$$

$$Pr_{\sigma_1} = \frac{\mu_{\sigma_1} c_{\sigma_1} g}{\lambda_{\sigma_1}}; \quad Po_{\sigma_1} = \frac{q_{\sigma_1} l^2}{\lambda_{\sigma_1} t_1}; \quad Eu = \frac{\rho}{\rho v^2};$$

$$K'_{\sigma_1, \sigma_2, \sigma_3} = \frac{\rho_{\sigma_1, \sigma_2, \sigma_3} \omega l_i^2}{c^2}; \quad K''_{\sigma_1} = \frac{\rho_{\sigma_1} \omega}{\sigma_{\sigma_1}};$$

$$K''_{\sigma_1} = \frac{\rho_{\sigma_1} \omega}{\sigma_{\sigma_1}}; \quad K''_{\sigma_2} = \frac{\rho_{\sigma_2} \omega}{\sigma_{\sigma_2}}; \quad K''' = \frac{V}{\omega l};$$

$$K^{IV} = \frac{e^2 \sigma}{\omega \rho v^2}; \quad K^V = \frac{k e^2 \sigma l^2}{\lambda t}.$$

The K' and K'' criteria are variant criteria of the electromagnetic field and with alternating sinusoidal current and $\omega = 1$,

and K^{IV} and K^V are Eu Po variants for ponderomotive forces and joule heat; K' is a similarity criterion of an electromagnetic field in moving media.

The K' criterion characterizes the ratio of the current conduction density to the rotation of the magnetic intensity in a

stationary medium;

K'' characterizes 1) the ration between the displacement current density and the conductance current in a stationary medium; b) the ration between the transfer current density of a moving polarized medium and the conductance current generated by the movement of the medium in a magnetic field; c) the density ratio between the ponderomotive forces in a stationary dielectric and the ponderomotive forces in a stationary conductor;

K''' characterized the density ratio between a conductance current generated by the movement of a conductor in a magnetic field and the conductance current in a stationary medium;

$(K''')^2$ characterizes the density ratio between the ponderomotive forces generated by the movement of a dielectric in an electrical field, and the ponderomotive forces in a stationary dielectric.

All the values in the criteria of the left part of equations (42) apply to the same flowing point. All the criteria in the right part of the equations, except $X, Y, Z, B_1', B_1'', \dot{E}_{rp4}, \Theta_h, \dot{E}_h, V_h$, have a strictly local meaning (it is recalled that the dimensionless characteristic equations are considered as fixed).

The resulting criterial relations fulfill the requirements of the π -theorem. Indeed, the number of physical values is $N = 50+1$; the number of values with independent dimension $b = 6$, and the number of criteria $N - b = 44+1$.

It is obvious that the simplifications we introduced in the

description of a stationary case are correct on condition that $K^{\text{IV}} \ll 1$ and $K^{\text{V}} \ll 1$.

To produce a similarity of electrical, temperature, velocity and pressure fields, the criteria K^{IV} , K^{V} , K^{VI} and Bu in the similar points of the model and sample should be the same. This would obviously occur if the following were equal in the model and sample

$$L_1, L_{11}, \dots, L_4, Fo, Re_{rps}, \Theta_r, Ko_s, Q_{ps}, Gr', \Sigma_s, K'_s, \\ K'_{s1}, K'_{s2}, K'_{s3}, K'_s, K'_{s1}, K'_{s2}, R_{s1}, R_{s2}, R_{s3}, Pr_s, \\ \Lambda_{s1}, \Lambda_{s2}, \Lambda_{s3}, C_s, C_{s1}, C_{s2}, C_{s3},$$

if Bi' , Bi'' and \dot{E}_{rps} were equal in the similar points on the boundary surfaces at the similar moments of time, and Θ_h , \dot{E}_h , V_h in the similar points of the volume; also if the dimensionless characteristic equations were correspondingly identical for the sample and model. This is the rule for modeling the process under investigation.

In a stationary case, the equations (30)-(41) with $\exp(j\omega\tau) = 1$ will produce the following binding equations:

$$\frac{c_{ss}e_0}{\omega_0 l_0^2} = \frac{c_0 e_0}{c_{ss}}; \quad \frac{\rho_0 l_0^2}{l_0} = \frac{\rho_0}{l_0} = \rho_0 g_0 = \frac{\rho_0 u_0}{l_0^2} = \frac{\rho_0 e_0^2}{\omega_0 l_0};$$

$$\frac{\lambda_0 l_0}{l_0} = k_0 c_0 e_0^2 = \frac{c_0 \rho_0 g_0 l_0 u_0}{l_0}; \quad q_{rps} = \frac{i_0 l_0}{l_0};$$

$$q_0 = i_0 l_0; \quad u_0 = c_0 l_0.$$

We will select 7 scales with independent dimensions:

$$\rho_0 = \rho_s; \quad g_0 = g_s; \quad c_0 = c_s; \quad l_0 = l_s; \quad c_{ss} = c_s; \quad k_0 = k; \quad c_0 = c_s.$$

By analogy with the previous case, we will get:

$$K^{IV} = K^{IV}(\Pi') = K^{IV}(X', Y', Z', L'_I, L'_{II}, \dots, L'_I,$$

$$K'_*, \dot{U}, Q, Q_{rp}, Q'_{rp}, Gr'_*, Pr_*);$$

$$K^V = K^V(\Pi'); \quad Re = Re(\Pi'); \quad Eu = Eu(\Pi'), \quad (43)$$

where

$$X' = \frac{xg}{c_c^4} \left(\frac{\sigma_* c_* t_*}{k} \right)^2; \quad Y' = \frac{yg}{c_c^4} \left(\frac{\sigma_* c_* t_*}{k} \right)^2;$$

$$Z' = \frac{zg}{c_c^4} \left(\frac{\sigma_* c_* t_*}{k} \right)^2; \quad L'_I, L'_{II}, \dots, L'_I = \frac{l_{I, II, \dots, I} g}{c_c^4} \left(\frac{\sigma_* c_* t_*}{k} \right)^2;$$

$$\dot{U} = \frac{u \sigma_*^2 c_* t_*}{\rho_* c_c^3 k}; \quad Q = \frac{qg}{\rho_* c_c^{10}} \left(\frac{\sigma_*}{k} \right)^6 (c_* t_*)^4;$$

$$Q_{rp} = \frac{q_{rp} \sigma_*}{\rho_* c_c^2 k g}; \quad Q'_{rp} = \frac{q'_{rp} \sigma_*}{\rho_* c_c^2 k g};$$

$$Re = \frac{v \rho l}{\mu}.$$

The other criteria are the same as in a nonstationary case. It follows from (43) that

$$Nu = \frac{a^m l}{\lambda} = Nu(\Pi').$$

Here the requirements of the π -theorem are also fulfilled: $N = 22 + i$;

$$b = 7; \quad N - b = 15 + i.$$

The gist of the modeling rule is that in the model and sample $L'_I, L'_{II}, \dots, L'_I, K^*, \dot{U}, Q, Gr', Pr_*$ must be correspondingly equal, and Q_{rp}, Q'_{rp} equally distributed on the smelting boundaries; the dimensionless characteristic functions must be respectively identical.

It is implied here that the order of relations between the relative conductances in the various parts of the furnace and its model is the same, and the size of the electrodes and the location of the voltmeter test circuit are included in the number of geometric parameters.

It is not difficult to see that when the nonpotential aspect of a field can be ignored /see expressions (34) and (35)/, the criterion K_I is excluded from the criterial dependences (43), and the K^{IV} criterion will look like

$$K^{IV} = \frac{\rho^2 c^2 l^2}{c_c^2 \rho v^2}$$

In the commercial ore-smelting electric furnaces of the non-ferrous metallurgy $K^* \ll 1$ and $K^{IV} \ll 1$. They can therefore be modeled according to the above-outlined rule.

If the linear scales of a model and sample are different, the use of the same smelting in them will result in the nonfulfillment of the $Gr_*^* = idem$ requirement. This brings up the problem of selecting modeling materials.

So far it has been impossible to select the suitable materials for modeling nonstationary operating conditions of furnaces in the nonferrous metallurgical industry.

The rule for modeling a stationary case, as shown by calculations and the experience in modeling commercial furnaces, can be easily followed by covering the smelting in the modeled furnace with a solid charge, and by using acidified glycerin (slag) and naphthalene (solid charge) as modeling materials.

Approximate modeling methods are now being developed with a view to reducing the size of the models and widening the assortment of modeling materials.

SUMMARY

Similarity conditions are analysed and rules for simulation of the processes occurring in the electrical melting furnace under stationary conditions are formulated. This analysis allows to obtain criterial equations (42 and 43) in a general form.

BIBLIOGRAPHY

1. Nus, G. S., IZFh (Journal of Engineering Physics) No. 8, 1962.
2. Eygenson, L. S., Modelirovaniye (Modeling), Published by Sovetskaya Nauka (Soviet Science), Moscow, 1952.
3. Benikov, V. A., Primeneniye Teorii Podobiya i Fizicheskogo Modelirovaniya v Elektrotekhnike (The Application of the Similarity and Physical Modeling Theory in Electrical Engineering), Gosenergoizdat (State Power Engineering Publishing House), 1949.

5132

CSO: 1880-D

THERMAL STRESSES AND HEAT RELEASE IN
RECTANGULAR CROSS-SECTION UNITS

by A. S. Trofimov

Certain parts of nuclear reactors are shaped like fairly long prisms ($l \gg 3a$, if $a < b$) with a rectangular cross section ($2a \times 2b$) (Fig. 1), or have a very similar shape (the reflector and decelerator units, etc.). Knowing the heat release q and the temperature field $T(x, y)$, it is quite simple to determine the magnitude of the thermal stresses in such units.

Disregarding the axial temperature gradients, we will have a condition of plane deformation $\epsilon_z = \text{const}$. Introducing the standard symbols (1), we will get a formula for the axial stress, assuming the lack of external loads on the prism

$$\sigma_z = \nu E \left[\frac{1}{4ab} \int_{-a}^a \int_{-b}^b T dx dy - T(x, y) \right] + \nu (\sigma_x + \sigma_y), \quad (1)$$

and for the tension function definable as

$$\sigma_x = \frac{\partial^2 \Phi}{\partial y^2}; \quad \sigma_y = \frac{\partial^2 \Phi}{\partial x^2}; \quad \tau_{xy} = -\frac{\partial^2 \Phi}{\partial x \partial y}, \quad (2)$$

we will get the following equation

$$\nabla^4 \Phi + \frac{\alpha E}{1 - \nu} \nabla^2 T = 0, \quad (3)$$

where

$$\nabla^4 = \frac{\partial^4}{\partial x^4} + 2 \frac{\partial^4}{\partial x^2 \partial y^2} + \frac{\partial^4}{\partial y^4}; \quad \nabla^2 = \frac{\partial^2}{\partial x^2} + \frac{\partial^2}{\partial y^2},$$

with the following boundary conditions on the cross-section contour

$$\Phi = \frac{\partial \Phi}{\partial n} = 0.$$

In a steady-state process we have:

$$\nabla^2 T = -\frac{q_v}{\lambda},$$

which, with $q_v = \text{const}$ produces the following problem for the dimension-

less stress function $u = \phi \frac{\lambda(1-\nu)}{aEt^2q_v}$:

$$\nabla^2 u = 1 \quad \begin{array}{l} -c \leq x \leq c, \\ -1 \leq y \leq 1, \end{array} \quad (4)$$

at

$$x = \pm c = \pm \frac{a}{b} \quad u = \frac{\partial u}{\partial x} = 0, \quad (4.a)$$

$$y = \pm 1 \quad u = \frac{\partial u}{\partial y} = 0 \quad (4.b)$$

(Hereinafter x and y will be used as dimensionless coordinates)

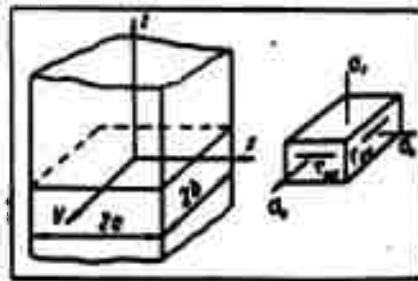


Fig. 1. Diagram of rectangular cross-section unit

We find solution (4) by using the variational method (2) and the n -th approximation for $u(x, y)$ in the form of

$$u_n = (x^2 - c^2)(y^2 - 1)^2 [a_1 + a_2 x^2 + a_3 y^2 + \dots]. \quad (5)$$

The system of equations for the unknown coefficients a_k in our case looks like the following

$$\int_{-c}^c dx \int_{-1}^1 \left[\nabla^2 \sum_{k=1}^n a_k \varphi_k - 1 \right] \varphi_s dy = 0, \quad s=1, 2, \dots, n, \quad (6)$$

where $\varphi_1 = (x^2 - c^2)^2 (y^2 - 1)^2$; $\varphi_2 = \varphi_1 x^2$; $\varphi_3 = \varphi_1 y^2$ || T. A. etc.

We shall limit ourselves to three terms of the series, then

$$\nabla^4 \sum_{k=1}^3 a_k \varphi_k = 8a_1 [3(y^2 - 1)^2 + 3(x^2 - c^2)^2 + 4(3x^2 - c^2)(3y^2 - 1)] +$$

$$+ 8a_2 [3x^2(x^2 - c^2)^2 + 3(y^2 - 1)^2(15x^2 - 2c^2) +$$

$$+ 2(3y^2 - 1)(15x^4 - 12x^2c^2 + c^4)] + 8a_3 [3y^2(y^2 - 1)^2 +$$

$$+ 3(x^2 - c^2)^2(15y^2 - 2) + 2(3x^2 - c^2)(15y^4 - 12y^2 + 1)].$$

Substituting quadratures in (6), we get the following system

$$a_1 \left(\frac{64}{7} c^4 + \frac{256}{49} c^2 + \frac{64}{7} \right) + a_2 c^2 \left(\frac{64}{77} c^4 + \frac{64}{49} \right) +$$

$$+ a_3 \left(\frac{64}{49} c^4 + \frac{64}{77} \right) = \frac{1}{2},$$

$$a_1 \left(\frac{64}{11} c^4 + \frac{64}{7} \right) + a_2 c^2 \left(\frac{192}{143} c^4 + \frac{256}{77} c^2 + \frac{192}{7} \right) +$$

$$+ a_3 \left(\frac{64}{77} c^4 + \frac{64}{77} \right) = \frac{1}{2},$$

$$a_1 \left(\frac{64}{7} c^4 + \frac{64}{11} \right) + a_2 c^2 \left(\frac{64}{77} c^4 + \frac{64}{77} \right) +$$

$$+ a_3 \left(\frac{192}{7} c^4 + \frac{256}{77} c^2 + \frac{192}{143} \right) = \frac{1}{2}.$$

The solution of this system for the different cross-section relations is given in Table 1.

c	Values of coefficients a_k		
	a_1	a_2	a_3
0,1	0,034896	0,0072160	0,2153200
0,2	0,036570	0,0076043	0,1884900
0,3	0,038924	0,0083781	0,1448520
0,4	0,040420	0,0090080	0,0986810
0,5	0,039910	0,0092298	0,0624880
0,6	0,037419	0,0090146	0,0385540
0,7	0,033574	0,0084531	0,0237190
0,8	0,029069	0,0076667	0,0147070
0,9	0,024481	0,0067707	0,0092205
1,0	0,020203	0,0058575	0,0058575

Consequently, we get the following formulas for stresses (2):

$$\sigma_x = kf_x; \quad \sigma_y = kf_y; \quad \tau_{xy} = kf_{xy} \quad (8)$$

where

$$k = \frac{\alpha E}{1-\nu} \frac{q_0 b^2}{k}$$

$$f_x = 2(x^2 - c^2)^2 \{ (3y^2 - 1) [2(a_1 + a_2 x^2) + a_3 (3y^2 - 1)] + 6a_2 y^2 (y^2 - 1) \};$$

$$f_y = 2(y^2 - 1)^2 \{ (3x^2 - c^2) [2(a_1 + a_2 y^2) + a_3 (3x^2 - c^2)] + 6a_2 x^2 (x^2 - c^2) \};$$

$$f_{xy} = -8xy(x^2 - c^2)(y^2 - 1) [2a_1 + a_3 (3x^2 - c^2) + a_3 (3y^2 - 1)].$$

The maximum normal stresses occur on the prism surface and are defined by the following formulas:

$$\sigma_{x \max} = \sigma_x(x=0, y = \pm 1) = kf_x^{\max}, \quad \text{with } \sigma_y = 0, \quad (9)$$

$$\sigma_{y \max} = \sigma_y(x = \pm c, y=0) = kf_y^{\max}, \quad \text{with } \sigma_x = 0.$$

Here the values f_x^{\max} and f_y^{\max} depend only on c , and can be tabulated (Table 2).

Table 2.

The f_x^{\max} and f_y^{\max} values in relation to c

c	$f_x^{\max} = 8c^4 (a_1 + a_2)$	$f_y^{\max} = 8c^4 (a_1 + c^2 a_2)$
0.1	0.00020018	0.0027973
0.2	0.00288100	0.0117500
0.3	0.01190900	0.0285700
0.4	0.02847500	0.0535800
0.5	0.05119800	0.0844300
0.6	0.07776800	0.1171100
0.7	0.11004800	0.1478500
0.8	0.14344000	0.1739800
0.9	0.17688000	0.1941700
1.0	0.20848000	0.2084800

If solution (5) were to involve only one term of the series, as is the case with formulas (3), the σ_{\max} would be placed too low (about 23% for a square cross section); but the addition of the

following terms of the series (functions $\varphi_4; \varphi_5$ etc.) in our solution amounts to approximately 5%, and this may probably be disregarded in view of the accurate definition of the constants etc.

The tangential stresses on the surface are reduced to zero, their maximum being found in the region where the normal stresses are low, and the absolute magnitude of τ_{\max} is considerably smaller than σ_{\max} (for $c = 1 \frac{\tau_{\max}}{\sigma_{\max}} = 0.234$); the tangential stresses will therefore not be limiting factors in the operation of the unit.

Bibliography

1. Gatewood, B. E. Temperaturniye napriasheniya (Temperature Stresses), Foreign Literature Publishing House, 1959.
2. Kantorovich, L. V., Krylov, V. I., Priblizhenniye metody vysshego analiza (Approximate Methods of Higher Analysis), Gostekhizdat (State Publishing House of Technical Literature), 1952.
3. Belov, A. V., Izvestiya Vsesoyuznogo nauchno-issledovatel'skogo instituta gidrotekhniki im. Vedeneyeva (Bulletin of the all-Union Vedeneyev Scientific-Research Institute of Hydraulic Engineering), 54, 1954.

5132

CSOF 1880-D

CONCERNING THE CRITICAL DIAMETER OF
SPHERICAL THERMAL INSULATION

by E. A. Niderov

As is known (1), the critical diameter of the thermal insulation of cylindrical and spherical bodies is usually referred to as the value of the insulation diameter corresponding to the minimum thermal resistance. The data on a critical diameter of the thermal insulation of a sphere, available in literature (2), apply only to a hypothetical case of a convective heat-exchange coefficient independent of the diameter of a sphere. The solution shown below reveals the precise variability of the heat-exchange coefficient.

We will record the general expression of the thermal resistance of spherical bodies

$$r = r_0 + \frac{1}{\pi d} \left[\frac{1}{2\lambda} \left(1 - \frac{1}{x} \right) + \frac{1}{a_x dx^2} \right]. \quad (1)$$

We will assume the relation $a_x = a_x(D)$ and, consequently, relation $a_x = a_x(x)$ to be known. Thus a convective heat exchange with the surrounding medium provides experimental data (3) on the nature of the relationship between the Nusselt number and the Reynolds number. These data can be expressed in the form of the following exponential relation

$$\text{Nu} = A \text{Re}^n, \quad (2)$$

with $R < 10$ $n = 0$, $A = 2$. As Re increases, the value n changes from $n = 0 (\text{Re} \rightarrow 0)$ to $n = 1 (\text{Re} \rightarrow \infty)$. On the basis of (2) we have

$$a_x = a_1 x^{n-1}, \quad (3)$$

where a_1 is the value definable by formula (2), with $x = 1$.

Substituting (3) in (1) and comparing the derivative $\frac{dr}{dx}$, we find the critical value

$$x_0 = \left[\frac{2(n+1)\lambda}{a_1 d} \right]^{1/n} \quad (4)$$

or the value of the critical diameter

$$D_0 = \frac{2(n+1)\lambda}{a_2} \quad (5)$$

The independence of a_2 of the sphere diameter corresponds to $n = 1$, and can actually occur only during a convective heat exchange with $R \rightarrow \infty$.

In this case, in accordance with (2), we have:

$$D_0 = \frac{4\lambda}{a_2} \quad (6)$$

But in all the other real cases, when $1 < n \leq 0$, the value of the critical diameter will be

$$\frac{2}{n+1} \text{ times less.}$$

SYMBOLS

r_0 is the thermal resistance of a spherical body to the insulation layer; $x = D/d$ the ratio of the variable external insulation diameter D to the constant value d of the internal insulation diameter; $a(x)$ the coefficient of the heat exchange on the external insulation surface.

SUMMARY

Equation (5) is obtained which relates the optimum thickness of spherical thermal insulation and the convective heat transfer mechanism, described by formula (2).

BIBLIOGRAPHY

1. Mikheyev, M. A. Osnovy Teploperedachi (The Basis of Heat Exchange), Gosenergoizdat (State Power Publishing House), 1956.
2. Voskresenskiy, K. D., Sbornik Raschetov i Zadach po Teploperedache (A Collection of Calculations and Problems in Heat Exchange), Gosenergoizdat, 1959.

3. Katsnel'son, B. D., and Timofeyev, F. A. Trudy Tsentral'nogo kotloturbinnogo instituta (Transactions of the Boiler and Turbine Institute), Vol 12, No. 3 Mashgis (State Publishing House of Scientific Literature), 1949.

5132
CSO: 1880-D

—

**FIRST INTERNATIONAL CONGRESS OF CHEMICAL
ENGINEERING (CHISA) IN BRNO**

by A.S. Ginsburg

The first International Congress of chemical engineering, machine-building and automation (CHISA) was held from the second through the eighth of September 1962 in Brno (Czechoslovakia). Participating in the congress were over 750 delegates representing 19 countries (Czechoslovakia, USSR, GDR, Poland, Hungary, Rumania, Bulgaria, Yugoslavia, England, Belgium, Holland, the U.S., France, West Germany, Japan, etc.).

The following three sections were simultaneously at work: 1) chemical engineering (chairman professor Zh. Standart, Prague); 2) chemical machine-building (chairman engineer I. Schreiber, Brno); 3) automation (chairman engineer I. Komurca, Prague).

The convening of the Congress was a significant event in the development of world science and technology not only because chemistry and chemical technology are a powerful force of modern technical progress, but also because of the concrete subjects of the reports which covered a variety of processes and apparatuses of various industries. For example, the sessions of the engineering section dealt with hydrodynamics, heat transfer and drying, absorption and extraction, distillation, etc.; the section on machine-building examined reports on the characteristics of materials used in chemical machine-building

(austenitic rustproof steel containing Cr-Mn-N, alloys with a nickel and titanium base, etc.), the protection of materials against corrosion (the chemical stability of acid-proof enamel, zinc-nickel electrolytic cover, the stability of polyvinyl chloride, etc.), the design and calculation of apparatuses and their elements (high-pressure pumps and compressors, heat exchangers, mixers, cylindrical vessels), as well as reports on the durability of the chemical industry apparatuses; the section on automation dealt with complex automation and the construction of automatic production control systems, the use of electronic computers for regulating processes and apparatuses, as well as certain problems of general interest such as the cascade regulation of the temperature in a blast furnace, the selection of the best heat exchanger design, the analytical determination of the properties of fractionating columns, the control of the blast process with the heat stream pick-up, thermistors in laboratory measuring facilities, apparatuses for gas chromatography, etc.

A review report on "The Investigation in the Field of Chemical Engineering in the USSR" was read by Academician N. M. Zhavoronkov at the opening of the Congress.

We shall dwell in greater detail on the performance of the engineering section where much attention was devoted to pseudoliquifaction, particularly the drying of granular materials in a boiling layer. The first session of that section was devoted to a discussion of hydrodynamics. A report on mechanical liquid mixing was made by

Professor G. Steidl (Department of Processes and Apparatuses of the Prague Chemical-Technological Institute). That report outlined the investigation results of such phenomena as the homogenation of inter-mixable liquids, the exhaustion of a granular solid phase and its dissolution. We should also point out such themes as the analytical and experimental investigation into the movement of non-Newtonian liquid (Ya. Ulbrecht, Scientific-Research Institute of synthetic rubber, Gottwaldow, Czechoslovakia); the determination of gas consumption by measuring the temperature drop in the adiabatic expansion in a venturi tube (T. Nobler and A. Burkhart, Laboratory of processes and apparatuses of the Polish Academy of Sciences, and Department of processes and apparatuses of the Polytechnical Institute at Glivice); the study of the mechanism of continuous evaporation of solutions and the investigation of "lower density" areas in a pseudoliquidified solid body-liquid system (H. Hassett, A. Lodson and N. Stokley, Department of processes and apparatuses of the Technological Institute at Laffborough, England). The latter report was illustrated by a special film demonstrating the formation of canals (or, as the authors called them "bands and pseudo-bubbles") in a boiling layer.

The second session was devoted primarily to the hydrodynamics of a boiling layer. This problem, now being widely tackled in Czechoslovakia, was dealt with in the reports by J. Beranek and D. Sokol (Scientific-Research Institute of Organic Synthesis in Pappubitzse).

Beranek dwelt on the uneven distribution of solid particles

in a boiling layer. The author distinguishes three types of a boiling layer: uniform, bubbly and reciprocating. Considerable differences in the specific gravity of the particles and liquid tend to disrupt the uniformity of a pseudoliquidified layer and result in the formation of bubbles. If the sizes of the individual bubbles are large enough to be commensurable with the diameter of the tubes, they produce a "piston effect" in the latter — the bubbles divide the particle "pistons". The fluidity of such a pseudoliquidified layer is characterized by two simplexes, d_n/d_r and d_n/d_{an} , where d_n is the diameter of the bubbles; d_r the diameter of the solid particles and d_{an} the diameter of the apparatus. A vertical channel in which the static pressure is less than the hydrostatic pressure may be formed in the layer; as the static pressure along the edges of the channel is greater than within it, the liquid is sucked into the channel. The size of the bubbles depends on the physical properties of the particles and their interfriction. An accurate physical picture of the state of a boiling layer will make it possible to proceed to the kinetic calculation of the apparatus.

D. Sokol discussed the abrasion of particles in a boiling layer which is frequently of decisive importance in the practical utilization of pseudoliquidification processes. The abrasion is determined by the hydrodynamics of the layer, the design of the apparatus and the physical properties (stability) of the particles. The author investigated the effect of the gas velocity, the height and

diameter of the apparatus on the abrasion of the particles. He found that abrasion occurs primarily when the material movement takes place in a horizontal plane.

The reports of G. Winterstein, K. Rose and G. Fivog (Institute of Designing Chemical Equipment in Leipzig, GDR) outlined the investigation results of the hydrodynamics of a pseudoliquidified layer in a multistep apparatus with overflow pipes. In these continuously operating apparatuses, usually of a counterflow type, the layer of a definite thickness should be maintained at each step, and the duration of the various particles should be characterized by some average value.

The authors presented equations and charts characterizing the relationship between the transportation process of the solid particles (up or down) and the geometric and dynamic characteristics of the apparatus.

Investigating the mixing of solid particles in a horizontal boiling layer, L. Musil (Scientific-Research Institute of Inorganic Chemistry at Usti-on-Labe, Czechoslovakia) checked the possibility of using a simple diffusion model. In view of the difficulty of solving the problem of the lengthy presence of the particles in the layer on the basis of physical laws alone, the author used the statistical method of investigating chance phenomena. He characterizes the intermixing of particles as a so-called diffusion coefficient which remains constant throughout the process.

Professor P. G. Romankov and docent N. B. Rozhkovskaya (the

[Leningrad Lenseviet Technological Institute) submitted a report on "The drying of paste-like materials in a boiling layer". This comprehensive report outlines a new method of drying paste-like materials and describes new designs of drying apparatuses and feeders. The effect of the design of irrigation facilities and the water temperature on the irrigation density is discussed in the works of T. Hobler, I. Synoviets, V. Granovskiy and Lu-Hsin Su (Laboratory of processes and apparatuses of the Polish Academy of Sciences at Gliwice). It contains information on the water consumption and a calculation of the irrigation density for horizontal and vertical pipes.

The third session was devoted primarily to the processes of drying materials in a boiling layer.

The major report on this theme was made by professor Ya. Tsiborovskiy (Warsaw polytechnical institute). It is practical to use apparatuses with a pseudoliquidified layer for drying paste-like and solid materials. An investigation of the heat exchange between gas and the layer showed that the temperature of the solid phase is practically the same at all points, and a layer of 150 mm high and more is characterized by a thermal equilibrium between the gas and the layer. According to the author, the drying in a pseudoliquidified layer is an adiabatic process. Referring to some design problems, he suggests that the gas be fed (tangentially) as in a dust extractor (cyclone) in order to prevent the formation of channels. To dry such powders, it would be practical to use impulse pseudoliquidification.

The speaker reported that grain dryers with a boiling layer and a capacity of 6 tons per hour are successfully at work in Polish agriculture; they are used for drying rye, buckwheat, oil plant seeds, etc. He suggests that the automatic control of the drying process in a boiling layer be based on the layer and gas temperature and the intensification of the feeding mechanism (by the use of a booster).

Dryers in a boiling layer are characterized by a high technical and economic indices: moisture removal $100-300 \text{ kg/m}^3\text{-hr}$ (instead of $15 \text{ kg/m}^3\text{-hr}$ in other types of dryers), specific heat consumption $2,940-5,460 \text{ joule/kg}$ of moisture; when a low residual moisture is desired, the heat consumption can be raised by increasing the desorption heat. The hydraulic resistance of the installation ranges from about 2,940, when the drying chambers are connected in parallel, to $9,800 \text{ n x m}^{-2}$, when connected in series.

In his detailed work, I. Valharzha (State Scientific Research Institute of Thermal Machinery in Prague) obtained a system of differential equations describing the process of drying monodispersed material in a jet dryer, and generalizes the same process for polydispersed materials. The polydispersed system is replaced by a certain number of monodispersed fractions which are characterized by various periods of their presence in the apparatus. The results of the theoretical investigations were checked on an experimental installation.

V. Vanecak (Scientific-Research Institute of Inorganic Chemistry at Usti-on-Labe) investigated the dehydration of crystalhydrates in a

laboratory dryer in a boiling layer as well as in a semiproduction continuous-operation installation. The characteristics of the dried materials are presented, and the basic technical and economic indices cited.

A. S. Ginzburg and V. A. Rezchikov (Moscow Technological Institute of the food industry, and the All-Union Scientific-Research Institute of grain) investigated the aerodynamics of the heat-and mass exchange in an apparatus with a boiling layer of grain.

The aerodynamic investigations revealed the existence of two stages in the pseudoliquidified state of the grain layer: an initial stage and a stage of turbulent boiling. In apparatuses without mechanical mixers the drying process should be carried out at the beginning of the second stage of pseudoliquidification. The investigations of grain drying in a boiling layer indicate that it would be practical to use that method for a preliminary drying of wet grain. The drying of thermolabile and moisture-inert grain materials in a boiling layer calls for the use of alternating heating and cooling processes.

The calculation of a drying installation with a boiling layer should take into account the duration of the material-heating process to a preset permissible maximum temperature. Such a formula was obtained by the authors by integrating the differential equation of a thermal balance. An empirical equation was obtained and a calculation nomogram compiled in order to determine the drying speed. The equation provides a good description of the experimental results obtained by the

investigators of various countries (USSR, Czechoslovakia, Poland, Canada, West Germany).

Ziolkovskiy (Institute of Physical Chemistry of the Polish Academy of Sciences) dwelt on the "sewing" (equivalent) heat conduction of a layer of granular materials in which the space between the individual grains is filled with gas that is either immobile or moving normally in the direction of the heat stream. He investigated the relationship between the heat conduction of the layer and that of the solid phase, the nature of the grain arrangement, the mean temperature of the layer and the speed of the gas flow; in particular, he established the exponential relationship between the coefficient of the heat conduction of the layer and its temperature.

The report of J. Jaris and K. Porter (Birmingham University, England) dealt with condenser designing. The authors developed a method calculating horizontal refrigerating devices designed for the condensation in the presence of noncondensable gases. The theoretical premises were checked in an experimental laboratory device by condensing the steam of ethyl alcohol and water in the presence of air or nitrogen.

The importance of the problem of drying in a boiling layer was emphasized by the discussion following the reports.

P. D. Lebedev (USSR) emphasized the value of the impulse method of drying finely dispersed materials, V. Vanecek (Czechoslovakia) pointed out with reason that drying in a medium with a considerable amount of steam cannot be considered as an adiabatic process, etc.

The main subject of discussion at the fourth session was heat transmission.

Unable to dwell in detail on the content of all the reports, we shall hereafter confine ourselves to a brief outline of some of the works and reports.

V. R. Van Vijk outlined the results of an investigation into the formation of steam bubbles in boiling liquid binary mixtures; the report was illustrated by a motion picture film (the filming speed was 4,000 frames per second).

The work of K. Kembłowski and M. Servinskiy (Technical Institute, Lodz') discussed the investigation of a heat transfer from a heated wall to a suspension of solid particles in water moving in a pipe, and cited a comparison of the heat transfer coefficients with reference to pure liquid and suspensions.

I. Moshchitskaya (Institute of physical chemistry of the Polish Academy of Sciences) experimentally determined the local heat transfer coefficients on models; the resulting coefficients were then compared with the values obtained from an analogy between the heat transfer processes and the mass.

The mass exchange of two-phase systems was the subject of discussion at the fifth session. Special mention should be made of the report submitted by professor Zh. Standart (Institute of theoretical bases of chemical machinery of the Czechoslovakian Academy of Sciences) who used the thermodynamic method of irreversible processes to

investigate the transfer phenomena on an interphase surface. Guided by the Bernoulli equation and the first law of thermodynamics, written with reference to heterogenic systems, the author obtained the well-known differential equations for a continuous phase and new expressions for the processes occurring on the surface of the phase division. Corresponding inequations for individual transfer processes were obtained on the basis of the second law of thermodynamics expressed in the form of an irreversible entropy increment. The linear correlation between the moving forces and the streams they generate, obtained from these inequations, are transformed and account is taken of the changing moving forces. Of the greatest interest are the correlations describing the superimposed processes of heat-and mass-exchange.

G. Linde (East German Academy of Sciences) investigated the hydrodynamic instability of the liquid interphase of a surface in the process of mass and heat exchange. Determining the coefficients of light ray diffraction on an interphase surface, the author showed that the instability of that surface is the cause of a more complex free convection mechanism in the mass and heat exchange processes on the boundary of the phase division. Under conditions of a compulsory turbulent convection, the hydrodynamic stability reduces the intensity of the process.

J. M. Smith (California University) studied the nature of the transfer in porous catalyzers which are considered as a system of macro-and micropores. The experimental data were processed with a view

to obtaining the relationship between the speed of gas diffusion and the distribution function of the macropore sizes, as well as the relationship between the seeming (equivalent) heat conduction and the distribution function of micropores and the length of the free run of gas molecules in them.

J. Niko and P. Le Hoff (University of Nancy, France) investigated the removal speed of solid particles (glass balls with a diameter of 63 micron) with reference to 1- and 2- component boiling layers (glass balls with a diameter of 63 and 160 micron). The authors draw an analogy between the diffusion of particles in a boiling layer and a turbulent diffusion in a continuum.

M. Mokhtadi (Birmingham University) and P. Bruz (Canadian Industrial Company) investigated the internal circulation and speed of a following drop with reference to binary mixtures of nonmiscible liquids.

P. Feldesh (Budapest Technical Institute) drew an analogy between mass transfer and hydrodynamics on reticular bubble plates of diffusion apparatuses.

Of the reports submitted to the sixth session, to shall mention that of Mr. Jorger (Prague Scientific Research Institute of thermo-technics) on "The effect of a jet flow on the mass transfer and the possibilities of using that method for drying purposes", and by M. E. Pozin (Leningrad Lensoviet Technological Institute) "Foam in the processing of gas with liquids".

M. Corger investigated the process of naphthalene evaporation.

under the effect of an air stream directed from a nozzle normally to the evaporation surface. The correlations required to determine the coefficient of the mass exchange were obtained on the basis of experiments carried out under different conditions (the speed of the air jet from the nozzle 10-40 m/sec, the width of the nozzle 5-40 mm, the distance between the nozzles 70-350 mm, and the distance between the nozzle and the control plate was 1-8 times greater than the width of the nozzle). The optimum distance between the nozzle and the material should be 8.5 times greater than the width of the nozzle.

M. E. Pozin's investigations in the use of the foam regime are widely known. This was indicated also by the lively discussion that followed his report. The various interaction processes between gas and liquids (cooling and heating gases and liquids, evaporating solutions, drying and moistening gases, etc.) are sharply intensified by the conversion of the gas-liquid system into a stable foam.

The considerable turbulence under such conditions leads to the creation of a constantly renewable interphase surface, the diffusion resistance decreases and the intensity of thermal and diffusion processes increases many times in comparison with the usual bubbling apparatuses and scrubbers. Used on a large scale are foamy gas purifiers whose efficiency is as high as 97-99%; the best results are achievable in cleaning the gas of dust consisting of particles with a diameter of about 5 microns.

The seventh session focused its attention on extraction

processes. The report submitted by S. Ellis and J. Jeffries (Birmingham University) contained an analysis of the existing theories of mass transfer and the quantity of movement in a system of a continuous and dispersed phase, and made an attempt to determine the efficiency of apparatuses by calculation methods. As an analysis was made for only one drop of liquid, a coincidence of calculation and experimental data was obtained only for simple apparatuses with a fairly accurate description of the hydrodynamic regime of the dispersed phase. Under conditions of a complex extract flow, the picture is changed by the interaction ("adhesion") of the drops.

F. Molino (Birkenditch Technical Institute, England) investigated the mass exchange by separating the liquid systems and suspensions in a hydrocyclone. He cited, in particular, the design parameters of an apparatus for the enrichment of minerals and the form of solid particle trajectories as well as the investigation results of extraction and oil separation.

Doctor Reiner (who spoke in place of K. Libhart, Lurgi Joint Stock Company, Frankfurt-am-Maine, West Germany) outlined the results of his research on equipment for liquid extraction. A higher efficiency is usually achieved by increasing the mass transfer surface or decreasing the film thickness of the respective phase. According to the authors of the proposed apparatuses which are of a more complex design than the packed and sifter columns, the degree of separation amounts to 90-95%. It is proposed to replace the mixing by centrifugation

which makes it possible to do without a mixer-separator. The investigations were made on a model about one-tenth the natural size.

G. P. Solomakha and A. N. Planovskiy (Scientific-Research Institute of organic semiproducts and dyestuffs, Moscow) investigated the mass transfer process in a gas phase during the absorption of ammonium by water from an air-ammonium mixture. Numerous tests revealed that the coefficient of the mass transfer on sieve plates is determined by the speed of gas in the column and the height of the static liquid level on the plate.

Schubert (Czechoslovakia), S. Koppacheva (USSR), etc. participated in the discussion.

The eighth session was devoted to absorption processes.

K. Asperger (Institute of chemical equipment designs, Leipzig, East Germany) cited a design of equipment for the production of nitric acid and developed a new equation for determining the equilibrium constants of nitrogen dioxide absorption. Admitting the possibility of using existing methods for designing plate-like absorption columns, the author finds it necessary to elaborate the design of packed columns and proposes a system of differential equations for characterizing the changing concentrations by the height of the column.

The reports of V. I. Konvisar who spoke on behalf of a group of authors (V. Atroshenko, A. Zazorin, V. Efinov, Ye. Kordysh) and I. Litvinenko (Kharkov Polytechnical Institute) outlined the results of a large-scale effort in designing columns to obtain nitric acid from

nitric oxides. The process of nitric oxide absorption by water solutions of nitric acid is considerably accelerated in a column with sifter plates. The report shows the efficiency of the plates as determined by the temperature, linear speed and general pressure of nitrous gas as well as by the acid concentration. A production type nitric acid with a concentration of 68-70% was obtained in a zonal absorber with sifter plates under a pressure of $(3.8-5) \times 9.8 \times 10^4 \text{ H x m}^{-2}$.

Ya. Bettelheim and R. Klimecek (Scientific-Research Institute of inorganic chemistry, Usti-on-Labe, Czechoslovakia) proposed and successfully tested on a new model an absorption installation consisting of a packed column made of wire spirals. The installation is designed to absorb sulfur dioxide from the flue gas of thermal electric power plants.

M. Belski and M. Adelmets (Scientific-Research Institute of inorganic chemistry, Usti-on-Labe, Czechoslovakia) reported on the construction and extraction results on a semiplant model of an absorber with "collapsing" (Russian term proval'niye) plates designed to wash the tail gases in the production of superphosphate. A study of the apparatus produced certain data characterizing the mass transfer coefficients and the drop in the column pressure.

V. Orlov (USSR), and others participated in the discussion.

Redistillation was discussed at the ninth session. V. V.

Kaforov's report (Moscow D. I. Mendeleev chemical-technological Institute) was titled "Certain problems of the contemporary state of

the theory and practice of redistillation". The report discussed the equilibrium in steam-liquid systems and the kinetics of redistillation processes; it introduced the concept of diffusion efficiency and cited equations of mass transfer with reference to the design of the various types of diffusion apparatuses; it cited the technical and economic indices of the redistillation columns (the output per unit of capacity and the consumption of energy per unit of the division height) and proposed certain methods of improving them.

K. Drozba's work (the Otto Gerike Polytechnical Institute, Magdeburg, East Germany) dealt with the investigation of a mass transfer on a hooded plate; the reports of M. Gumlia, M. Rylec and A. Standart (Czechoslovak friendship plants, Zaluzhi, Czechoslovakia, and the Institute of theoretical bases of chemical machinery of the Czech Academy of Sciences) discussed the dynamics and mass transfer of collapsing plates; T. G. Somer (Technical University, Ankara) discussed the experimental investigation into the designing of redistillation columns with sifter plates; T. Hobler, R. Crupicka and I. Chaika (Laboratory of processes and apparatuses of the Polish Academy of Sciences) investigated the hydrodynamics of sifter and collapsing plates.

Distillation was the subject of discussion at the tenth session. Mention should be made of the work of K. Lukasi, I. Gaker and D. Galbin (Leina werke, East Germany) discussing the production of trimethyl amine with the use of an extractive distillation mixture of methyl

amine with water. The relationship between the number of theoretical plates and the amount of added water was obtained as a result of the design of the column with the use of a computing machine.

We should also mention the report by Vilim (Scientific-Research Institute of synthetic rubber, Gotwaldow, Czechoslovakia) on the use of azeotropic distillation to dehydrate certain partially water soluble hydrocarbons. That report defines the physico-chemical parameters which determine the relationship between the amounts of water in a liquid and steam phase as well as the final water content in a liquid subjected to distillation.

The eleventh and twelfth sessions were devoted to chemical reactors.

The report on the "Effect of chemical reaction on diffusion phenomena" by D. F. Otmer (Technological Institute, Brooklyn, N. Y., U.S.) dwelt on the general characteristics of diffusion phenomena, and particularly, the simultaneous transfer of heat and mass. It would be practical to use electronic computers for the solution of the corresponding differential equations. The experimental investigation of drying processes calls for the use of high precision apparatus.

The solution of important problems in chemical kinetics should be based on the following scheme: the formulation of the initial concept of the process mechanism, a mathematical analysis, an experimental study of the process, the design of the installation, its production and operation. The experimental method of investigation is of major

importance, but mathematical patterns are also established. The best method of analysis is the presentation of the differential equations of the process in dimensionless form. Analogic computing devices should be used for calculating the streams of heat and mass in chemical reactions.

Unfortunately, the reporter touched only on general formulations but did not provide any mathematical or graphic interpretation.

I. I. Yoffe and L. M. Pis'zen (Scientific-Research Institute of organic semiproducts and dyestuffs, Moscow) substantiated the selection of optimum operating conditions and designed various schemes of chemical reactors. As pointed out by the authors, dynamic programming is the most effective method of solving such problems.

The work of D. R. Mason and J. Eoulas (University of Michigan, Ann Arbor, Michigan, U.S.) discusses the mathematical modelling of a tubular reactor with a fixed layer in a transitional regime; I. Nlitz (Research Laboratory of the Unilever Company, Vlardingem, Holland) speaks of the mathematical comparison of periodic and constant condensation reactions of ethylene oxide; J. J. Carberry, (Division of Processes and Apparatuses, Notre Dame University, Indiana, U.S.) discusses the effect of heat- and mass transfer on the activity and yield of catalytic heterogeneous reactions; M. Grupa (Scientific-Research Institute of Macromolecular chemistry, Brno, Czechoslovakia) devoted his work to a study of the boiling and condensation processes occasioned by a direct removal of the heat from liquid systems; the report of O. Kantakly

(chemical plants of Czech-Soviet friendship, Zluzhi, Czechoslovakia) dealt with a synthesis of ammonium in the presence of oxygen-containing substances; I. Sedlacek and L. Kubicek (Research Institute of the Cralovopolaki machine-building plant in Brno, Prague department) discussed the catalytic method of removing gas mixtures from oxygen and hydrogen, etc.

After the JHISA Congress the delegates attended the opening of the International fair at Brno with its large exhibition of apparatuses of the chemical machine-building industry from many countries.

In conclusion it should be pointed out that the convening of the Congress contributed to the establishment and strengthening of friendly contacts between the scientists of various countries.

There is no doubt that these creative contacts will contribute to the development of science and technology in such an important area as processes and apparatuses of various branches of industry.

5132

CSO:1880-D

- END -

UNCLASSIFIED

UNCLASSIFIED